A THEORETICAL MODEL OF FULLY DEVELOPED FIRE IN MASS TIMBER ENCLOSURES

COLLEEN ALICE WADE

A thesis submitted in partial fulfilment of the requirements for the degree of

Doctor of Philosophy

Department of Civil and Natural Resources Engineering
University of Canterbury
Christchurch, New Zealand

November 2019

Once asked by Denis Lawson (a past Director of FRS) as to his ambition in his further work, Kawagoe answered – after some hesitation – "To abolish the fire resistance test". This objective has not yet been achieved but its limitations are increasingly recognized ...

— Philip H. Thomas [1]

Colleen Alice Wade: *A theoretical model of fully developed fire in mass timber enclosures.* A thesis submitted in partial fulfilment of the requirements for the degree of Doctor of Philosophy. © November 2019

SUPERVISORS:
Prof. Charles Fleischmann
Dr. Anthony Abu
Dr. Michael Spearpoint

Science may be described as the art of systematic oversimplification.

— Karl Popper

For bet than never is late. [Better late than never.]

— Geoffrey Chaucer, The Yeoman's Prologue and Tale, Canterbury Tales, circa 1386.

This thesis is dedicated to Anne
– my lovely, caring and beautiful mum.

ABSTRACT

Existing practices for the fire design of mass timber buildings based on traditional fire resistance frameworks previously developed for non-combustible enclosures are inadequate. The contribution of mass timber surfaces to a fully developed enclosure fire is coupled to the design fire such that timber charring rates determined from standard fire resistance tests or parametric time temperature relationships may not apply. This is particularly important when considering structural fire performance of tall mass timber buildings.

This thesis describes a theoretical fire model for calculating the thermal environment within enclosures constructed from fully or partially exposed mass timber elements such as cross-laminated timber. The fire model includes two new pyrolysis submodels to enable calculation of the mass loss rate, energy release and char depth within wood surfaces burning in the enclosure. Phenomena such as debonding of lamellae in engineered wood panels is included and discussed. The pyrolysis submodels are coupled to the two-zone fire model B-RISK enabling the fire dynamics in small mass timber enclosures to be predicted. Model predictions for heat release rate, gas temperatures and/or char depths are compared with data from 19 full-scale fire experiments previously published in the literature.

The thesis also describes a submodel for predicting the enclosure thermal enhancement and ventilation effects on the mass loss rate of a burning fuel package. Model predictions have been evaluated with good agreement for an inert reduced-scale enclosure based on a series of heptane pool fires and a series of upholstered chair fires in a full-size enclosure. The application of the submodel to mass timber enclosures in combination with the previously developed pyrolysis submodels is discussed however additional experiments with well characterised fuel sources are required to more thoroughly evaluate this feature of the model. Potential applications of the model include generating thermal boundary conditions for a more advanced thermal/structural finite element code and for deriving modified fire load energy density values applicable to mass timber for use in simplified fire severity formula.

It is concluded that where mass timber structures must be designed to 'not collapse' in fire then satisfying prescriptive time periods in standard fire resistance tests is not sufficient. The fire performance of these structures need to be specifically engineered considering the expected fire growth, duration and decay periods. This requires a coupled interaction between the moveable fire load and the combustible enclosure surfaces to be considered.

Deputy Vice-Chancellor's Office
Postgraduate Office

UNIVERSITY OF CANTERBURY
Te Whare Wānanga o Waitaha
CHRISTCHURCH NEW ZEALAND

Co-Authorship Form

This form is to accompany the submission of any thesis that contains research reported in co-authored work that has been published, accepted for publication, or submitted for publication. A copy of this form should be included for each co-authored work that is included in the thesis. Completed forms should be included at the front (after the thesis abstract) of each copy of the thesis submitted for examination and library deposit.

Please indicate the chapter/section/pages of this thesis that are extracted from co-authored work and provide details of the publication or submission from the extract comes:

Wade, C.A., Hopkin, D., Su, J., Spearpoint, M.J. and Fleischmann, C.M. Enclosure fire model for mass timber construction – Benchmarking with a kinetic wood pyrolysis submodel. Paper accepted for presentation at INTERFLAM 2019. July 1-3, London, UK.

Content from this paper is included in Chapters 5 and 6.

Please detail the nature and extent (%) of contribution by the candidate:

The candidate was the primary author for this paper (80% contribution) with the co-authors reviewing and commenting upon the draft paper prior to publication.

Certification by Co-authors:
If there is more than one co-author then a single co-author can sign on behalf of all
The undersigned certifys that:

- The above statement correctly reflects the nature and extent of the PhD candidate's contribution to this co-authored work
- In cases where the candidate was the lead author of the co-authored work he or she wrote the text

Name: *Charles Fleischmann* Signature: Date: 5-6-19

Deputy Vice-Chancellor's Office
Postgraduate Office

UNIVERSITY OF CANTERBURY
Te Whare Wānanga o Waitaha
CHRISTCHURCH NEW ZEALAND

Co-Authorship Form

This form is to accompany the submission of any thesis that contains research reported in co-authored work that has been published, accepted for publication, or submitted for publication. A copy of this form should be included for each co-authored work that is included in the thesis. Completed forms should be included at the front (after the thesis abstract) of each copy of the thesis submitted for examination and library deposit.

Please indicate the chapter/section/pages of this thesis that are extracted from co-authored work and provide details of the publication or submission from the extract comes:

Jessop, D., Abu, A.K., Wade, C.A., Spearpoint, M.J., Gerlich, J.T., 2019. Performance of a light timber-framed compartment in natural fire subjected to lateral load. Fire and Materials 43, 175–188. https://doi.org/10.1002/fam.2684

Content from this paper is included in Chapter 9.

Please detail the nature and extent (%) of contribution by the candidate:

The candidate was a co-author for this paper (15% contribution) and contributed part of the content along with reviewing and editing the paper.

Certification by Co-authors:
If there is more than one co-author then a single co-author can sign on behalf of all
The undersigned certifys that:

- The above statement correctly reflects the nature and extent of the PhD candidate's contribution to this co-authored work
- In cases where the candidate was the lead author of the co-authored work he or she wrote the text

Name: *Anthony Abu* Signature: Date: 5-6-19

Deputy Vice-Chancellor's Office
Postgraduate Office

UNIVERSITY OF CANTERBURY
Te Whare Wānanga o Waitaha
CHRISTCHURCH NEW ZEALAND

Co-Authorship Form

This form is to accompany the submission of any thesis that contains research reported in co-authored work that has been published, accepted for publication, or submitted for publication. A copy of this form should be included for each co-authored work that is included in the thesis. Completed forms should be included at the front (after the thesis abstract) of each copy of the thesis submitted for examination and library deposit.

Please indicate the chapter/section/pages of this thesis that are extracted from co-authored work and provide details of the publication or submission from the extract comes:

Wade, C.A., Spearpoint, M.J. and Fleischmann, C.M. Engineering Methods for Evaluating the Contribution of Exposed Timber to Post-Flashover Enclosure Fires. SFPE Europe Magazine. Issue 11. 2018.

Content from this article is included in Chapters 5 and 6.

Please detail the nature and extent (%) of contribution by the candidate:

The candidate was the primary author for this paper (90% contribution) with the co-authors reviewing and commenting upon the draft paper prior to publication.

Certification by Co-authors:
If there is more than one co-author then a single co-author can sign on behalf of all
The undersigned certifys that:

- The above statement correctly reflects the nature and extent of the PhD candidate's contribution to this co-authored work
- In cases where the candidate was the lead author of the co-authored work he or she wrote the text

Name: *Charles Fleischmann* Signature:  Date: 5-6-19

Deputy Vice-Chancellor's Office
Postgraduate Office

UNIVERSITY OF CANTERBURY
Te Whare Wānanga o Waitaha
CHRISTCHURCH NEW ZEALAND

Co-Authorship Form

This form is to accompany the submission of any thesis that contains research reported in co-authored work that has been published, accepted for publication, or submitted for publication. A copy of this form should be included for each co-authored work that is included in the thesis. Completed forms should be included at the front (after the thesis abstract) of each copy of the thesis submitted for examination and library deposit.

Please indicate the chapter/section/pages of this thesis that are extracted from co-authored work and provide details of the publication or submission from the extract comes:

C.A. Wade, M.J. Spearpoint, C.M. Fleischmann, G.B. Baker, A.K. Abu, Predicting the fire dynamics of exposed timber surfaces in compartments using a two-zone model, Fire Technol. 54 (2018) 893–920. doi:10.1007/s10694-018-0714-2.

Content from this paper is included in Chapters 5 and 6 of this thesis.

Please detail the nature and extent (%) of contribution by the candidate:

The candidate was the primary author for this paper (90% contribution) with the co-authors reviewing and commenting upon the draft paper prior to publication.

Certification by Co-authors:
If there is more than one co-author then a single co-author can sign on behalf of all
The undersigned certifys that:

- The above statement correctly reflects the nature and extent of the PhD candidate's contribution to this co-authored work
- In cases where the candidate was the lead author of the co-authored work he or she wrote the text

Name: *Charles Fleischmann* Signature: Date: 5-6-19

Deputy Vice-Chancellor's Office
Postgraduate Office

UNIVERSITY OF CANTERBURY
Te Whare Wānanga o Waitaha
CHRISTCHURCH NEW ZEALAND

Co-Authorship Form

This form is to accompany the submission of any thesis that contains research reported in co-authored work that has been published, accepted for publication, or submitted for publication. A copy of this form should be included for each co-authored work that is included in the thesis. Completed forms should be included at the front (after the thesis abstract) of each copy of the thesis submitted for examination and library deposit.

Please indicate the chapter/section/pages of this thesis that are extracted from co-authored work and provide details of the publication or submission from the extract comes:

Wade, C.A., Fleischmann, C.M., Spearpoint, M.J. & Abu, A.K. 2017. Prediction model for compartment effects on burning upholstered furniture. Fire Safety 2017 International Conference on Research and Advanced Technology in Fire Safety. Santander, Spain.

Content from this paper is included in Chapter 7 of this thesis.

Please detail the nature and extent (%) of contribution by the candidate:

The candidate was the primary author for this paper (85% contribution) with the co-authors reviewing and commenting upon the draft paper prior to publication.

Certification by Co-authors:
If there is more than one co-author then a single co-author can sign on behalf of all
The undersigned certifys that:

- The above statement correctly reflects the nature and extent of the PhD candidate's contribution to this co-authored work
- In cases where the candidate was the lead author of the co-authored work he or she wrote the text

Name: *Charles Fleischmann* Signature: Date: 5-6-19

Deputy Vice-Chancellor's Office
Postgraduate Office

UNIVERSITY OF CANTERBURY
Te Whare Wānanga o Waitaha
CHRISTCHURCH NEW ZEALAND

Co-Authorship Form

This form is to accompany the submission of any thesis that contains research reported in co-authored work that has been published, accepted for publication, or submitted for publication. A copy of this form should be included for each co-authored work that is included in the thesis. Completed forms should be included at the front (after the thesis abstract) of each copy of the thesis submitted for examination and library deposit.

Please indicate the chapter/section/pages of this thesis that are extracted from co-authored work and provide details of the publication or submission from the extract comes:

Wade, C.A., Fleischmann, C.M., Spearpoint, M.J., Abu, A.K., 2015. Revisiting normalised heat load and its application in a compartment fire model, in: Proceedings Fire and Materials 2015. InterScience Communications Limited, San Francisco, USA.

Content from this paper is included in Chapter 9 of this thesis.

Please detail the nature and extent (%) of contribution by the candidate:

The candidate was the primary author for this paper (85% contribution) with the co-authors reviewing and commenting upon the draft paper prior to publication.

Certification by Co-authors:
If there is more than one co-author then a single co-author can sign on behalf of all
The undersigned certifys that:

- The above statement correctly reflects the nature and extent of the PhD candidate's contribution to this co-authored work
- In cases where the candidate was the lead author of the co-authored work he or she wrote the text

Name: *Charles Fleischmann* Signature: Date: 5/6/19

Deputy Vice-Chancellor's Office
Postgraduate Office

UNIVERSITY OF CANTERBURY
Te Whare Wānanga o Waitaha
CHRISTCHURCH NEW ZEALAND

Co-Authorship Form

This form is to accompany the submission of any thesis that contains research reported in co-authored work that has been published, accepted for publication, or submitted for publication. A copy of this form should be included for each co-authored work that is included in the thesis. Completed forms should be included at the front (after the thesis abstract) of each copy of the thesis submitted for examination and library deposit.

Please indicate the chapter/section/pages of this thesis that are extracted from co-authored work and provide details of the publication or submission from the extract comes:

Wade, C.A., Gerlich, J.T., Abu, A.K., 2014. The Relationship between Fire Severity and Time-Equivalence (BRANZ Study Report No. 314). Porirua, New Zealand.

Content from this paper is included in Chapter 9.

Please detail the nature and extent (%) of contribution by the candidate:

The candidate was the primary author for this report (70% contribution) with the co-authors contributing additonal content, reviewing and commenting upon the draft report prior to publication.

Certification by Co-authors:
If there is more than one co-author then a single co-author can sign on behalf of all
The undersigned certifys that:

- The above statement correctly reflects the nature and extent of the PhD candidate's contribution to this co-authored work
- In cases where the candidate was the lead author of the co-authored work he or she wrote the text

Name: *Anthony Abu* Signature: Date: 5-6-19

We have seen that computer programming is an art,
because it applies accumulated knowledge to the world,
because it requires skill and ingenuity, and especially
because it produces objects of beauty.

— Donald E. Knuth [2]

ACKNOWLEDGEMENTS

My sincere thanks go to my supervisors - Charley Fleischmann, Mike Spearpoint and Tony Abu for their support, encouragement, guidance and patience over the past six years. While at times I questioned the wisdom of embarking on this journey in the latter part of my career, I am now pleased that I did and thankful for the opportunity I was given. Special thanks to Charley who as senior supervisor agreed to my part-time enrolment from a remote location and for having faith in my ability to complete.

I also thank my current and former BRANZ colleagues who contributed in various ways - Greg Baker, Kevin Frank, Amanda Robbins and Haejun Park for providing inspiration, encouragement and setting good examples. Thanks to Peter Collier, Ed Soja, George Hare, Peter Whiting, Paul Chapman and the rest of the fire team who were always willing to help. To the BRANZ managers and leaders who supported me and facilitated the research - Chelydra Percy, Chris Litten, Richard Capie, Janet Geritzlehner, Anna de Raadt, Paul Shortis, Trish Shaw and Jacquie Harper and to other BRANZ staff including Andries Labuschagne for the many papers and articles he managed to track down for me and Moyra Shelton for always seeming to get the right signatures on the right forms on my behalf.

My appreciation also extends to my external collaborators, Danny Hopkin (OFR Consultants) and Joseph Su (NRCC) who both became involved with my research more recently but who most importantly provided valuable ideas and data that were used extensively in this thesis. Also thanks to Hans Gerlich and Daniel Jessop for the helpful discussions along the way.

I would particularly like to acknowledge BRANZ Inc and the Building Research Levy for helping to fund not only this research but also the development of the B-RISK model over many years. And finally, thanks to all the users of the software who ultimately provided the incentive to keep the model development alive.

CONTENTS

LIST OF FIGURES

LIST OF TABLES

ACRONYMS

AST Adiabatic Surface Temperature

BRANZFIRE A computer fire model

B-RISK A computer fire model

CBUF Combustion behaviour of uphostered furniture study

CFAST Consolidated model of fire growth and smoke transport

CLT Cross-laminated timber

CO Carbon monoxide

CO_2 Carbon dioxide

C/VM2 New Zealand verification method for protection from fire

DLT Dowel-laminated timber

EC_5 EN 1995-1-1: Eurocode 5

EPI Emulsion-polymer-isocyanate

EWC Engineered wood construction

FDS Fire Dynamics Simulator (a computer fire model)

FLED Fire load energy density

FPRF Fire Protection Research Foundation

FTP Flux time product

GER, GE Global equivalence ratio

Glulam Glue-laminated timber

HCN Hydrogen cyanide

HRR Heat release rate

HRRPUA Heat release rate per unit area

ISO International Organisation for Standardisation

LVL Laminated veneer lumber

MF Melamine formaldehyde

MLR Mass loss rate

MUF Melamine urea formaldehyde

NIST National Institute of Standards and Technology

NLT Nail-laminated timber

NRCC National Research Council of Canada

NZBC New Zealand Building Code

NZS New Zealand Standard

O_2 Oxygen

PRF Phenol resorcinol formaldehyde

PU, PUR Polyurethane

PVAc Poly(vinyl acetate), PVA glue

SMA Wood pyrolysis submodel A (equivalence ratio)

SMC Wood pyrolysis submodel C (kinetic)

A	Area [m^2]
A	Reaction pre-exponential factor [s^{-1}]
A_{Fp}	Surface area of fuel exposed to radiation [m^2]
B	Sill elevation above the floor [m]
Bi	Biot no. [-]
C	Fraction of fuel that can be burned with available oxygen [-]
D	Diameter [m]
D	Fuel/stick thickness [m]
E	Experiment measured value
E	Reaction activation energy [J mol^{-1}]
F	View factor [-]
Fo	Fourier no. [-]
H	Height [m]
L	Length [m]
L_g	Latent heat of gasification [kJ g^{-1}]
MW	Molecular weight
M	Model prediction value
N	Neutral plane elevation above the floor [m]
P	Pressure [Pa]
Q	Heat release [kJ]
$\dot{Q}$	Rate of heat release [kW]
$\dot{Q}''$	Rate of heat release per unit area [kW m^{-2}]
R	Universal gas constant [8.3145 kJ $kmol^{-1}$ K^{-1}]
S	Stick spacing [m]
T	Temperature [K]

V Volume [m^3]

W Width [m]

X Mass fraction of char [-]

Y Mass fraction [kg kg^{-1}]

a Proportion of surface area exposed [-]

b Thermal diffusivity [m^2 s^{-1}]

c Initial fraction of the unheated solid represented by a component e.g. lignin, cellulose or hemicellulose [-]

c_p Specific heat [kJ g^{-1} K^{-1}]

d Depth [m]

f Contraction factor [-]

g Acceleration of gravity [9.81 m s^{-2}]

$\dot{h}$ Rate of change in enthalpy [kW]

h Convective heat transfer coefficient [W m^{-2} K^{-1}]

k Thermal conductivity [W m^{-1} K^{-1}]

$\dot{m}$ Mass rate of change [kg s^{-1}]

$\dot{m}''$ Mass loss rate of change per unit area [kg s^{-1} m^{-2})]

$\dot{m}_p$ Plume flow rate [kg s^{-1}]

m Mass [kg]

m Mass of fuel remaining [kg]

m_o Original mass of fuel [kg]

n Reaction order [-]

$\dot{q}''$ Heat flux [kW m^{-2}]

$\dot{q}''_c$ Characteristic heat release rate per unit area [kW m^{-2}]

q Dose of blackbody thermal radiation [kJ]

r Stoichiometric oxygen to fuel mass ratio [-]

s Stoichiometric air to fuel ratio [-]

t Time [s]

u Moisture content fraction [-]

ν_p Surface regression rate [m s^{-1}]

w Reaction rate [s^{-1}]

x Position, dimension [m]

z Layer height [m]

Greek

α Absorptivity [-]

α Fire growth rate coefficient [kW s^{-2}]

β Ratio of convective gain and radiative loss with incident heat flux [-]

ΔH_c Heat of combustion [kJ g^{-1}]

Δt Timestep [s]

δ Bias factor [-]

ϵ Emissivity [-]

γ Ratio of specific heats $c_p/c_\nu = 1.4$ [-]

λ Fraction of total energy released inside the enclosure [-]

ν Char residue yield [-]

Ω Excess fuel factor [-]

ϕ Global equivalence ratio [-]

Ψ Yield of species i [kg kg^{-1}]

ρ Density [kg m^{-3}]

σ Standard deviation [-]

σ Stefan-Boltzmann constant [5.67×10^{-8} W m^{-2} K^{-4}]

$\tilde{\sigma}$ Relative standard deviation [-]

Subscripts

abs Absorbed

avg Average

b Burning

con	Convection
c	Char
c	Crib
ceil	Ceiling
dry	Dry
res	Residue
emi	Emitted
ext	External, non fire exposed side
FB	Free burn (well-ventilated)
f	Fuel, flame
fs	Fuel surface
g	Gas
init	Initial
i	Component, species
in	In, entering
inc	Incident
int	Internal, fire exposed side
lim	Limit
L	Losses
l	Lower layer
max	Maximum
nc	Noncombustible, inert
o	Opening
p	Plume
rad	Radiation
R	Room
s	Solid
s	Surface
tot	Total

u	Upper layer
v	Vapourisation
out	Out, leaving
vm	Vent mixing
water	Water
w	Wood
wall	Wall
∞	Ambient

1 INTRODUCTION

1.1 BACKGROUND AND MOTIVATION

There is growing world-wide interest in constructing taller buildings with mass timber and engineered wood products [3, 4]. Mass timber is typically a term used to describe a family of engineered wood products of large section size (including thick panel products) that offers the construction industry a viable alternative to steel and concrete [5]. Brandon [6] defines mass timber structures as having a smallest dimension not less than 80 mm. Mass-timber products include variants such as cross-laminated timber (CLT), nail-laminated timber (NLT), laminated veneer lumber (LVL), dowel-laminated timber (DLT) and glue-laminated timber (glulam) and are typically formed into solid wood panels or heavy structural elements in contrast to traditional light-timber frame and cavity construction. In New Zealand, mass timber construction mainly comprises of LVL, Glulam and CLT [7] and is mostly manufactured with Radiata pine with lesser quantities of Douglas fir [8].

Various structural solutions for tall buildings are also available, which use mass timber as the primary structural material e.g. Figure 1.1. In New Zealand, innovative post-tensioned timber frame technology has been developed for multi-storey buildings [9] being cost competitive with concrete or steel frame buildings [10].

There are many advantages to using mass timber in addition to its architectural qualities, including [12, 13]:

- easy handling during construction
- amenable to a high degree of offsite prefabrication
- fast construction times
- light-weight panels allow smaller less expensive foundations
- high in-plane and out-of-plane strength and stiffness
- improved dimensional stability allows longer and larger panels
- high strength to weight ratios allows good seismic performance
- less carbon intensive to manufacture, transport and erect than other common structural materials so contributes to reducing the carbon impact of construction.

Figure 1.1: Concept design by Michael Green Architecture for a 20-storey tall timber building [11]. Reprinted from [5] with permission.

Fire performance of mass timber is also often promoted as an advantage due to the development of a surface layer of char that helps to insulate and protect the underlying wood. In solid wood, the rate and depth of char is predictable and can be accounted for in the engineering design of the structure [14]. However, wood is clearly a combustible material and has contributed to severe damage [15] and loss of life in some fires [16]. Many of the documented fires involve light-timber frame but there are also examples of fire in heavy timber structures such as a glue-laminated timber gynamasium in Hiroshima, Japan [17] and most recently at the Notre Dame cathedral in Paris where it appeared the heavy timber roof structure contributed significantly to the severity of the fire [18]. This paradox is acknowledged by Buchanan [19] who commented:

> *"Modern fire engineering designs of steel and concrete buildings rely on full 'burnout' of any fire compartment, with no fire spread and no collapse, through the full period of fire development and decay. For timber buildings, the achievement of*

burnout is less certain, because of the residual fuel which is always present in the large timber structural elements."

The concept of burnout and what it means for timber stuctures is further explored by Law and Hadden [20]. They identify two distinct schools of thought regarding how structural fire safety may be achieved in tall timber buildings. These are:

1. undertake standard fire-resistance tests assuming there are no fundamental differences between timber, steel or concrete buildings; or

2. recognise the differences between combustible and non combustible construction materials and explicitly require that a structure should resist burnout.

Law and Hadden [20] go on to explain *"it is not possible to define a meaningful period of fire resistance for an exposed timber element within the existing fire resistance framework. Any design that includes exposed structural timber elements and does not consider the coupled interaction between the structure and the fire leaves structures at risk of unwanted failures."*

Fire resistance ratings specified in codes and standards have traditionally been derived on the assumption that compartments are non-combustible where the structure does not contribute to the fuel load or the severity of the fire. While is it still possible in most countries to design mass timber buildings following the traditional fire resistance framework, there is no assurance that building code objectives or functional requirements, such as Clause C6.3 in the New Zealand Building Code (NZBC), requiring that "*Structural systems in buildings that are necessary to provide firefighters with safe access to floors for the purpose of conducting firefighting and rescue operations must be designed and constructed so that they remain stable during and after fire* [21]" will actually be achieved in practice.

There are further considerations necessary for mass timber such as CLT. For example, Deeny et al. [22] have summarised the key challenges for designers of modern high-rise timber construction using CLT. These are:

- It is necessary to be able to determine the size of the fire incorporating the contribution of exposed CLT and a corresponding need to determine the proportion of the burning which is external to the compartment. This is needed for guidance on external and vertical fire spread.

- It is necessary to understand the conditions governing the self-extinguishment and prevention of debonding of CLT lamellae.

- It is necessary to understand when and what encapsulation products are required to control the number and area of CLT

surfaces which interact with the fire. This is particularly important for buildings with high consequence of failure and where reliance is placed on 'stay in place' evacuation strategies.

- There is a need for charring rate calculation methods that account for the increase in fuel and the effects of any CLT debonding.
- There is a need to confirm the applicability of the currently available reduced cross section methods to determine load bearing fire resistance of timber structures.
- There is a need for reliable fire design methods based on a fundamental understanding of the response of CLT to fire.

Developing a good understanding of fire dynamics in compartments constructed with combustible materials was also identified by Gerard et al. [23] as one of the biggest research needs to achieve fire-safe tall wood structures. This was reinforced by Barber [4] who stated that the development of a calculation methodology to account for the change in compartment fire dynamics when two or more timber surfaces are exposed is the next step in the advancement of fire safety engineering. Even as recent as 2017, Östman et al. [24] report that accurate models are still not available for post-flashover fires in non-combustible compartments and that there is even less accuracy for modelling consequences in enclosures with combustible structural materials available. It is this topic that is the primary focus of this thesis.

1.2 RESEARCH HYPOTHESIS AND OBJECTIVES

The objective of this research was to develop an improved fully developed fire model that can be used to generate thermal exposures suitable for the purpose of structural design and for assessing the fire resistance of separating elements. The research intended to make use of an existing fire model B-RISK [25]. This model was the result of a collaborative research effort between BRANZ and the University of Canterbury that extended over a six year period from 2008-2013. B-RISK is a combined probabilistic-deterministic multi-room enclosure fire model addressing a range of mostly pre-flashover fire phenomena useful for fire design. B-RISK is now used by most fire engineering consultancies in New Zealand and also in some consultancies overseas and therefore was expected to provide an effective means of introducing any improved design approach for modelling fully developed fire to practicing engineers. The author of this thesis was also the principal developer and custodian of the B-RISK software code and therefore had access to, and was able to work efficiently with, the model where required as part of the proposed research.

The research hypothesis can be expressed as follows:

> *If the pyrolysis of exposed wood surfaces can be adequately described and integrated with a traditional enclosure fire model based on mass and energy conservation then the time-varying thermal environment over the duration of the fire can be be predicted and shown to be in general agreement with full-scale enclosure fire experiments conducted in mass timber enclosures.*

The primary objective of this research has been to therefore develop a new theoretical model for predicting the time-varying thermal environment during a fully developed fire within a mass timber enclosure, and to evaluate the accuracy of the predictive model by comparison with a series of full-scale experiments (by others) in mass timber enclosures. The specific research tasks that contribute to achieving this objective are:

1. Quantifying the mass and energy contribution of exposed wood linings with a wood pyrolysis submodel. Several wood pyrolysis submodels have been investigated and two of them are presented and evaluated in this thesis.

2. Quantifying the fuel response effects due to thermal feedback and restricted ventilation within an enclosure, since this is most commonly ignored in existing fire models. This research has implemented a fuel response effects submodel within B-RISK - initially for a noncombustible or inert enclosure and then for a mass timber enclosure.

3. Quantifying fire severity such that time-varying thermal boundary conditions are calculated in a manner that would be compatible with other more detailed thermal/structural finite element models of mass timber structural elements. Equivalent time of fire severity is also considered for possible application to non structural elements in mass timber enclosures.

1.3 THESIS STRUCTURE

This thesis consists of ten chapters, as follows:

1. INTRODUCTION. Chapter 1 (the current chapter) describes the motivation and objectives of the research.

2. ENCLOSURE FIRES. Chapter 2 introduces the conceptual model of the enclosure fire with emphasis on the fully developed post-flashover fire. The principles and history of zone models are presented. Other model types are briefly discussed with their advantages and disadvantages.

3. Basis for an Enhanced Fire Zone Model. Chapter 3 introduces the specific enclosure fire model used in this research and the reasons for its selection. The applicability of the existing model to the demands of mass timber enclosures is discussed.

4. Mass Timber Construction. Chapter 4 introduces the salient features of mass timber construction with respect to its fire performance and gives an overview of the combustion and pyrolysis of timber. Past efforts to study and predict the contribution of mass timber surfaces to enclosure fire development are described including a review of the relevant literature on pyrolysis models, debonding of CLT lamella, significance of adhesive type, autoextinction of burning timber surfaces, influence of oxygen and air flow, encapsulation of timber and engineering methods that have been developed to aid in the fire design of mass timber buildings.

5. Fire Dynamics Model for Mass Timber Enclosures. Chapter 5 describes the theoretical basis for two new pyrolysis submodels incorporated within the B-RISK zone model for predicting the fire environment within an enclosure with partially exposed or fully exposed mass timber surfaces. A separate submodel for debonding of the CLT lamella based on the temperature reached at the adhesive line is also described.

6. Benchmarking Pyrolysis Submodels. Chapter 6 presents data from nineteen full-size enclosure fire tests involving encapsulated, partially exposed or fully exposed timber wall and ceiling surfaces and compares them with predictions (using the two new wood pyrolysis submodels described in Chapter 5) of the enclosure gas temperature, rate of heat release and/or char depth with the experimental data.

7. Fuel Response Effects in Inert Enclosures. Chapter 7 describes an extension of the B-RISK zone model to consider the fuel response effects. This allows the user to specify a mass loss rate curve for a fuel package within the enclosure applicable to a free-burning well-ventilated condition. The thermal feedback within the enclosure and oxygen vitiation effects are calculated and incorporated into the B-RISK fire model. Applications of the model to the burning of heptane pool fires and upholstered chairs within noncombustible enclosures are presented.

8. Fuel Response Effects in Mass Timber Enclosures. Chapter 8 extends the previous fuel response submodel to a mass timber enclosure, with the wood surfaces also contributing to the fully developed fire.

9. MODEL APPLICATIONS. Chapter 9 suggests how the modified B-RISK fire dynamics model can be used to generate thermal boundary conditions for use in more advanced two- or three-dimensional finite element thermal and structural response models. It also suggests how equivalent time of fire severity could be applied to non structural elements in mass timber enclosures.

10. CONCLUSIONS AND RECOMMENDATIONS. Chapter 10 gives the conclusions from the research and identifies where future research effort would be beneficial.

1.4 MODEL VERSIONS

The submodels developed as part of this thesis have evolved over time as the research progressed. Unless otherwise stated in the relevant section, the version of the B-RISK model used to generate results is 2019.031 - the most recent at the time of writing.

1.5 LIST OF PUBLICATIONS

The following publications were written or co-authored during the course of this study with content included in this thesis (or closely related to that included).

- Wade, C.A., Hopkin, D.J., Su, J., Spearpoint, M.J., Fleischmann, C.M., 2019. Enclosure fire model for mass timber construction - benchmarking with a kinetic pyrolysis submodel, in: Interflam 2019: 15th International Conference on Fire Science and Engineering. InterScience Communications Limited, Royal Holloway College, Windsor, UK [26].

- Jessop, D., Abu, A.K., Wade, C.A., Spearpoint, M.J., Gerlich, J.T., 2019. Performance of a light timber-framed compartment in natural fire subjected to lateral load. Fire and Materials 43, 175–188 [27].

- Wade, C.A., Spearpoint, M.J., Fleischmann, C.M., Baker, G.B., Abu, A.K., 2018. Predicting the fire dynamics of exposed timber surfaces in compartments using a two-zone model. Fire Technol 54, 893–920 [28].

- Wade, C.A., Spearpoint, M.J., Fleischmann, C.M., 2018. Engineering Methods for Evaluating the Contribution of Exposed Timber to Post-Flashover Enclosure Fires. SFPE Europe Magazine [29].

- Wade, C.A., Fleischmann, C.M., Spearpoint, M.J., Abu, A.K., 2017. Prediction model for compartment effects on burning upholstered furniture, in: Alvear, D. (Ed.), Proceedings of Fire Safety

2017 International Conference on Research and Advanced Technology in Fire Safety. Presented at the Fire Safety 2017 International Conference on Research and Advanced Technology in Fire Safety., Editorial de la Universidad de Cantabria, Santander, Spain, pp. 315–330 [30].

- Wade, C.A., Fleischmann, C.M., Spearpoint, M.J., Abu, A.K., 2015. Revisiting normalised heat load and its application in a compartment fire model, in: Proceedings Fire and Materials 2015. InterScience Communications Limited, San Francisco, USA [31].
- Wade, C.A., Gerlich, J.T., Abu, A.K., 2014. The Relationship between Fire Severity and Time-Equivalence (BRANZ Study Report No. 314). Porirua, New Zealand [32].

The following publications were written or co-authored while enrolled in this PhD however their content while related is not part of this thesis.

- Wade, C.A., 2019. Fire hazard assessment of wall and ceiling fire spread in rooms, in: Apte, V. (Ed.), Flammability Testing of Materials Used in Construction, Transport and Mining. Woodhead Publishing Limited, Cambridge, England (2nd edition in preparation) [33].
- Wade, C.A., Frank, K., 2019. Fire resistance requirements in single storey industrial and warehouse buildings (Study Report No. SR417). BRANZ, Porirua, New Zealand [34].
- Wade, C.A., Frank, K., 2019. Evaluating fire resistance requirements in New Zealand industrial and storage buildings. SFPE Europe Magazine [35].
- Baker, G.B., Wade, C.A., Frank, K., 2017. Reaction-to-Fire Behaviour of Partial Quantities of Timber Surface Linings in Compartments, in: Alvear, D. (Ed.), Research and Advanced Technology in Fire Safety. Presented at the Fire Safety 2017 International Conference on Research and Advanced Technology in Fire Safety., Editorial de la Universidad de Cantabria, Santander, Spain, pp. 331–346 [36].
- Wade, C.A., Baker, G.B., Frank, K., Harrison, R., Spearpoint, M.J., 2016. B-RISK 2016 User guide and technical manual (Study Report No. SR364). BRANZ, Porirua, New Zealand [37].
- Peel, H., Wade, C.A., Spearpoint, M.J., Fleischmann, C.M., 2016. Experiments to develop a performance based assessment method for rooms partially lined with timber. Presented at the 11th Conference on Performance-Based Codes and Fire Safety Design Methods. Warsaw, Poland [38].

- Peel, H., Wade, C.A., Spearpoint, M.J., 2016. Comparison of partially lined timber room experiments with the modified B-RISK flame spread capability, in: Proceedings of 14th International Conference on Fire Science and Engineering (INTERFLAM). University of London, UK [39].

- Jessop, D., Abu, A.K., Wade, C.A., Spearpoint, M.J., Gerlich, J.., Buchanan, A.H., 2016. Full-scale fire test of a laterally loaded light timber-framed compartment, in: Proceedings of the 9th International Conference on Structures in Fire. Princeton, USA [40].

- Quintiere, J.G., Wade, C.A., 2015. Chapter 29 Compartment Fire Modeling, in: SFPE Handbook of Fire Protection Engineering. Springer, pp. 981–995 [41].

2

ENCLOSURE FIRES

2.1 INTRODUCTION

A convenient framework for describing the evolution of a fire within an enclosed space or compartment is shown in Figure 2.1 and is represented by a rise in temperature with time starting from ignition. Drysdale [42] identifies that the enclosure fire can be divided into the following three stages.

1. Growth (or preflashover) stage - here the average temperature is low and the fire is localised near its origin. During this stage the fire may continue to growth and increase in size.
2. Fully developed (or postflashover) stage - here all the items in the enclosure are involved and flames are present throughout the volume. [1]
3. Decay stage - here the fuel is becoming depleted and average temperatures decline. Flaming will eventually cease.

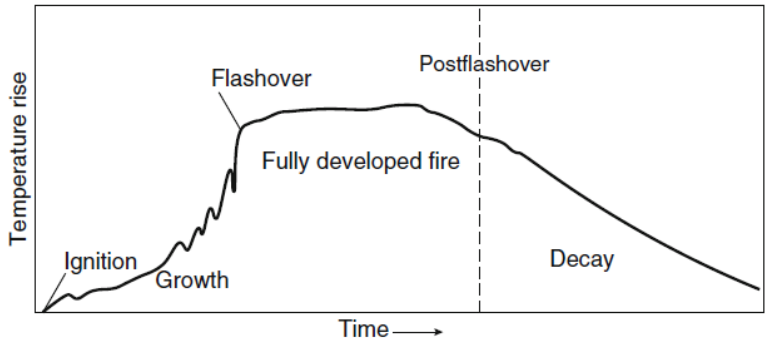

Figure 2.1: General description of a room fire. Reprinted from Walton and Thomas [45] with permission from Springer Nature.

The transition period between the growth stage and the fully developed stage is referred to as 'flashover'. Drysdale points out that this is not an 'event' like 'ignition' although it is tempting to treat it as such since it marks the beginning of the fully developed stage [42]. Flashover criteria are usually based on the temperature at which the radiation from the hot gases in the enclosure will ignite all the combustible contents. Gas temperatures of 500–600 °C are widely used

1 This depends on the geometry and size of the enclosure and may not be strictly true for a large enclosure where travelling fires have been proposed [43, 44].

[46]. It is generally accepted that conditions inside an enclosure following flashover are not survivable for its occupants.

This thesis will focus particularly on the fully developed or post-flashover fire where the average enclosure temperatures are the greatest since it is the most damaging period for building structures and is of most interest for structural fire design.

2.2 THE POST-FLASHOVER ENCLOSURE FIRE

In the 1950's Kawagoe [47] was the first to systematically study the behaviour of the enclosure fire by burning wood cribs in enclosures including different wall opening sizes. He found that the size and shape of the openings had a strong effect on the burning rate $\dot{m}_b$ and determined the following empirical correlation where A_o is the area of the opening and H_o is the height of the opening.

$$\dot{m}_b = 0.09 A_o \sqrt{H_o} \tag{2.1}$$

This correlation applies over a limited range of $A_o\sqrt{H_o}$ where the fire can be described as ventilation-controlled since it is related to the rate at which air can enter the compartment. Drysdale shows how this same relationship can be derived from a theoretical analysis of the flow of gases in and out of an enclosure where the fuel is wood burning under stoichiometric conditions [42]. The theoretical analysis requires a large number of simplifying assumpions and Drysdale argues that the precise agreement is fortuitious but says the relationship between the burning rate and the ventilation factor - $A_o\sqrt{H_o}$ was significant.

Equation 2.1 does appear to be at odds with the observation that burning rate increases when the fuel is subjected to increasing radiant heat feedback from the gases and compartment surfaces. Drysdale therefore concluded that the exact relationship only applies to wood cribs in which the burning surfaces are largely shielded from the influence of the compartment feedback [42]. Harmathy further investigated the distinction between ventilation-controlled and fuel-controlled burning regimes and recommended the following relationships applying to wood fuels to distinguish between the two regimes [48].

$$\frac{\rho\sqrt{g}A_o\sqrt{H_o}}{A_{fs}} < 0.235 \text{ (for ventilation control)} \tag{2.2}$$

$$\frac{\rho\sqrt{g}A_o\sqrt{h_o}}{A_{fs}} > 0.290 \text{ (for fuel control)} \tag{2.3}$$

Harmathy's form of the ventilation factor was normalised by the fuel surface area A_{fs} and therefore represented the ratio of the air flow to the fuel flow. Harmathy also describes the transition as a critical regime with $0.235 < \rho\sqrt{g}A_o\sqrt{H_o}/A_{fs} < 0.290$ where the rate of burning is often smaller than predicted using either of the above two equations [48]. Harmathy questioned the belief that in ventilation-controlled fires a shortage of air limits the rate of burning. Instead he proposed that for charring materials it was the oxidation of surface char that was the limiting factor [49]. For non-charring fuels he found that burning was virtually unaffected by ventilation [50]. Oxygen vitiation and radiation thermal enhancement effects on the burning rate of fuel is discussed in more detail in Chapter 7.

2.3 FIRE MODELS

2.3.1 *General*

Fire models consist of mathematical formula to describe the physical processes encountered in enclosure fires using interrelated expressions based on physics and chemistry [45]. These processes involve heat transfer, fluid dynamics and combustion. They can include both simple hand-calculations and complex computer models able to rapidly solve equations of transient and coupled phenomena. The use of computer fire models accelerated with the arrival of personal computers in the 1980's. Emmons [51] acknowledged, in 1985, that the way of the future in fire engineering was through various levels of modelling aided by the modern computer. More than thirty years on, this has indeed been the case facilitated by a better understanding of the science along with ever-faster and more powerful computers.

Quintiere [52] outlined the three main purposes of a fire model. They are:

- To underpin fire test methods and enhance the universality of fire test data allowing it to be used in engineering analysis replacing methods that are empirical and that only provide a means to rank materials relative to each other.
- To provide investigative tools for the analysis of fire growth in accidental fires.
- To provide quantative and versatile tools for building designers including methodology able to be used as a basis for performance based building codes.

There are two main types of physics-based mathematical fire model in common use. They are the zone model and the computational fluid dynamics (CFD) model. A brief description of both types is given in this chapter, however since the content of this thesis mainly concerns the first model type, only a brief overview of CFD models is given.

2.3.2 *Zone models*

A zone model solves equations for the conservation of mass and energy for one or more distinct control volumes. Most commonly there are just two control volumes (per enclosure), one corresponding to a hot upper layer and another representing a cooler lower layer. However, some zone models may be formulated differently, for example a single control volume might be used to represent a postflashover fire, or a series of control volumes representing multiple enclosures with interconnected openings between them.

The simplest essence of a zone model is therefore to solve mass and energy conservation equations for the control volumes (CV1 and CV2) shown in Figure 2.2. CV1 encloses the gases in the upper layer along with the plume, while CV2 encloses the remaining volume within the room representing the lower layer. The interface between the two layers can move up or down as the respective control volumes change. Combustion of the fuel source releases mass and energy which is transported by the buoyant plume to the upper part of the room. Air is entrained from the lower layer (CV2) into a plume as a result of buoyancy, increasing the volume of the upper layer and moving the layer interface closer to the floor. As the layer descends below the top of an opening some of the gases leave the room removing mass and enthalpy from control volume CV1. Hydrostatic pressure differences over the height of the opening then cause air from outside the room to enter the room through the opening at low level. The properties (including temperature, gas density and concentrations etc) of each control volume or layer zone are assumed to be spatially uniform, but can vary with time. It is also assumed that the gases transported in the plume are instantaneously distributed across the entire ceiling.

The zone model approach typically uses a series of submodels and source terms to quantify the various mass and energy flows. These can vary in complexity and usually include empirical relationships to describe phenomena such as the entrainment into the fire plume, shear mixing of flows near the openings as well as the vent flows. Along with the heat enthalpy flows that accompanying the transport of mass terms, additional heat transfer calculations to account for heat losses to the room bounding surfaces are typically included. Some models also include additional submodels designed to predict detector or sprinkler operation, visibility or tenability estimates and other parameters that may be useful for fire safety engineering.

Quintiere and Wade [41] list other assumptions made in applying the conservation laws to the control volumes or 'zones'. These include:

- The gas is treated as an ideal gas.

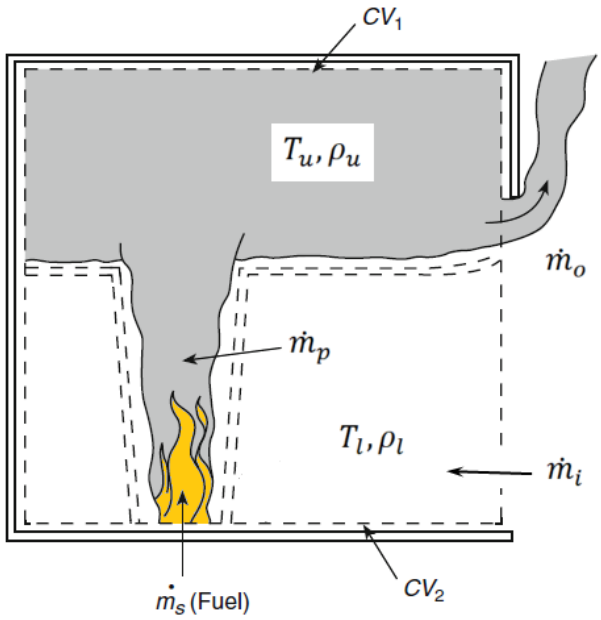

Figure 2.2: Zone model concept showing control volumes. Adapted from [41] with permission from Springer Nature.

- Mass flow across the free boundaries is due to pressure differences or shear mixing effects.
- Combustion is treated as a source of mass and energy.
- The plume instantly arrives at the ceiling. The time required to transport mass vertically to the ceiling or horizontally to the far ends of a compartment is ignored.
- The mass or heat capacity of room contents is considered negligible compared to the enclosure wall, ceiling and floor elements.
- The horizontal cross-section of the enclosure is a constant area but this assumption need not always be made.
- The pressure in the enclosure is considered to be uniform in the energy equation, but hydrostatic variations account for the pressure differences at free boundaries of the enclosure which in turn governs the vent flows.
- Mass flow into the fire plume is due to turbulent entrainment.
- Friction between the gases at solid boundaries is ignored.

Excellent descriptions of the principles of zone models are given by Quintiere [53] and Janssens [54] and these papers are highly recommended.

2.3.3 *History of zone model development*

The zone modeling approach emerged in the mid-1970s when the effort to study the developing fire in an enclosure intensified [41]. The first to publish a basis for the zone model approach was Fowkes [55] in relation to bedroom fire experiments at Factory Mutual. A number of computer models based on the two-zone approach quickly followed including the Harvard computer fire code [56, 57] and the Japanese BRI model [58]. The Harvard project ended in 1982 with Mark V of the Harvard Computer Fire Code [57, 59]. Further development was carried out at the National Bureau of Standards and a model called FIRST [60] resulted.

The 1980's and 1990's saw many more zone models arrive with an emphasis on compartment smoke-filling for preflashover fires. These included ASET [61], FPETOOL [62], FAST/CFAST [63], WPI Fire [64, 65], CCFM.VENTS [66], BRANZFIRE [67, 68], JET [69] amongst others. In 1992 Janssens [54] listed some 23 major pre-flashover zone models developed between 1978 and 1991.

Since the 2000's there was MAGIC [70], BRI2 [71], B-RISK [25, 37] and a recently revised version of CFAST [72–75].

A small subset of zone models have been specifically targeted at fully developed or postflashover fires. One of the first in this category was that of Magnusson and Thelanderson [76]. This was later revised by Wickstrom [77] and used in the development of the parametric time temperature equations in EN 1991-1-2 [78]. Other similar one-zone models included COMPF/COMPF2 [79–82] developed in the mid-70's by Babrauskas and more recently the European model OZONE [83–85].

2.3.4 *CFD models*

Computational fluid dynamics (CFD) is a general analysis tool for a wide range of fluid flow problems including those associated with fire. CFD has become an important analysis method used in fire safety engineering with many applications beyond those able to be addressed by zone models which are generally limited to relatively simple fire scenarios that can be described in terms of a small number of idealised enclosures [86].

CFD models solve partial differential equations for the conservation of mass, momentum and energy within the fire and its surroundings. Unlike zone models, CFD models enforce the conservation laws in thousands or millions of relatively small control volumes. Modelling the turbulent flows in fire requires special treatment and there are different approaches used including large eddy simulation (LES) and Reynolds averaged Navier-Stokes (RANS) equations [86].

Novozhilov provides a review of progress in CFD modeling for fire simulation as at 2001 [87].

Olenick and Carpenter [88] list about a dozen CFD models developed specifically for fire. Some of the more common models in use by the fire community today include the Fire Dynamics Simulator (FDS) [89], SMARTFIRE [90] and FireFOAM [91].

2.3.5 *Equation-based fire models*

An even simpler approach than the zone-type model are parametric relationships that use analytical equations to describe the time-history of the enclosure fire temperature. One example is a series of analytical expressions from Lie [92] for ventilation-controlled fires. Lie's expressions were said to be derived from approximations to curves based on the work of Kawagoe and Sekine [93, 94].

Perhaps the best known equation-based fire model in current use are the parametric time temperature equations from EN 1991-1-2 [78]. These equations are presented as valid for enclosures up to 500 m^2 with a maximum enclosure height of 4 m and they assume that the fire load will be completely burned out. The required input parameters are the room dimensions, the opening dimensions, the fuel load energy density, and the thermal characteristics of the enclosure bounding surfaces. The theoretical basis for these curves and their relationship to the standard fire curve was described by Wickström [77].

Ma and Mäkeläinen [95] also developed a parametric time temperature curves where the fire loads, opening factor, geometry and thermal properties of the enclosure determine the maximum gas temperature and fire duration. Another similar method called the BFD curve was developed by Barnett [96, 97]. This has the advantage of using only one equation for the final temperature–time curve compared to the multiple equations utilised by the Eurocode providing an easily applied method.

Pope and Bailey [98] compared the Eurocode and BFD parametric methods along with the CFD model FDS with large scale post-flashover test data and found that the BFD curve gave better predictions than the other two methods and consistently resulted in more accurate solutions than the method adopted in the Eurocode. They concluded that more advanced methods of modelling fire in compartments do not necessarily result in more realistic and accurate predictions of the fire temperatures in post-flashover fires.

While equation-based fire models are simple to use and suitable for including in spreadsheets, they lack the flexibility of models that solve the mass and energy conservation governing equations for an enclosure.

2.3.6 *Model type selection*

CFD analysis represents the state-of-the-art in fire modelling and is now routinely used in fire safety engineering as computers have become cheaper and faster. However compared to zone models they are numerically intensive and relatively complex.

In arguing the case for using CFD in preference to zone models, Novozhilov [87] lists several key major limitations of zone models . These include:

- Variables of interest are averaged over zones, therefore resolution is poor and some local effects cannot be distinguished.
- Knowledge of the nature of the flow structure is needed in advance and therefore the validity of the assumptions should be confirmed in each case.
- In rapidly growing fires there may not be sufficient time for the different zones to develop and be distinguishable from each other.
- The flow structure may change as a result of small changes in input parameters (bifurcation).

In 2008 Jowsey et al. [99] comment that to their knowledge, there had been no systematic evaluations of zone models when predicting heating of structural elements in fire. They note that the Reynolds number cannot be calculated properly and therefore convective heat transfer needs to be calculated differently and cannot be affected by any details of a complex geometry. Pyrolysis models are lacking and for fully developed fires heat release rates are ultimately determined by the ventilation with very limited data sets available. However, Jowsey et al. [99] also acknowledge that zone models are simple to use, robust in nature and can provide good insight on fire development for simple scenarios.

Regardless of the type of model selected, they will all be severely limited if the fundamental properties of the parameters affecting fire growth are improperly defined. Very often material properties specified are very simple or approximate. The errors resulting from incomplete material properties can be more important than those caused by improperly specifying parameters associated with the detailed fluid flow and combustion models [99]. This should not be forgotten in the context of building design where the exact characteristics of the moveable fire load representing the enclosure contents may be uncertain when the building is first complete let alone what it may be 10 years later. To that end, Torero comments that the increased level of precision gained from CFD is not necessarily justified where the model is used for mainstream design [100]. With respect to the use

of pyrolysis models embedded within CFD codes this may be even more true with Barber et al. [101] stating (as recently as 2018) that the computational time required to undertake pyrolysis modelling using FDS was extensive, and the simulation run times may be considered too long to be used as a viable design tool.

Considering a fixed amount of computing resource, an engineer may choose to dedicate it to a detailed analysis of a small number of CFD scenarios or they may choose a much larger number of simulations using a simpler tool that allows for treatment of uncertainty by perhaps using Monte Carlo sampling techniques. The latter has been conducted as part of probabilistic analysis that explicitly considers uncertainty in the different input and output parameters, such as that conducted by Notarianni [102], Elicson et al. [103] and Baker et al. [104–106]. From a design perspective zone models remain a valuable analysis tool alongside more detailed CFD approaches and has been used as the underlying model type in the research described in the remainder of this thesis.

3

BASIS FOR AN ENHANCED FIRE ZONE MODEL

3.1 EXISTING B-RISK MODEL

3.1.1 *Model selection*

The existing B-RISK model [37] developed at BRANZ in conjunction with the University of Canterbury has been used as a starting point for the further research described in this thesis. Not only does it provide a working model whereby standard mass and energy conservation equations are solved within a zone model framework, it is also well-known to the author of this thesis being the primary developer of the B-RISK model. B-RISK has been successfully used in related research efforts in recent years including balcony spill plumes [107], flame spread on timber linings [39], a design fire generator [106], a radiative item-to-item fire spread model [108–110] and modelling the activation of multiple sprinklers [111, 112]. B-RISK is a derivative of the earlier BRANZFIRE model [67, 68, 113] but with added functionality including Monte Carlo capability. It has been coded using Microsoft® Visual Studio® 2017 and the Visual Basic .NET framework.

This chapter will provide an overview of the B-RISK model building upon the general description of the zone modelling approach presented in the previous chapter. A more detailed and complete description of the B-RISK model can be found in the technical guide [37] with various benchmarking against experimental data presented in [114]. The model is freely available from the BRANZ website.

3.1.2 *Model overview*

3.1.2.1 *Governing equations*

Conservation of mass and energy can be expressed in a set of first order differential equations which when solved provides solutions for the upper layer volume, upper and lower layer temperatures, and pressure advancing in time. The specific form of the equations follows that given by Peacock et al. for the CFAST model [115].

The equation for the rate of change in pressure in the room is:

$$\frac{dP}{dt} = \frac{\gamma - 1}{V_R}(\dot{h}_l + \dot{h}_u) \tag{3.1}$$

The pressure is nominally that at floor level, and is relative to the atmospheric pressure at a nominated reference elevation. The offset

pressure is used to avoid unnecessary loss of significant digits when solving vent flow equations, where the pressure differences across the vent are small.

The equation for the rate of change in the volume of the upper layer is:

$$\frac{dV_u}{dt} = \frac{1}{\gamma P}\left[(\gamma - 1)\dot{h}_u - V_u \frac{dP}{dt}\right] \tag{3.2}$$

The lower layer volume is the difference between the room volume (a fixed value) and the upper layer volume. The height of the smoke layer or interface above the floor for an enclosure of uniform area and flat ceiling is then given by:

$$z = \frac{V_R - V_u}{A_{ceil}} \tag{3.3}$$

The equation for the rate of change in temperature of the upper layer is:

$$\frac{dT_u}{dt} = \frac{1}{c_p \rho_u V_u}\left[(\dot{h}_u - c_p \dot{m}_u T_u) + V_u \frac{dP}{dt}\right] \tag{3.4}$$

The equation for the temperature of the lower layer is:

$$\frac{dT_l}{dt} = \frac{1}{c_p \rho_l V_l}\left[(\dot{h}_l - c_p \dot{m}_l T_l) + V_l \frac{dP}{dt}\right] \tag{3.5}$$

The equations for the rate of change of mass in the upper and lower layers are given by:

$$\frac{dm_u}{dt} = \dot{m}_p + \dot{m}_f - \dot{m}_{vm} - \dot{m}_{out} \tag{3.6}$$

$$\frac{dm_l}{dt} = \dot{m}_{in} + \dot{m}_{vm} - \dot{m}_p \tag{3.7}$$

$\dot{m}_{vm}$ is a vent shear mixing flow from the upper layer to the lower layer. $\dot{m}_p$ is the mass flow entrained into the plume, $\dot{m}_{in}$ and $\dot{m}_{out}$ are the mass flows entering the lower layer and leaving the upper layer through the openings respectively.

Two additional equations are included to determine species concentrations in the respective layers. Species tracked in the model are soot, CO, CO_2, HCN, water vapour, unburned fuel and O_2.

$$\frac{dY_{i,u}}{dt} = \frac{1}{m_u}\left[\dot{m}_p (Y_{i,l} - Y_{i,u}) + \dot{m}_f (\Psi_i - Y_{i,u})\right] \tag{3.8}$$

$$\frac{dY_{i,l}}{dt} = \frac{1}{m_l}\left[\dot{m}_i(Y_{i,\infty} - Y_{i,l}) + \dot{m}_d(Y_{i,u} - Y_{i,l})\right] \tag{3.9}$$

m_u and m_l are obtained from the ideal gas law such that $m_i = MW_i PV_i/(RT_i)$ where i corresponds to the upper or lower layer and MW_i is the average molecular weight of the layer based on the gas composition of the layer and R is the universal gas constant.

The mass fractions of soot, HCN and CO initially present in the room are considered to be negligible, while the initial mass fraction of O_2 is set equal to 0.231 (ambient), and of CO_2 equal to 0.0005. Unburned fuel is only generated under a ventilation-limited burning regime.

3.1.2.2 *Heat Transfer*

B-RISK incorporates a four wall radiation exchange algorithm using the equations described by Forney [116]. The method allows the ceiling, upper wall, lower wall and floor to transfer radiation independently between each other. The fire is treated as point source of radiation that intercepts each of the surfaces. Soot particles are assumed to emit radiation and carbon dioxide and water vapour are assumed to absorb radiation. The boundary between the upper and lower wall is distinguished by the position of the layer interface and it changes with time. The radiation exchange submodel determines the net radiant heat flux emitted or absorbed by each room surface (i. e. upper and lower walls, ceiling and floor). These radiant fluxes are combined with the convective heat flux and used as the boundary condition for the heat conduction calculations described later.

The following assumptions are made in developing the four wall radiation exchange model [116].

1. Both gas layers and each of the wall, ceiling and floor surfaces are assumed to be at a uniform temperature. This is generally not true where the surfaces meet each other.

2. The surfaces and gas layers are assumed to be in quasi-steady state, remaining constant over the duration of the time step of the associated differential equations.

3. For the purposes of estimating the radiation heat transfer from the flame, the total radiant energy of the fire is assumed to radiate uniformly in all directions from a single point source positioned on the plume centreline at one-half the calculated flame height.

4. The radiation emitted by the room surfaces, gas layers and the fire is assumed to be diffuse and gray (i.e. the radiant flux is assumed independent of direction and wavelength).

5. The room surfaces are assumed to be opaque (i. e. incident radiation is either reflected or absorbed not transmitted) and the gases are assumed to be non-reflective.

6. The room is assumed to be a rectangular box with each surface either perpendicular or parallel to every other surface. Radiation losses through room openings are included.

The interior convection coefficient used in the heat transfer calculations between the gas layers and the room surfaces are calculated following the method described by Peacock et al. [115], however for the simulations presented in this thesis a constant convection coefficient of 35 W/m^2K has been used as specified in Eurocode 1 [117] for simple fire models. The reader should refer to the B-RISK manual [37] for a complete description of the equations used in the radiative exchange submodel and for the convective boundary conditions (see also the sensitivity analysis in Appendix B).

3.1.2.3 *Differential equation solver*

The ordinary first-order differential equations are solved using a stiff differential equation solver. The numerical solution was from that provided in a mathematics library, BNALib [118]. The equations relate to upper layer volume, upper and lower layer temperature, oxygen, soot, unburned fuel, water vapor, carbon monoxide and carbon dioxide concentrations. The numerical solver comprises an adaptive driver that estimates the error and adapts the step size to achieve the specified accuracy. An initial timestep of 1 second is generally used which the solver will reduce as necessary.

3.2 CURRENT LIMITATIONS AND NEW RESEARCH TASKS

3.2.1 *Combustible construction*

The current B-RISK zone model does already include capability for surface flame spread and fire growth over combustible wall and ceiling linings that was previously developed by Wade [67, 113, 119] for simulating ISO 9705 room corner tests [120]. It is based on thermal flame spread theory as presented by Quintiere [121] with both wind-aided flame spread and opposed flow (or lateral) flame spread modelled. The surface materials are characterised by ignition and heat release rate data from cone calorimeter [122] experiments carried out at a range of different external heat fluxes as well as data obtained from the ASTM 1321 (LIFT apparatus) test method [123] where lateral flame spread is also included. However, this submodel is considered mainly applicable to pre-flashover fires because the input data characterising the combustible surface materials is determined in cone calorimeter experiments at heat fluxes (typically 20 to

60 kW/m^2) that are representative of pre-flashover rather than post-flashover fires. It is also usual that soon after flashover, the extent of flame spread across the ceiling and upper wall is at a maximum having reached the far ends of the enclosure (at least for small enclosures). The existing surface linings submodel was recently modified to simulate the fire growth in enclosures with internal surfaces partially lined with timber in a study by Peel [39, 124]. Peel compared B-RISK predictions with seven full-scale ISO 9705 experiments [38] and found that the modelled fires showed good agreement with early fire growth in the experiments but underestimated the times to flashover which was considered acceptable for engineering purposes.

The existing submodel is mainly concerned with ignition, flame spread and early fire growth involving combustible lining materials, and while these are important for evaluating the life hazard, they are less important for assessing the effects of fully developed post-flashover fire on the building structure. Therefore, for mass timber enclosures, suitable wood pyrolysis submodels to determine the contribution of the mass timber surfaces to a fully developed fire are still needed. In such a model however, it may still be necessary to account for the contribution from burning surface lining materials before as well as after flashover.

3.2.2 *Fuel response effects*

Pyrolysis models are rarely included within zone models with the fire source term, such as the rate of heat release versus time curve, usually provided by the user as input to the model. However it is well known that the rate of burning of fuel inside a compartment is influenced by the thermal and combustion environment to which it is exposed i.e. radiative feedback from the gases and hot surfaces inside the room to the surface of fuel, as well as the oxgyen availability in the gases feeding the flame. Different fuels may respond differently to the enclosure environment depending on its combustion properties and configuration in the room.

A fuel response effects submodel for inclusion in B-RISK is described in Chapter 7 with applications of the submodel for heptane pool fires and upholstered furniture burning inside a small room given. The submodel is then extended for application to mass timber enclosures as described in Chapter 8.

3.2.3 *Evaluating fire severity*

For a mass timber enclosure, the logical fire severity measure would be related to the maximum depth of char in the wall or ceiling resulting from a given fire exposure. The fire dynamics enclosure model is relatively simple with regards to the one-dimensional heat transfer

conduction calculation to determine the char depth. For more complicated geometries involving two or three-dimensional timber surfaces, it may be appropriate to use the fire dynamics model to generate an adiabatic surface temperature time curve and for this to be used as a thermal boundary condition in a more detailed finite element thermal-structural model. Possible applications of the model are discussed in Chapter 9.

4

MASS TIMBER CONSTRUCTION

4.1 GENERAL

Mass timber is defined as a group of engineered wood products of large section size [125] including thick panels of wood engineered for strength through laminations of different layers. The panels vary in size but can range upwards of 20 m x 2.4 m [11]. The main types of mass timber are cross-laminated timber, nail-laminated timber, laminated veneer lumber and dowel laminated timber.

CLT is a multi-layered wood panel system with each layer (or lamella) comprising wood boards assembled and glued perpendicular to each other as illustrated in Figure 4.1 and Figure 4.2. Typically, there are between three and seven layers with the layer thickness in the range 16 to 51 mm, and the width in the range 60 to 240 mm [12].

Figure 4.1: Cross-laminated timber panel. Reprinted from Green [11]. This image is distributed under the terms of the Creative Commons Attribution License CC BY 4.0.

NLT is a very old construction method also found today in historic structures as well as new construction [127]. Individual lengths of timber are stacked on edge and nail-fastened into a single structural element as illustrated in Figure 4.3.

LVL is made up of layers of wood veneers laminated together using a waterproof structural adhesive (typically phenol formaldehyde (PF) or phenol-resorcinol formaldehyde (PRF)). The veneer thickness is typically in the range 2.5 to 4.8 mm. LVL is illustrated in Figure 4.4.

DLT illustrated in Figure 4.5 has the advantage of having no nails and no adhesive. To form the DLT members, lumber panels are stacked

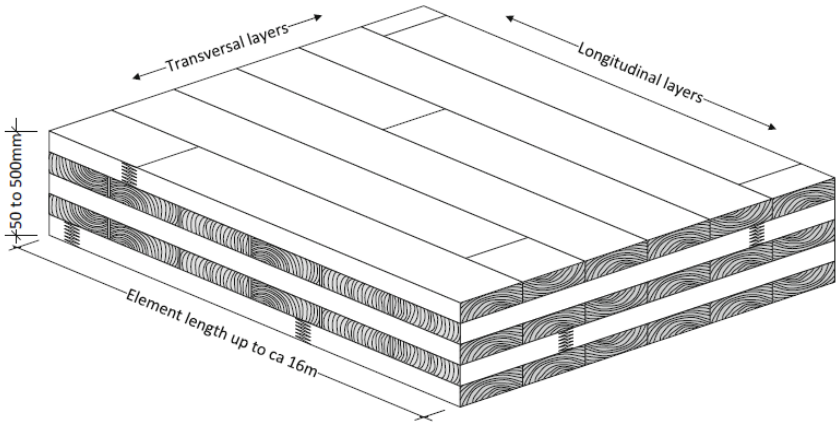

Figure 4.2: Example of cross-laminated cross-laminated timber panel. Reprinted from Schmid et al. [126] with permission from Springer Nature.

Figure 4.3: Nail laminated timber. Reprinted from Think Wood [127] with permission.

like NLT and are friction-fitted together with hardwood dowels. The dowels hold the boards together [128].

Since timber is a combustible material, the mass timber panels provide an additional source of fuel that may change the fire dynamics and severity of the compartment fire. This influences the rate at which the timber surfaces burn and the gas temperatures and heat fluxes generated within the enclosure.

While many building codes may tolerate structural collapse in low-rise buildings provided life safety is ensured, when determining fire performance for tall buildings in particular, common practice is to assign a fire resistance rating to the structure (as would typically be done for non-combustible enclosures) in the expectation that it

Figure 4.4: Laminated veneer lumber. Reprinted from Green [11]. This image is distributed under the terms of the Creative Commons Attribution License CC BY 4.0.

Figure 4.5: Dowel laminated timber. Reprinted from StructureCraft [129] with permission.

is sufficient for the compartment structure to survive until burnout of the room contents. However, this may not be appropriate when that structure itself is combustible. One approach to mitigating the contribution of timber is to protect it by encapsulating the surfaces with a non-combustible lining such as gypsum plasterboard. However, if the timber is exposed to a fire, there is a need for design methods that account for the burning surfaces and the effect on the fire dynamics as well as determining if the combustion of timber will cease or continue to burn after the contents have burned out. Thus, if 'withstanding complete burnout' is a design objective, the construction intended to perform as fire-resistant separations or load-carrying structure within a building must be evaluated considering the real fire behaviour. Traditional fire calculation models for estimating temperatures in compartments for fully developed fires e.g. [76, 78] do not consider the additional fuel contributed by the timber structure and therefore a calculation methodology to account for the change in

compartment fire dynamics when mass timber surfaces are exposed or insufficiently protected is required.

4.2 CHEMICAL STRUCTURE OF WOOD

Abu Ghalia and Dahman [130] give the chemical composition of wood as 50% carbon, 5% hydrogen and 40% oxygen with the remainder being nitrogen and various metal ions. All wood types contain carbohydrates typically as polysaccharides. The three main constituents of wood are cellulose, hemicellulose and lignin (see Figure 4.6) along with smaller amounts of organic extractives and inorganic species that form the ashes after the fire [131]. Cellulose consists of a large number of glucose molecules in a chain-like polymer and is given the formula $(C_6H_{10}O_5)_n$. Other sugars combine to form hemicelluloses being branch-chain polymers. Lignin is a phenolic-like high molecular weight polymer that acts as a binding agent within and between the cell walls [132]. The relative proportions of cellulose, hemicellulose and lignin in dry softwoods are typically in the ranges 40-44%, 20-32% and 25-35% respectively [132].

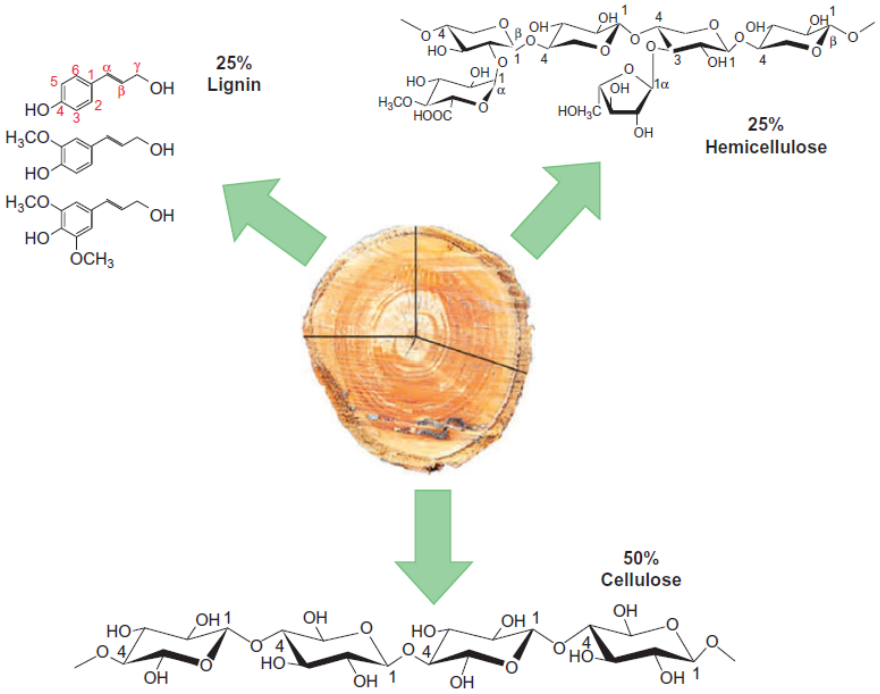

Figure 4.6: Chemical structures of wood. Reprinted from [130] with permission from Elsevier.

4.3 BURNING OF WOOD

There are many references in the literature providing detailed overview and review of the pyrolysis, ignition and combustion of wood e.g. [133–135]. This section gives a brief overview along with previous research relevant to developing a suitable new enclosure fire model including wood surfaces.

When solid fuels such as wood are exposed to external heating they decompose producing a mixture of volatiles and solid carbonaceous residue (or char) [136]. In an oxidising environment charring materials can either exhibit flaming combustion or smouldering combustion depending on the magnitude of the external heat flux as described in Figure 4.7 and with degradation zones illustrated in Figure 4.8.

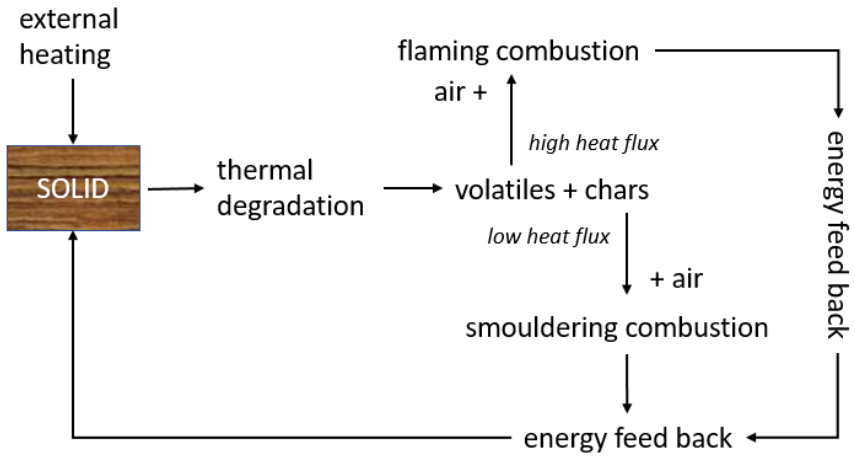

Figure 4.7: Combustion of charring materials. Adapted from Di Blasi [136] with permission.

Browne [133] described four zones (A to D) that develop when wood is heated with the zones demarcated by temperature.

- Zone A - up to 200°C

  This zone becomes dehydrated with water vapour evolved and with traces of carbon dioxide, formic and acetic acid and glyoxal (an organic dialdehyde compound) formed. The water vapour mostly migrates towards the heated side and escapes through the exposed surface. A fraction also migrates in the opposite direction, and re-condenses at a location where the temperature is below 100°C [138].

- Zone B - 200 to 280°C

  With further heating, pyrolysis is slow with water vapour, carbon dioxide, formic and acetic acids, and glyoxal continuing to be produced with possibly some carbon monoxide. Wood is

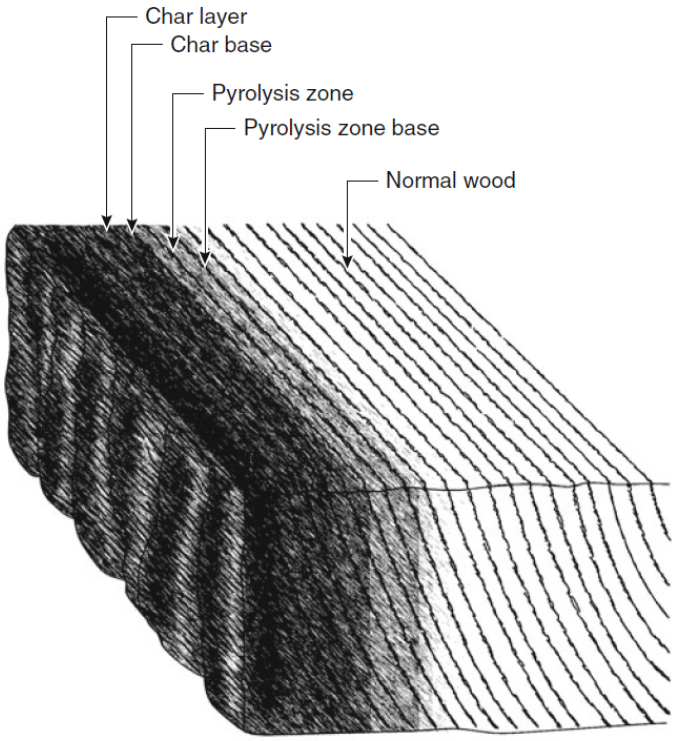

Figure 4.8: Degradation zones in a wood section. Reprinted from White [137] with permission from Springer Nature.

slowly converted to char. The reactions so far are endothermic and the gases produced are noncombustible.

- Zone C - 280 to 500°C

  The rate of pyrolysis rapidly increases and temperatures rise producing heat and combustible gases including carbon monoxide, methane, formaldehyde, formic and acetic acids, methanol, and later hydrogen (diluted with carbon dioxide and water vapour). Tar droplets are produced as smoke and the residue is char. Secondary reaction may also occur. The volatiles that are generated again migrate mostly toward the heated side, but also partly in the opposite direction.

- Zone D - above 500°C

  Char is formed with further secondary reactions in which the gaseous products and tars originating from deeper layers are further pyrolyzed to give more highly combustible products ie. carbon dioxide and water vapour react with carbon to form carbon monoxide, hydrogen, and formaldehyde.

Figure 4.9 identifies the major physical and chemical phenomena associated with the pyrolysis of a slab of wood.

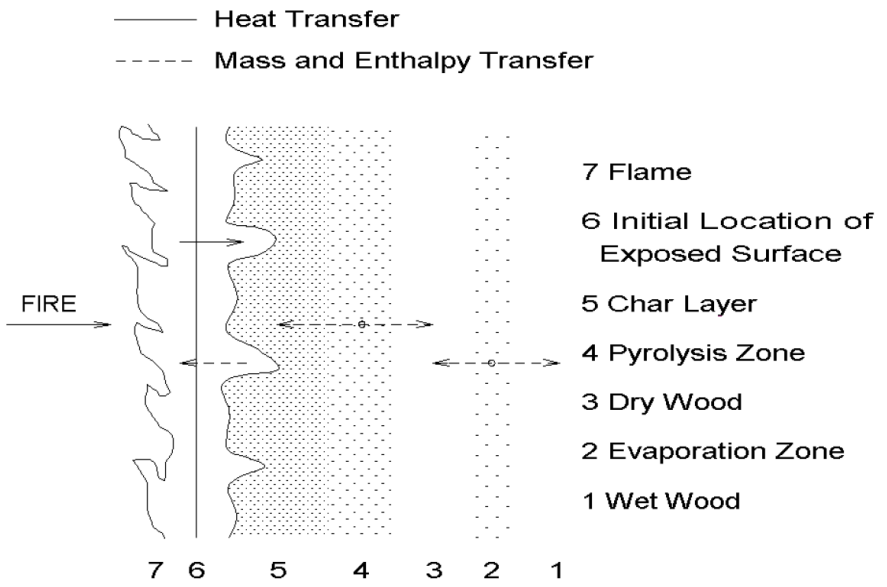

Figure 4.9: Heat and mass transfer in a pyrolysing slab of wood. Reprinted from Janssens [138] with permission.

When heated, wood changes colour. At 250°C, wood is dark brown; above 300°C, wood is black. The brown colour is associated with the onset of pyrolysis [139]. The 300°C isotherm is widely accepted as a rounded value to represent the charring depth [140]. The burning behaviour of wood is characterised by charring including both pyrolysis and oxidation processes. In addition, the outer surface of the char may be subject to mechanical disintegration or erosion. The process of converting wood to char and gas also results in a reduction in the wood's apparent density [137].

A great deal of attention has been given to determining charring rates which generally refers to the rate at which the wood depth is converted to char often expressed as a value in mm/min. The char rate enables the loss of cross-section and the reduction in structural loadbearing capacity of timber structures to be estimated. However the majority of effort in measuring charring rates has focussed on heating regimes following standard fire resistance tests e.g. [141, 142] rather than the actual heating (and cooling regime) of real fires. Babrauskas [143] provides an extensive review of experimental studies of charring rates, in furnaces, cone calorimeter as well as in compartments undertaken prior to 2005. Charring rates in standard fire resistance tests tend to be fairly constant after a higher initial rate [137]. Collier measured char rates of New Zealand radiata pine glulam beams in standard fire resistance tests and found density and moisture content to be the two main factors influencing char rate [144]. A design value of 0.65 mm/min was then adopted in the New Zealand timber design standard NZS 3603 [145]. This is consistent with design char rates in Eurocode 5 [146] for solid-sawn or glulam-

inated timber. In addition to density and moisture content, charring rate is also influenced by heat flux and local oxygen concentrations. Differences in charring rates for different wood species can partially be explained by differences in material properties. The kinetics due to the composition of wood can also play a role, however Richter et al. [147] argue that the difference in kinetics, at the mesoscale, is insignificant for temperature and mass loss rate predictions. They also found that the influence of kinetics reduced from microscale to mesoscale, and that it was reasonable to expect that the prediction of charring at the macroscale would also be unaffected by the variation in kinetics within the timber. Their advice was that *"Modellers should, therefore, focus on the difference in material properties between different wood species."*

4.4 PYROLYSIS MODELS FOR BURNING WOOD

A pyrolysis model allows the charring rate to be predicted over time. Janssens provided references to more than 50 different mathematical models for the pyrolysis (or thermal degradation) of wood developed since the second world war [138]. Janssens concluded that none of the models included all of the important features that needed to be addressed. The simplest type of pyrolysis model is an empirical analytical expression for char rate of wood exposed to a standard fire resistance test mentioned as discussed in Section 4.3 but since pyrolysis is a very complex process it can also be much more detailed model requiring partial differential equations for the decomposition of individual wood constituents to be solved. Fredlund's model [148] is one of the more complete including algorithms for mass transfer and char oxidation (but not char contraction). Fredlund verified the model with standard fire resistance experiments and was able to show that the distribution of temperature in the specimens tested was described very well for both moist and dry wood.

Janssens [138] also developed a new pyrolysis model to predict the charring rate of and temperature distribution in wood members exposed to specified fire conditions. This model was a function of the dry density, moisture content, lignin content and char contraction and was calibrated on the basis of correlations for the charring rate of wood members exposed to the standard ASTM E119 fire [149].

Lautenberger developed a generalized model that can be used to simulate the pyrolysis, gasification, and burning of a wide range of solid fuels encountered in fires [150]. The model considers a user–specified number of gas phase and condensed phase species, each having its own temperature–dependent thermophysical properties. Model calculations agreed well with the experimental data including blind simulations indicating that the predictive capabilities of the model are generally good, particularly considering the complexity of the problems simulated [150].

In solid phase kinetics, pyrolysis reaction rates may be described by Arrhenius type functions of the temperature shown in Equation 4.1 [151]. In the case where the degradation of the fuel is not dependent on oxygen, $m_i = 0$.

$$\dot{w} = A_i Y_{O_2}^{m_i} Y_s^{n_i} \exp\left(-\frac{E_i}{RT}\right) \tag{4.1}$$

Generally, solid-phase pyrolysis can be assumed to follow the Arrhenius equation with three parameters defining the reaction kinetics. These kinetic parameters are reaction order (n_i), activation energy (E_i) and pre-exponential factor (A_i). This type of pyrolysis submodel will be described later in Section 5.7 and used to calculate the contribution of the exposed surfaces to fire development in mass timber enclosures.

4.5 ENCLOSURE FIRE EXPERIMENTS

A recent literature review by Brandon and Östmann [152] on the contribution of CLT to enclosure fires provides a comprehensive summary of 41 fire tests of enclosures comprising both exposed and protected wood based construction. They also provide an overview of relevant results such as peak heat release rates, charring rates, time to decay of a fire and encapsulation times. Brandon and Östmann [152] listed two main causes for re-growth in the fire growth rate. They are:

- failure of the adhesive bond line within a CLT element allowing lamella to fall away prematurely exposing fresh timber,
- fire protective boards (e.g. gypsum plasterboard) falling away from the protected timber surface, and

A summary of a number of relevant full-size enclosure fire experiments involving protected and unprotected heavy timber or CLT construction follows. This list of experimental studies involving timber enclosures is not exhaustive.

4.5.1 *Hakkarainen 2002*

As part of a Nordic research effort, Hakkarainen [153] conducted three experiments in enclosures with dimensions 4.5 m × 3.5 m × 2.5 m high with an opening 2.3 m wide × 1.2 m high opening and construction with heavy laminated timber. The protection to the heavy laminated timber (presumed to be glulam) varied in each test - either none, or one layer of 12.5 mm thick Type A gypsum plasterboard or two layers of gypsum plasterboard (comprising 12.5 mm thick Type

A and 15.4 mm thick Type F gypsum plasterboard) screwed fixed to the timber structure. The fuel load comprised 680 kg of wood cribs and 230 kg of particleboard flooring.

Hakkarainen reported that the average gas temperature inside the enclosure without gypsum plasterboard protection was relatively low, approximately 700°C (attributed to insufficient ventilation), for the main part of the experiment. Towards the end of the experiment when most of the movable fire load had burned out, the temperature was observed to increase. Hakkarainen attributed this to the reduction in the generation rate of pyrolysis gases allowing more oxygen to enter the enclosure. In this experiment intense combustion outside the room was observed. In the case of protected timber construction, approximately 15% of the burning took place outside the compartment whereas the proportion of external burning was approximately 50% for the unprotected construction.

4.5.2 *Frangi and Fontana 2005*

Frangi and Fontana reported on full-scale tests on wooden modular hotels under natural fire conditions conducted in Switzerland [154]. In addition to a shorter time to flashover (compared to tests with noncombustible linings), they also clearly observed the influence of combustible linings after flashover. For the module with combustible wall and ceiling linings, the external burning outside the window was much more severe than for the modules with noncombustible wall and ceiling linings. This observation was consistent with the experiment conducted by Hakkarainen [153]. From Equation 2.2 it can be estimated that the minimum fuel surface area for ventilation controlled combustion is approximately 54 m^2 and this can be provided by the enclosure wall surfaces alone. Given the burning is expected to be ventilation controlled then external flaming is also likely. However for other fuel-controlled cases such as in enclosures with a much larger window area relative to the floor area, it may still be possible for external flames to be observed that are result of flame extension through the opening.

4.5.3 *Frangi et al. 2008*

Frangi et al. [155] presented results from a natural full-scale fire test of a three-storey CLT (XLam) timber building conducted at the Building Research Institute in Tsukuba, Japan. The building had a foot-print of about 7 m $\times$ 7 m and a height of about 10 m. The main building structure comprised 85 mm thick panels. The CLT walls were protected by either one or two layers of 12.5 mm thick gypsum plasterboard over 27 mm thick mineral wool. Both standard and fire grades of gypsum plasterboard were used. The CLT ceiling was protected

with 27 mm thick mineral wool and 12.5 mm thick fire grade gypsum plasterboards and unspecified fixings. The fire load was estimated to be 780 MJ/m^2.

Flashover occurred after about 40 minutes. After 55 minutes the fire intensity declined and the fire was manually extinguished after 60 minutes. During the last 10 minutes it was observed that the gypsum plasterboards partially fell off. After the fire test it was observed that the gypsum plasterboards in the fire room had completely fallen off confirming the visual observations during the fire test and the temperatures measured in the wall and floor assemblies [155]. The test did show that it was possible to prevent fire spread from the room of origin with no elevated temperatures or smoke recorded in the enclosure above the fire room.

4.5.4 *McGregor 2013*

Full-scale fire experiments on compartments constructed with CLT include those in Canada reported by McGregor [156]. These included CLT enclosures with fully protected with gypsum plasterboard and fully exposed timber surfaces. The fuel load represented a bedroom fire with estimated fire load energy density (FLED) of 366 MJ/m^2. In all cases, the peak temperatures inside the compartment were similar and were what might be expected in a ventilation-controlled fire for the given compartment geometry. However, the peak heat release rate resulting from internal and external burning to the compartment varied. In the experiment with the fully exposed CLT, debonding of CLT lamellae occurred, which allowed newly exposed timber to burn, contributing additional fuel and energy to the fire and preventing flaming extinction. In this thesis, where the term debonding is used, it is assumed to be accompanied by the char falling away and virgin timber being freshly exposed to the fire. This is discussed further in Section 4.6.

4.5.5 *Medina Hevia 2014*

Medina Hevia [157] continued the research of McGregor, by conducting further experiments with partial coverage (one and two walls) of exposed CLT. Both series of experiments were the subject of publications by Li et al. [158, 159]. It was also found that flaming extinction only occurred in the experiment where just one wall was unprotected and where debonding was not observed.

4.5.6 *Su and Lougheed 2014*

In a series of four full-scale apartment fire experiments conducted to evaluate the performance of encapsulation for protecting combustible

structural elements, one experiment included 3-ply 105 mm thick CLT construction protected with 2 layers of 12.7 mm thick Type X gypsum board. The experiment represented a three-storey section of a building bounded on four sides (three internal walls and an exterior wall) within the lower storeys of a mid-rise (e.g. six-storey) building [160]. Peak gas temperatures reached were in the range 1100-1200°C. The Type X gypsum board encapsulation system performed very well in the CLT experiment. The gypsum plasterboard stayed in place on most surface areas until the end of the test (180 min). The peak heat release rate (HRR) was 8.4 MW [161].

4.5.7 *Hox and Baker 2015*

Hox and Baker [162, 163] reported on an enclosure experiment on a student bedsit apartment in Norway constructed with 100 mm thick CLT. The fire compartment was a real-size mock-up of the apartment with internal dimensions 5.75 m × 2.3 m × 2.75 m high, with an open door leading to an open corridor outside. The typical fire load from the furniture was calculated to be 660 MJ/m^2. The ceiling in the fire room collapsed at 96 min with a reasonably constant plateau in the gas temperature of approximately 1000°C up until that time.

4.5.8 *Janssens 2015*

Janssens [164] reported two tests carried out at the Southwest Research Institute in Texas for the American Wood Council to evaluate the performance of CLT and NLT construction protected with two layers of 16 mm thick Type X gypsum board. The fire represented a severe living room fire in a compartment that measured 4.11 m × 3.6 m × 2.38 m high with a 1.87 m wide × 2.07 m high opening. The walls were 175 mm thick CLT and the ceiling 140 mm deep NLT. The ceiling was loaded with concrete blocks (1.9 kN/m^2). The fuel load in the room was living room furniture with an estimated fire load density of 570 MJ/m^2. After about 3 hours the enclosure was completely burned out and the experiment terminated. The measured peak HRR was 5.5 MW (the actual HRR may have been slightly higher since the exhaust system was not able to collect all the combustion gases during the peak burning period). The protected CLT and NLT did not exceed 100°C during or after the experiment. The maximum gas temperature measured was 1245°C. A second similar enclosure was constructed, measuring 4.46 m × 3.25 m × 2.38 m with the same opening but with a CLT ceiling. The fire load density was 601 MJ/m^2. This experiment was terminated after 2 hr 15 min. The peak HRR was 4.9 MW. Again, the protected CLT did not reach 100°C with a maximum gas temperature of 1222°C in the enclosure. These experiments demonstrated the effectiveness of 2 layers of 16 mm thick Type X gyp-

sum plasterboard in preventing any charring of the protected CLT or NLT elements. However, there was some superficial charring at one or two locations near the floor, where the wall was exposed for a long time to the heat from a pile of smouldering residue of cellulosic fuel.

4.5.9 *Hadden et al. 2017*

Hadden et al. [165] conducted compartment experiments as part of investigations into the extinction behaviour of CLT. These experiments are described more fully in Section 4.8. They found that autoextinction was achieved in the compartment with two surfaces of exposed CLT, but this depended on the char layer remaining attached i.e. no debonding of the CLT lamellae. Autoextinction was not observed for compartments with three exposed CLT surfaces.

On the topic of combustible linings, Hadden et al. [165] noted that in previous experiments by Butcher et al. [166] in compartments with fibre insulation board linings, higher temperatures were reached more quickly than when burning cribs of the same fire load in compartments with inert linings. Hadden et al. [165] suggest that the large surface area of fuel and the fixed ventilation conditions resulted in production of pyrolysis gases at a rate greater than could be oxidised by the air inflow to the compartment. They also suggested that correlations such as Equation 2.1 may not hold for compartments with significant areas of exposed combustible material.

4.5.10 *Emberley et al. 2017*

Emberley et al. [167] conducted a full-scale fire test on a compartment constructed from CLT. The internal faces of the compartment were lined with non-combustible board, with the exception of one wall and the ceiling where the CLT was exposed directly to the fire inside the compartment. Extinction of the fire occurred without intervention. This is consistent with the findings of Hadden et al. [165]. Wood cribs were used as the fuel and self-extinction of the exposed CLT followed soon after the decay of the cribs. They also conducted a small-scale study to establish the range of incident heat fluxes for which autoextinction of the CLT could occur. The small-scale tests showed that the critical heat flux for (flaming) auto-extinction of Radiata pine CLT is 45 kW/m^2.

4.5.11 *Su et al. 2017*

Su et al. [168] at the National Research Council in Canada conducted a series of six large CLT compartment experiments as part of a Fire Protection Research Foundation (FPRF) research program with the goal of quantifying the contribution of CLT building elements (wall

and/or floor-ceiling assemblies) in compartment fires. The compartments were 9.1 m long × 4.6 m wide × 2.7 m high constructed using 175-mm thick 5-ply CLT structural panels with testing carried out in the NIST Fire Research Laboratory. The CLT panels were manufactured using 100 x 50 mm spruce-pine-fir lumber glued with a polyurethane structural adhesive (with a brand name of HBE1) compliant with the ANSI/APA PRG 320 manufacturing standard in effect at that time. Two sizes of opening were investigated and various combinations of exposed and protected CLT.

These experiments are described more fully in Section 6.4 with the data used in the benchmarking of the pyrolysis submodels described in Section 5.5.

4.5.12 *Janssens 2017*

Following the FPRF experiments, Janssens [169] conducted three enclosure fire experiments with exposed CLT ceiling panels manufactured using different adhesives with protected walls. This was part of an investigation to develop a fire test method for assessing the performance of different CLT adhesives (see Section 4.7). The ceiling panel was loaded with concrete blocks during the testing (0.96 kN/m^2). The interior dimensions of the test enclosures were 9 ft (2.74 m) × 19 ft (5.79 m) × 8 ft (2.44 m) high and with an opening 36 in (0.91 m) wide × 75 in (1.91 m) high. The test series used a propane gas burner to duplicate the heat flux measured in the test 1-1 in the FPRF test series [168].

The tests included:

- Test 1: E1 grade SPF lumber and a polyurethane adhesive
- Test 2: V1 grade Douglas fir lumber with an melamine formaldehyde resin
- Test 3: V1 grade Douglas fir lumber with an improved polyurethane adhesive

Test durations were in the range 3 to 4 hours. Debonding occurred in the first test accompanied by fire regrowth in the room. No debonding was observed in Tests 2 and 3 with lower temperatures and heat fluxes measured compared to Test 1. The data obtained in these tests confirmed the validity of the room test procedure for qualifying CLT adhesives, which was incorporated in the 2018 edition of the PRG 320 standard [170].

4.5.13 *Su et al. 2018 (NRC)*

Following development of the proposed screening test method for CLT adhesives and the associated compartment experiments by Janssens

[169], Su et al. [171] conducted a further series of experiments on CLT manufactured using a thermally resistive adhesive that met the new proposed evaluation procedures of ANSI/APA PRG-320 [170]. The experiments included two with glulam beams and columns. While debonding of CLT lamellae did not occur, meaning the construction burned more like solid wood, there was still some contribution to the fire development from the CLT in places where the CLT charred behind failing gypsum board protection.

These experiments were carried out at the National Research Council in Canada and are described more fully in Section 6.5. They are also used in benchmarking the pyrolysis submodels also described in Section 6.5.

4.5.14 *Zelinka et al. 2018*

Most recently, Zelinka et al. [172, 173] conducted a series of large experiments in CLT (5-ply 175 mm thick Douglas Fir - Larch) enclosures at the Forest Products Laboratory (FPL). There were five enclosure experiments of 2-floor specimens intended to be apartment-style structures with two 9.1 × 9.1 × 2.7 m high rooms. There were also corridors on both levels. The first three experiments had two unglazed window openings (3.66 m wide × 2.44 m high). The last two experiments with fire sprinklers had glazed windows. One experiment had automatic sprinkler activation and one had delayed sprinkler activation. Varying amounts of exposed mass timber ranging from full protection using gypsum plasterboard to no protection were investigated in the experiments.

This dataset is rather unique being both multi-room and multi-level with oxygen calorimetry. The peak HRR measured for the three unsprinklered experiments were in the approximate range 19 - 24 MW. The peak HRR for the experiment with delayed sprinkler activation was 5.7 MW and the peak HRR was reported as negligible for the automatic sprinkler activation. These experiments were not part of the benchmarking for the pyrolysis submodels described in Chapter 6 but would be a very useful dataset for comparison with model predictions at some future time.

4.6 DEBONDING (DELAMINATION) OF CLT LAMELLAE

Bartlett et al. [174, 175] defined delamination as a phenomenon in which the fire-exposed lamella(e), or part(s) thereof, detach from the main mass of timber. They observed that debonding occurred not by entire lamellae falling off at once, but rather by small pieces of charred timber, generally 2 to 5 cm in length, detaching from the lamella beneath. This was also observed by Aguanno for CLT floor panels in standard fire resistance tests [176]. In the literature, the

term delamination and debonding are both used to describe this phenomenon.

Frangi et al. [177] had also conducted fire resistance tests and observed fall off of the charred layers was followed by an increased charring rate and occurred at times consistent with the estimated position of the 300°C isotherm (i.e. the nominal char depth). They also concluded that CLT with thicker layers showed better fire behaviour compared to that with thinner layers. Klippel et al. reports that ceilings are more prone to delamination than exposed walls [178, 179]. Hadden et al. [165] agreed with this with the reasoning that the char on the ceiling falls earlier than char on the walls (under the action of gravity).

Emberley et al. [180] reviewed the research into debonding existing at that time and expressed considerable concern that the understanding of debonding was not sufficient and its implications not adequately recognised by designers. They emphasised the need for further research.

Bartlett conducted experiments to investigate the debonding process in CLT [181] using two different apparatus. A modified BS476-7 apparatus was used to study CLT specimens 220 mm thick with seven lamellae of various thickness bonded with a polyurethane adhesive. A radiant panel was also used to subject CLT samples to a constant heat flux of 100 kW/m^2 with charring rates determined using data from embedded thermocouples. These samples were 100 mm thick with three lamellae bonded with a melamine formaldehyde adhesive. They observed debonding for both parallel and perpendicular lamellae. In the latter experiments they observed some debonding when the temperature at the glue line was only 90-125°C. Following debonding rapid increases in charring rate of up to 2 mm/min were observed.

As part of an investigation to develop a full-scale enclosure test for evaluating adhesives in CLT, Janssens [169] reported that the temperatures measured within a CLT ceiling at the first glue line when debonding was observed were consistent with a polyurethane adhesive failure temperature of 200-220°C.

Barber [4] identified possible solutions to limit the onset of early debonding such as specifying thicker outer layers for the CLT or by using improved adhesives. Hoehler et al. [182] also concluded there was a need to use better heat-resistant adhesives following the series of FPRF CLT compartment experiments.

4.7 INFLUENCE OF ADHESIVE TYPE

Klippel provides a brief history of the use of adhesives in engineered wood structures reporting that originally casein adhesives were used [183]. This was replaced in the 1940's by phenolic-formaldehyde ad-

hesives and then, to improve the bond strength and reduce the hardening temperature, resorcinol was added giving (phenolic)-resorcinol-formaldehyde adhesives (RF/PRF). These had excellent structural performance and were resistant to elevated temperatures. Less expensive melamine-(urea)-formaldehyde (MF/MUF) adhesives were then introduced followed by polyurethane adhesives in about 1985 [183]. In recent times one-component polyurethane (PU) adhesives for engineered wood products have become very popular for various reasons including: no mixing, easy handling; fast bonding at room temperature; reduced coating weight; no solvents, formaldehyde or volatile organic compounds; invisible bondlines and long shelf life [184]. However, they do not perform as well in fire and fail at modest temperatures. Clauß et al. [184–186] revealed there were strong decreases in tensile shear strength at temperatures between 180-200°C. The shear strength versus temperatures of the different adhesives (including PUR, MF, PRF, MUF, EPI, PVAc and UF) investigated in their study is shown in Figure 4.10 along with the shear strength of Beech timber.

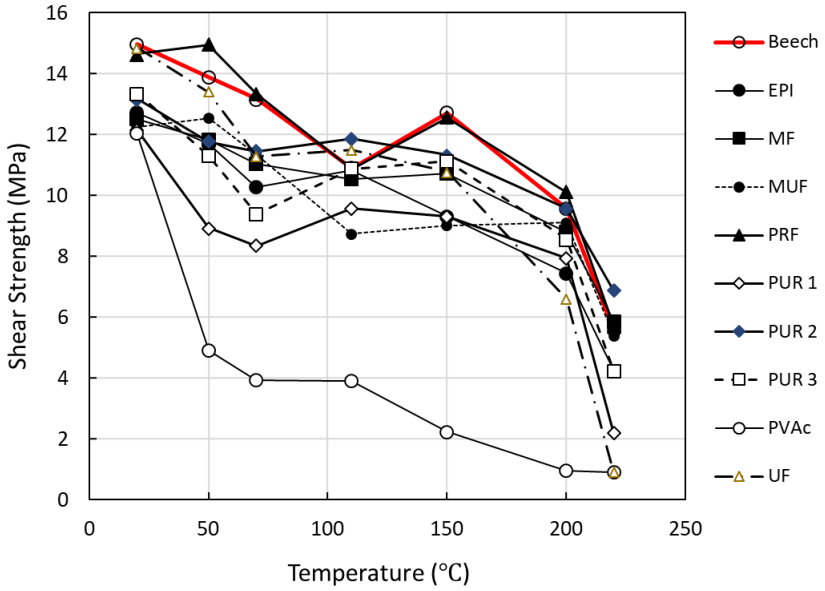

Figure 4.10: Shear strength of different adhesives compared with solid Beech wood according to EN 302-1 versus temperature. Data from Clauß et al. [185].

Klippel [183] reported that the thermal stability of adhesives had been investigated by various researchers in experiments at constant elevated temperatures. He noted that in these tests, the strength reduction with increasing temperature followed a similar trend with most of the adhesives providing sufficient strength up to 200°C.

Frangi et al. [177, 187] conducted small-scale tests following standard fire resistance procedures and showed that the fire behaviour of CLT depended on the performance of the adhesive used for bonding the timber panels. They commented that the thermal behaviour

of one component PU adhesives can vary a great deal by modifying their chemical structure. They cautioned that test results based on one particular polyurethane adhesive may not be valid for other PU adhesives. They included five different PU adhesives and one melamine urea formaldehyde (MUF) adhesive in their test programme and found that for the specimens manufactured with less temperature-sensitive adhesives the charred layers almost remained in place until the end of the fire test [177]. Further it is now seen that some formulations of PU adhesive recently developed are more thermally resistive and were successfully used to avoid debonding in full-scale enclosure experiments carried out by Su et al. [171].

Craft et al. [188, 189] reported there was considerable variability in the elevated temperature performance of different adhesives as shown by a variety of test methods including the results from an elevated temperature adhesive tension test which they proposed. In their results, they found phenol-resorcinol formaldehyde (PRF) and melamine formaldehyde (MF) adhesives did not fail without considerable wood damage whereas polyurethane and PVA samples failed accompanied by little or no wood failure. Their test results for these latter adhesives are shown in Figure 4.11. All their tests were carried out at an oven temperature of 220°C and since wood failure was typically not observed within the two hour exposure, they argued that it was an appropriate oven temperature to be used for the evaluation.

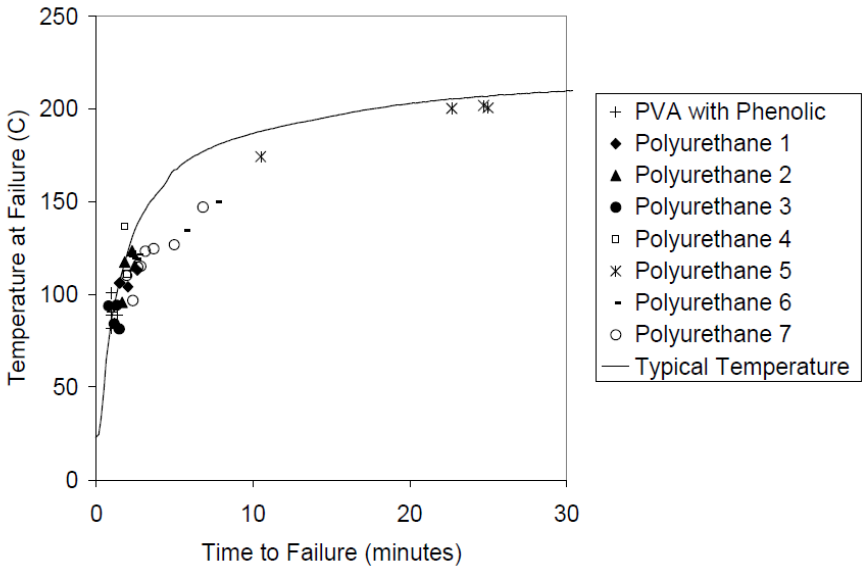

Figure 4.11: Results of elevated temperature tension tests showing point of failure for eight different adhesives. Reprinted from Craft et al. [189] with permission.

Bartlett [181] observed delamination for both formaldehyde and polyurethane based adhesives, however could draw no conclusions regarding the underlying physical/controlling mechanisms.

Aguanno [176] conducted standard fire resistance tests on CLT floor-ceiling panels and found that adhesive failure and ply falloff occurred once the temperature at the back of the ply increased to around 200°C. He observed that lamellae would not fall off as a single layer all at once, but instead broke away in small pieces at first, on the order of a few cm which gradually increased in size as more pieces fell. He reported that this process took several minutes for each layer.

Note that in Eurocode 5 [146] the following is stated - *"For bonding of wood to wood, wood to wood-based materials or wood-based materials to wood-based materials, adhesives of phenol-formaldehyde and aminoplastic type 1 adhesive according to EN 301 may be used. For plywood and LVL, adhesives according to EN 314 may be used."* EN 301 [190] is a standard for classifying phenolic and aminoplastic adhesives (i.e. including MUF and PRF adhesives) for load-bearing timber structures. The classification is for moisture and temperature resistance with Type I adhesives being permitted for full outdoor exposure and for use in temperatures above 50°C [191]. One-component polyurethane adhesives (PU) are covered by EN 15425 [192] which includes a table indicating their adhesive type rating for moisture and temperature resistance [191]. EN 15416 [193] provides a series of different test methods for adhesives for load bearing timber structures other than phenolic and aminoplastic. The temperature resistance in all these standards is in relation to the ambient environment rather than fire temperatures.

Janssens [169] developed a full-scale fire test method for assessing the performance of CLT adhesives and evaluated the performance of three ceiling panels using three different adhesives. The interior dimensions of the room were 2.85 × 5.79 × 2.44 m with an opening of 0.91 m wide × 1.9 m high. A propane gas burner provided the source fire exposure. The three CLT ceiling panels were: E1 grade SPF lumber and polyurethane adhesive (the same as used in the FPRF experiments); V1 grade Douglas fir lumber and melamine formaldehyde resin; and V1 grade Douglas fir lumber and an improved polyurethane adhesive. E1 and V1 are stress grades of CLT panels according to the PRG320 standard – referring to machine grading (E) and visual grading (V) respectively. For the first panel, debonding and fire regrowth in the room was observed with the debonding reported as being consistent with a failure temperature of 200 - 220°C. No debonding with lower temperatures and heat fluxes were recorded for the latter two tests [169].

ANSI/APA PRG-320 [170] specifies requirements for lamination and adhesive materials (referring to existing adhesive standards), as well as methods of testing and quality assurance. It does not include NLT or CLT products manufactured without adhesive face bonds [194]. Following the Janssens investigation, Annex B of the 2018 version of ANSI/APA PRG-320 was developed. This involves full-scale

room fire testing to ensure that the CLT does not exhibit fire regrowth when subjected to an exposure similar to the FPRF test 1-4 (compartment test 1-4 [168]; See also Config L in Table 6.1). It also includes a vertical load on the ceiling panel of 25% of the allowable stress design (ASD) reference flatwise bending moment of the CLT. The unprotected panel is required to sustain the load for a period of 240 minutes without char layer falloff resulting in a significant temperature increase during the cooling phase of the fully developed fire.

Independently, Brandon and Dagenais [195] conducted a series of intermediate-scale furnace ($1 \times 1 \times 1$ m^3) experiments that successfully simulated the fire exposure and oxygen content of the FPRF compartment test 1-4 [168] with CLT specimens made with five different types of structural adhesive - two one-component polyurethanes (PU1 and PU2); one melamine formaldehyde (MF); one emulsion polymer isocyanate (EPI) and one phenol resorcinol formaldehyde (PRF). Their aim was to assess whether and when delamination would have occurred in the full scale compartment test 1-4 if the given adhesive had been used instead. Brandon and Dagenais recommended their smaller intermediate scale furnace test as an alternative to the full scale testing method described in Annex B of the 2018 version of ANSI/APA PRG-320.

Brandon and Dagenais [195] also assessed whether a small-scale heat performance test would be a suitable and economical method to differentiate delaminating adhesives from non-delaminating adhesives used for face bonding CLT elements, however did not draw strong conclusions regarding the correspondence between the two tests and recommended further research.

Earnshaw et al. [196] in the context of discussing a new adhesive standard for load-bearing timber products in New Zealand expressed concern about the fire performance of newer structural timber adhesives used in load-bearing structures in the event that the char layer integrity is compromised by adhesive failure. They argued that the base requirement for a structural adhesive is that it should maintain its integrity at least as long as the wood it joins.

In New Zealand AS/NZS 4364:2010 [197] gives requirements for bond performance of adhesives formed in structural finger-jointed timber and glulam products. For serviceability purposes it includes a creep resistance test (Method A) subjecting a sample to min 70°C for a period of seven days. There are no specific fire-related requirements. Where engineered wood products are required to achieve a fire resistance rating then standard fire resistance testing e.g [141] will be required but this does not preclude debonding and does not provide useful information regarding the effect of debonding on the fire dynamics in real enclosure fires.

In summary, heat debonding in fire due to failure of the adhesive bondline in engineered timber structures can be avoided by selecting

a suitable adhesive. Currently, these could be identified with the furnace test proposed by Brandon and Dagenais [195] or by using the test described in Annex B of the 2018 version of ANSI/APA PRG 320 [170]. There is a current need to further investigate the fire performance of adhesives used in engineered timber structures sourced from within New Zealand.

A prediction submodel for occurrence of debonding of lamella in mass timber panels and its effect on enclosure fire dynamics is developed and described later in Section 5.8.

4.8 AUTO-EXTINCTION OF BURNING TIMBER

Emberley et al. [198] pose the question - *"if a compartment fire consumes all the furnishings' fuel, does exposed structural timber continue to burn?"* It is important to be able to answer this question because if the timber does continue to burn the outcome may be unacceptable and lead to a need to encapsulate the exposed timber with a protective board. On the other hand, if the answer is no, then the timber can be left exposed enhancing the architectural and sustainability features of the building. In either case the maximum depth of char may still need to be known in order to evaluate the structural adequacy and fire resistance of the element.

Solid timber will not burn unless an external heat flux is applied since the flame heat flux is not sufficient to sustain its own burning [42]. Therefore it is necessary to understand more precisely the conditions under which extinction will occur.

Crielaard [199, 200] investigated the self-extinguishment of CLT and identified the three stages of combustion of CLT as flaming combustion, smouldering combustion and self-extinguishment. In this thesis the term auto-extinction (and flaming and smouldering extinction where appropriate) is used instead. Crielaard concluded that smouldering extinction of CLT occurs when the externally applied heat flux falls below 5 to 6 kW/m^2. He also noted that the transition from smouldering combustion to auto-extinction depended on the airflow across the timber.

Recent CLT compartment experiments with various configurations of surfaces exposed have also been conducted by Hadden et al. [165]. They observed auto-extinction in a compartment with two surfaces of exposed timber. However, they also repeated an experiment (see Section 6.3.2) for the same configuration and did not observe auto-extinction. Auto-extinction was also not observed in the remaining two experiments. Auto-extinction depended on the char layer remaining attached, i.e. debonding did not occur for the full duration of the fire (including decay).

Bartlett et al. [201] conducted a series of small scale tests in a Fire Propagation Apparatus (FPA) to investigate the conditions for flam-

ing extinction to occur. They determined a critical mass loss rate at extinction of 3.5 g/m^{2}s or a temperature gradient of 28 K/mm at the charline. External heat flux and airflow did not affect the critical mass loss rate at the range they investigated.

Emberley et al. [167, 202] carried out small-scale and full-scale fire tests on a compartment with exposed CLT on the walls and ceiling. Based on small-scale results using a cone heater, they concluded the critical heat flux for the flaming self-extinction of Radiata Pine CLT to be 45 ± 1 kW/m^2 with a corresponding mass loss rate of 3.7 ± 0.2 g/m^{2}s which was similar to Bartlett [201]. Their results also showed that the critical mass loss rate was dependent upon the timber species but did not show a clear dependency with the timber density [202]. The full-scale compartment geometry had internal dimensions of $3.5 \times 3.5 \times 2.7$ m where they also observed self-extinction of the CLT wall and ceiling in the full-scale experiment when the maximum incident heat flux reduced below 45 kW/m^2. Emberley et al. urge caution in the direct application of their results, pointing out that any debonding, or failure of construction detailing leading to a secondary fire on the opposite side of the panel, could prevent auto-extinction. Comparing Crielaard's [200] and Emberley et al.'s [167] results indicates that the minimum heat flux for smouldering combustion is significantly lower than the minimum heat flux for flaming combustion [201].

Bateman et al. [203] conducted a series of five reduced-scale compartment fire experiments and determined that sustained burning was dependent on both the configuration of exposed faces and, to a lesser extent, the imposed fuel load. They observed auto-extinction when the mass loss rate dropped below 3 g/(m^{2}s). This is lower but comparable to that recorded by Bartlett et al. [201] and Emberley et al. [167].

In this thesis, the term smouldering extinction is used as the criterion for auto-extinction. The premise is that flaming extinction may not be sufficient because the timber could reignite with an increased in air flow across the surface, or it could continue to undergo smouldering combustion and degrade even in the absence of flame. If the timber were to continue to degrade during the decay phase while the gas temperatures are declining there is a risk that the extent of charring could reach a critical depth for structural failure.

4.9 INFLUENCE OF OXYGEN CONTENT AND AIRFLOW

Craft et al. [204] carried out medium-scale fire-resistance tests on three-ply CLT panels following the standard CAN/ULC S101 test method to investigate the charring rate of the panels with and without gypsum protection. They made the significant observation that if the CLT panel fails to prevent the flow of air through the panel, it

is quite likely the fire resistance will be governed by integrity failure as opposed to structural failure. A flow of air through small gaps between boards lining up in the panel, which in this case was driven by a lower pressure in the furnace, leads to oxidation of the char layer on the hot exposed surface and loss of the char in the vicinity of the gap.

Schmid et al. [205] conducted experiments investigating charring in CLT beams using a gas-fired furnace and varying the oxygen concentration and gas velocity. They showed that glowing combustion influences the char layer at oxygen concentrations above about 15% leading to char contraction while oxygen concentration of 10 and 5% gave no significant effect. The effect became more significant when the gas velocity was increased. They questioned many fire resistance tests simulating entire fires, where the ventilation conditions (oxygen content, gas velocity) in the cooling phase were not controlled nor documented. They suggested there was a limit for significant glowing combustion between 10 and 15% and this was in line with another study of calorimetric experiments by Jervis where the critical oxygen limit was found to be 14 % [206]. Further study of char oxidation and contraction in the decay phase of the fire is required and may be important for performance-based design considering real fire exposures. Following Schmid et al. [205] findings, Brandon and Dagenais [195] chose to allow the oxygen content in their intermediate-scale furnace experiments simulating the fire exposure and oxygen content of FPRF compartment test 1-4 to be in the range 0 to 5%.

Brandon et al. [207] successfully replicated the extent of charring in the FPRF test 1-4 enclosure fire [168] in a furnace by controlling both the temperature using a plate thermometer and the oxygen concentration in the exhaust, so that it resembled the conditions measured in the full-scale compartment test. They emphasise that it is not sufficient to control only the temperature or heat flux to match the compartment experiment but matching the oxygen levels is also required. Standard fire resistance tests typically have lower than ambient oxygen levels. For example, Collier [208] measured the furnace oxygen concentration during a standard fire resistance test of a light timber-frame wall lined with gypsum plasterboard using the BRANZ furnace and found that the oxygen concentration initially dropped to about 6% as the temperature rapidly increased but then settled in a band 10-12% as the temperature became more steady after about 30 minutes. During the fully developed period in real enclosure fires the oxygen concentration could be less than 6%. However, for the decay phase in an enclosure fire, the oxygen levels could be higher than 10-12% leading to char oxidation and flaming at the combustible surface and therefore a higher charring rate could be expected. It is also acknowledged that oxygen concentrations could vary between different furnaces depending on their design. Radiant panel appa-

ratus e.g. [209] have previously been used to expose specimens to a heat flux simulating a compartment fire but since these would be conducted under ambient oxygen levels in the case of timber specimens they may overestimate the charring rate for the same imposed heat flux time history compared to either a furnace environment or the ventilation-controlled period of a real enclosure fire but they could be helpful in studying the decay phase.

These findings also infer that the common application of the time-equivalent formula from the Eurocode relating fire severity in a standard fire resistance test with fire severity in a compartment fire is likely to be nonconservative when applied to combustible specimens like CLT, even if the additional fuel contributed by the specimen has been accounted for. This is because the charring rate in the decay stage of the fire with elevated oxygen levels may be higher than some equivalent time in the furnace with reduced oxygen levels.

4.10 TIMBER PROTECTION (ENCAPSULATION)

The main method of limiting the amount of timber exposed to fire is to encapsulate it with protective boards such as gypsum plasterboard. However, depending on the specification and detailing of the protection, it may either prevent the timber from contributing to the fire or it may just delay the involvement of timber. While protective boards may be used to contribute to the fire resistance of timber structures, in the current context the purpose is to prevent the timber burning and contributing to the fire severity.

Moser and Spearpoint conducted small-scale experiments using four types of non combustible board (including gypsum plasterboard and MgO board) to determine their ability to delay onset of charring when used to protect CLT [210]. At a constant irradiance of 50 kW/m^2, the greatest delay was 26.5 min achieved by a 13 mm thick fire-rated gypsum plasterboard. However, performance in real fires will also depend on a range of factors including the thermal exposure and heating rate, the durability, number and thickness of the board and how it is fixed to the underlying CLT.

Su and Lougheed [160] investigated encapsulation systems for mid-rise wood buildings. Three materials were evaluated as encapsulation for combustible structural elements: Type X gypsum board, cement board and gypsum-concrete. Bench-scale, intermediate-scale and full-scale fire tests were conducted to investigate the performance of the encapsulation materials. Criteria for evaluating the performance of the encapsulation systems were proposed based on the temperature reached at the interface between the timber and the encapsulation material. It is important to note that the time the encapsulation could protect the timber beneath is dependent on the fire exposure. In real fire situations, this can vary greatly, and the more severe the fire ex-

posure, the shorter the time that the encapsulation protects the underlying timber may be.

Brandon [211] established that in the FPRF test series, the exposed gypsum layer from the ceiling was observed to fall-off when the temperature behind the exposed gypsum board was between 300 and 500°C. He suggests that a temperature of 300°C on the unexposed side of the exposed gypsum layer could be used as a criterion for the failure/fall-off of the gypsum board protection. Brandon [211] also said that this fall-off criterion is conservative compared to the results of fire resistance tests summarized by Just [212] which comprised an extensive database of results in which none of the temperatures measured behind the exposed gypsum board was below 300°C at the time the protection failed. In the most recent report from Brandon [6] strategies including procedures for predicting gypsum board fall off are presented.

4.11 FIRE SAFETY ENGINEERING METHODS

The fire risk computer model CU-RISK was developed at Carleton University with the main objective of facilitating the evaluation of fire safety designs for four-story timber-frame commercial buildings [213]. Zhang et al. [214] modified the CU-RISK fire risk analysis model (which includes a two-zone model) to include timber surfaces considering the growth, full development and decay periods of a compartment fire. In this model, simple assumptions were made for both the mass loss rate of the burning contents and the combustible structure. The decay phase was assumed to start when the remaining FLED reduces below some specified value. Model predictions were compared with four full-scale experiments and were reported to be in good agreement. Two of these were CLT construction and are included in the benchmarking discussed later in Chapter 6.

Barber [4] described a two-step engineering methodology principally based on simple calculation using analytical equations that generally followed an example given by Crielaard [199] for determining auto-extinction of CLT. Firstly, a critical lamella thickness for avoiding debonding or layer fall-off is determined based on a calculated char depth in the real fire condition. The charring rate, assuming a parametric fire exposure from Eurocode 1 Part 1-2 [78], is calculated following the guidance in Eurocode 5 (EN 1995 Part 1-1) [146]. Given the depth of char determined, the additional fuel load due to the charred CLT is added to the FLED assumed in the calculation of the parametric fire. This requires iteration to ensure that the depth of char calculated and the FLED assumed are consistent. Secondly, to check for smouldering-extinction of CLT, a calculation of the incident radiant heat flux on the timber surface is done, and if this is below

a critical value proposed by Crielaard, smouldering-extinction of the timber is assumed.

Brandon [211] summarized engineering methods for predicting the structural damage of CLT members and falloff of gypsum plasterboard with design fires which are dependent on the design of the compartment and the contribution of CLT to the fuel load. He proposed an engineering method based on the parametric fire equations in conjunction with an iterative procedure to estimate the char depth adjusting the fuel density at each iteration. This model presented by Brandon [211] is not equipped to consider the effects of delamination or fall-off of the base layer and the limitations of the parametric fire equations apply.

A similar iterative procedure was demonstrated by Salminen and Hietaniemi [215] for the performance-based fire design of a 14-storey residential mass timber building in Finland with up to 25% of the apartment walls and or ceiling left unprotected.

Brandon also developed a one-zone model with wood combustion for CLT called SP-Timfire [216]. This model calculated the heat release rate of the CLT by assuming a linear relationship with charring depth of 5.39 MJ/m^2 per mm of char depth. As discussed later in Section 5.3.2, this value had been determined experimentally by Schmid et al [217] and for wood density of 515 kg/m^3 it can be converted to an effective heat of combustion of 10.5 MJ/kg. Brandon's model was used iteratively with the heat conduction calculations done using the finite element program SAFIR [218]. Thermal properties for wood from König and Walleij [219] were adopted. Delamination was said to be simulated by removing the exposed lamella from the model when temperatures in the bond line reached a specified temperature.

Hopkin et al. [220] subsequently presented a zone model for appraising exposed or partially exposed timber structures subject to fire using effective thermal properties. This tracked the 300°C isotherm through bounding surfaces, estimating a mass loss rate and exposed surface contribution to the heat release rate of the enclosure fire. They found the approach yielded acceptable results when compared with fire experiments involving partially or fully exposed CLT structures and where debonding was not observed.

Barber et al. [101] also presented a methodology where the pyrolysis functionality within FDS was used to determine the response of a mass timber structure. Pyrolysis model inputs were based on previous research by Wang et al. [221]. The method was validated against the results from five full-size compartment fire tests [168] with exposed cross laminated timber. They showed the modelling to predict char depths within 20% based on a fully developed fire. However CLT char fall-off (debonding) was not captured; nor any gypsum board fall off and charring of CLT behind the gypsum board. Barber et al. [101] also acknowledged that the computational time required

to undertake pyrolysis modelling using FDS was extensive, and the simulation run times may be considered too long to be used as a viable design tool. Most recently, Brandon [6] presented strategies for the fire design of mass timber buildings involving analytical methods using parametric fires.

The calculation model described in the next chapter uses a two-zone fire model solving mass and energy conservation equations over the full fire duration. The modified model includes both the dynamic contribution of timber surfaces (without iteration) via two different pyrolysis submodels for the wood combustion and the contents fuel load during the fire and includes the calculation of char depth over time. A separate submodel for the effect of debonding of lamellae is also included.

5

FIRE DYNAMICS MODEL FOR MASS TIMBER ENCLOSURES

5.1 GENERAL

The two-zone model B-RISK is used considering both pre-flashover and post-flashover fire behaviour. The model is described more fully elsewhere [37] with an overview previously given in Chapter 3 with some further key characteristics and modifications noted here.

Conservation of mass and energy leads to a set of first-order differential equations which allow the upper layer volume, upper and lower layer temperatures, and the pressure equation to be solved. The form of the equations is as given by Peacock et al. [222].

The mass flow of air and hot gases through the compartment wall opening is driven by buoyancy. Bernoulli's equation is used to calculate the mass flows generally following subroutines developed by Cooper and Forney [223, 224]. A near vent mixing correlation developed by Utiskul [225] has been applied where the incoming cold air behaves like a jet entering the vent with a characteristic velocity and diffusing downward because of buoyancy.

The strong plume model of Heskestad as described by ISO 16734 [226] for the buoyant plume is used for entrainment in the far field. For fully developed post-flashover fires where the entrainment height is small due to the layer height being close to the floor, the buoyant plume model is not appropriate (i.e. for near field entrainment). In this case the McCaffrey correlation for the flaming region is used [227]. When the fire is ventilation-limited, the oxygen-constrained heat release rate is used in the plume correlation instead of the well-ventilated free-burning heat release rate. This produces a plume flow that is in balance with the oxygen inflow through the openings (i.e. the mass flow of oxygen in the plume matches the mass flow of oxygen entering the compartment). Under these conditions, the energy balance for the upper layer control volume is not particularly sensitive to the total plume entrainment but is instead driven by the oxygen entering the compartment much like a one-zone well-stirred reactor. Further analysis and supporting evidence for this is included in Appendix A.

The model includes a four-wall radiation exchange algorithm following the method described by Forney [228]. This allows the ceiling, upper wall, lower wall and floor to transfer radiation independently between the different surfaces taking into account the absorption or blocking and emission of radiation by the gas-soot mixture. Radiant

heating of these surfaces by the flames is also considered by treating the fire as a point source. The emission of radiation by soot particles and absorption by carbon dioxide and water vapour for both layers is included and used as energy source terms in the ordinary differential equations of the zone model. The fraction of energy passing through a soot-air mixture depends on the absorption coefficient of the soot and the path length through the gas. The absorption coefficient is approximated using the average extinction coefficient for the layer based on the concentration of soot in the gas layer. The soot yield is fuel-dependent and in the present study a value of 0.015 g/g for well ventilated flaming combustion of wood was used [229]. This yield is modified during the simulation based on the global equivalence ratio using a correlation developed by Tewarson et al. [230]. The radiation exchange sub model determines the net radiant heat flux emitted or absorbed by each room surface. These radiant fluxes are combined with the convective heat flux and used as the boundary condition for the surface heat conduction calculations.

5.2 HEAT CONDUCTION MODEL

An implicit one-dimensional, finite-difference scheme is used to calculate heat conduction through the ceiling, walls and floor of the compartment. This allows the temperature at any internal node to be calculated by solving a set of simultaneous equations for the unknown nodal temperatures at each time step. Under transient conditions with constant properties and no internal generation the appropriate form of the heat equation for a one-dimensional system is [231]:

$$\frac{1}{b}\frac{\partial T}{\partial t} = \frac{\partial^2 T}{\partial x^2} \tag{5.1}$$

The finite difference approximation of the time derivative can be expressed by equation 5.2 with the m subscript denoting the x location of the nodal points and the superscript p used to denote the time dependence such that the time derivative is stated in terms of the difference in temperatures associated with the new $(p+1)$ and previous p times [231].

$$\left.\frac{\partial T}{\partial t}\right|_m \approx \frac{T_m^{p+1} - T_m^p}{\delta t} \tag{5.2}$$

The temperature at each node is calculated by solving a set of simultaneous equations for the unknown nodal temperatures at each time step [231]. The implicit method has the advantage of being unconditionally stable and therefore allows a larger time step to be used in the

calculations compared to using an explicit method. The implicit form of the one-dimensional finite-difference scheme for a surface node is given by Incropera and deWitt [231] as:

$$(1+2Fo)T_1^{p+1} - 2FoT_2^{p+1} = \frac{2Fo\ Bi\dot{q}''_{int}}{h} + T_1^p \tag{5.3}$$

Where $\dot{q}''_{int}$ is the incident heat flux to the exposed surface and the Fourier and Biot numbers are given by:

$$Fo = \frac{b\Delta t}{(\Delta x)^2} \text{ with } b = \frac{k}{\rho c_p} \tag{5.4}$$

$$Bi = \frac{h\Delta x}{k} \tag{5.5}$$

In B-RISK, the interior convection coefficient (h) used in the convective heat transfer calculations between the gas layer and the room surface are by default calculated following the method described by Peacock et al. [115] assuming natural convection, however for the simulations presented in this thesis a constant convection coefficient of 35 W/m^2K has been used as specified in Eurocode 1 [117] for simple fire models. A sensitivity analysis (see Appendix B) comparing the predicted gas temperatures using both assumptions reveals only a very small difference thus either assumption would be acceptable for the types of fires and enclosures considered in this thesis.

The implicit form for an interior node is given as:

$$-FoT_{m-1}^{p+1} + (1+2Fo)T_m^{p+1} - FoT_{m+1}^{p+1} = T_m^p \tag{5.6}$$

Writing an equation for each node gives n equations which must be solved simultaneously for each timestep. This is done using the matrix inversion method by expressing the equations in the form [A][T]=[C], where:

$$[A] = \begin{bmatrix} 1+2Fo & -2Fo & 0 & 0 & \cdots & 0 \\ -Fo & 1+2Fo & -Fo & 0 & \cdots & 0 \\ 0 & -Fo & 1+2Fo & -Fo & \cdots & 0 \\ \vdots & \vdots & \ddots & \cdots & \cdots & \vdots \\ 0 & \cdots & \cdots & 0 & -2Fo & 1+2Fo \end{bmatrix} \tag{5.7}$$

$$[C] = \begin{bmatrix} 2FoBi_{int}\dot{q}''_{int}/h + T_1^p \\ T_2^p \\ T_3^p \\ \vdots \\ 2FoBi_{ext}(T_{ext} - T_n^p) + T_n^p \end{bmatrix} \tag{5.8}$$

While the simplest form of the heat conduction equation is shown here with constant properties and no internal generation as assumed in the existing B-RISK model, for the calculations for wood pyrolysis discussed later in this chapter temperature-dependent properties have been introduced. However, constant properties have been assumed for the non-participating surfaces including the floor and plasterboard protected surfaces which should ideally be corrected in future work.

A limitation of the one-dimensional analysis is that it does not account for any cracking that occurs in the char (see Figure 5.1) which increases the relative importance of radiative heat transfer through the char pores and reduces the importance of in-depth conduction into the solid [135]. This potentially compromises the assumptions described in this section, and remains an area of possible further research.

Figure 5.1: Photo of typical cracking that occurs in the charred surface of a LVL specimen subjected to radiant heat.

5.3 THERMOPHYSICAL AND RELATED PROPERTIES OF WOOD AND CHAR

Thermophysical and related properties of wood and char for use in the pyrolysis submodels are presented in this section. Different properties for the wood and char are used.

5.3.1 *Char yield*

Tran and White [232] define the char yield Y_c where m_c is the mass of residue including char, $m_{w,res}$ is the mass of residue without the char and m_{init} is the original mass of the sample.

$$Y_c = \frac{m_c - m_{w,res}}{m_{init} - m_{w,res}} \tag{5.9}$$

They also define a char contraction factor f_c related to char yield, and the densities of wood and char through the following equation.

$$f_c = Y_c \frac{\rho_w}{\rho_c} \tag{5.10}$$

Their measured properties for wood species which included redwood, southern pine, red oak and basswood found contraction factors in the range 0.4 to 0.83, and char yields in the range 0.20 to 0.31 with char densities from 156 to 360 kg/m^3. Tran [233] states that for most wood samples the residual char is about 20% of the original mass. Ragland and Aerts [139] also give a mass fraction of 0.20 for char from dry wood. White reported that a higher lignin content in the wood results in a greater char yield [137].

Janssens provides data for the percentage of wood pyrolysed as a function of density based on an extensive collection of Cone Calorimeter data [234]. He determined the regression equation shown in Equation 5.11 with $R^2 = 0.49$. In general, there was large scatter in the data so that the regression equation obtained may have a large uncertainty attached.

$$\%P = 81.8 - 0.0208(\rho_{w,dry} - 600) \tag{5.11}$$

If the mass of residual ash is ignored then the char yield could be estimated as a function of the oven dried density as shown in Equation 5.12.

$$Y_c = 0.182 + 0.000208(\rho_{w,dry} - 600) \tag{5.12}$$

Spearpoint and Quintiere [235] estimated char fraction by direct measurement following testing of several wood species, making judgement on the final height, char depth and volume shrinkage of the sample. They produced a plot of the measured char fraction against dimensionless irradiance (β) as shown in Figure 5.2 and with β given by Equation 5.13.

$$\beta \equiv \frac{\sigma(T_s^4 - T_o^4) + h_c(T_s - T_o)}{q_i''} \tag{5.13}$$

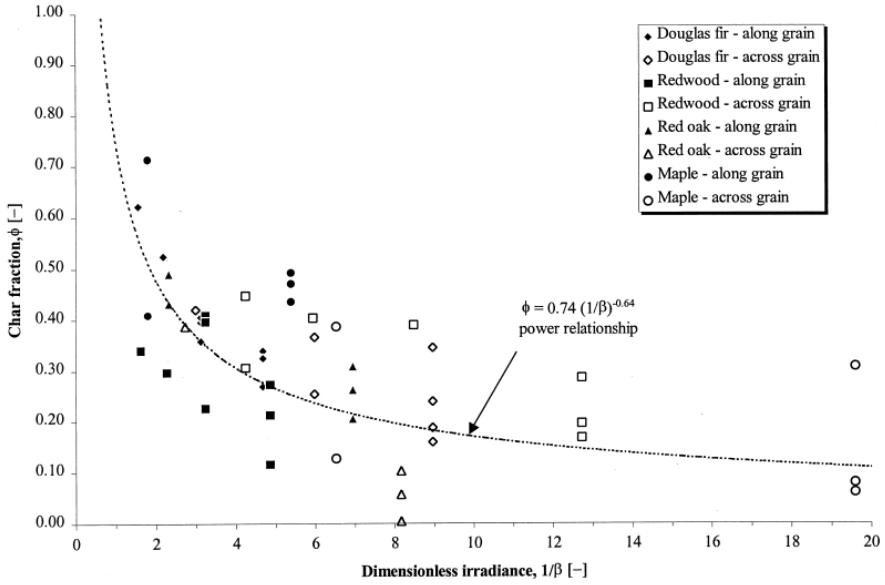

Figure 5.2: Char fraction against dimensionless irradiance. Reprinted from Spearpoint and Quintiere [235] with permission from Elsevier.

Char yield is an input to the kinetic wood pyrolysis model described in Section 5.7 and a typical value for wood of 0.25 is used in simulations presented later in Chapter 6. This is in the range reported by Tran and White [232] and Spearpoint and Quintiere [235].

5.3.2 *Heat of combustion of wood*

Gross heat of combustion values are measured in a bomb calorimeter resulting in typical values of around 20 MJ/m^2 for oven dry wood [233] for complete combustion of the wood and char. The actual heat of combustion observed in real fires is not the gross value. Spearpoint and Quintiere [236] discuss the heat of combustion of wood where the main constituent of wood char is carbon and the net heat of combustion for a carbon and oxygen to carbon dioxide reaction is 32 MJ/kg. Given that the average net heat of combustion of wood for a complete reaction is 17 MJ/kg and assuming a typical char yield for dry wood of 1/3 by mass allows the mean heat of combustion of the wood volatiles during the flaming stage ($\Delta H_{c,fl}$) to be solved.

$$1/3(32) + 2/3(\Delta H_{c,fl}) = 17 \tag{5.14}$$

This gives a value of 10 MJ/kg for the heat of combustion of the wood volatiles during the flaming stage. Spearpoint and Quintiere [236] concluded that only about 60% of the energy of wood is released during the flaming stage of combustion. Using the same methodology with assumed char yields of 0.25 and 0.20 give 12 MJ/kg and 13.3

MJ/kg for the respective values of heat of combustion of the wood volatiles during the flaming stage.

For an irradiance of 50 kW/m^2, Tran [233] measured the effective heat of combustion for a range of wood products to be in the range 12.8 to 13.5 MJ/kg on an actual basis and in the range 14.0 to 15.1 MJ/kg on a dry basis. The effective heat of combustion of wood depends on the wood species and the heat flux. Tran derived the following correlations for the average effective heat of combustion for different wood species for a range of heat fluxes from 20 to 50 kW/m^2 in the OSU apparatus [233].

$$\Delta H_{c,dry} = 0.057\dot{q}''_{ext} + 11.88 \tag{5.15}$$

$$\Delta H_{c,actual} = 0.068\dot{q}''_{ext} + 9.95 \tag{5.16}$$

The net heat of combustion of the wood volatiles is reported as being slightly higher for lignin (14.7 MJ/kg) compared to cellulose (13.8 MJ/kg) and even lower values for some hemicelluloses of Douglas fir [132].

Janssens provides data for the effective heat of combustion of wood as a function of density based on an extensive collection of Cone Calorimeter data [234]. He determined the regression equation shown in Equation 5.17 with $R^2 = 0.43$.

$$\Delta H_{c,dry} = 11.9 - 0.0048(\rho_{w,dry} - 600) \tag{5.17}$$

Brandon's one-zone model [216] calculated the heat release rate of CLT by assuming a linear relationship with charring depth of 5.39 MJ/m^2 per mm of char depth. This had been previously determined experimentally by Schmid et al. [217] from cone calorimeter experiments at an incident flux of 75 kW/m^2 and for char depths > 10 mm. Another way of interpreting this value is to convert it to an effective heat of combustion by dividing by the density of wood. For a density of 515 kg/m^3, the effective heat of combustion would be 10.5 MJ/kg. This is very close to Spearpoint and Quintiere [236] estimate of the energy released during the flaming stage of combustion.

Eurocode 5 [146] specifies a constant heat of combustion for wood of 17.5 MJ/kg but with an assumed combustion efficiency of 0.8, giving an effective heat of combustion value of 14 MJ/kg. This value has generally been used in all subsequent analysis presented in the following chapters. The sensitivity of the kinetic model results to the assumed effective heat of combustion value is discussed in Section 5.7.4.

5.3.3 *Density*

The density of oven-dry wood depends on species and is typically in the range 320 to 720 kg/m^3 [237]. Virgin wood density of 515 kg/m^3 [238] has been used for calculations in this thesis (see Table 6.2) being typical of the CLT used in many of the full-scale experiments described in Chapter 6. A range of values for the density of char is found in the literature. For example, Shi et al. [239] determined the density of carbonized wood for six wood species having very different initial characteristics and found whatever their initial characteristics were (such as oven dry density, dimension of the growth rings) the density of carbonized wood could be deduced from the initial oven dry density by the simple relationship in Equation 5.18. The correlation of their data is shown in Figure 5.3. It is noted that the measured density of the carbonised wood shown in Figure 5.3 is derived from dimensional measurements that includes the char contraction.

$$\rho_c = 0.63\rho_{w,dry} \tag{5.18}$$

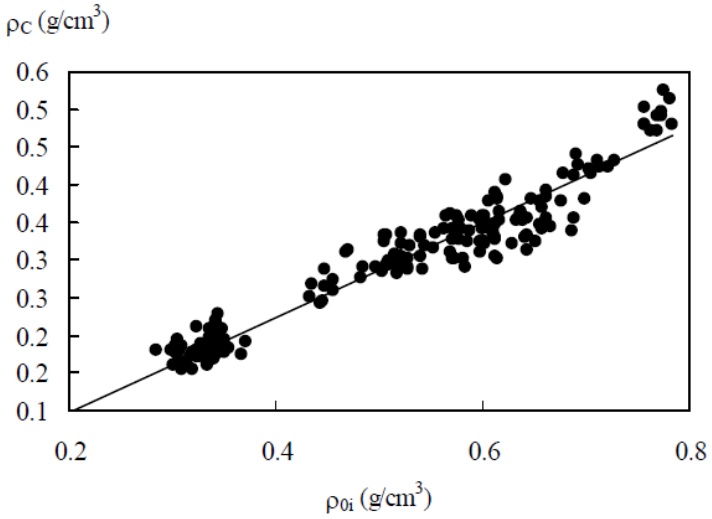

Figure 5.3: Variation of the density of carbonized wood as a function of the initial oven dry density. Reprinted from Shi et al. [239] with permission requested.

Given a wood density value ρ_w at ambient with moisture content u and ignoring any expansion term, the oven dry density can be given by Equation 5.19 [132] and the char density given by Equation 5.20.

$$\rho_{w,dry} = \frac{\rho_w}{(1+u)} \tag{5.19}$$

$$\rho_c = \frac{0.63\rho_w}{(1+u)} \tag{5.20}$$

Beall also correlated char density at 600°C as a function of ρ_o [240] as given in Equation 5.21.

$$\rho_{c,600} = 0.75\rho_w - 63 \tag{5.21}$$

Wang et al. [241] used 150 kg/m^3 for the density of char saying it was based on 26% of the density of the original wood consistent with the bulk density estimated from cone calorimeter experiments but she also gives the residue yield from TGA experiments on wood as 13%. Spearpoint and Quintiere [235] use 200 kg/m^3 for density of char. The value for char density assumed for simulations conducted as part of this thesis is determined as summarised later in Table 5.1.

5.3.4 *Thermal conductivity*

Thermal conductivity of wood generally increases with temperature, moisture content and density. Wood is also anisotropic and thermal conductivity along the grain may be 1.5 to 2.8 times the conductivity across the grain [242].

Hankalin et al. [243] proposed the temperature dependent thermal conductivity values in Equation 5.22 to Equation 5.24 for a pyrolysing wood particle where thermal conductivity at ambient temperature is given as the average of the longitudinal and radial directions so may be higher than actually applicable for this application. Although Hankalin indicated Equation 5.24 applied up to 923 K, it has been used for higher temperatures (up to 1200°C) in this study. Furthermore, the thermal conductivity of 'char' is treated as being non-reversible such that the maximum temperature reached is used for any subsequent determination of thermal conductivity. Any wood that has reached a minimum temperature of 300°C is considered to be 'char'.

$$k = 0.285 \text{ for } T \leqslant 473 \text{ K} \tag{5.22}$$

$$k = -0.617 + 0.0038T - 4 \times 10^{-6}T^2 \text{ for } 473 < T \leqslant 663 \text{ K} \tag{5.23}$$

$$k = 4.429 \times 10^{-2} + 1.477 \times 10^{-4}T \text{ for } 663 < T \leqslant 923 \text{ K} \tag{5.24}$$

In Eurocode 5 [146] the thermal conductivity values of the char layer are stated to be apparent values rather than measured values, in order to take into account increased heat transfer due to shrinkage cracks above about 500°C and the erosion of the char layer at about 1000°C. They were intended for use with the heating regime in the standard fire resistance test. These properties were included in a

study by König and Walleij [219]. Figure 5.4 show both the Eurocode 5 and Hankalin's equations for thermal conductivity as a function of temperature.

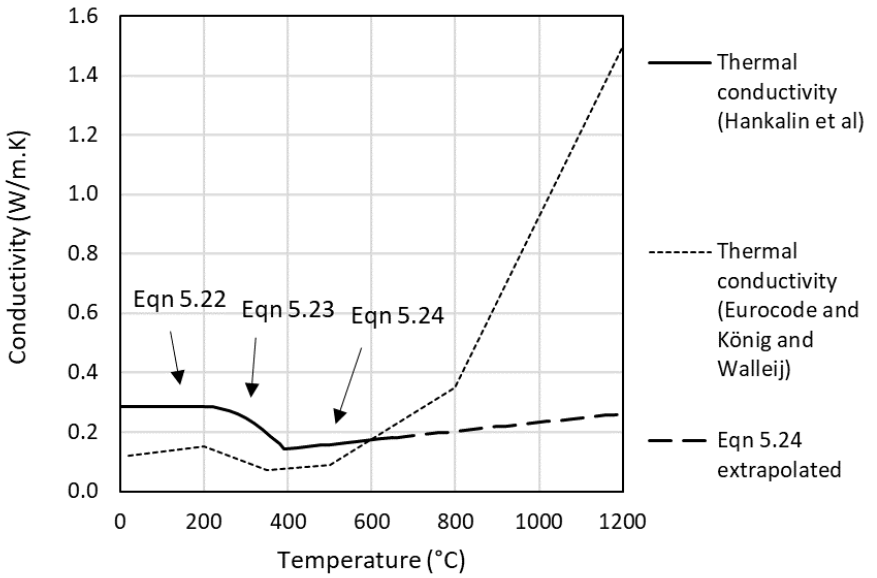

Figure 5.4: Thermal conductivity of wood and char as a function of temperature.

Hopkin [244] investigated how the conductivity properties of the char layer influence the depth of char in parametric fires. He proposed a conductivity model for softwood exposed to natural fires and modified the model given in Annex A of Eurocode 5 [146] that assumed standard ISO 834 fire exposure. Hopkin et al. [245] presented a framework for how 'effective' thermal properties of timber can be extended to incorporate parametric fires through consideration of heating rates and fire load densities and negating the need for complex mass and heat transfer models. Through calibration of an effective conductivity of the char layer against the parametric charring method contained in Annex A of EN 1995-1-2, they were able to establish a relationship between the heating rate and the effective conductivity of the char layer, in the heating phase of parametric fires. His modified conductivity model was shown to be applicable to a range of densities and moisture contents of timber and also variations in heating rate and fire load density [245].

5.3.5 *Specific heat*

Specific heat depends on temperature and moisture content but not on density or species [139]. The specific heat of dry wood in J/kg.K is given by Tenwolde et al. [242] in Equation 5.25.

$$c_{p,w,dry} = 103.1 + 3.867T \tag{5.25}$$

The specific heat of wood at a given moisture content is given by Janssens and Douglas [132] in Equation 5.26.

$$c_{p,w,u} = \frac{c_{p,w,dry} + 4187u}{1+u} + (23.55(T-273) - 1326u + 2417)u \tag{5.26}$$

Janssens and Douglas [132] give the specific heat for wood char in Equation 5.27 with temperature units K, also shown in Figure 5.5 with temperature units in °C.

$$c_c = 714 + 2.3(T-273) - 8\times10^{-4}(T-273)^2 - 3.7\times10^{-7}(T-273)^3 \tag{5.27}$$

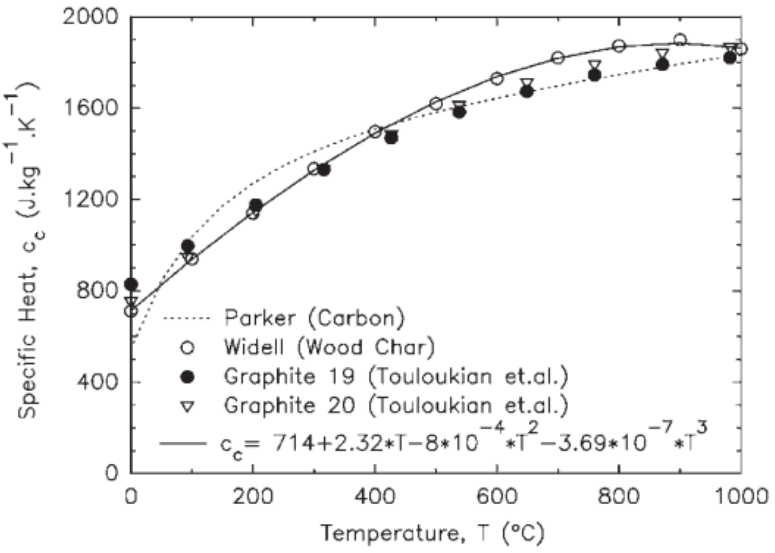

Figure 5.5: Specific heat of char as a function of temperature. Reprinted from Janssens and Douglas [132] with permission.

Equation 5.25, Equation 5.26 and Equation 5.27 are shown in Figure 5.6. They do not include any latent heat effect. In contrast, the specific heat from Eurocode 5 [146] in Figure 5.7 shows the latent heat effect included separately over the narrow temperature range 99 to 120°C.

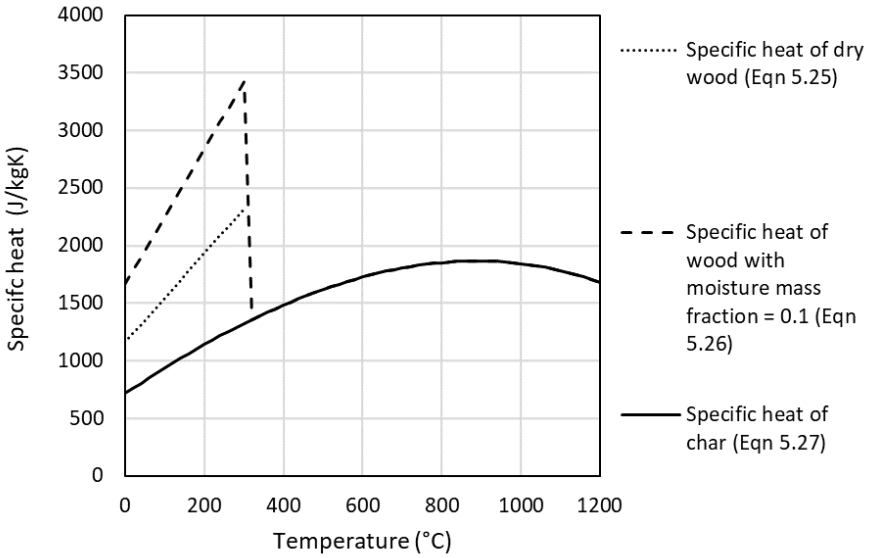

Figure 5.6: Specific heat of wood as a function of temperature.

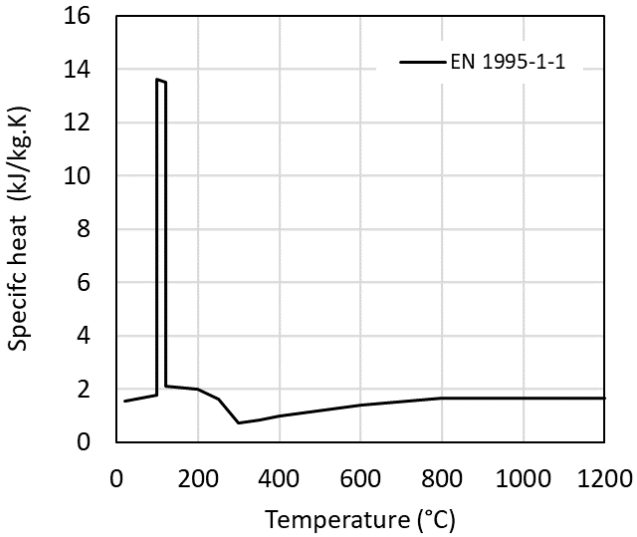

Figure 5.7: Specific heat of wood and char as a function of temperature as given in EN 1995-1-1 [146].

5.3.6 *Summary*

Later in this Chapter, two wood pyrolysis models called SMA (Section 5.5) and SMC (Section 5.7) for determining the contribution of the burning mass timber surfaces to the enclosure fire are described in detail. A summary of the assumptions associated with density, thermal conductivity and specific heat of wood and/or char used in these wood pyrolysis submodels is given in Table 5.1.

Property	Submodel SMA	Submodel SMC
Char yield	n/a	0.25
Density	Finite elements are designated 'char' or 'wood' based on the maximum temp reached. If maximum temp is $\geqslant$ 300°C then Equation 5.20 for char density is used otherwise the ambient density for the wood is used.	An apparent density of each finite element is calculated based on the mass fraction of water, cellulose, hemicellulose, lignin and char as described later in Equation 5.47.
Thermal conductivity	If maximum temp reached by finite element is $\geqslant$ 300°C then Equation 5.22 to Equation 5.24 are used with that maximum temp. A sensitivity analysis for thermal conductivity supporting the use of these equations is discussed later in Section 6.5.3.	
Specific heat	If maximum temp reached by finite element is $\geqslant$ 300°C then Equation 5.27 is used for the specific heat of char, otherwise Equation 5.26 is used.	
Effective heat of combustion	14 MJ/kg	

Table 5.1: Summary of thermophysical property assumptions for wood pyrolysis submodels.

5.4 PYROLYSIS OF THE MOVEABLE FIRE LOAD

During the initial growth period, before flashover and while the fire is well ventilated, the heat release and other characteristics supplied by the user for the item first ignited are used, with the mass loss rate given by:

$$\dot{m}_f = \frac{\dot{Q}}{\Delta H_c} \tag{5.28}$$

Since the early growth rate of the fire was not a focus for this thesis, in this chapter, for convenience, the initial fire growth rate is represented as $\dot{Q} = \alpha t^2$ where the α coefficient has been selected to provide a reasonable match for the experiments under consideration. Following flashover a switch to a fully developed regime occurs where the moveable fuel load is then represented as equivalent wood cribs. Flashover is not a precise term and criteria are usually based on the temperature at which the radiation from the hot gases in the compartment will readily ignite the combustible contents. Gas temperatures of 500–600°C are widely used [46] as a criterion. The flashover criterion used for the simulations described in this paper is an average upper layer of 500°C. The fully-developed regime determines the fuel mass loss rate $\dot{m}_f$ (kg/s) for two cases; a fuel surface

area-controlled mass loss rate, and a ventilation-controlled mass loss rate. For the case of actual wood cribs being the fuel source a third case of porosity-control is also included.

The fuel surface area-controlled mass loss rate is given by Equation 5.29 representing crib fires (see Figure 5.8) where D (m) is a characteristic fuel or stick thickness, v_p (m/s) is a surface regression rate - for wood taken as $0.0000022D^{-0.6}$, m (kg) is the mass of fuel remaining and m_{init} (kg) is the original mass of fuel (determined using the specified floor area and fuel load energy per unit floor area) [246]. This equation assumes cribs are ignited instantaneously.

$$\dot{m}_f = \frac{4}{D} m_{init} v_p \sqrt{\frac{m}{m_{init}}} \tag{5.29}$$

The mass loss rate for crib porosity-controlled burning is given by Equation 5.30 where S is the stick spacing and H_c is the crib height.

$$\dot{m}_f = 4.4 \times 10^{-4} \frac{S}{H_c} \frac{m_{init}}{D} \tag{5.30}$$

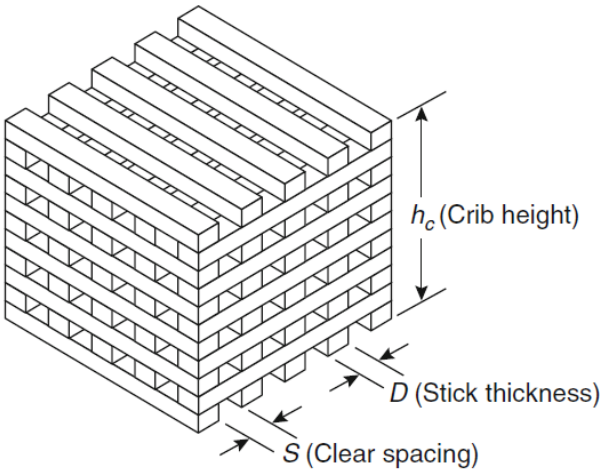

Figure 5.8: General arrangement of a wood crib. Reprinted from Babrauskas [246] with permission from Springer Nature.

The mass loss rate for ventilation-controlled burning is given by Equation 5.31 where $13100\dot{m}_p Y_{O_2,l}$ is the maximum rate of heat release (kW) that can be supported by the oxygen in the plume flow and ΔH_c (kJ/kg) is the heat of combustion of the fuel. The constant (13100) in Equation 5.31 is the oxygen calorimetry constant representing the energy released per unit mass of oxygen consumed (in kJ/kg) and is applicable to a wide range of common fuels [246, 247]. Assuming the oxygen flow in the plume represents the total available oxygen for combustion is a more generally applied method for a two-zone model compared to calculating the oxygen inflow through a

single opening from the outside and can also be used where there are multiple openings or where other rooms are connected to the room of fire origin.

$$\dot{m}_b = \frac{13100\dot{m}_p Y_{O_2,l}}{\Delta H_c} \tag{5.31}$$

This mass loss rate corresponds to that able to burn inside the room given the available oxygen and is not necessarily the total mass loss rate. After flashover, the governing mass loss rate is the lesser of the fuel-controlled, porosity-controlled and ventilation-controlled rates. For the ventilation controlled case, the mass loss rate is then multiplied by Ω where Ω is a user-defined input. In B-RISK, Ω can be expressed as the ratio between the total mass loss rate and the burning rate inside the room as given by Equation 5.32. This also corresponds to the global equivalence ratio as defined by Pitts [248].

$$\Omega = \frac{\dot{m}_{f,tot}}{\dot{m}_b} = \frac{\Delta H_c \dot{m}_{f,tot}}{13100\dot{m}_p Y_{O_2,l}} \tag{5.32}$$

This means the user is effectively specifying the global equivalence ratio (GER) as it determines the proportion of gasified fuel burning inside and outside the room. $\Omega = 1$ corresponds to all the fuel generated burning within the room to match the available oxygen (i.e. stoichiometry), and $\Omega = 1.3$ has been used as a default value for wood cribs in a non-combustible or protected-timber compartment. It has been observed experimentally that wood cribs do not burn more than 30 to 40% fuel rich, with Babrauskas reporting an upper limit of approximately 37% fuel rich ($\Omega = 1.37$) [246]. Since enclosure effects on the mass loss rate of the cribs is not included here, this approach gives the user more control over the burning regime and can be used to provide a closer match to experimental observations. This user input (Ω) to the post-flashover fire model will be referred to as GER or GE in this thesis.

B-RISK keeps track of the total amount of fuel consumed during the simulation and when all the fuel is consumed (based on the user supplied input for the FLED and the floor area) the mass loss rate becomes zero. An illustration of the general form of the design fire is shown in Figure 5.9.

5.5 WOOD PYROLYSIS SUBMODEL A (EQUIVALENCE RATIO MODEL)

5.5.1 *Wood surface burning rate model SMA*

This submodel estimates the depth of char based on a 300°C isotherm [146] below the surface of the timber lining as a function of time

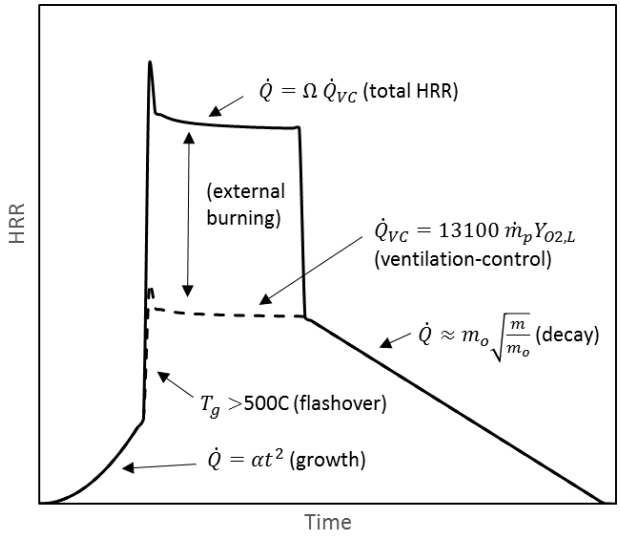

Figure 5.9: Conceptual design fire. Reprinted from Wade et al. [28] with permission from Springer Nature.

based on one-dimensional heat conduction calculations of the bounding surfaces. The mass of charred material is determined based on the predicted change in the isotherm position over the previous timestep and expressed as an equivalent FLED and added to the fuel load for the contents of the room. B-RISK provides a calculation of the 300°C isotherm for each of the four surfaces (ceiling, floor, upper wall, lower wall). Char depths are determined for only two surfaces here – the ceiling using the 300°C isotherm data for the ceiling and the wall surfaces using 300 °C isotherm data for the portion of the wall height predicted by the model to be in the hot upper layer. It is assumed char depth determined for the ceiling applies uniformly across the entire ceiling, and in the case of the wall, applies uniformly to all the wall surfaces. This is likely to be conservative, however in the future, the char depth in both the upper wall and lower wall could be separately determined if required. The floor surface has also been ignored but could also be included in future.

The volume V of timber contributed to the fire from the ceiling and walls is given by Equation 5.33 Equation 5.34 and Equation 5.35 where d_c is char depth (m), W, L and H are the room width, length and height (all in m) respectively. The proportion of 'exposed timber' for the ceiling and walls is α_c and α_w respectively. The equivalent FLED (MJ/m^2) is given by equation 5.36 where ρ_w is the density of wood (kg/m^3). $FLED_{w,tot}$ is added to the contents fuel load energy density per unit floor area and updated at each time step as the char depth increases with time.

$$V_{w,wall} = d_{c,wall}\, \alpha_w \left[2\,(W + L)\, H\right] \tag{5.33}$$

$$V_{w,ceil} = d_{c,ceil} a_c WL \tag{5.34}$$

$$V_{w,tot} = V_{w,ceil} + V_{w,wall} \tag{5.35}$$

$$FLED_{w,tot} = \frac{V_{w,tot} \Delta H_c \rho_w}{LW} \tag{5.36}$$

When calculating the surface area of contributing surfaces, the area of any openings present is also included (i.e. not subtracted from the total wall surface area). The area of openings can be accounted for indirectly by choosing an appropriate value for k_w ie as a fraction of the total surface area including the openings. This method also assumes no in-depth burning i.e. the material is inert with the char depth determined only from the position of the 300°C [167] isotherm generated by the thermal environment within the room.

A flow chart illustrating the coupling of moveable fire load and the contribution of the mass timber when the GER submodel SMA is used is shown in Figure 5.10.

5.5.2 *Sensitivity to excess fuel factor*

The result of an example calculation showing the effect that the GE ratio has on the predicted enclosure gas temperature when using pyrolysis submodel SMA is presented here. The enclosure fire experiment designated as Config. P in the benchmarking discussed later in Section 6.5.3) is used here. The enclosure in this experiment had dimensions 4.5 × 2.4 × 2.7 m high with an opening 0.76 m × 2.0 m high. 33% of the wall and 10% of the ceiling were exposed CLT and the fuel load was 360 kg of wood cribs.

Simulations using submodel SMA with GE ratios of 1.0, 1.3 and 2.0 have been run and the predicted gas temperatures are shown in Figure 5.11. Measured gas temperatures from the experiment are also shown in Figure 5.11.

For this experiment, a GE ratio of 2 (i.e. equal burning inside and outside the opening) provides the best agreement for the peak gas temperature and the time to reach the peak gas temperature. This GE ratio is consistent with the findings previously observed by Hakkarainen [153]. Lower GE ratio increases the fire duration by burning more fuel inside the room with GE 1.0 corresponding to the case where the burning rate corresponds to stoichiometric combustion such that all the mass is burned inside the room (over a longer period) with no external burning. GE 1.0 therefore provides the most conservative prediction of the fire severity within the enclosure, although may not be conservative when considering external fire spread vertically above the opening or horizontally to adjacent property.

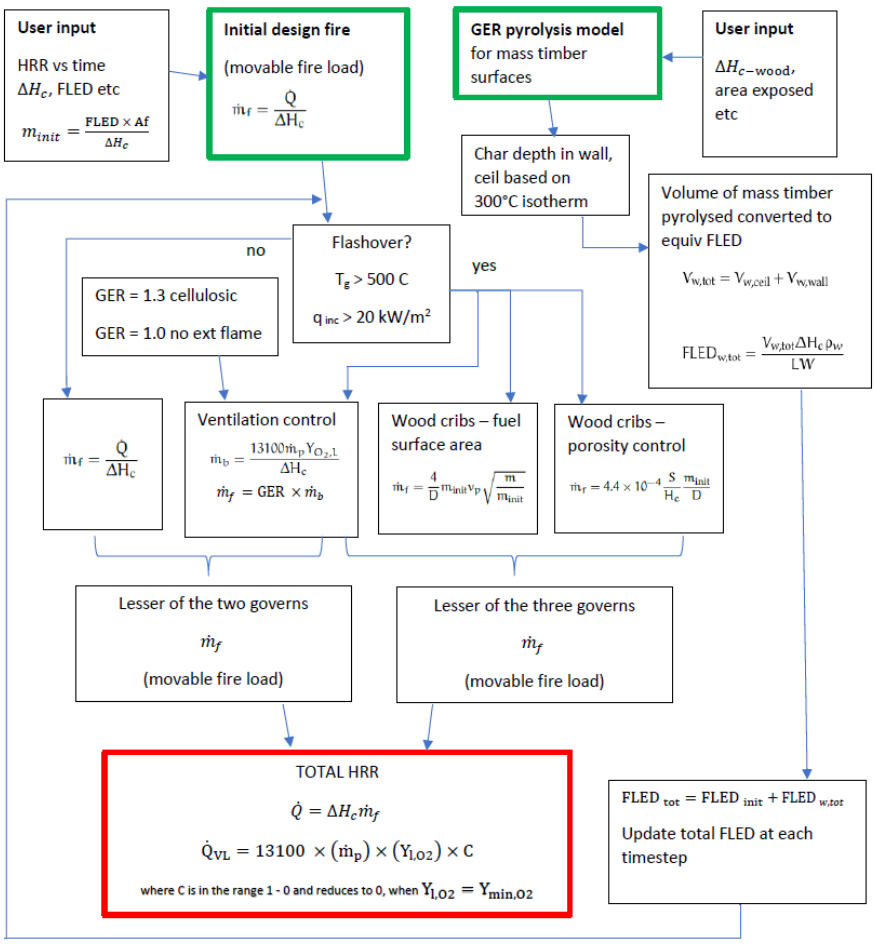

Figure 5.10: Flow chart for the moveable fire load coupled with the GER submodel SMA for mass timber.

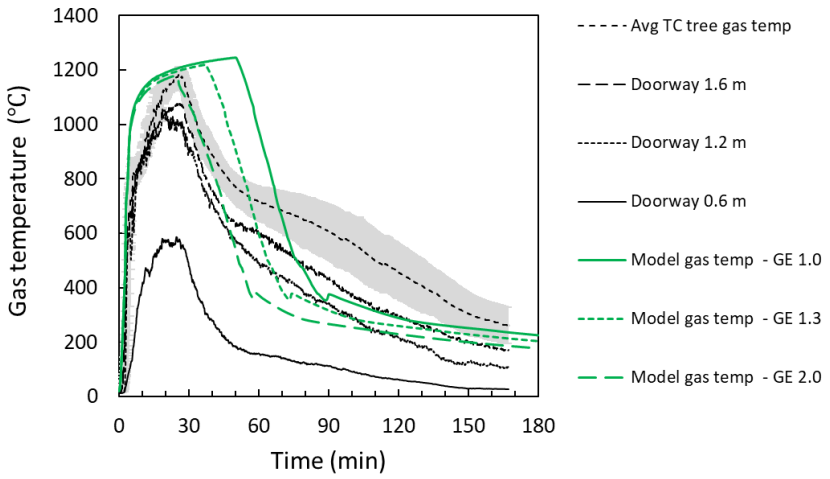

Figure 5.11: Measured and predicted enclosure gas temperatures for Config. P using using SMA pyrolysis submodel with GE factors of 1.0, 1.3 and 2.0.

5.6 WOOD PYROLYSIS SUBMODEL B (INTEGRAL MODEL)

The one-dimensional integral model described by Spearpoint and Quintiere [235, 236] for the transient pyrolysis of a semi-infinite charring solid exposed to a constant radiant heat flux was investigated and subsequently trialled within B-RISK. A limited number of simulations were made with variable results. Due to limited time, no conclusions were drawn and the submodel was not included in the benchmarking cases discussed later. However, further investigation and evaluation of this submodel could be considered at some time in the future.

5.7 WOOD PYROLYSIS SUBMODEL C (KINETIC MODEL)

5.7.1 *Wood surface burning rate submodel SMC*

In this wood pyrolysis submodel, the decomposition of solid wood is described by an Arrhenius equation that gives a relationship between the reaction rate and temperature of the solid. This requires the kinetic properties - activation energy E_i, pre-exponential factor A_i and reaction order n_i (also known as the kinetic triplet) to be specified to determine the decomposition rate. A multiple-component scheme is used that assumes a solid material is composed of several components with each component undergoing a single independent reaction to generate products [136]. The constituent components of solid wood included in the model are cellulose, hemicellulose, lignin and water. The reaction rate for each component $w_{i,j}$ at a given time can be described with a first order differential equation where $Y_{i,j}$ is the mass fraction $(m_i/m_{i,init})$ of component i at time j, m_i is the mass of component i and $m_{i,init}$ is the initial mass of component i. For each component the initial mass fraction is $Y_{i,init} = 1$ at the start of the simulation. c_i is the initial fraction of the overall unheated composite solid represented by component i i.e. $m_{i,init}/m_{init}$. Equation 5.37 is solved using numerical methods to give the value of Y_i at each time step.

$$w_{i,j} = \frac{Y_{i,j}}{dt} = c_i A_i \exp\left(-\frac{E_i}{RT_{i,j}}\right)(Y_{i,j})^{n_i} \tag{5.37}$$

The solid is represented by the one-dimensional finite difference scheme illustrated later in Figure 5.19 and the overall reaction rate at a given time is the sum of the reaction rates of all the components (i) within a given layer or slice of the solid material at a given temperature. The mass loss rate is derived from the reaction rates for each layer and summed over all the layers to give a total rate for the wood material at a given time as described next.

For the cellulose, hemicellulose and lignin components, a char residue yield ν_i is specified (discussed in Section 5.3.1) with the mass fraction of char $X_{i,j}$ at time j given by Equation 5.38 and Equation 5.39. There is of course no char associated with the liquid water component which evaporates.

$$X_{i,j} = (1 - Y_{i,j})\nu_i \tag{5.38}$$

The mass fraction of char residue at time j for each layer and for the three components (excluding moisture/water) is:

$$X_j = \sum_{i=1}^{3}(X_{i,j}c_i) = \sum_{i=1}^{3}((1 - Y_{i,j})\nu_i c_i) \tag{5.39}$$

At a given time j, the mass of solid wood that remains per unit volume is given by Equation 5.40 where ρ_{init} is the initial mass of wood per unit volume.

$$m_j''' = \sum_{i=1}^{3}\left(Y_{i,j}c_i\rho_{init}\right) \tag{5.40}$$

The total mass loss rate in $kg/(m^3 s)$ can then be given by:

$$\frac{dm}{dt} = -\frac{(m_j - m_{j-1})}{\Delta t} \tag{5.41}$$

Ignoring any char oxidation, the gasification rate of fuel available to be converted to combustion energy in the fire model ($\dot{m}_{s,j}$) in a single layer of the finite difference scheme is given by:

$$\frac{dm_{s,j}}{dt} = -\frac{(m_{s,j} - m_{s,j-1})}{\Delta t} \tag{5.42}$$

At each time step this can be summed over all the layers (L=1 to N) in the finite difference scheme as per Equation 5.43 where Δx is the thickness of each layer, assuming that the gases are instantly transported to the fire-exposed surface of the material where they may burn.

$$\dot{m}_j'' = \sum_{L=1}^{N}\left(\sum_{i=1}^{3}\left(Y_{i,j} - Y_{i,j-1}\right)c_i\rho_{init}\Delta x\right) \tag{5.43}$$

The rate of heat release ($\dot{Q}''$) from the combustible gases determined from the mass flux ($\dot{m}''$) and the heat of combustion ΔH_c is

given by Equation 5.44 adapted from Wang et al. [241] with the temperatures inside the solid found using a one-dimensional heat conduction equation to compute the solid phase temperature gradient at x depth.

$$\dot{Q}'' = \Delta H_c \dot{m}'' = \Delta H_c \rho_{init} \int_{L=1}^{N} \sum_{i=1}^{3} (1-\nu_i) A_i \left(\frac{\rho_i}{\rho_{init}}\right)^{n_i} \exp\left(\frac{-E_i}{RT(x)}\right) dx \tag{5.44}$$

A flow chart illustrating the coupling of moveable fire load and the contribution of the mass timber when the kinetic submodel SMC is used is shown in Figure 5.12.

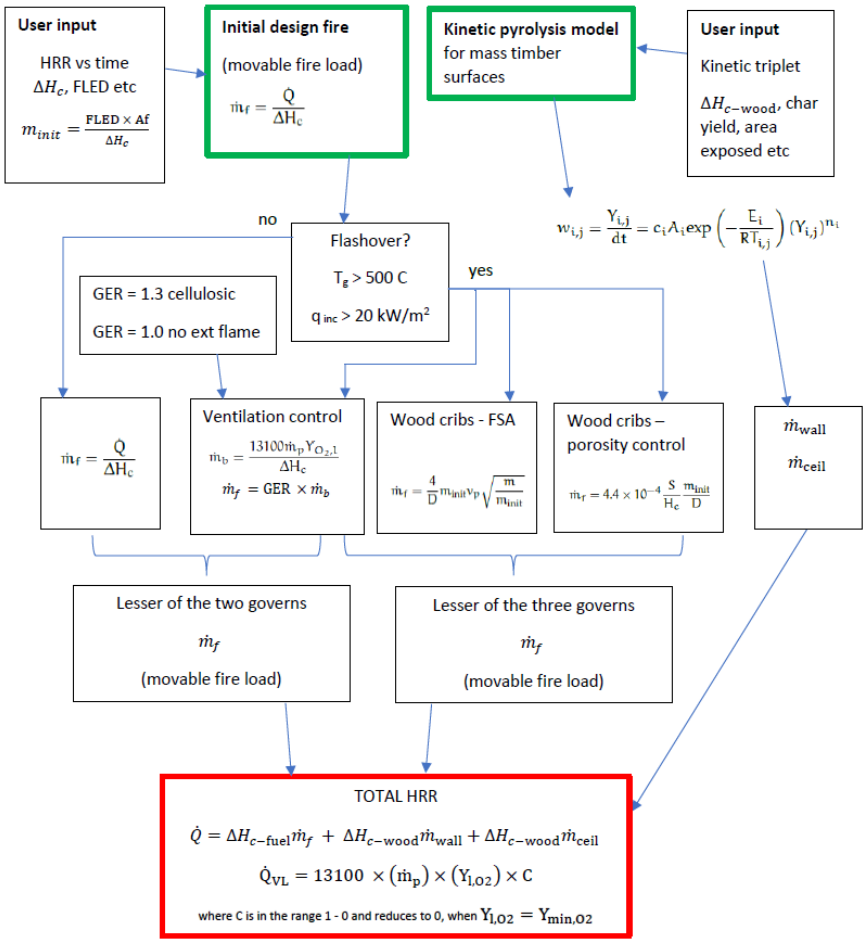

Figure 5.12: Flow chart for the moveable fire load coupled with the kinetic submodel SMC for mass timber.

5.7.2 *Material kinetic properties*

In addition to the thermophysical and related properties of wood and char discussed earlier in Section 5.3, the kinetic parameters for wood determined by Wang et al [241, 249] using a hand calculation method for a three component scheme have been applied in this model as given in Table 5.2.

The kinetic properties for water in Table 5.2 have been derived assuming a reference temperature of 100°C, a reaction rate of 0.0016 s^{-1} and a heating rate of 5 K/min following the procedure described in the FDS User Guide [250] with water evaporating in the region of 100°C.

This set of kinetic properties has been used in all the simulations using the kinetic wood pyrolyis submodel presented in this thesis. Richter et al. [147] found that variations in kinetics were found to have only a small effect (± 1 $gm^{-2}s^{-1}$) on the predicted mass loss rate at both the microscale (mg-samples) and mesoscale (kg-samples) and to have a negligible effect on the predicted temperatures (±16 K) across different depths, heat fluxes and oxygen concentrations at the mesoscale. They stated that the variation in kinetics is negligible for predicting charring across scales and a kinetic model of charring derived for one wood species should be valid for all wood species [147].

Component	E_i (J/mol)	A_i (s^{-1})	n_i	c_i	Ref
Hemicellulose	1.64×10^5	3.25×10^{13}	2.1	0.37	[249]
Cellulose	1.98×10^5	3.51×10^{14}	1.1	0.44	[249]
Lignin	1.52×10^5	8.41×10^{13}	5.0	0.09	[249]
Water	6.04×10^5	1.53×10^{83}	1.0	0.10	[250]

Table 5.2: Kinetic properties for wood.

The mass of water that remains at a given time j per unit volume can be expressed by Equation 5.45 where $Y_{water,j}$ is determined by solving Equation 5.37 for water as the component i.

$$m_{water,j} = Y_{water,j} c_{water} \rho_{init} \tag{5.45}$$

The mass of char present at a given time per unit volume is:

$$m_{c,j} = X_j \rho_{init} \tag{5.46}$$

The total mass present at a given time per unit volume (which is also the apparent density of the material) is therefore:

$$m_j = m_{s,j} + m_{water,j} + m_{c,j} \tag{5.47}$$

5.7.3 *Example application of the kinetic submodel*

The result of an example calculation presenting intermediate output from the kinetic model as implemented in B-RISK is described here. This example is the same case as discussed earlier in Section 5.5.2 for an enclosure experiment designated as Config. P and also discussed later in the benchmarking presented in Section 6.5.3. The enclosure had dimensions 4.5 × 2.4 × 2.7 m high with an opening 0.76 m × 2.0 m high. 33% of the wall and 10% of the ceiling were exposed CLT. The fuel load was 360 kg of wood cribs.

To illustrate the calculation, the predicted residual mass fractions for each component and for the char residue within the discrete single layer located 50 mm below the wood surface for the experiment is shown in Figure 5.13. The wall is 175 mm thick CLT and each layer in the finite difference scheme is 1 mm thick giving a total of 175 layers for the full depth of wall. The corresponding predicted mass loss rate for all components contributed by the individual layers located at depths of 25, 50 and 60 mm below the wood surface is shown in Figure 5.14 to illustrate how the rate of decomposition varies with increasing depth (and decreasing temperature) below the surface. The area underneath each of these curves represents the total mass contributed by the given layers and reflects different degrees of thermal decomposition. The layer closer to the exposed surface is fully decomposed whereas deeper layers are only partially decomposed.

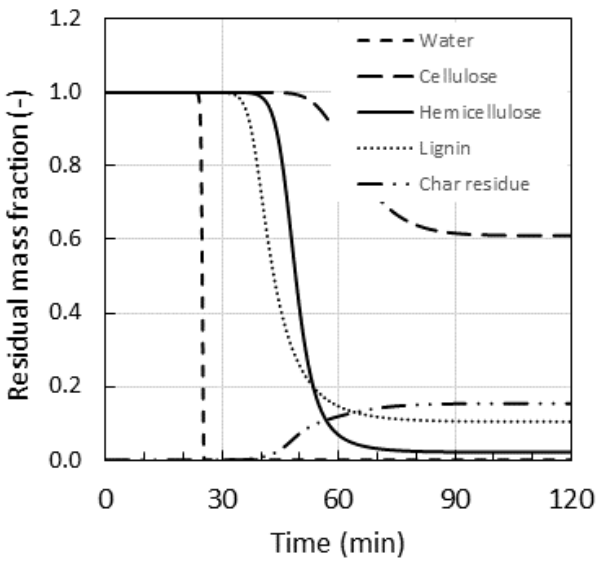

Figure 5.13: Example of the predicted residual mass fraction for each component within the wall element located at a depth of 50 mm below the surface of the wall for Config. P.

The total mass loss rate (kg/s) contributed by all areas of the exposed wall and exposed ceiling summed over all elements for all com-

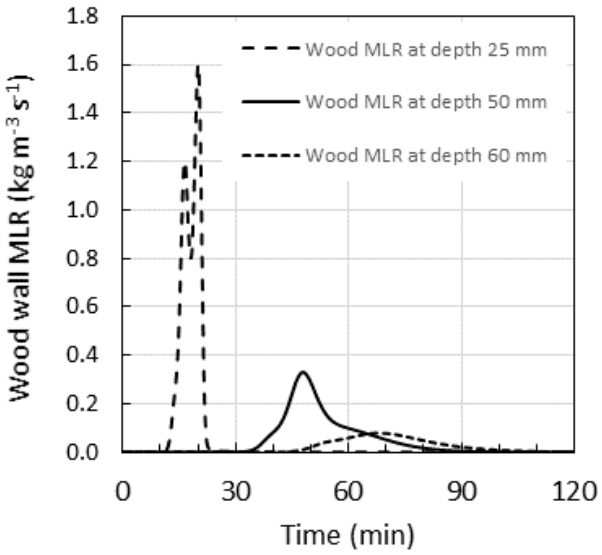

Figure 5.14: Example of the predicted mass loss rate (kg m^{-3} s^{-1}) for all components contributed by elements located at depths of 25, 50 and 60 mm below the surface of the wall for Config. P.

ponents is shown in Figure 5.15. Since, in this experiment, only 10% of the ceiling was exposed compared to 33% of the wall, the ceiling contribution is relatively small compared to the wall as also seen in Figure 5.15. The model assumes that the combustible gases from the decomposition of the wood surfaces are instantly transported to the fire-exposed surface of the material where they are available to burn.

Since this research is predominantly concerned with the fire during its fully developed phase, for simplicity in these simulations, the initial fire growth is represented as a fast t-squared fire until flashover where a switch to a fully developed regime occurs. The mass loss rate contributed by the moveable fire load (wood cribs) during the fully developed regime was calculated using equations for wood cribs given in Section 5.4. The sum of the mass loss rate of the moveable fire load and from the exposed wood surfaces gives the total mass loss rate shown in Figure 5.15 and this is used in the calculation of the rate of heat release. The oxygen-constrained rate of heat release is determined from the predicted concentration of oxygen inside the enclosure. The total rate of heat release which includes burning external to the enclosure is taken as the product of the total mass loss rate and the effective heat of combustion. Continuing the present example calculation, the predicted total heat release rate is shown in Figure 5.16 assuming an effective heat of combustion of 14 MJ/kg as discussed in Section 5.3.2.

It is observed in Figure 5.16 that the ratio of the total heat release and the heat released inside the enclosure in the early part of the ventilation controlled stage is in the order of 2 i.e. similar amounts of

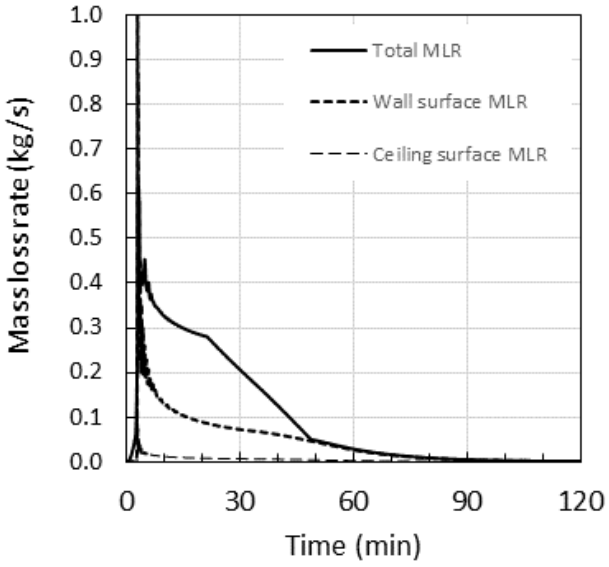

Figure 5.15: Example of the predicted mass loss rate (kg/s) contributed by all elements in the exposed wall, exposed ceiling and the total mass loss rate including the moveable fire load (wood cribs) for Config. P.

heat released inside and outside the enclosure and this is consistent with the observations previously noted in Section 4.5.1.

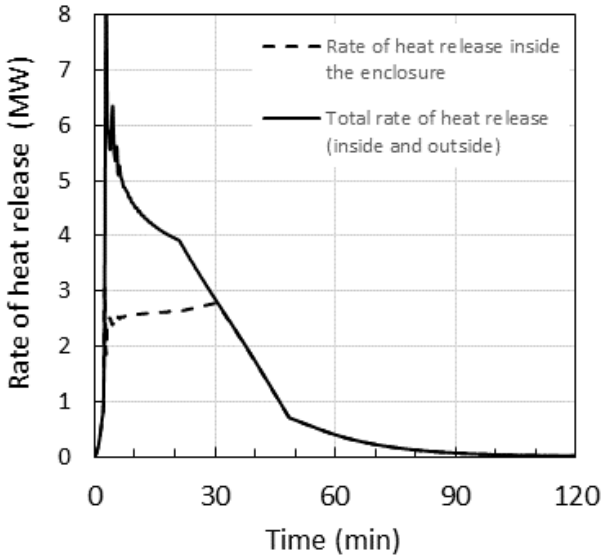

Figure 5.16: Example of the predicted total heat release rate (inside and outside) the enclosure contributed by all areas of exposed walls and ceiling and the moveable fire load for Config. P.

5.7.4 *Sensitivity to effective heat of combustion*

The result of an example calculation showing the effect that the effective heat of combustion has on the predicted enclosure gas temperature when using pyrolysis submodel SMC is presented here. The enclosure fire experiment designated as Config. P in the benchmarking discussed later in Section 6.5.3 is used here and is same example from the previous section. Figure 5.17 shows the predicted gas temperature for the three cases compared with the measured data. The effective heat of combustion within the range 12 - 16 MJ/kg has only a small effect increasing the peak predicted gas temperatures. However, the effect might be more significant in the case of a fuel controlled rather than ventilation controlled fire.

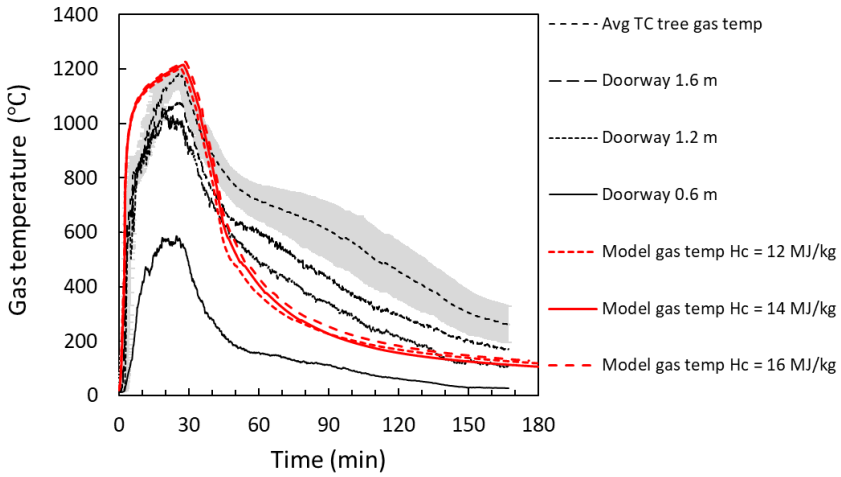

Figure 5.17: Measured and predicted enclosure gas temperatures for Config. P using SMC pyrolysis submodel with effective heat of combustion = 12, 14 and 16 MJ/kg.

Figure 5.18 shows the predicted total HRR for the three cases. The effect of a higher heat of combustion value is to increase the total HRR as shown.

5.8 DEBONDING OF THE WOOD LAMELLAE

5.8.1 *Debonding submodel*

This section describes an adaptation of the previously described heat conduction submodel used to predict the time that each lamella of a CLT wall or ceiling element would debond. An assumed adhesive debonding temperature is specified by the user along with the number of lamellae used and their thickness. Further to the discussion in Section 4.7 a value of 200°C is used as the default debonding temperature but this can be changed by the model user. In addition, this

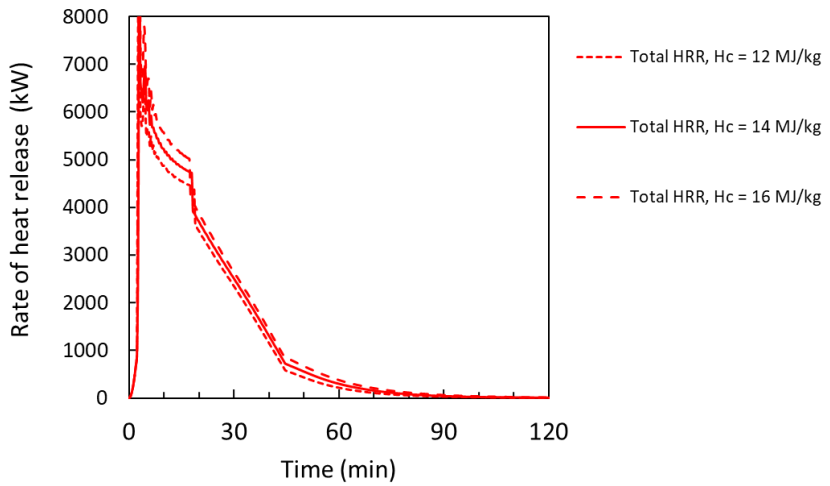

Figure 5.18: Predicted enclosure total HRR for Config. P using SMC pyrolysis submodel with effective heat of combustion = 12, 14 and 16 MJ/kg.

heat conduction submodel also allows the position of the char depth with time to be determined so that the pyrolysed material can be added to the fuel load as described in Section 5.5.1. This accounts for any potential change in the char rate following debonding of any fire exposed lamellae.

The time for the specified adhesive debonding temperature to be reached at the depth below the surface corresponding to the position of the adhesive line is determined from the heat conduction submodel described in Section 5.2. This is the time that the first lamella debonds. A simple schematic of the finite difference scheme is illustrated in Figure 5.19.

At that time, the finite difference scheme is reformulated to remove the fire exposed lamella from the scheme thus exposing the next layer to the radiative and convective boundary conditions computed by the zone model of the fire compartment. The procedure is repeated with each subsequent lamellae removed if the required temperature at each adhesive line is reached. The reformulated schematic of the finite difference scheme is illustrated in Figure 5.20.

Once lamella are discarded following debonding, the temperature of that element is set equal to the char temperature thereafter. The element is able to contribute additional mass and energy to the enclosure consistent with the assumed char temperature of 300°C. As noted previously by Bartlett et al. [174, 175] and Aguanno [176] it is unlikely that the entire lamella would instantaneously fall away upon the adhesive line reaching the nominated debond temperature. The debonding submodel was coded into the B-RISK zone model and requires the user to specify the lamella thickness and the adhesive debonding temperature.

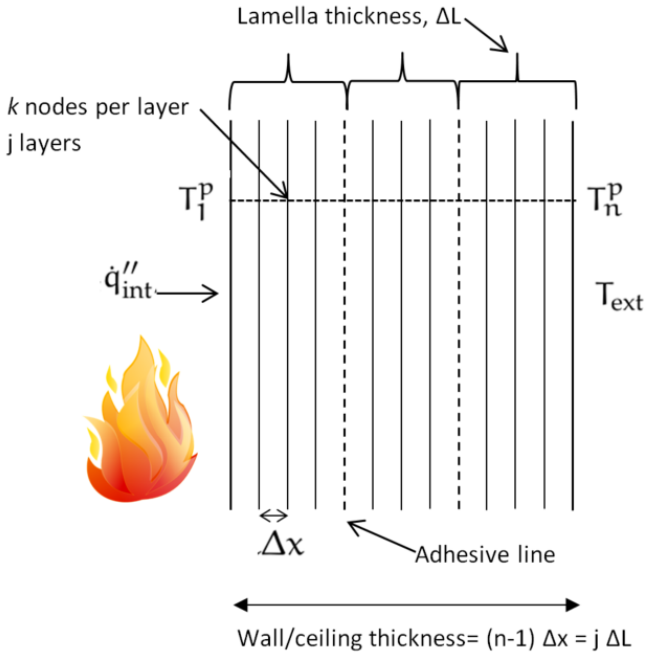

Figure 5.19: Schematic view of finite difference scheme before layer debonding.

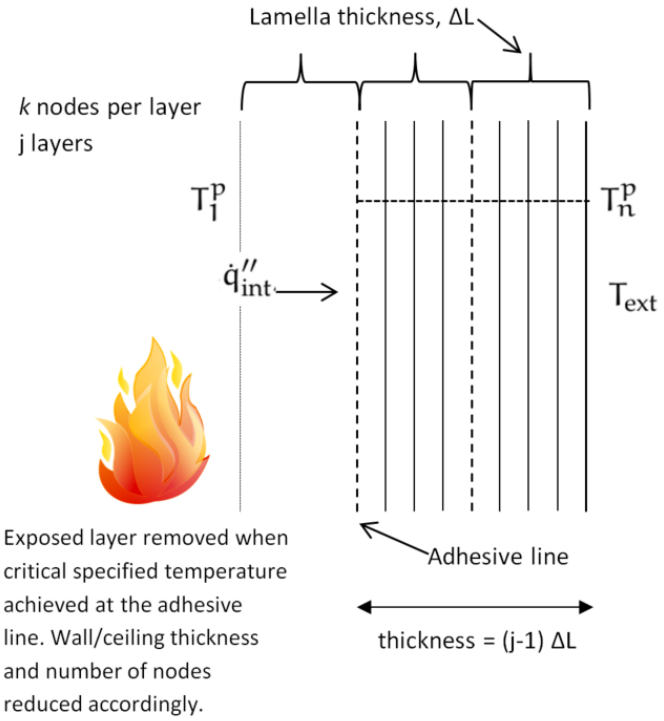

Figure 5.20: Schematic view of finite difference scheme after layer debonding.

5.8.2 *Sensitivity to the assumed debonding temperature*

To illustrate an example of the effect of the debonding submodel, and its sensitivity to the assumed adhesive debonding temperature, an experiment conducted by Hadden et al. [165] is used. An approximately cubic compartment of internal dimensions $2.72 \times 2.72 \times 2.77$ m^3 (width $\times$ length $\times$ height) was constructed with CLT elements with the CLT on the ceiling, rear wall and one side wall exposed to the fire and other surfaces protected. There was a door opening 1.84×0.76 m^2 (height $\times$ width) and the fuel load was relatively low (56 kg of wood crib) with the intention to ensure burnout of the wooden cribs within a short period of time after flashover. The CLT comprised five layers of 20 mm thick predominantly Spruce wood bonded with a polyurethane adhesive. The thermal properties for room materials used in this example are given by Hadden et al. as shown later in Table 6.2. The finite difference scheme represented each layer with 10 nodes per layer giving a total of 46 nodes for the overall 100 mm thick CLT element. The wood pyrolysis submodel SMA was used with GE taken as 2.0.

Three simulations using the submodel were performed where the only change in input was the assumed adhesive debonding temperature which was given a value of 150, 200 and 250°C respectively. The submodel results are quite sensitive to this parameter with more extensive debonding predicted as the debonding temperature is lowered. This leads to re-growth in the fire development and an increasing fire gas temperature as each layer falls away as shown in Figure 5.21.

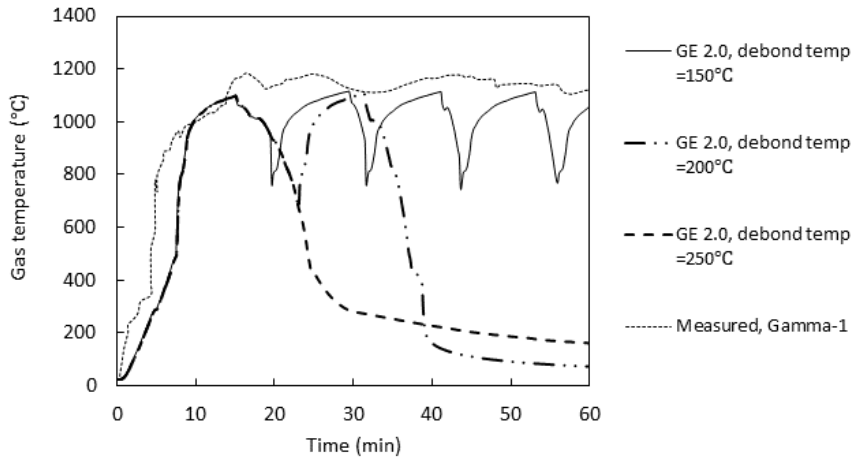

Figure 5.21: Effect of the adhesive debonding temperature on the upper layer gas temperature.

The total rate of heat release is compared for the different cases in Figure 5.22. This is the sum of the heat release rate inside the room

and that burning outside the room. The predicted peak rate of heat release is comparable to the measured values indicating that the assumed GER of 2.0 (which governs the relative proportion of fuel mass burning inside and outside the room) is reasonable. Figure 5.22 also shows the model predicting transitions between ventilation-controlled and fuel surface area-controlled burning. The debonding of lamella causes a period of ventilation-controlled burning followed by a transition back to fuel-control as the fire decays.

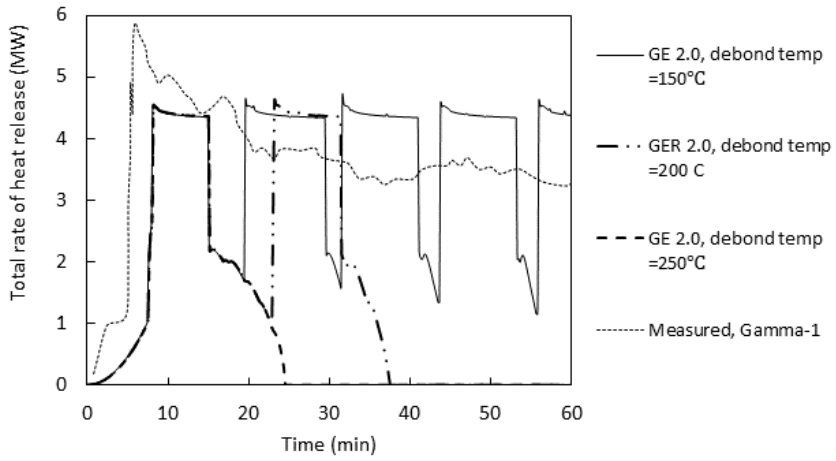

Figure 5.22: Effect of the adhesive debonding temperature on the total rate of heat release.

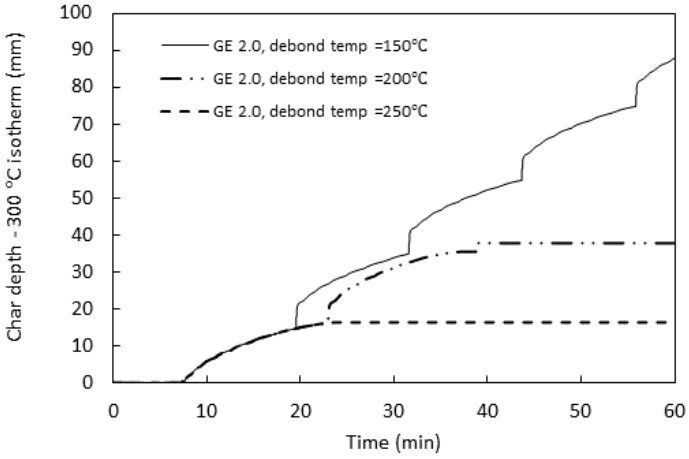

Figure 5.23: Effect of the adhesive debonding temperature on the predicted depth of char in the ceiling element.

The progression of the char below the exposed surface within the CLT ceiling element for the three cases is shown in Figure 5.23 clearly indicating the debonding of each layer and the time at which it is predicted to occur. Using the lower 150°C debonding temperature,

debonding of multiple layers is predicted whereas for the higher debonding temperature of 250°C no debonding is indicated. The predicted total fuel mass loss is compared in Figure 5.24 illustrating the extent to which debonding of CLT lamella contributes to the overall fuel load. Nodal temperatures within the CLT ceiling element is shown in Figure 5.25 where debonding of the surface layer is clearly shown followed by a rapid increase in temperatures within the freshly exposed layer. The debonding behaviour in the model is such that each lamella in its entirety is assumed to fall completely away at the predicted time of debonding. In reality, there will be some variability in the internal temperatures and a more progressive debonding process.

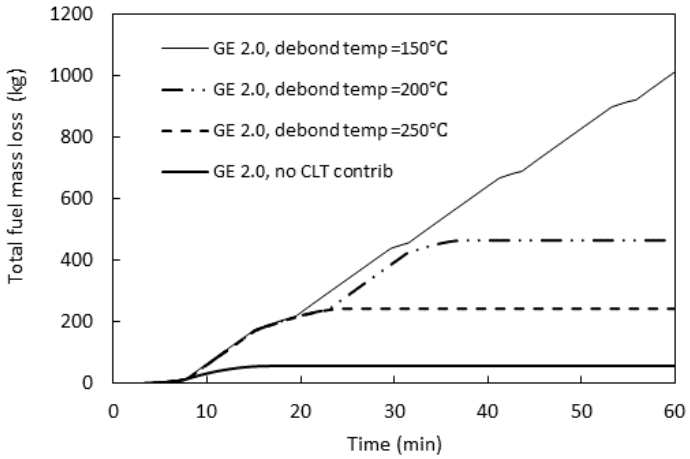

Figure 5.24: Effect of the adhesive debonding temperature on the predicted total fuel mass loss.

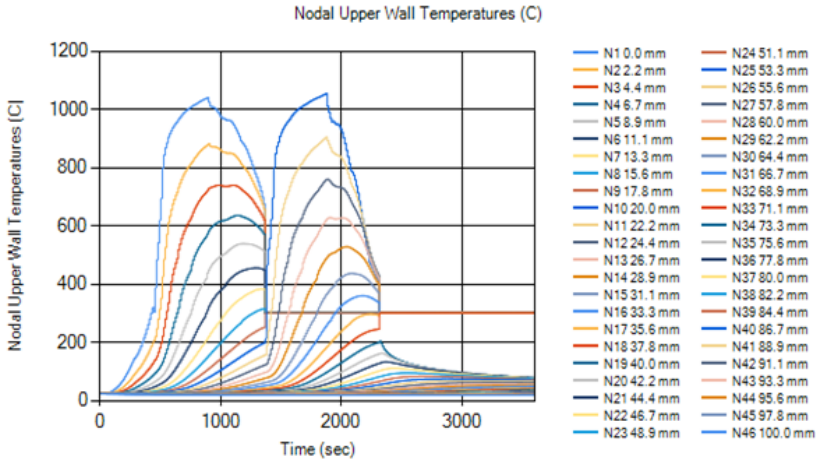

Figure 5.25: Nodal temperatures in the upper wall for the simulation using the adhesive debonding temperature of 200°C.

This debonding model could in the future be adapted to also predict the case of a protected mass timber element i.e. a surface layer of inert gypsum plasterboard that falls off when the temperature at the gypsum-timber interface reaches a pre-defined temperature, exposing a contributing timber material.

5.9 OTHER ASSUMPTIONS AND CONSIDERATIONS

As previously noted, the fire model calculates the incident radiant heat flux to the interior surfaces considering re-radiation between the different surfaces. Absorption and emission by carbon dioxide, water vapour and soot in the respective gas layers is considered. Contribution to generation of these species from the timber surfaces are also included.

However, the model is not able to account for any difference in the position of exposed wood surfaces other than as a ceiling or a wall. Medina Hevia [157] showed that exposed CLT on opposite walls was worse than CLT on adjacent walls (at least in small rooms) which is attributed to the increased thermal feedback between two opposite surfaces.

The compartment heat loss calculation currently does not allow more than one material to be specified for the wall. Where part of the wall is exposed CLT and another part is CLT protected with plasterboard, only thermal properties of wood will be used for calculating total heat losses through the walls. For the case where some of the CLT is encapsulated with a less insulating material than wood (e.g. plasterboard), it means that the overall surface conductive heat losses may be underestimated. This is likely to lead to slightly higher calculated gas temperatures than otherwise expected depending on the relative material surface areas concerned. This is considered a conservative assumption for most applications but the model could be refined to account for this in the future.

Where a protection system such as gypsum plasterboard encapsulation is used to protect timber surfaces from the fire, the model does not determine the ability of the system to remain in place during the fire. It is assumed that the protection is sufficient to prevent any contribution of the protected wood to the fire development.

While the dynamic changes in charring rate determined from the 300°C isotherm eventually ceases as the fuel depletes, additional criteria to address the potential for smouldering combustion during the decay period might be necessary. Crielaard proposed a criterion of 5 kW/m^2 for the maximum incident radiant flux be used to determine if auto-extinction has been achieved [199, 200].

6 BENCHMARKING THE PYROLYSIS SUBMODELS

6.1 GENERAL

This chapter presents and discusses results obtained by comparing model predictions with data from experiments undertaken by others and previously reported in the literature.

Table 6.1 lists a series of 19 enclosure fire experiment configurations taken from four different series of experiments. These are used for benchmarking the performance of the modified enclosure fire model with the two new wood combustion pyrolysis submodels described in Chapter 5 for the exposed mass timber surfaces. Configs. A – E were nominally identical except for the location and amount of exposed timber surfaces within the enclosure. Similarly, Configs. F – H were also nominally identical except for the location and amount of exposed timber surfaces within the enclosure. Configs. I - N varied by the opening size as well as the location and amount of exposed timber surfaces within the enclosure. Configs. O - S varied by the type, location and amount of exposed timber surfaces.

In Configs. A, I, J and O the timber surfaces were fully protected and these experiments provided a baseline comparison for the other Configs with exposed timber. In Configs. O - S, the CLT for enclosure construction was manufactured with a thermal resistive adhesive meaning the CLT in those experiments was expected to perform similarly to solid wood.

In this chapter, SMA refers to the global equivalence wood pyrolysis submodel A described in Section 5.5 while SMC refers to the kinetic pyrolysis submodel C described in Section 5.7. In all the benchmarking cases discussed here, a common set of temperature dependent thermal properties for CLT have been used as given in Section 5.3. A constant effective heat of combustion value for wood of 14 MJ/kg was also adopted as discussed in Section 5.3.2.

CONFIG	ROOM SIZE m	OPENING m	WOOD EXPOSED	REF.
A.	$4.5 \times 3.5 \times 2.5$	1.069×2.0	none	[156]
B.	$4.5 \times 3.5 \times 2.5$	1.069×2.0	4 walls, ceil	[156]
C.	$4.5 \times 3.5 \times 2.5$	1.069×2.0	2 adj walls	[157]
D.	$4.5 \times 3.5 \times 2.5$	1.069×2.0	2 opp walls	[157]
E.	$4.5 \times 3.5 \times 2.5$	1.069×2.0	rear wall	[157]
F.	$2.72 \times 2.72 \times 2.77$	0.76×1.84	back, side wall	[165]
G.	$2.72 \times 2.72 \times 2.77$	0.76×1.84	back wall, ceil	[165]
H.	$2.72 \times 2.72 \times 2.77$	0.76×1.84	back, side wall, ceil	[165]
I.	$9.1 \times 4.6 \times 2.7$	1.8×2.0	none	[168]
J.	$9.1 \times 4.6 \times 2.7$	3.6×2.0	none	[168]
K.	$9.1 \times 4.6 \times 2.7$	3.6×2.0	side wall	[168]
L.	$9.1 \times 4.6 \times 2.7$	1.8×2.0	ceil	[168]
M.	$9.1 \times 4.6 \times 2.7$	1.8×2.0	side wall	[168]
N.	$9.1 \times 4.6 \times 2.7$	1.8×2.0	side wall, ceil	[168]
O.	$4.5 \times 2.4 \times 2.7$	0.76×2.0	none	[171]
P.	$4.5 \times 2.4 \times 2.7$	0.76×2.0	33% wall, 10% ceil	[171]
Q.	$4.5 \times 2.4 \times 2.7$	0.76×2.0	36% walls[a]	[171]
R.	$4.5 \times 2.4 \times 2.7$	0.76×2.0	19% wall[a], 100% ceil	[171]
S.	$4.5 \times 2.4 \times 2.7$	0.76×2.0	35% wall, 100% ceil	[171]

a This was exposed Glulam beams/columns represented as an equivalent area of wall.

Table 6.1: Summary of enclosure fire experiment configurations used in benchmarking the pyrolysis submodels.

6.2 CARLETON UNIVERSITY EXPERIMENTS (CONFIG. A-E)

6.2.1 *Description*

Five configurations of room fire experiments conducted at Carleton University representing bedroom fires with different room construction types are presented in this section [28].

In Test 1 and 2 from [158] (both Config. A), CLT walls were protected with two layers of 12.7 mm thick gypsum board. These were identical tests with no contribution from the CLT. The average HRR of Test 1 and 2 was reported, and due to system malfunction, only the gas temperature for Test 2 was reported [158]. In Test 3 (Config. B), the wall and ceiling CLT panels were totally exposed. Three additional experiments in the same series (Tests 4, 5 and 6) are not relevant to the present study because the CLT panels were protected with light frame plasterboard-lined construction so these are not included here but were similar to Tests 1 and 2. Three further room fire experiments (Configs. C, D, E) were carried out by Medina Hevia [157] with the goal of determining the maximum percentage of exposed CLT that would result in auto-extinction of the CLT room surfaces.

All rooms were constructed from CLT panels manufactured by Nordic Engineered Wood [238]. They were 105 mm thick with nominal density 515 kg/m^3 and comprised three layers each 35 mm thick. The layers were adhered with a polyurethane-based adhesive. The enclosure geometry and ventilation were as given in Table 6.1. The CLT floor panel in each room was protected with a layer of 15.9 mm (5/8 inch) thick Type X fire-rated gypsum board with a layer of 12.7 mm thick cement board installed on top. Over the cement board, a layer of 19 mm thick hardwood tongue and groove maple flooring was installed.

Since the actual thermal properties of the construction materials were not reported, the temperature properties shown in Table 6.2 were assumed (with Hankalin et al. properties [243] for the thermal conductivity of wood) for the subsequent modelling described in this section. Emissivity is assumed to be 0.7[1] for all wood surfaces based on a graphite material [251]. The fuel load was bedroom furniture and clothing and also included maple boards on the floor. The furniture layout in the room is shown in Figure 6.1.

The HRR was recorded for each test using oxygen consumption calorimetry and therefore burning just outside the room opening was captured along with burning inside the room. Gas temperatures were measured with unshielded Type K thermocouple wire on thermcouple trees. Each thermocouple tree included 6 thermocouples at

1 This value may be too low for wood char with a value of 1.0 being considered more reasonable [132]. A sensitivity analysis on the effect of using emissivity 0.7 vs 1.0 showed it made almost negligible difference to the predicted gas temperatures.

Property	Timber	Plasterboard
Thermal conductivity W/(m K)	see Section 5.3	0.24 [165]
Density kg/m^3	515 [238]	784 [165]
Heat capacity J/(kg K)	see Section 5.3	950 [165]

Table 6.2: Thermal properties used as model input.

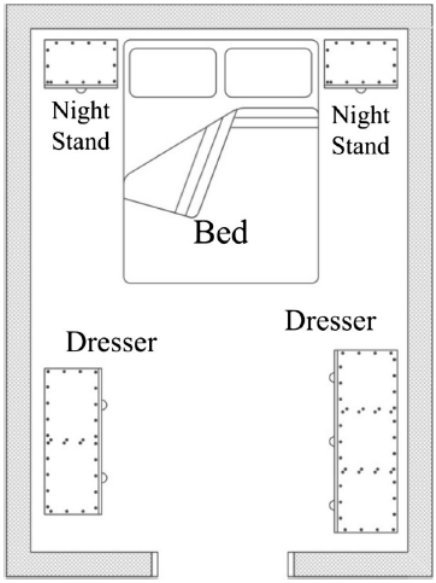

Figure 6.1: Furniture layout in Config. A – E. Reprinted from Li et al. [158] with permission from Springer Nature.

heights of 0.4, 0.8, 1.2, 1.6, 2.0 and 2.4 m from the floor. The thermocouple wire ends were twisted together to make the connection and the trees were covered with a 12.7 mm fibreglass insulation layer. Trees were located at the doorway, two near the centre of the room and one at the rear of the room [156]. Temperature data presented in the following figures are the average of all the trees.

6.2.2 *Config. A prediction – timber fully protected*

This configuration allows the fire model to be evaluated for the burning contents without any contribution from linings to give a baseline against which to compare the other configurations. Integrating the measured heat release rate curves from calorimetry, McGregor [156] estimated the actual energy release from the furniture for this case as 366 MJ/m^2 and the wood equivalent fuel load on a floor area basis as 30.2 kg/m^2. The maple flooring was included as part of this fuel load. An effective average heat of combustion for the fuel can then be calculated as 366/30.2 = 12.1 MJ/kg. This is typical for wood during the early pyrolysing period when mostly flaming combustion occurs [233].

In these simulations, a heat of combustion for wood of 17.5 MJ/kg from Eurocode 5 [146] with an assumed combustion efficiency of 0.8 is used giving an effective value of 14 MJ/kg. The characteristic fuel thickness for the wood crib representation assumed in the simulations (Equation 5.29) is 50 mm. Since the CLT was fully protected it is assumed there is no contribution to the burning. For the case of the moveable fire load, simulations with GER of 1.3 and 2.0 are done. GER of 1.3 means that, for ventilation control, the mass loss rate from the fuel will be 30% higher than can burn inside the room, and this is of the same order as noted previously for wood cribs burning in an enclosure. Li et al. [158] estimated the GER to be 1.18 for this experiment.

Figure 6.2 shows the total rate of heat release predicted by the model. The rate of heat release is the sum of the energy generated inside the enclosure plus any combustion outside the opening. The prediction is comparable to the average rate of heat release (for Test 1 and 2 [156, 158]) from oxygen calorimetry in the experiment also shown in Figure 6.2.

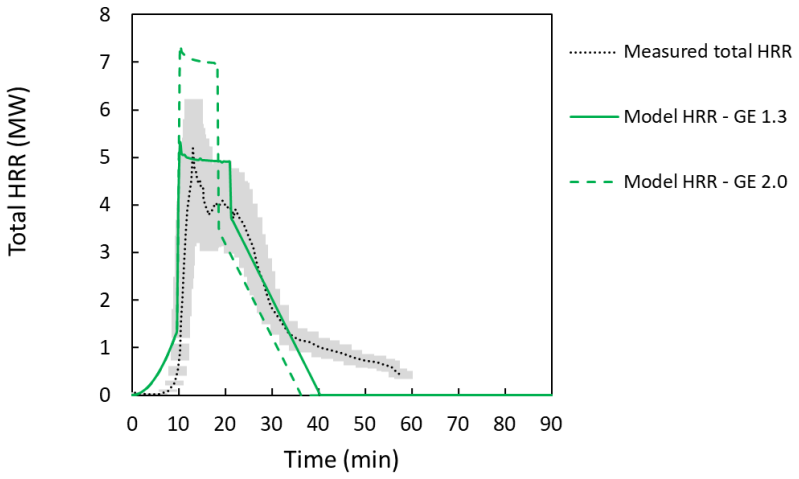

Figure 6.2: Measured and predicted total HRR for Config. A - no pyrolysis submodels.

Figure 6.3 shows the gas temperature history predicted by the model. This is comparable to (with a slightly higher peak) the gas temperature history for Test 2 also shown in Figure 6.3. An estimate of the combined relative uncertainty (95% confidence interval) of 0.20 and 0.14 for rate of heat release and gas temperature respectively for the measurement is shown as grey shading based on typical uncertainty estimates from the literature [252]. These are also shown on subsequent figures for the other configurations (B-H).

Since the initial growth rate was not the focus in this study, it is set to $\dot{Q} \approx 0.004t^2$ (kW) to give a time to flashover that approximately matches the experiments. The flashover time from visual observation

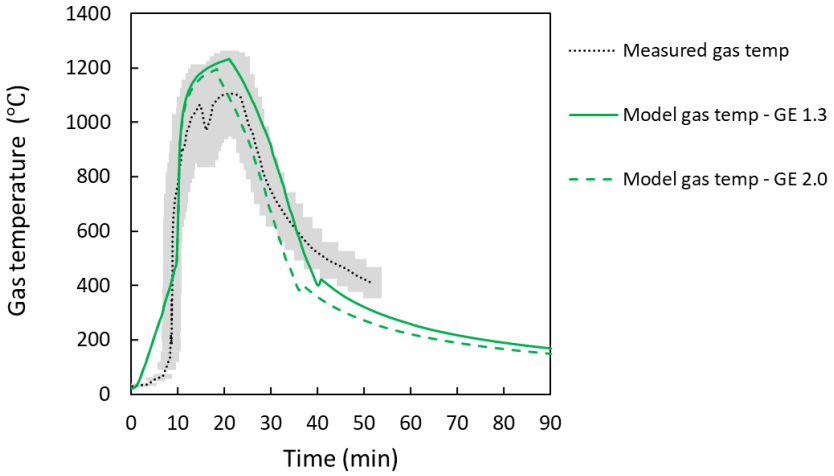

Figure 6.3: Measured and predicted enclosure gas temperatures for Config. A - no pyrolysis submodels.

was reported by Li et al. [158] for the repeated Test 1 and Test 2 as 6.5 and 8.6 min respectively. However, based on time for the gas temperatures to reach 500°C, flashover in Test 2 was closer to 10 min (see Figure 6.3) and is 10.2 min in the simulation.

6.2.3 *Config. B prediction – timber fully exposed*

For Config. B, the CLT ceiling and walls were fully unprotected and contributed fuel to the fire. GER of 2.0 is assumed in submodel SMA generally consistent with previous experiments of fully timber-lined rooms reported in the literature. For example, Hakkarainen [153] conducted a fire experiment in an unprotected heavy laminated timber enclosure and estimated the proportion of fuel burning externally to be 50%. This means, for ventilation control, the mass loss rate from the fuel was twice that able to burn inside the room based on the available oxygen. Li et al. [158, 159] estimated the GER to be about 3.1 for Config. B, while McGregor [156] noted that the energy release rate in the unprotected configuration was approximately twice that of the protected configuration. This also means that external burning and external flame projection was more pronounced for an unprotected timber enclosure compared to a fully protected or non-combustible enclosure.

In these simulations, the initial growth rate is set to $\dot{Q} = 0.012\alpha t^2$ (kW) to give a time to flashover that approximately matches the experiments. Figure 6.4 shows the measured and predicted total heat release rate for both GER = 2.0 and GER = 3.1 cases for SMA and SMC in the absence of any debonding. SMC predicts a much sharper

initial peak followed by a rapid decline that is not apparent in the measured data.

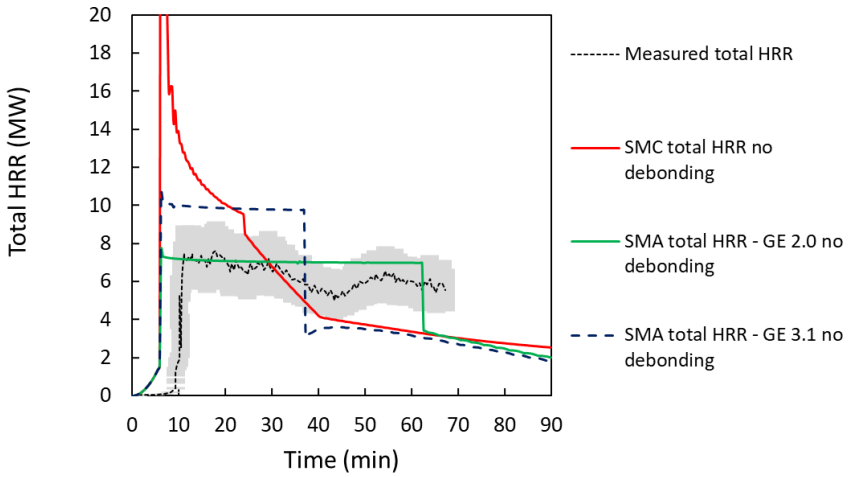

Figure 6.4: Measured and predicted total HRR for Config. B - without debonding.

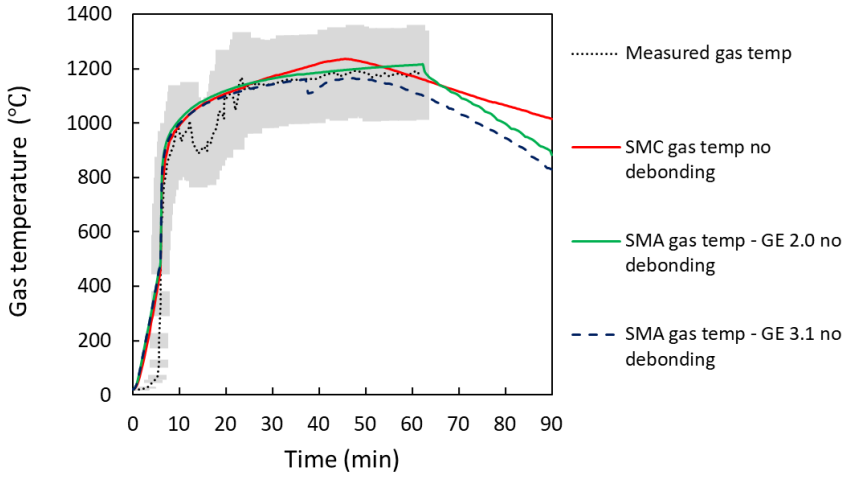

Figure 6.5: Measured and predicted enclosure gas temperatures for Config. B - without debonding.

Figure 6.5 shows the gas temperature history in the room predicted by the submodel for Config. B. This also compares well with the mean temperature measurements in the experiment (also shown in the same Figure). A plate thermometer was included in the room and it is noted that it gave measurements that were approximately 180°C lower than the average of the thermocouple trees.

An assumed value of GER = 2.0 in the simulation with SMA provides a better match to the measured total HRR than does Li et al.'s estimate of 3.1, while the gas temperature predictions are similar. How-

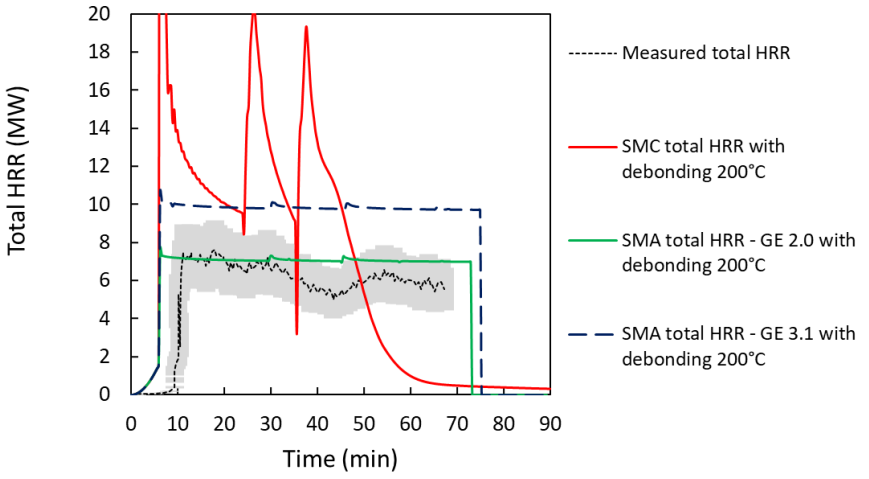

Figure 6.6: Measured and predicted total HRR for Config. B - with debonding.

ever, there is uncertainty in whether all the gasified fuel is completely burned as well as uncertainties in the means used by Li et al. to estimate GER in the experiment. However, it seems reasonable that the actual GER in the experiment was likely not lower than 2 and could have been as high as 3.1.

McGregor observed that all items in the room became fully involved at 5:55 minutes when the floorboards in the doorway ignited. He also noted that at 39 minutes, the HRR began to rise again entering a second growth phase, at which time pieces of the first CLT lamella were observed to fall off.

To illustrate the effect of including debonding in the model simulations of total HRR for both the SMA and SMC cases 'with debonding' is shown in Figure 6.6 and the gas temperature in Figure 6.7. The effect of the debonding in contributing fresh fuel to the fire can be clearly seen in the case of SMC (the kinetic submodel), however it is barely noticeable in the SMA cases. This is because the debonding occurs while the burning is already ventilation-controlled such that a release of additional mass following debonding would lead to an extended burning duration for SMA but would be immediately released in the vent flow to burn outside in the case of SMC.

McGregor estimated the overall average charring rate to be 0.85 mm/min based on a charring depth of 24 mm in 40 min [156]. This is less than the predictions illustrated in Figure 6.8. At 40 minutes the model predicted char depths of about 35 mm and 37 mm for SMA and SMC respectively. Overall for Config. B, SMA with GE 2.0 gives the best overall agreement with the experimental data considering heat release rate, gas temperatures and char depth.

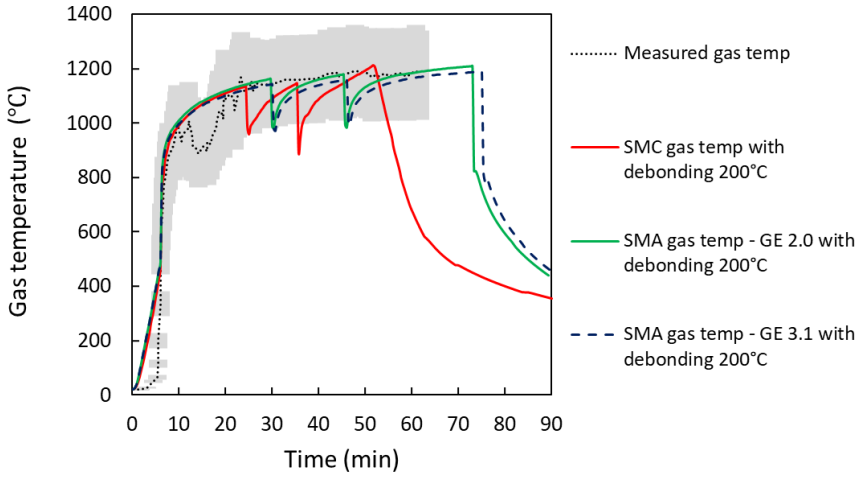

Figure 6.7: Measured and predicted enclosure gas temperatures for Config. B - with debonding.

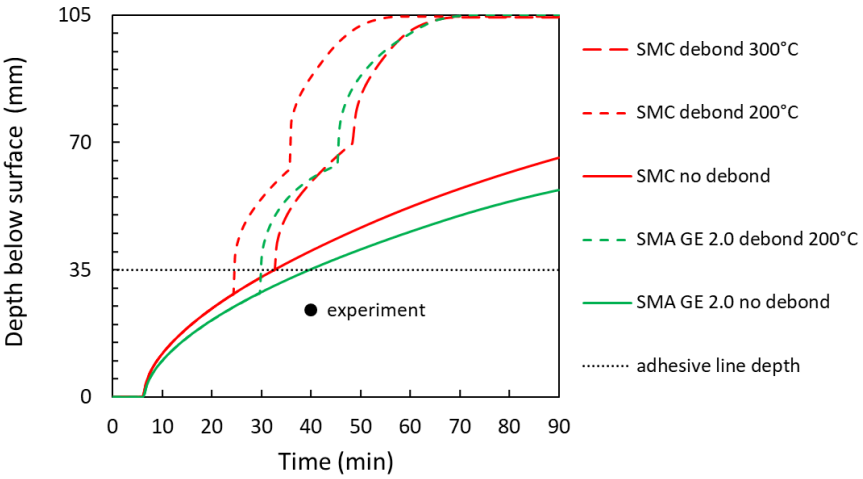

Figure 6.8: Config. B - Char depth in wall based on 300°C isotherm.

6.2.4 *Config. C prediction - two adjacent walls with timber exposed*

In this configuration, CLT panels on the rear wall and one side wall were exposed with other surfaces protected [157]. This was test 5 reported by Medina Hevia [157]. Flashover was observed at about 5 min with the gas temperature reaching a peak of about 1200°C after 20 min. The initial growth rate is set to $\dot{Q} = 0.017\alpha t^2$ (kW) to give a time to flashover that approximately matches the experiments. From Figure 6.9, the measured rate of heat release started to increase for a second peak around 65 min being the result of some debonding exposing fresh timber to the fire. A second flashover then occurred

following the rapid rise in temperature shown at around 75 min. The gas temperatures are shown in Figure 6.10.

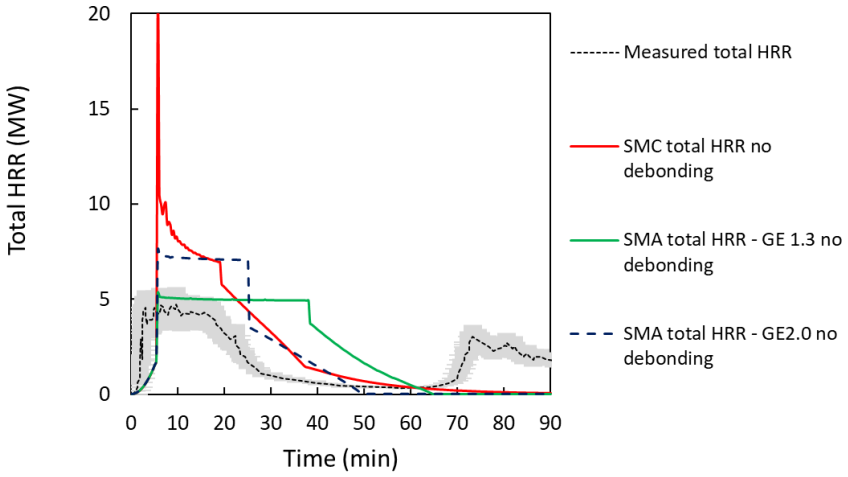

Figure 6.9: Measured and predicted total HRR for Config. C - without debonding.

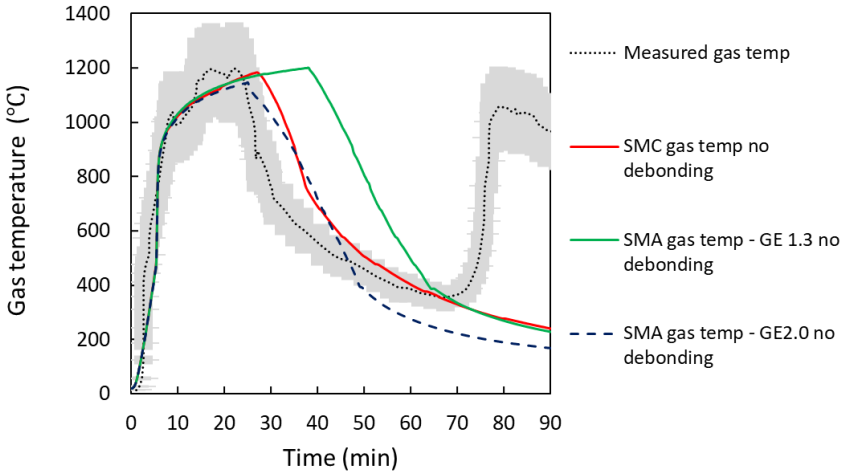

Figure 6.10: Measured and predicted enclosure gas temperatures for Config. C - without debonding.

Model simulations for this configuration were run for SMA with GE 1.3 and GE 2.0 and for SMC with and without the debonding submodel. The HRR curves with the debonding submodel utilised are shown in Figure 6.11 and the corresponding gas temperatures in Figure 6.12. Prior to debonding at 65 min, the predicted total HRR with GER = 1.3 provides a better match with the measured peak HRR in the experiment, whereas for the gas temperature, SMA with GER = 2.0 and SMC provide the better match due to predicted shorter times to reach the peak temperature. However, with respect to gas tem-

perature and fire severity, GER = 1.3 provides the more conservative prediction as seen in Figure 6.10. The corresponding comparisons for HRR and gas temperature with the debonding submodel included are shown in Figure 6.11 and Figure 6.12 respectively.

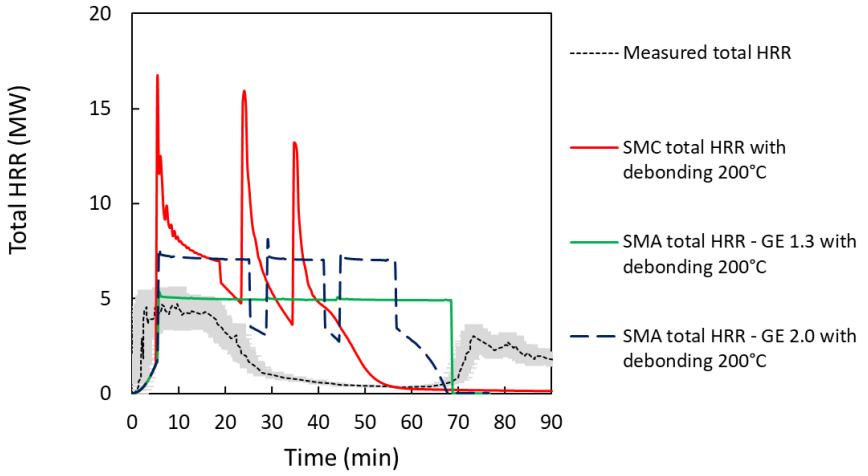

Figure 6.11: Measured and predicted total HRR for Config. C - with debonding.

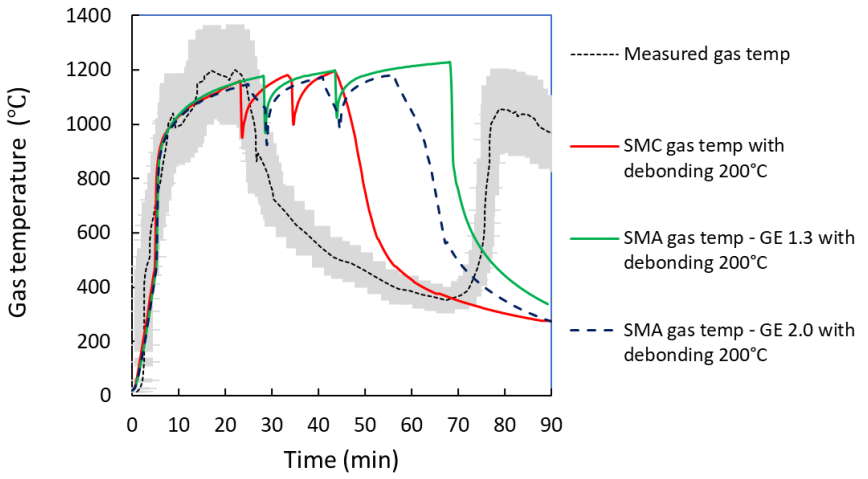

Figure 6.12: Measured and predicted enclosure gas temperatures for Config. C - with debonding.

The predicted debonding times (about 23-28 min) from both SMA and SMC when the 200°C criterion for temperature at the adhesive line is used is significantly less than the observed time in the experiment of about 65 min. The predicted char depths versus time are shown in Figure 6.13. Medina Hevia [157] reported char depths of 71 - 80 mm in the exposed CLT walls. The prediction using SMA and

utilising the debonding submodel is reasonable and conservative as shown in Figure 6.13.

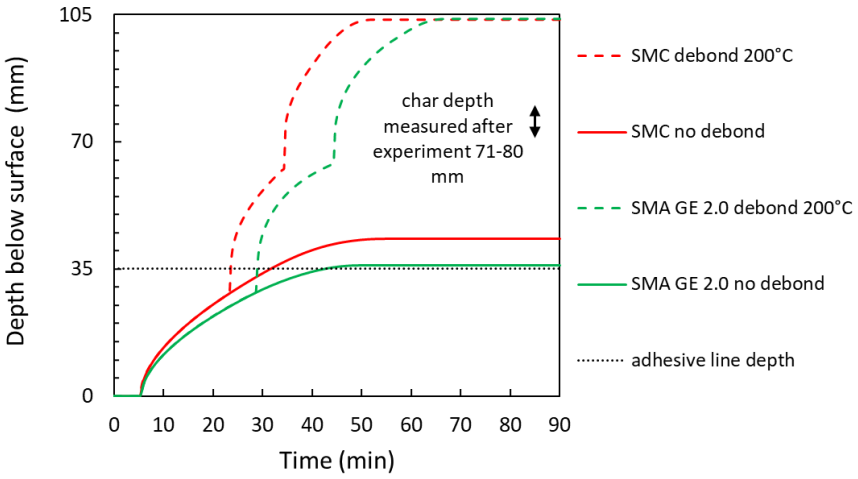

Figure 6.13: Config. C - Char depth in wall based on 300°C isotherm.

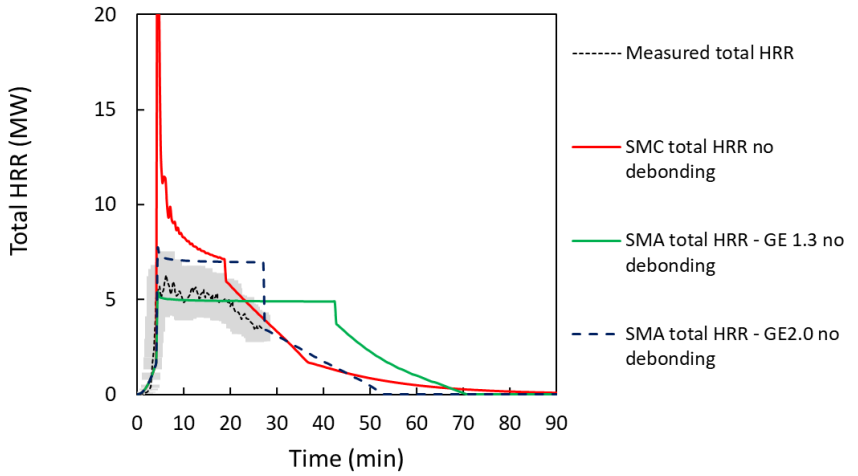

Figure 6.14: Measured and predicted total HRR for Config. D - without debonding.

6.2.5 *Config. D prediction - two opposite walls with timber exposed*

In this configuration, CLT panels on two opposite side walls were exposed representing 59.4% of the total wall surface area. Flashover was observed at about 4 min and was earlier than for Config C. The initial growth rate is set to $\dot{Q} = 0.029\alpha t^2$ (kW) to give a time to flashover that approximately matches the experiment. The furniture was reported to have been consumed by 16 min. Figure 6.14 and Fig-

ure 6.15 shows the measured and predicted total HRR without and with the debonding submodel included.

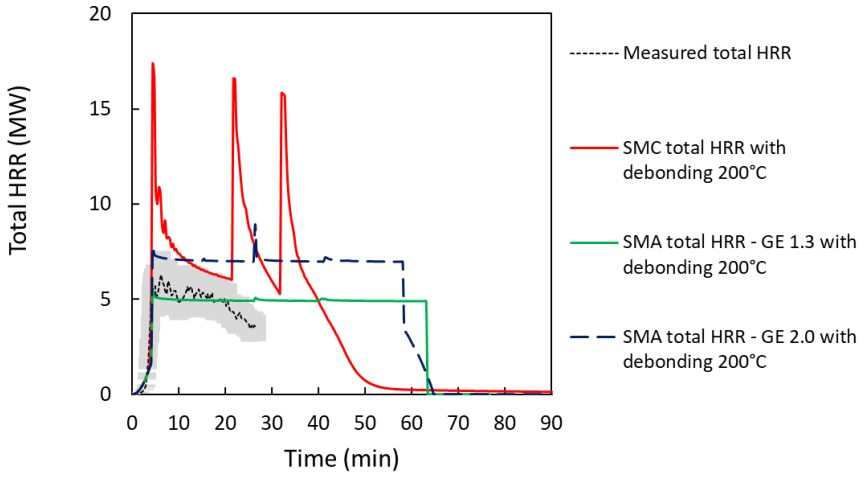

Figure 6.15: Measured and predicted total HRR for Config. D - with debonding.

The surface layer of CLT debonded during the experiment leading to a second flashover as illustrated by the increase in gas temperature after 45 min in Figure 6.16. Corresponding gas temperatures with the debonding submodel included are shown in Figure 6.17. The peak measured total HRR lies between the predicted values for SMA with GE 1.3 and SMA with GE 2.0 - with GE 1.3 again providing the more conservative prediction for the gas temperature and fire severity, but GE 2.0 better matching the measured data. There was a reported instrumentation failure in the HRR measurement around 30 min.

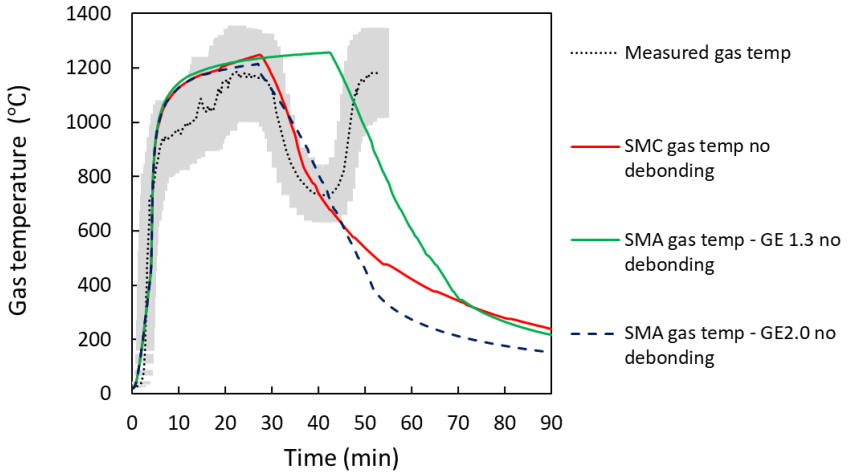

Figure 6.16: Measured and predicted enclosure gas temperatures for Config. D - without debonding.

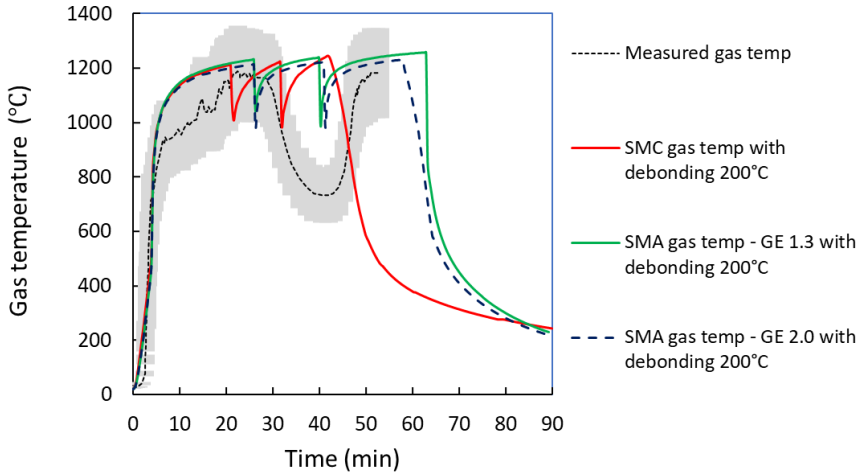

Figure 6.17: Measured and predicted enclosure gas temperatures for Config. D - with debonding.

The predicted char depths versus time are shown in Figure 6.18. Medina Hevia [157] reported char depths of 53 - 60 mm in the exposed CLT walls which was less than for the two adjacent walls in Config. C. The prediction using SMA and utilising the debonding submodel is reasonable and conservative as shown in Figure 6.18.

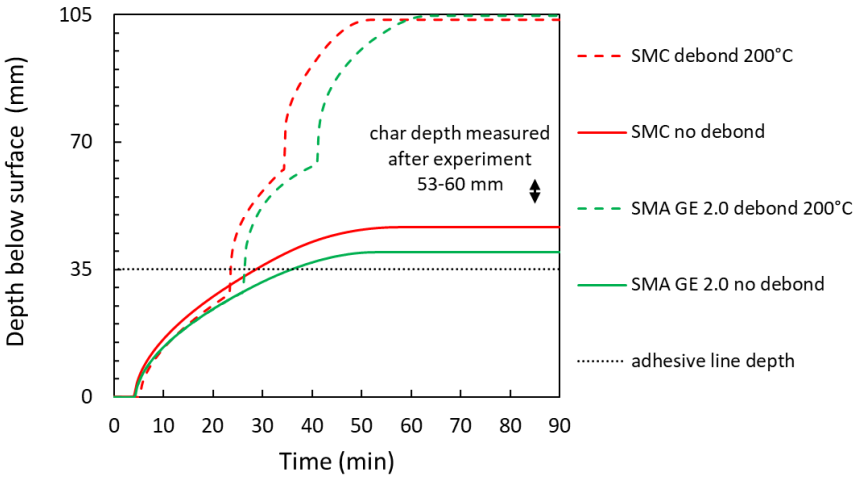

Figure 6.18: Config. D - Char depth in wall based on 300°C isotherm.

6.2.6 *Config. E prediction - one wall with timber exposed*

In this configuration, CLT panels on the rear wall were exposed representing 29.7% of the total wall surface area. The initial growth rate is set to $\dot{Q} = 0.029\alpha t^2$ (kW) to give a time to flashover that approximately matches the experiment. Figure 6.19 shows the measured and

predicted heat release rate without debonding and Figure 6.20 shows the same with the debonding submodel included. Debonding was not observed in this experiment, however is predicted to occur if a debonding temperature of 200°C is specified with either the SMA or SMC submodels.

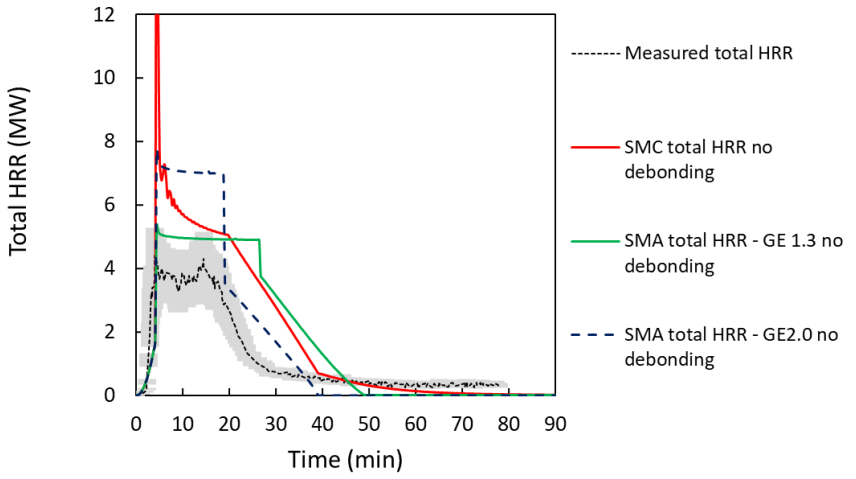

Figure 6.19: Measured and predicted total HRR for Config. E - without debonding.

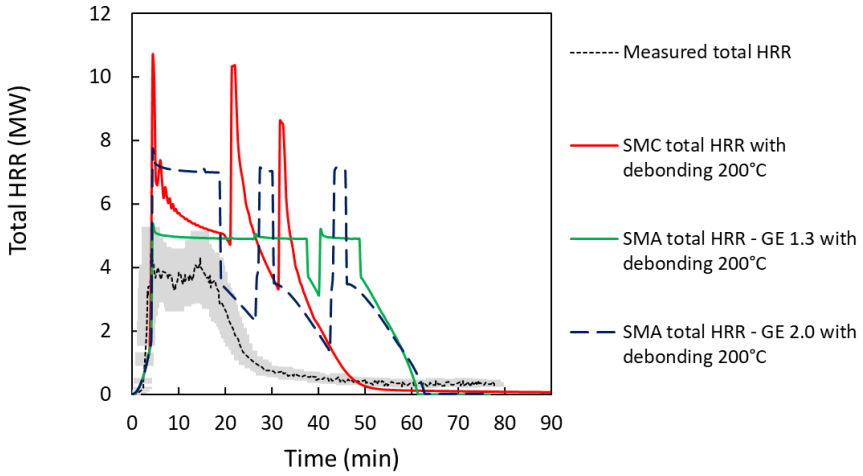

Figure 6.20: Measured and predicted total HRR for Config. E - with debonding.

Figure 6.21 and Figure 6.22 show the measured and predicted gas temperature without and with debonding respectively for SMA with GE 1.3 and GE 2.0.

The predicted char depths versus time are shown in Figure 6.23. Medina [157] reported char depths of 21 - 44 mm in the exposed

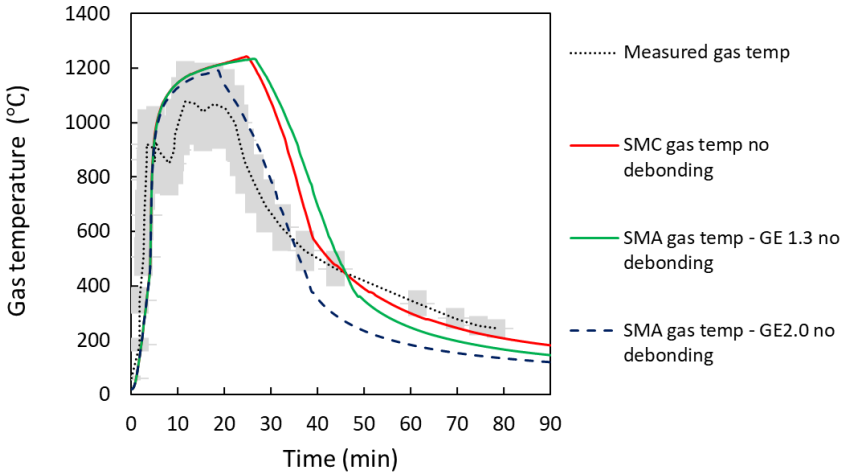

Figure 6.21: Measured and predicted enclosure gas temperatures for Config. E - without debonding.

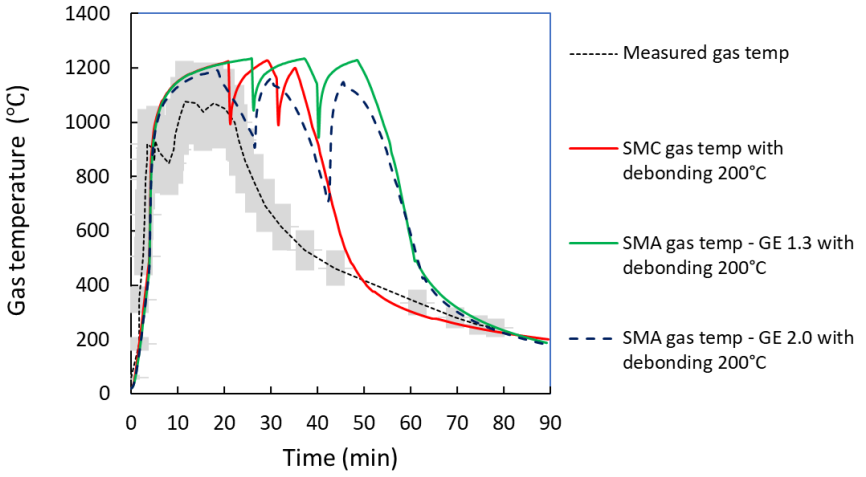

Figure 6.22: Measured and predicted enclosure gas temperatures for Config. E - with debonding.

CLT wall. The prediction using SMA and utilising the debonding sub-model is reasonable and conservative as shown in Figure 6.23.

6.3 EDINBURGH UNIVERSITY EXPERIMENTS (CONFIG. F-H)

6.3.1 *Description*

These configurations were investigated by Hadden et al. [165] in a room measuring 2.72 × 2.72 × 2.77 m high with an opening 1.84 m high and 0.76 m wide as summarised in Table 6.1. The timber used in these experiments was a CLT panel comprising five layers of spruce

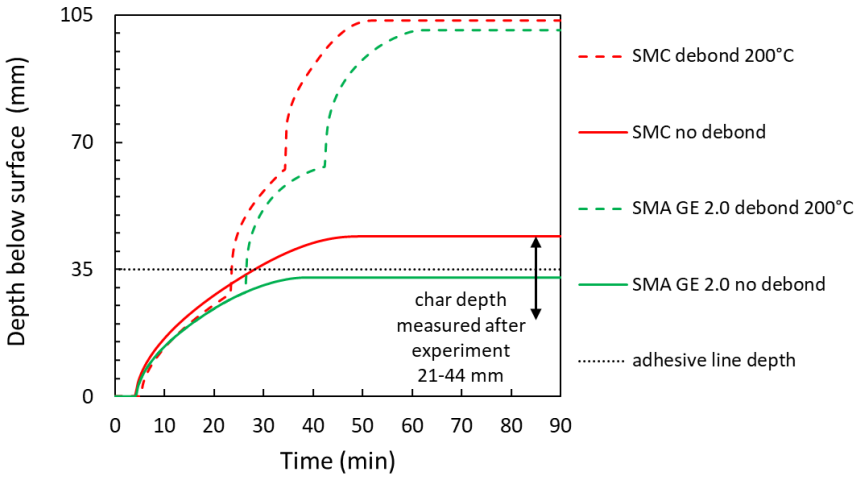

Figure 6.23: Config. E - Char depth in wall based on 300°C isotherm.

wood bonded with a polyurethane adhesive. The total panel thickness was 100 mm, and each layer (lamella) had a uniform thickness of 20 mm. The thermal properties for room materials were as given by Hadden et al. as shown previously in Table 6.2.

The contents fuel load was four wood cribs, with each crib consisting of five layers of sticks of cross-section 25 × 25 mm at a spacing 75 mm. The total mass of timber was approximately 56 kg in each experiment. Assuming an effective heat of combustion of 14 MJ/kg, the wood crib fuel load is estimated to be 106 MJ/m^2. The initial growth rate is set to $\dot{Q} = 0.014\alpha t^2$ (kW) for this set of simulations. A typical interior view of the enclosures is shown in Figure 6.24.

6.3.2 *Config. F prediction - rear and one side wall with timber exposed*

This configuration was designated 'Alpha' by Hadden et al. [165] and had CLT panels on the rear wall and one side wall exposed. The experiment was repeated with a change made to the protection system such that, for Alpha-1, the gypsum plasterboard protection was fixed directly over the timber surfaces, while for Alpha-2, stone wool insulation was installed between the plasterboard and the timber. Plasterboard was observed to fall during both experiments, but previously protected timber surfaces only contributed to the fire after falling off occurred for experiment Alpha-1.

In experiment Alpha-2, pieces of gypsum plasterboard started to fall from 25 min, but none of the protected timber contributed to the fire. Following the first peak in HRR and decline, the HRR increased again from 32.4 min. This was attributed to debonding of the surface layer. Figure 6.25 shows the measured and predicted heat release rate. Figure 6.26 shows the measured and predicted gas tem-

Figure 6.24: View inside a typical enclosure prior to ignition. Reprinted from Hadden et al. [165] under a Creative Commons License.

perature. While the GE 2.0 assumption matches the peak total HRR more closely, GE 1.3 provides a better prediction for the gas temperature history up until the time debonding was observed.

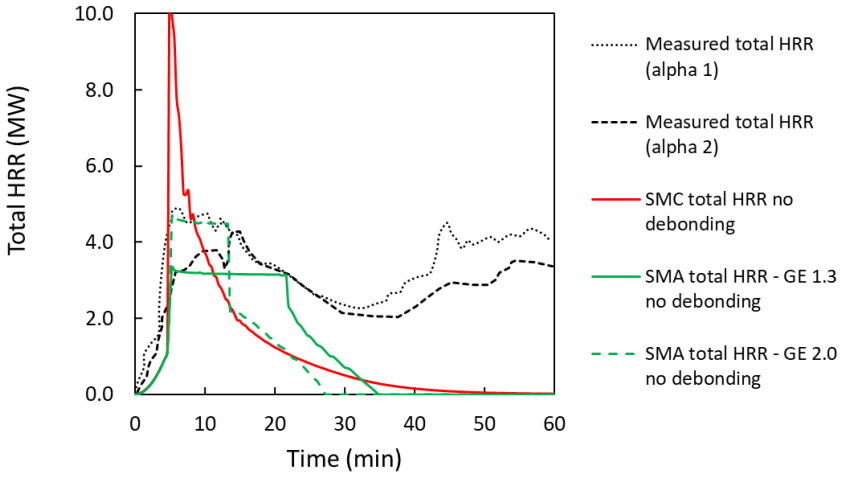

Figure 6.25: Measured and predicted total HRR for Config. F - without debonding.

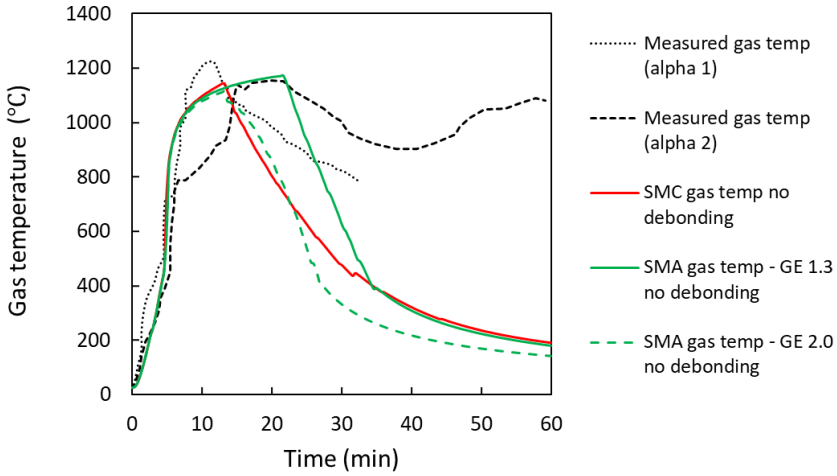

Figure 6.26: Measured and predicted gas temperature for Config. F - without debonding.

The HRR curves with the debonding submodel utilised are shown in Figure 6.27 and the corresponding gas temperatures in Figure 6.28.

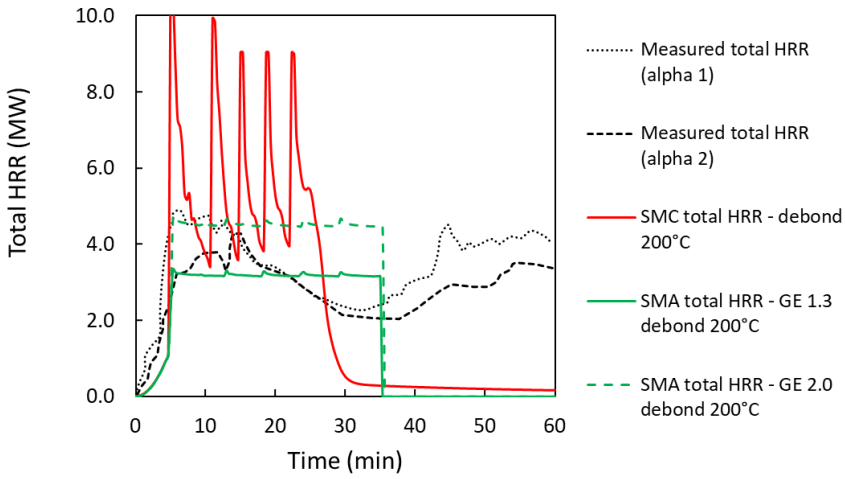

Figure 6.27: Measured and predicted total HRR for Config. F - with debonding.

Based on the predicted time for the temperature at the adhesive line to reach 200°C, debonding is predicted to occur at about 15.5 min for the GER 1.3 case. This is earlier than observed in the experiment. The predicted gas temperatures in the enclosure prior to the time of predicted debonding agree well with the experiment.

Hadden et al. [165] reported that the maximum char depth in the exposed timber was 53 mm after 60 min. Figure 6.29 shows the predicted char depth versus time for submodels and SMA and SMC without debonding and with debonding for SMA with GE 2.0. Simulations were made using a debond temperature of 200°C and 300°C. It

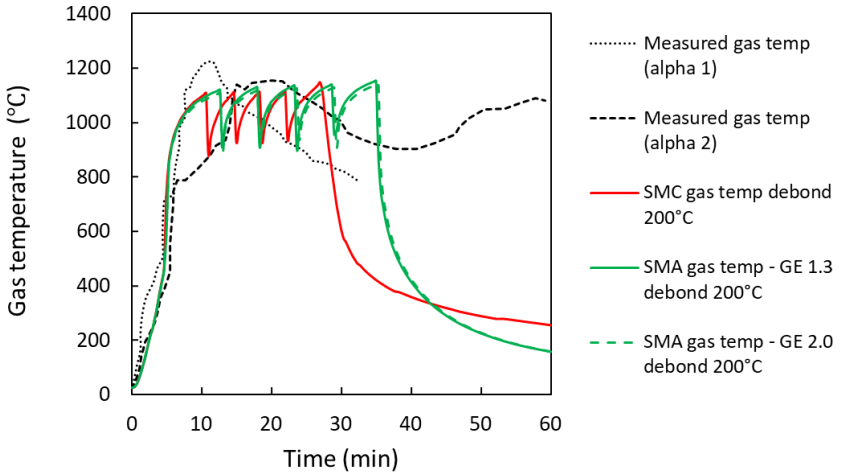

Figure 6.28: Measured and predicted gas temperature for Config. F - with debonding.

can be seen that the debonding submodel predicts the exposed wall to be completely charred through with a charring rate that is more rapid than measured in the experiment.

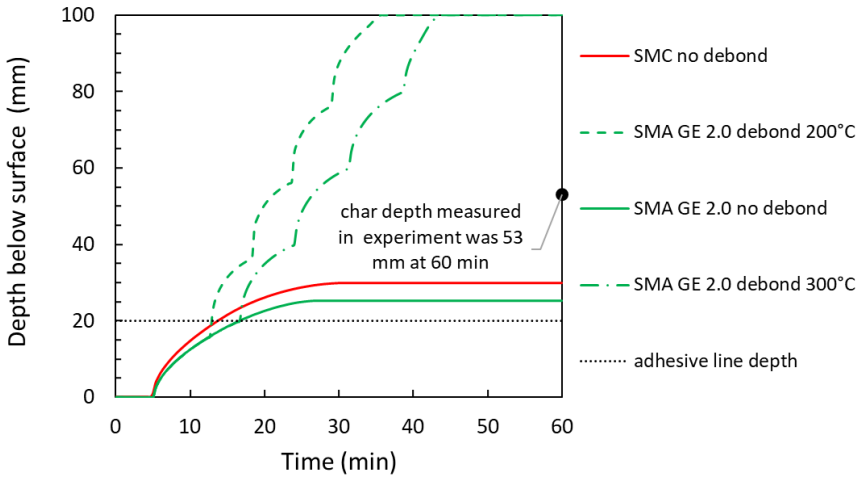

Figure 6.29: Config. F - Char depth in wall based on 300°C isotherm.

6.3.3 *Config. G prediction - rear wall and ceiling with timber exposed*

This configuration was designated 'Beta' by Hadden et al. [165] with CLT panels on the ceiling and rear wall exposed. The experiment was repeated (designated Beta-1 and Beta-2). The different behaviour observed for the repeated experiments was attributed by Hadden et al. to the uncertainties in the duration of the enclosure fire. Figure 6.30 shows the measured and predicted heat release rate. Fig-

ure 6.31 shows the measured and predicted gas temperature (without debonding). Both the SMA GE 2.0 and SMC submodels provide good agreement with the gas temperatures prior to when debonding was observed.

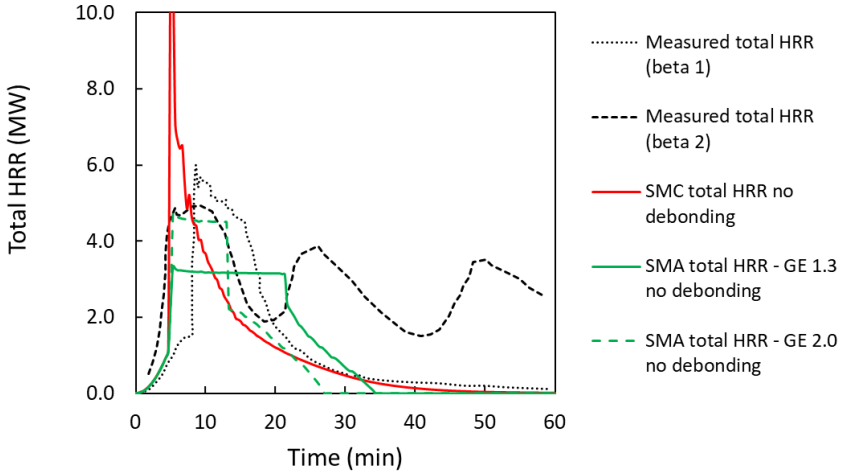

Figure 6.30: Measured and predicted total HRR for Config. G - without debonding.

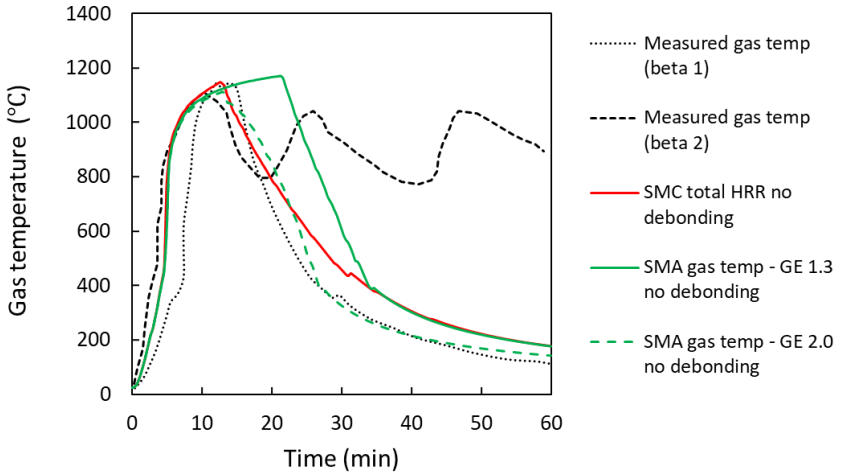

Figure 6.31: Measured and predicted gas temperature for Config. G - without debonding.

Figure 6.32 and Figure 6.33 show the predicted HRR and gas temperatures respectively with the debonding submodel included. Submodel SMA predicts debonding at about 16 min compared to about 20 min in experiment Beta-2. In Figure 6.33 the time between successive temperature peaks for experiment Beta-2 was about 15 min however it is half this time for the SMA predictions, with debonding

occurring every 6 min or so until the char penetrates the full depth of the wall.

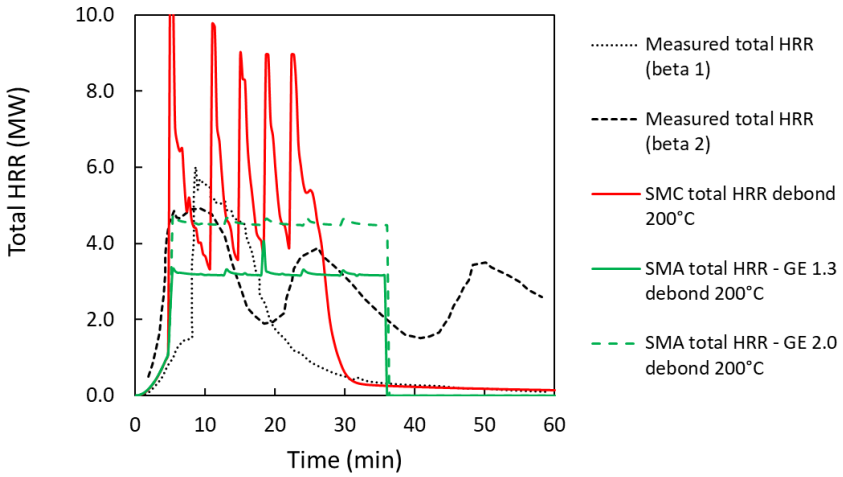

Figure 6.32: Measured and predicted total HRR for Config. G - with debonding.

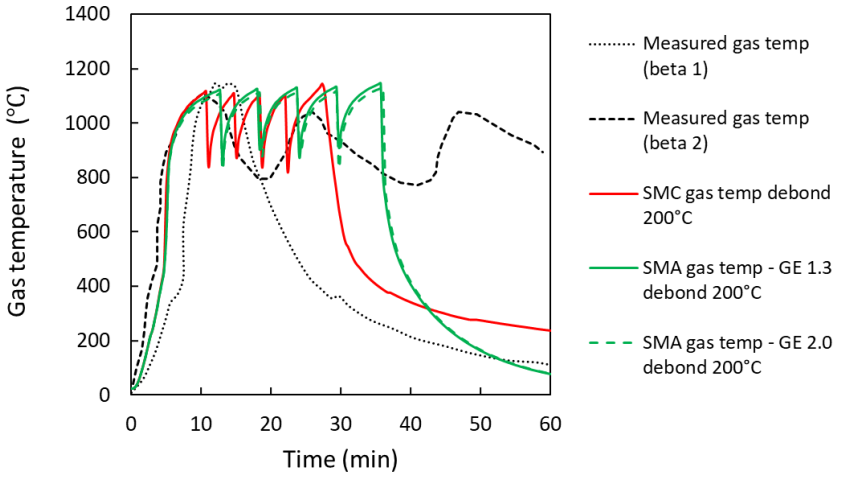

Figure 6.33: Measured and predicted gas temperature for Config. G - with debonding.

The maximum char depth measured in experiment Beta-1 and Beta-2 after 60 min was 11 mm and 44 mm respectively [165]. Figure 6.34 shows the predicted char depth versus time for submodels and SMA and SMC without debonding and with debonding for SMA with GE 2.0. Simulations are made using a debond temperature of 200°C and 300°C. As was the case for Config. F, it can be seen that the debonding submodel predicts the exposed wall to be completely charred through with a charring rate that is more rapid than measured in the experiment.

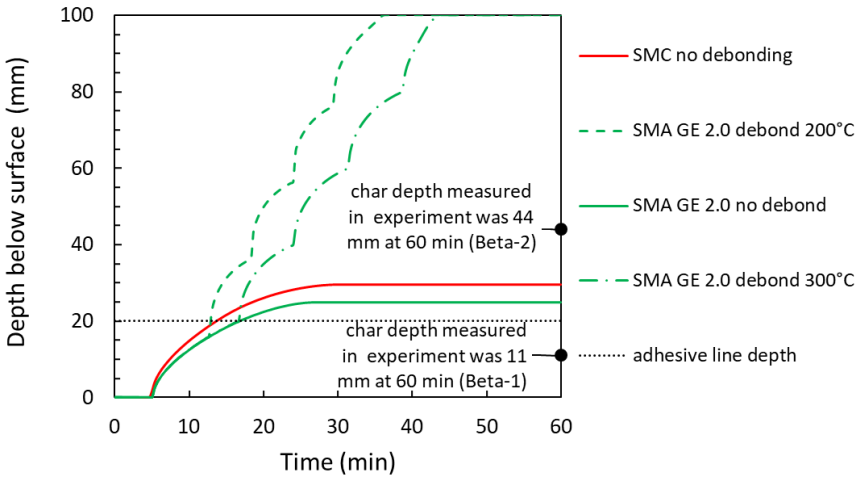

Figure 6.34: Config. G - Char depth in wall based on 300°C isotherm.

6.3.4 *Config. H prediction - rear, side wall and ceiling with timber exposed*

This configuration was designated 'Gamma-1' by Hadden et al. [165] with CLT panels on the ceiling, rear wall and one side wall exposed. Figure 6.35 shows the measured and predicted total heat release rate. Figure 6.36 shows the measured and predicted gas temperature. Again SMC and SMA GE 2.0 both provide good agreement with the experiment up until the time debonding and regrowth in the fire was observed.

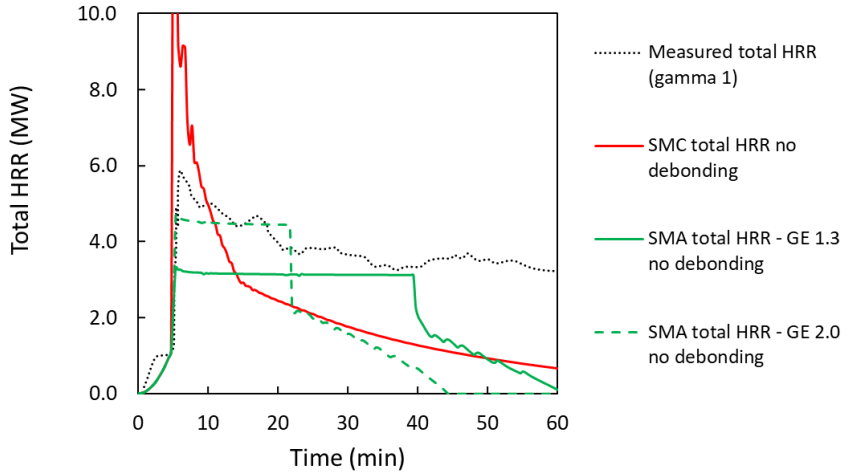

Figure 6.35: Measured and predicted total HRR for Config. H - without debonding.

Figure 6.37 and Figure 6.38 show the predicted HRR and gas temperatures respectively with the debonding submodel included. The predicted time for the 200°C isotherm to reach the adhesive line is

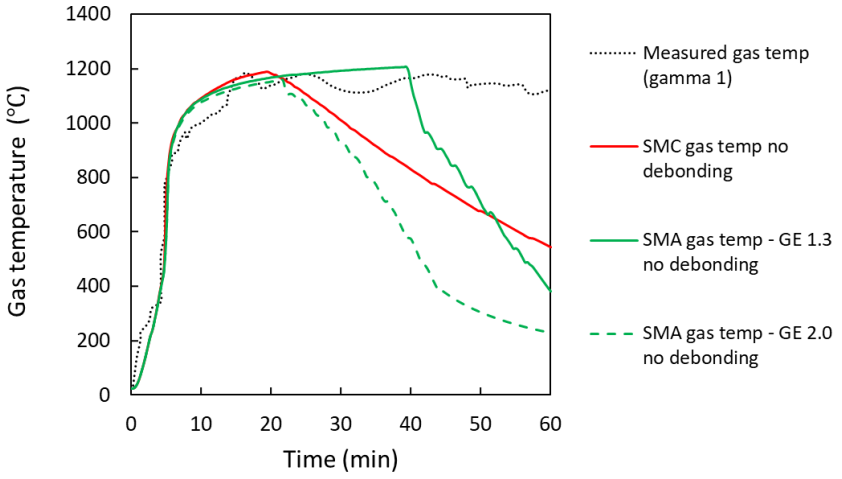

Figure 6.36: Measured and predicted gas temperature for Config. H - without debonding.

about 16 min for SMA and about 13 min for SMC. This is the same as for Config. G. For this configuration, Hadden et al. [165] indicated that the critical heat flux for sustained burning and continued pyrolysis was able to be maintained within the enclosure was due to radiative exchange between the surfaces. This meant the effect of debonding was not as distinctly obvious in the measured gas temperature Figure 6.36 when compared with Config. G.

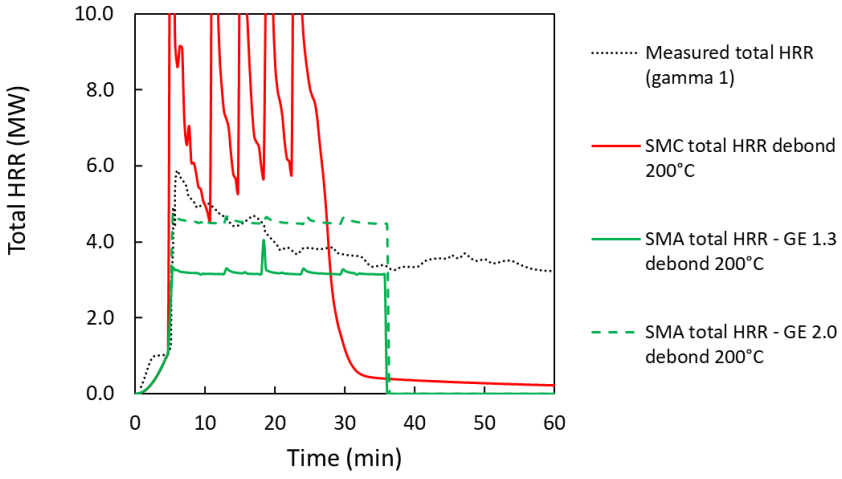

Figure 6.37: Measured and predicted total HRR for Config. H - with debonding.

The maximum char depth measured in experiment Gamma-1 after 60 min was 58 mm [165]. This is compared with the predicted char depth for SMA and SMC in Figure 6.39. As for the Config. F and Config. G, the debonding submodel predicts debonding of successive

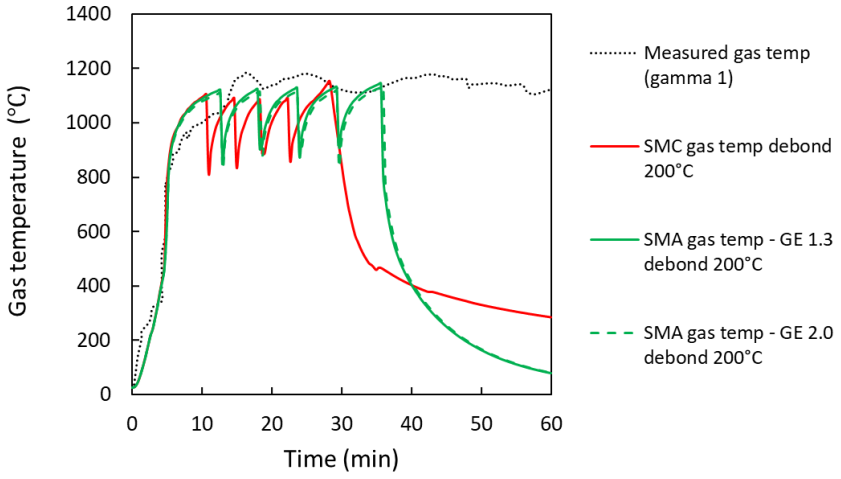

Figure 6.38: Measured and predicted gas temperature for Config. H - with debonding.

lamella at a faster rate than is observed in the experiment. This could indicate that the assumed debonding temperature of 200°C is too low and/or that the calculation of the heat conduction into the wall is not sufficiently accurate.

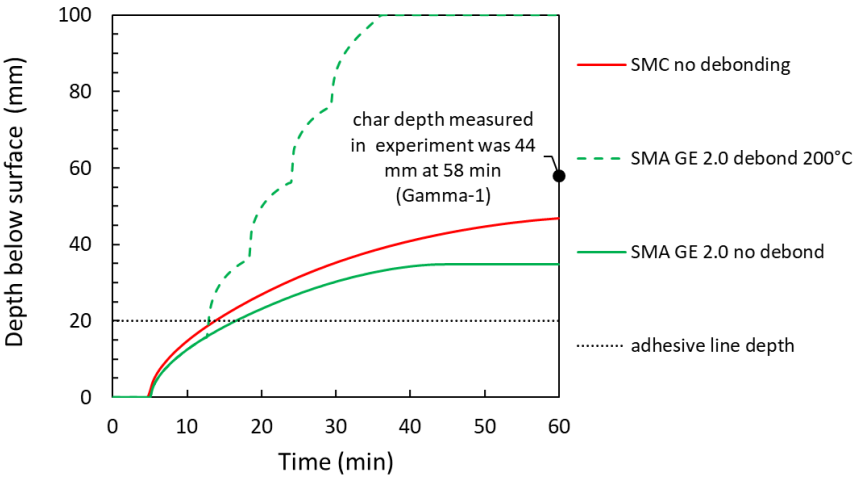

Figure 6.39: Config. H - Char depth in wall based on 300°C isotherm.

6.4 FPRF/NRCC EXPERIMENTS (CONFIG. I-N)

6.4.1 *Description*

These configurations were reported by Su et al. [168] in a room measuring 9.1 × 4.6 × 2.7 m high with an opening 2.0 m high and either 1.8 or 3.6 m wide as summarised in Table 6.1. These enclosures were

intended to represent a studio sized apartment unit. In addition to these openings, there were two additional small openings in the opposite (rear) wall. Each one was 150 mm diameter and positioned 0.3 m and 1.8 m above the floor. These were intended to simulate leakage of gases through a protected entrance doorway.

All rooms were constructed from CLT panels 175 mm thick and comprising five lamellae each 35 mm thick and manufactured from spruce-pine-fir lumber. The lamellae were adhered with a one component polyurethane adhesive (with a brand name of HBE). The panels were stated to conform to American National Standard ANSI/APA PRG-320-2012 [253].

The fuel load comprised mostly cellulosic furniture (white pine, hardboard and douglas fir) with a small amount of polyurethane foam (about 3% by mass) which was intended to provide a FLED of 550 MJ/m^2. Closer inspection of the report revealed the average heat of combustion assumed was 19.7 MJ/kg which was unlikely to have been the effective heat combustion realised in the experiments during the flaming stage as there was no allowance for a combustion efficiency (see also Section 5.3.2). Therefore, for the simulations reported here the FLED was downgraded to 391 MJ/m^2 to correspond to an average effective heat of combustion of 14 MJ/kg as discussed in Section 5.3.2. A view of the fuel load is shown in Figure 6.41 and the layout in Figure 6.40. For this series of experiments, the gas temperature presented in the figures is the average reading from the four thermocouples located on tree 3 opposite the opening over the height range 1.1 to 2.6 m above the floor.

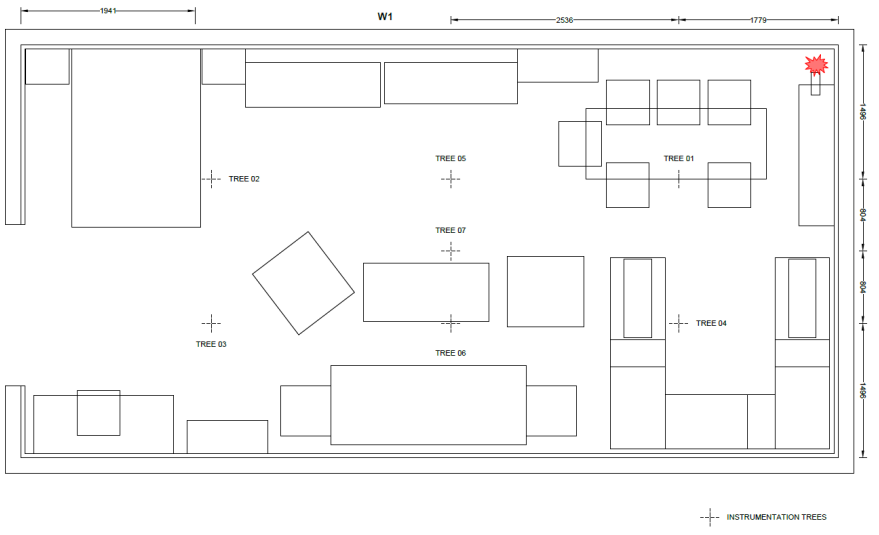

Figure 6.40: Configs. I - N. Layout of room contents showing location of instrumentation trees. Reprinted from [168] with permission.

Figure 6.41: Configs. I - N. View of room contents. Reprinted from [168] with permission.

6.4.2 *Config. I prediction - timber fully protected*

This configuration was referred to as Test 1-1 by Su et al [168]. There was an opening 1.8 m wide × 2.0 m high in one wall. Walls and ceiling were fully protected with 3 layers of 15.9 mm Type X gypsum plasterboard. The t^2 growth rate coefficient used is 0.0037 kW/s^2 to approximately match the experimental time to reach 500°C (flashover). The experiment is modelled assuming both the walls and ceiling were 175 mm thick wood covering with 48 mm of gypsum plasterboard.

Figure 6.42 shows the measured and predicted gas temperatures and Figure 6.43 shows the measured and predicted total rate of heat release. In both cases the agreement between the model and the measured values is considered to be very good. Since neither of the wood surface pyrolysis submodels are required for these simulations the model results reflect the underlying performance of the fire model. The model results indicate a short period of ventilation-controlled burning after flashover followed by a fuel-controlled regime in the decay phase. The user specified GE ratio influences the burning rate of the room contents with either GE 1.0 or GE 1.3 appearing to provide acceptable results in comparison with the measured data. GE 2.0 is too high for this experiment where there was no contribution from the surface linings and confirms that GE 1.3 is a reasonable default value to use in the model.

6.4.3 *Config. J prediction - timber fully protected*

This configuration was referred to as Test 1-2 by Su et al [168]. There was an opening 3.6 m wide × 2.0 m high. The walls and ceiling were fully protected with 2 layers of 15.9 mm Type X gypsum plasterboard. The t^2 growth rate coefficient used was 0.0052 kW/s^2 to approximately match the experimental time to reach 500°C (flashover). This configuration differed from Config. I by having double the area of ventilation for the largest opening. Flashover occurred at 15.3 min fol-

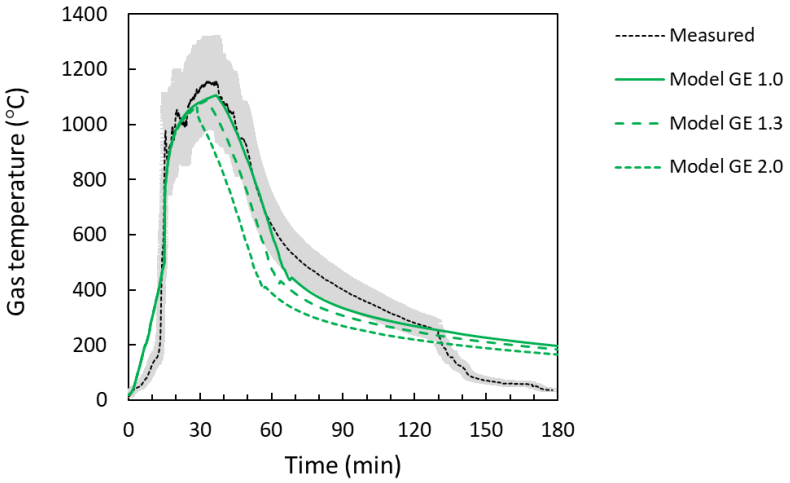

Figure 6.42: Config. I - measured and predicted gas temperature.

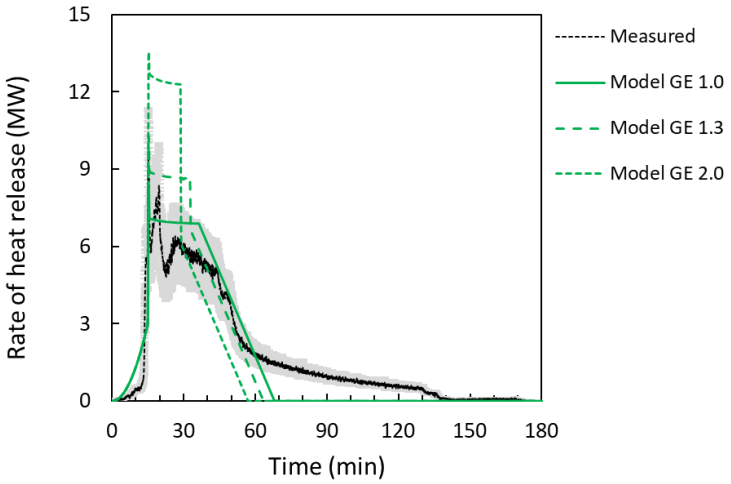

Figure 6.43: Config. I - measured and predicted total heat release rate.

lowed by a large external fire plume. The fire started to decay at 37 min and external flaming ceased from 40 min.

The model prediction of the peak gas temperature is clearly lower than measured in this experiment as seen in Figure 6.44 unlike for Config. I where a good prediction of the peak gas temperature is achieved. On the other hand the prediction of the total rate of heat release appears in good agreement as seen in Figure 6.45. The model considered this experiment to be fuel surface area controlled and not ventilation limited unlike Config. I. where a period of ventilation controlled burning of about 20 minutes duration is apparent from the plateau in the predicted rate of heat release curve (Figure 6.43). The poor agreement for the gas temperature might be interpreted as suggesting that the fuel surface controlled (free-burning) mass loss rate

for the wood cribs was not a good representation of the real furniture used in this experiment.

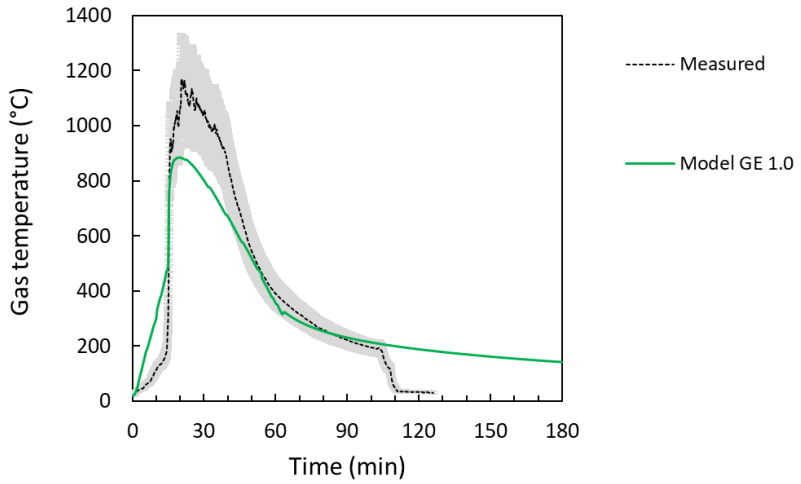

Figure 6.44: Config. J - measured and predicted gas temperature.

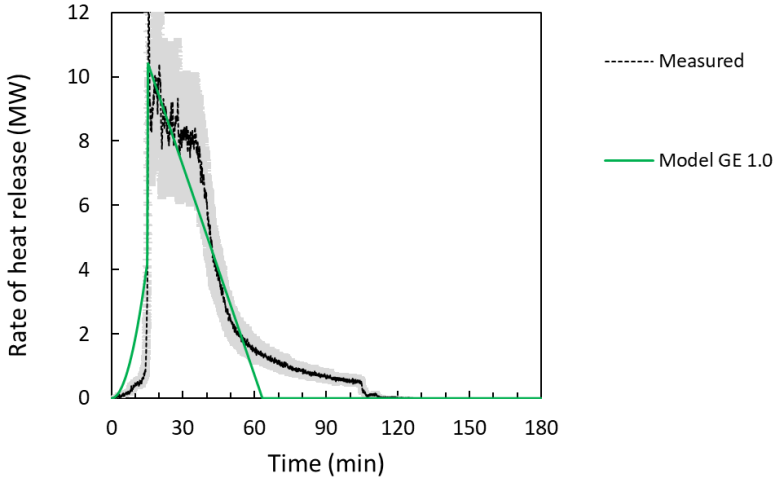

Figure 6.45: Config. J - measured and predicted total heat release rate.

6.4.4 *Config. K prediction - one wall with timber exposed*

This configuration was referred to as Test 1-3 by Su et al [168]. There was an opening 3.6 m wide × 2.0 m high (the same as Config. J). One wall was exposed (33%) with the remainder protected with 2 layers of 15.9 mm Type X gypsum plasterboard. The ceiling was fully protected with 3 layers of 15.9 mm Type X gypsum plasterboard. The t^2 growth rate coefficient used is 0.0083 kW/s^2 to approximately match the experimental time to reach 500°C (flashover).

Figure 6.46 shows the measured and predicted gas temperatures and Figure 6.47 shows the measured and predicted total rate of heat release. The predicted gas temperature curve for GE ratios of 1.3 and 2.0 are identical indicating that the model treats this experiment as fuel surface area controlled (as previously noted also for Config. J) and not ventilation limited. This is consistent with using Equation 2.1 and an assumed heat of combustion of 14 MJ/kg which gives 12.8 MW for ventilation controlled HRR for a 3.6 × 2.0 m high opening and which wasn't quite reached in the experiment. The peak gas temperature predicted from SMA is also lower than the measured temperature by at least 100°C. On the other hand the prediction of the total rate of heat release appears comparable. SMC matches the peak gas temperature more closely.

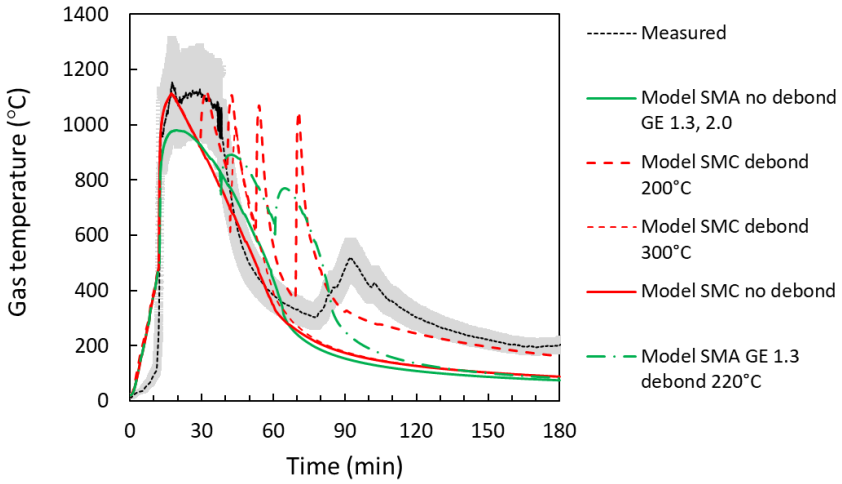

Figure 6.46: Config. K - measured and predicted gas temperature.

Char depth was measured in the exposed CLT wall at heights of 0.6, 1.1 and 1.6 m after the experiment and were found to be in the range 60-85 mm [168]. This is shown is Figure 6.48 along with the predicted char depths using submodel SMC with and without the debonding submodel. SMA with an assumed debonding temperature of 200°C resulted in a final char depth of 126 mm - well in excess of the maximum measured value of 85 mm. An assumed debonding temperature of 220°C gives a final char depth of 93 mm, however if a debonding temperature of 300°C is used the predicted final char depth is only 34 mm, only 1 mm short of reaching the adhesive line meaning no debonding is predicted. Therefore, final char depths can be very sensitive to the assumed debonding temperature for the adhesive used.

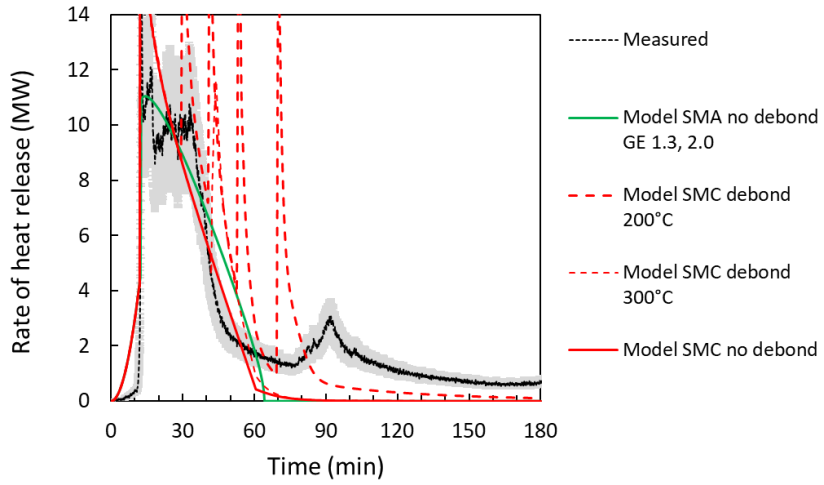

Figure 6.47: Config. K - measured and predicted total heat release rate.

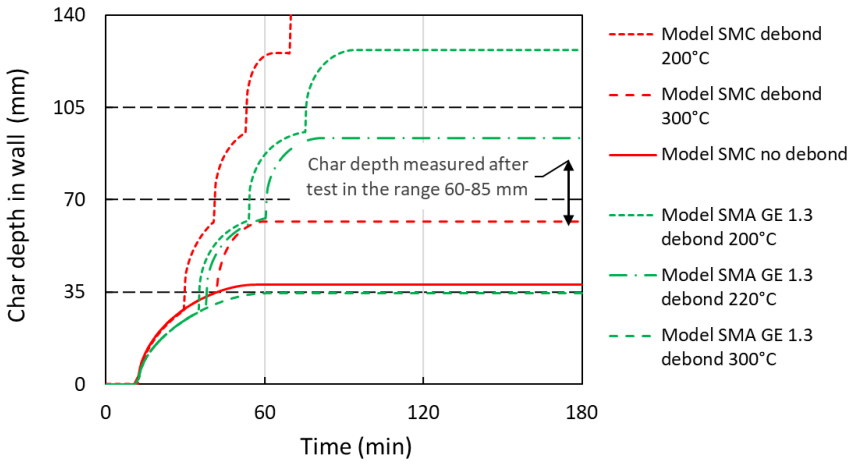

Figure 6.48: Config. K - measured and predicted char depth.

6.4.5 *Config. L prediction - ceiling with timber exposed*

This configuration was referred to as Test 1-4 by Su et al [168]. There was an opening 1.8 m wide × 2.0 m high (the same as Config. I). The walls were fully protected with 3 layers of 15.9 mm Type X gypsum plasterboard. The ceiling was fully exposed. The t^2 growth rate coefficient used is 0.0037 kW/s^2 to match Config. I. Flashover occurred at 11.5 min with the exposed ceiling fully involved. The fire started to decay at 75 min after the charred first lamella of the CLT panels fell off the ceiling. At 85 min external flaming ceased and oxygen volume fraction returned to above 15% in the enclosure. The enclosure temperatures kept decreasing until 140 min. The test was terminated by manual fire suppression at 159 min after the second lamella of the CLT panels fell from the ceiling at about 150 min and the third

lamella became involved. After the test two and half lamellae of CLT were lost at the centre of the ceiling [168].

The simulations assumed the ceiling and walls were both 175 mm thick wood comprising 5 layers each 35 mm thick however only the ceiling contributed to the fire. Figure 6.49 shows the measured and predicted gas temperatures and Figure 6.50 shows the measured and predicted total rate of heat release. Submodel SMA with GE 1.3 appears to most closely match the measured gas temperature and total heat release rate. The submodels SMA with GE 2.0 and SMC both predict a similar time to peak burning that is quicker than observed in the experiment.

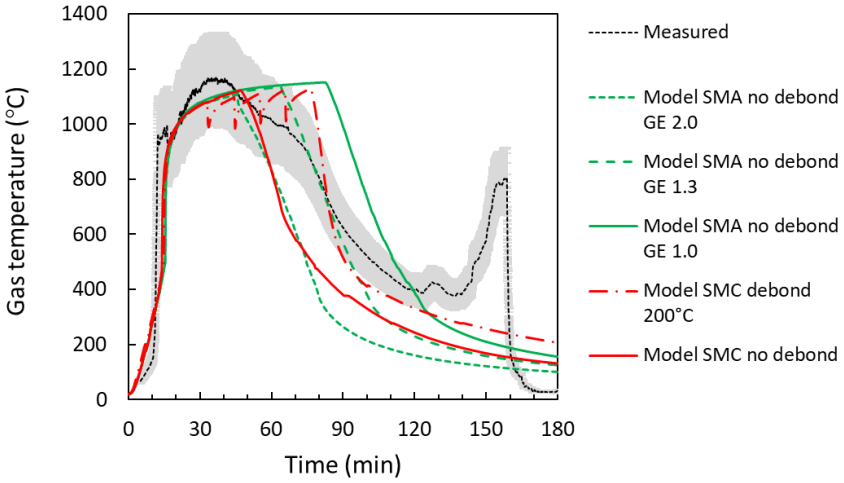

Figure 6.49: Config. L - measured and predicted gas temperature.

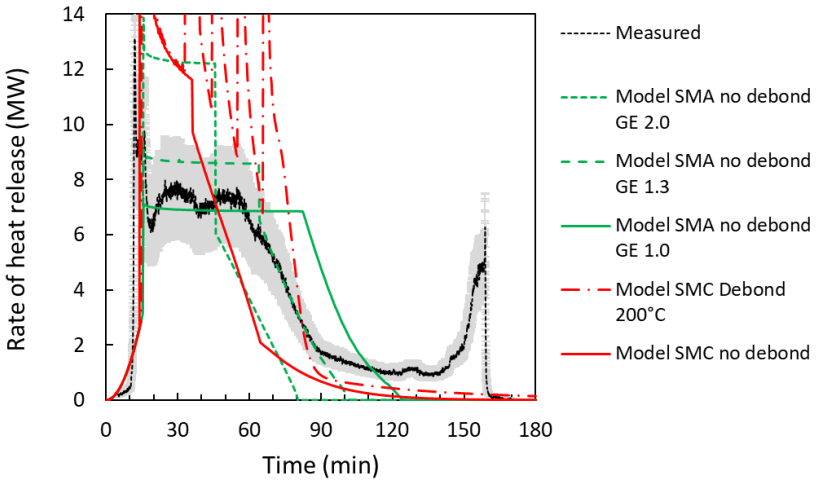

Figure 6.50: Config. L - measured and predicted total heat release rate.

After the test the depth of char in the ceiling panels was determined to be in the range 66 to 90 mm. This is shown is Figure 6.51 along with the predicted char depths using submodel SMC with and without the debonding submodel.

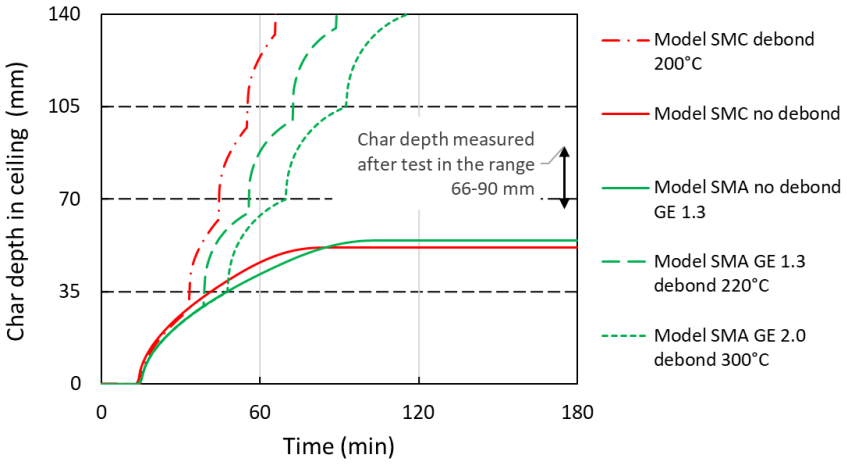

Figure 6.51: Config. L - measured and predicted char depth.

The simulations with the debonding submodel give char rate predictions that are too quick compared to the measured data and this becomes more apparent as the temperature at the adhesive line reaches the specified debonding temperature and each successive lamella is predicted to fall away. This is expected to be a result of the simplying assumption that each layer is removed from the entire surface at the debonding time. In reality the process of debonding is a much more progressive one occurring over a longer timeframe. Debonding may still need to be included in the model, at least for CLT where a thermal resistive adhesive has not been used, as ignoring the phenomenon in these cases would be non conservative.

6.4.6 *Config. M prediction - one wall with timber exposed*

This configuration was referred to as Test 1-5 as reported by Su et al [168] and a short summary of their observations follow. There was an opening 1.8 m wide × 2.0 m high (the same as Config. I and Config. L). The walls and ceiling were fully protected with 3 layers of 15.9 mm Type X gypsum plasterboard except for one wall representing 33% of the total wall area left exposed. The t^2 growth rate coefficient used is 0.0037 kW/s^2 to match Config. I. In the experiment, flashover occurred at 11.5 min followed by a large external fire plume. The contents were consumed by 40 min but the exposed wall continued to burn. From 52 min to 75 min pieces of the first lamella of the exposed wall was observed to gradually fall away. External flaming ceased at 67 min. The second lamella continued to burn until 100 min. From 100

to 130 min there was little visible flame on the exposed wall but from 130 to 140 minutes flaming resumed. At 140 min external flaming also resumed. The gypsum board protection started to fail with the ceiling contributing from 150 min and the other walls became fully involved from 185 min after their protection fell off. The experiment was manually suppressed at 202 minutes. Key events with room gas temperature are shown in Figure 6.52.

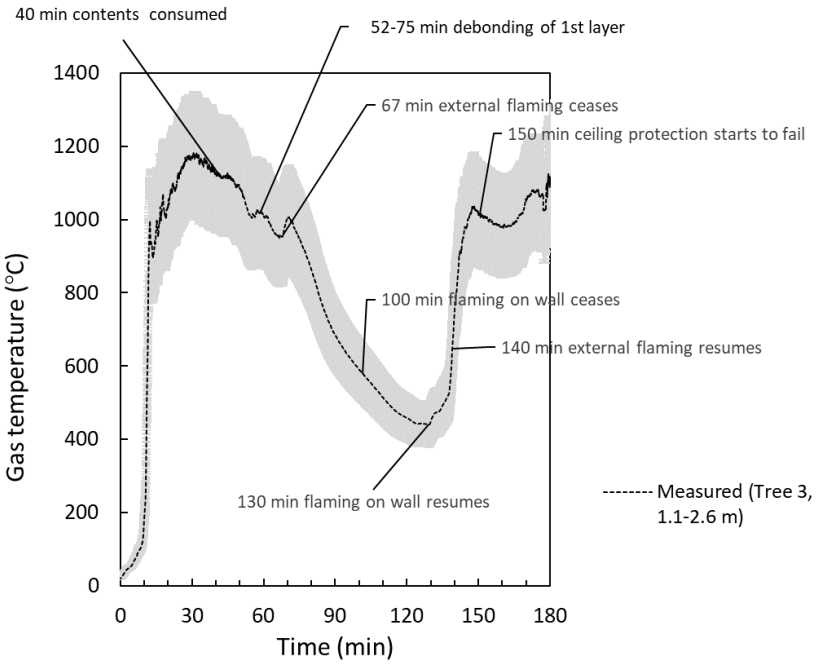

Figure 6.52: Config. M - Measured gas temperature with key events.

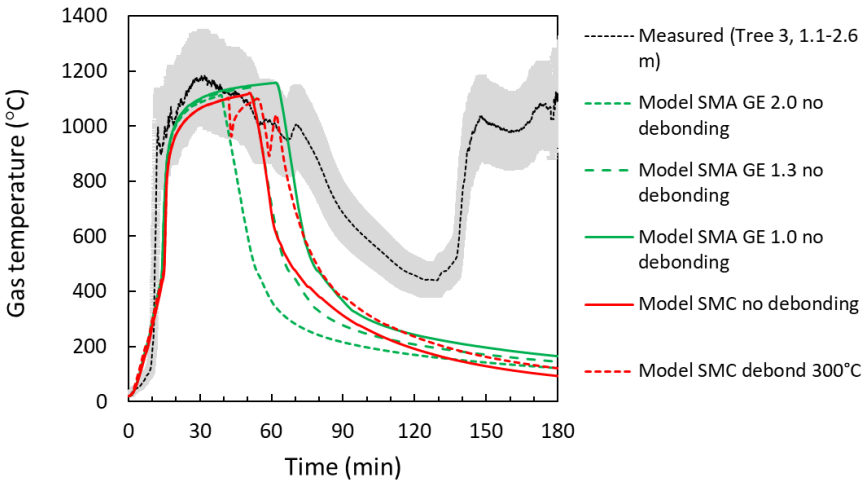

Figure 6.53: Config. M - measured and predicted gas temperature.

It is noted that debonding of the first lamella is occurring after the room contents have mostly burned out and with the fire starting to return to fuel-surface control. Since only a small part of the wall was exposed to start with, the regrowth in the fire is not very apparent from the gas temperature measurements during this phase of the fire.

The simulations assume the ceiling is 48 mm thick plasterboard and the walls are modelled as 175 mm thick wood comprising 5 lamella each 35 mm thick. Figure 6.53 shows the measured and predicted gas temperatures and Figure 6.54 shows the measured and predicted total rate of heat release. The prediction for submodel SMC with debonding at 300°C is also included.

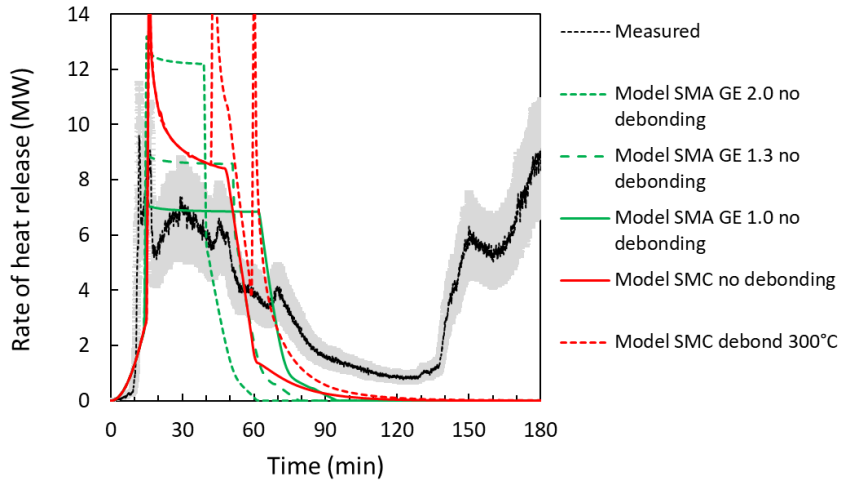

Figure 6.54: Config. M - measured and predicted total heat release rate.

The failure of gypsum plasterboard protection during the experiment, which is not accounted for in the model is partly responsible for the variation between measured and predicted gas temperature and heat release rate. After the test, the depth of char in the wall was measured to be in the range 102 to 141 mm. This is shown in Figure 6.55 along with the predicted char depths. The char depth predictions for the submodel SMC for debonding temperatures of both 200°C and 300°C is shown and clearly demonstrates the sensitivity of the char depth prediction to the debonding behaviour and if and when it occurs.

6.4.7 *Config. N prediction - one wall and ceiling with timber exposed*

This configuration was referred to as Test 1-6 as reported by Su et al [168]. There was an opening 1.8 m wide × 2.0 m high (the same as Config. I, L and M). The ceiling and one wall was fully exposed with the remaining walls protected with 3 layers of 15.9 mm Type X gypsum plasterboard. Again the t^2 growth rate coefficient used is 0.0037

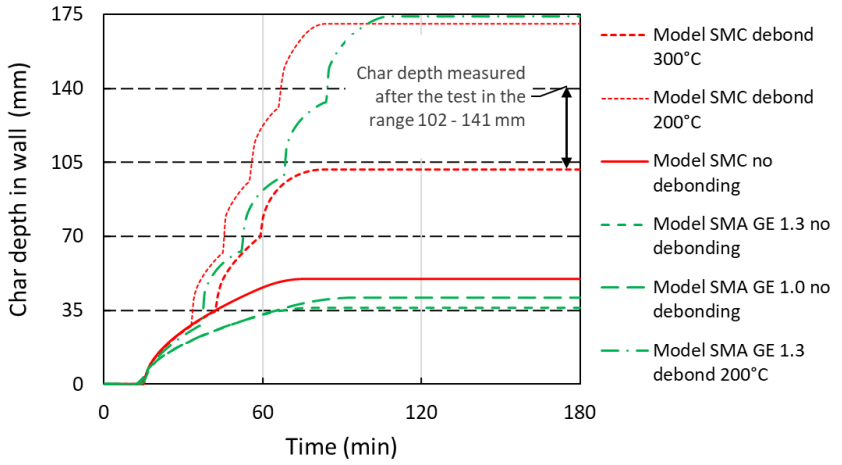

Figure 6.55: Config. M - measured and predicted char depth.

kW/s^2 to match Config. I. In the experiment, flashover occurred at 9.8 min followed by external flaming. At 80 min the external flaming reduced in size and the inside of the room became partly visible. At 100 min the external flaming increased once more obstructing the view. At 120 min the ceiling appeared to sag. At the end of the test, one of the ceiling panels collapsed into the room after manual fire suppression was commenced.

The measured predicted gas temperatures are shown in Figure 6.56 and the total heat release rate in Figure 6.57. Similar trends are seen as for the previous experiments.

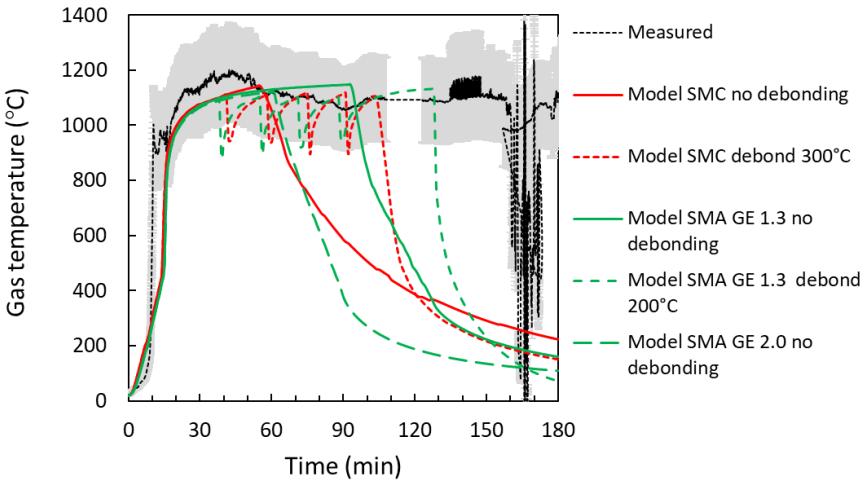

Figure 6.56: Config. N - measured and predicted gas temperature.

Char depths after the test were measured in the range 89 - 143 mm for the exposed wall and in the range 116 - 154 mm in the ceiling. The predicted char depth in the exposed wall is shown in Figure 6.58

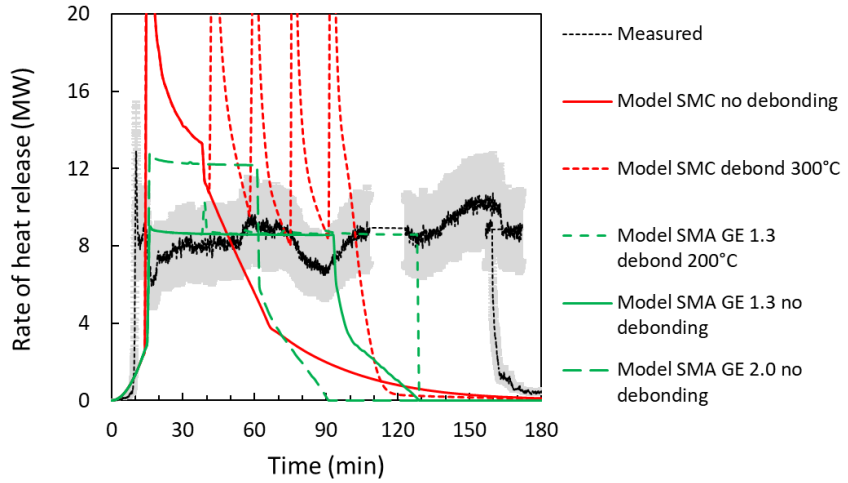

Figure 6.57: Config. N - measured and predicted total heat release rate.

with almost identical predictions shown in Figure 6.59 for the ceiling. Again, use of the debonding submodel results in charring rate predictions that are too quick and too deep compared to that seen in the experiment.

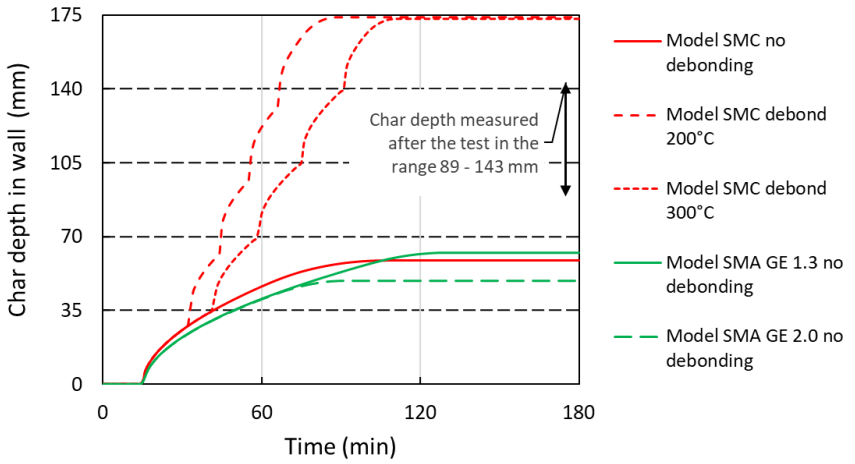

Figure 6.58: Config. N - measured and predicted char depth in the wall.

6.5 NRCC EXPERIMENTS (CONFIG. O-S)

6.5.1 *Description*

A series of five enclosure fire experiments incorporating combinations of CLT panels and Glulam structural elements were conducted at the National Research Council of Canada by Su et al. [171]. The enclosures were constructed from 175 mm thick CLT manufactured

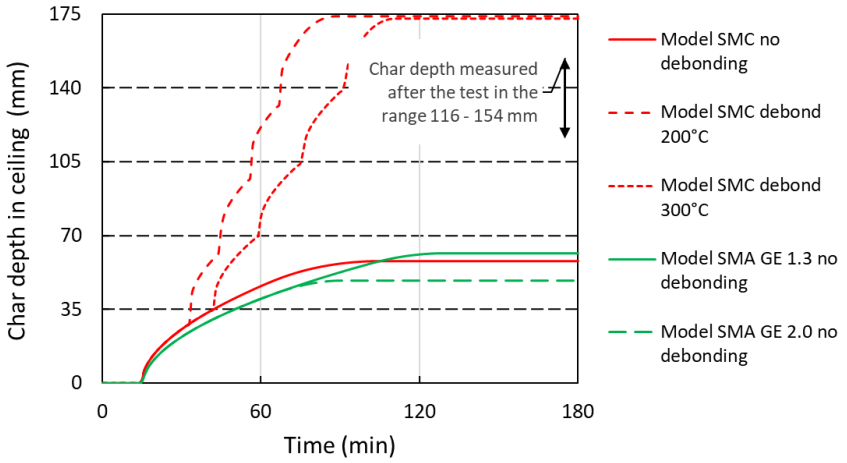

Figure 6.59: Config. N - measured and predicted char depth in the ceiling.

from spruce-pine-fir lumber using five lamellae each 35 mm thick and bonded together with a thermal resistive polyurethane adhesive which met the full-scale fire test requirements recently added to ANSI/APA PRG-320-2018 [170]. The density of the CLT was not reported by Su et al. [171] but the same CLT specification was reported by Janssens [169] to have a nominal density of 31.5 lb/ft^3 (505 kg/m^3) and similar to the nominal density of 515 kg/m^3 for the CLT used in experiments by McGregor [156]. The enclosure measured 4.5 m long × 2.4 m wide × 2.7 m high with a single doorway opening in one of the longer walls measuring 0.76 m wide × 2.0 m high. The fuel contents in each experiment comprised three wood cribs each weighing 120 kg. The wood cribs were constructed from 0.9 m long sticks of 95 × 38 mm spruce and are shown in Figure 6.60. The CLT was encapsulated with gypsum board to varying degrees as summarised in Table 6.3. The proportion of the wall and ceiling area exposed is given in Table 6.4 where the Glulam is represented as an equivalent wall area for modelling purposes based on the surface area directly exposed to the fire.

The use of a thermal resistive adhesive to bond the CLT lamella meant that debonding was not observed in these experiments. However, in some cases, there was still some additional CLT contribution later in the fire development which was attributed to charring and pyrolysis of wood behind some of the failing gypsum board encapsulation. It was therefore expected that the CLT in these experiments would burn in a manner similar to solid wood, providing a useful set of experiments for benchmarking the submodels without the added complexity of the lamellae debonding.

Three thermocouple trees were installed in the enclosure to measure the enclosure gas temperatures. Each thermocouple tree had five thermocouples at heights of 0.6, 1.2, 1.6, 2.0 and 2.4 m above

Figure 6.60: View of wood cribs used in Configs. O to S. Reprinted from Su et al. [171] with permission.

CONFIG.	WALLS	CEILING	FLOOR	GLULAM
O	3GB [a]	3GB	3GB	-
P	33% exposed rest 2GB [b]	10% exposed rest 2GB	2GB	-
Q	2GB	2GB	2GB	beam ≈ 11.5% wall column ≈ 24.5% wall
R	2GB	100% exposed	2GB	beam ≈ 6.4% wall column ≈ 12.6% wall
S	35% exposed rest 2GB	100% exposed	2GB	-

a 3 GB: 1 / 15.9 mm Type X gypsum board + 2 / 12.7 mm Type X gypsum board

b 2 GB: 2 / 12.7 mm Type X gypsum board

Table 6.3: Summary of room fire test with configurations of exposed timber as reported by Su et al. [171].

CONFIG.	WALL AREA EXPOSED	CEIL AREA EXPOSED	MOIST. CONTENT
O	0%	0%	8.9%
P	33%	10%	7.0%
Q	36%	0%	7.5%
R	19% [a]	100%	8.1%
S	35%	100%	7.1%

a This was exposed Glulam beams/columns represented as an equiv. area of wall.

Table 6.4: Proportion of the wall and ceiling area exposed as assumed in simulations.

the floor. Another thermocouple tree was located at the centreline of the opening to record the smoke temperature exiting the enclosure. Three thermocouples were at heights of 0.6, 1.2 and 1.6 m above the floor within the doorway opening. The thermocouples on the trees were Type K, stainless steel sheathed, 3.18-mm diameter, grounded junction thermocouples shielded for radiation. Thermocouples were also embedded inside the CLT at various locations at the depths of 17.5, 35, 52.5, 70 and 105 mm from the interior CLT surface. There were no mass loss or calorimetry measurements made during these experiments.

Based on the mass of wood cribs (360 kg) and an assumed effective heat of combustion of 14 MJ/kg [146], it is determined that the fire load energy density for the moveable fire load is 467 MJ/m^2. The initial fire growth is assumed to be a Fast t^2 fire until flashover after which the mass loss rate of the moveable fire load is determined from the lesser of the ventilation-controlled burning rate, crib porosity-controlled burning rate and the fuel-controlled burning rate for wood cribs. The calculated mass loss from the exposed wood surfaces is additional to the moveable fire load with the mass loss rate provided by the applicable wood combustion submodel. The heat conduction calculations for the 175 mm thick CLT walls and ceiling use finite difference layers that are 1.0 mm thick. The emissivity of the CLT is taken as 0.7 (see note in Section 6.2.1) regarding this value) and the initial density as 515 kg/m^3.

The actual measured moisture content for the CLT was in the range 7.0 to 8.9% as shown in Table 6.4 and these values were also used in the simulations. A sensitivity analysis for Config. P showed an almost negligible difference in the predicted enclosure gas temperatures with a moisture content in the range 7 to 10%.

Simulations of each of the five experiments are carried out. For the four experiments with exposed wood elements, multiple simulations are made using submodel SMA (with GE ratios of 1.0, 1.3 and 2.0) as well as the kinetic submodel SMC. For the SMC submodel the burning rate for the moveable fire load during the ventilation-controlled burning period is assumed to be 1.3 $\times$ stoichiometric. Simulations with SMC assume three different thermal conductivity relationships for the wood – temperature dependent properties from Hankalin et al. [243], Eurocode 5 (EC5) [146] along with an assumed constant thermal conductivity of 0.13 W/mK.

6.5.2 *Config. O - timber fully protected*

This experiment was designated experiment 1 by Su et al. [171] and did not include any wood surface contribution and therefore is useful to compare with the other four experiments that only varied due to the amount of exposed CLT or Glulam beams/columns present.

The average gas temperature shown in Figure 6.61 is the average temperature reading from the TC trees inside the enclosure. The shaded region shown corresponds to the range of temperatures measured by individual thermocouples on the thermocouple trees. Figure 6.61 also shows the gas temperature measured in the doorway opening at heights of 0.6, 1.2 and 1.6 m above the floor. The peak average gas temperature in the room of 1129°C was measured at about 19 min. The gas temperature predicted by the fire model (peak 1146°C at 21 min) provides good agreement with the measured average gas temperature from the thermocouple trees until the latter part of the decay where the predicted temperatures are higher than those measured. This change in slope in the predicted temperature occurs following predicted burnout of the contents and is due to the 'hot' layer ceasing to vent once the layer interface in the enclosure lifted to reach the top of the opening.

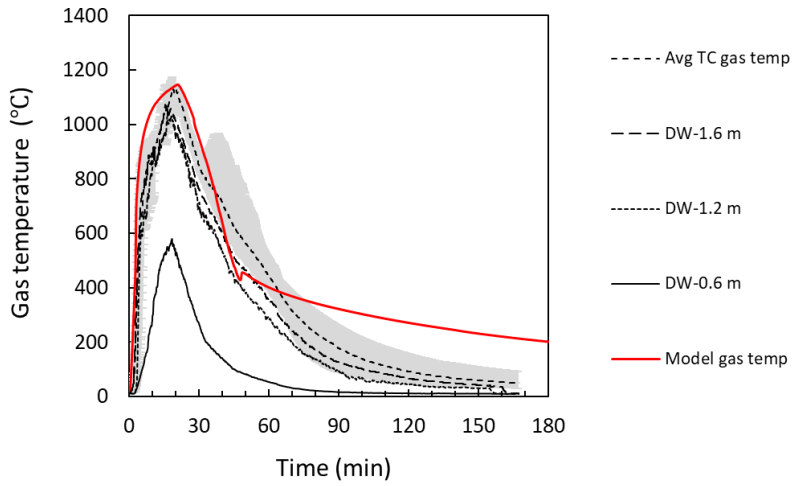

Figure 6.61: Measured and predicted enclosure gas temperatures for Config. O with no contribution from exposed wood surfaces.

6.5.3 *Config. P - timber partially exposed*

This experiment was designated experiment 2 by Su et al. [171]. A view of the room is shown in Figure 6.62 showing the exposed wall and ceiling.

With some exposed CLT introduced to the walls and ceiling the period of intense burning was extended with the peak average gas temperature of 1184°C recorded at about 26 min. Figure 6.63 shows the predicted gas temperature with the various pyrolysis submodels compared with the average temperature recorded by two thermocouple trees along with the thermocouples in the doorway opening. The grey shaded band represents the range of temperature readings recorded

Figure 6.62: Config. P - view of the room showing exposed wall and part of ceiling. Reprinted from Su et al. [171] with permission.

by the 10 individual room thermocouples. In addition, the gas temperature measured at elevations of 1.6 m, 1.2 m and 0.6 m above the floor in the opening are also shown.

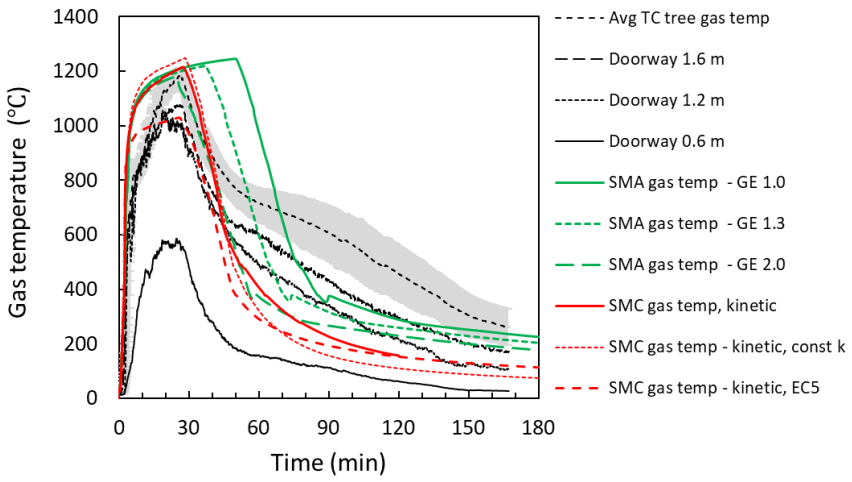

Figure 6.63: Measured and predicted enclosure gas temperatures for Config. P using kinetic and GE (with 3 different GE factors) pyrolysis submodels.

The predicted gas temperature using submodel SMA with an assumed GE ratio of 2 (i.e. equal burning inside and outside the opening) provides the best agreement for the time to reach the peak gas

temperature consistent with previous observations by Hakkarainen [153]. Lower GE ratio increases the fire duration by burning more fuel inside the room. For the kinetic submodel the closest overall agreement is obtained using the Hankalin et al. properties [243]. For the simulation using thermal conductivity from EC5 the predicted peak gas temperatures are appreciably lower and this is perhaps unexpected. The EC5 equations may work better when simulating standard fire resistance tests where the boundary condition gas temperature or heat flux is prescribed. In the case of a enclosure fire that solves the governing energy conservation equation, assuming higher thermal conductivity for the solid/char at higher temperatures (i. e. nearer to the surface) as used in EC5 has the counter effect of cooling the fire gas temperature since more of the energy from the fire is conducted into the wall (and less is used to increase the fire gas temperature). When simulating a standard fire resistance test (or a prescribed parametric time temperature curve) in a finite element heat transfer model the assumed energy of the fire (in a broad sense) does not change. It is also generally seen that the predicted gas temperature corresponds more closely with the outflow temperatures in the door opening than with the average readings from the thermocouple trees inside the room. The outflow temperatures may be more representative of a 'well-mixed' room gas temperature. The constant thermal conductivity simulation initially closely follows the gas temperature using the Hankalin properties but the temperature drops off more rapidly during the decay phase.

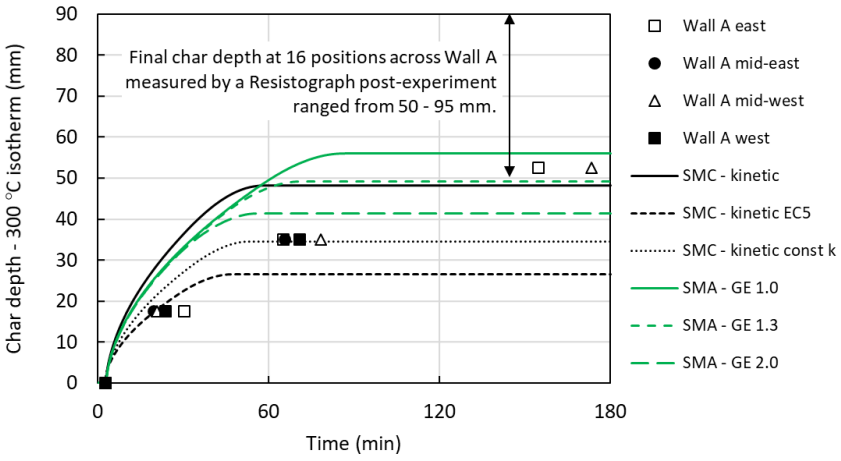

Figure 6.64: Measured versus predicted char depth in the exposed wall based on the time to reach 300°C determined from the predicted temperature/depth profile below the surface of the exposed wall for Config. P.

Figure 6.64 shows measured and predicted char depth in the wall. While the kinetic submodel (with Hankalin et al. thermal conductiv-

ity) gave a predicted maximum depth of char of 48 mm (being 5 mm less than indicated by the internal thermocouple readings) the initial char rate appears to be over-predicted. A resistograph was also used to measure char depth at 16 locations across the surface of the wall after the experiment and maximum depths recorded were in the range 50 – 95 mm (average 68.5 mm) [171]. The embedded thermocouples within the wall were at a height of 1.8 m and recorded maximum char depths of 53 mm. The resistograph readings at a similar height were in the range 50 to 70 mm.

6.5.4 *Config. Q - Glulam beams and columns exposed*

This experiment was designated experiment 3 by Su et al. [171]. The only exposed timber surface in this enclosure was due to the glulam beams and columns and these were represented in the model as an equivalent area of wall. The walls and ceiling were protected with gypsum plasterboard and are assumed not to contribute any fuel to the fire.

The fire was in the fully developed stage from flashover to 40 min with the measured peak average temperature reaching 1127°C shown in Figure 6.65. The fire then started to decay. In the period from 50 min to 85 min, the room temperatures increased again because the protected CLT panels started to char behind the gypsum board protection, causing flaming to occur at cracks and joints in the gypsum board which contributed heat to the room. This behaviour is not captured in the model where it is assumed there would be no contribution by any protected CLT. The model provides reasonable agreement for the time to reach peak gas temperatures and for the initial period of decay. However, thereafter the rate of decline in the predicted room gas temperature is much faster than that recorded by the thermocouple trees, but comparable to the measurements in the doorway opening. The same prediction trends apply when using submodel SMA where the GE ratio is controlled between 1 (i.e. stoichiometric MLR) and 2 (i.e. 2 × stoichiometric MLR). Once again the peak predicted gas temperatures using the kinetic submodel SMC with EC5 properties are appreciably lower than obtained using Hankalin's thermal conductivity.

6.5.5 *Config. R - Ceiling, Glulam beams and columns exposed*

This experiment was designated experiment 4 by Su et al. [171]. The additional exposed surface timber in this enclosure is provided by the ceiling (100%) and glulam beams and columns which are estimated to provide the same surface area as 19% of the wall. The average measured gas temperature from two different thermocouple trees is shown in Figure 6.66. The peak average gas temperature measured

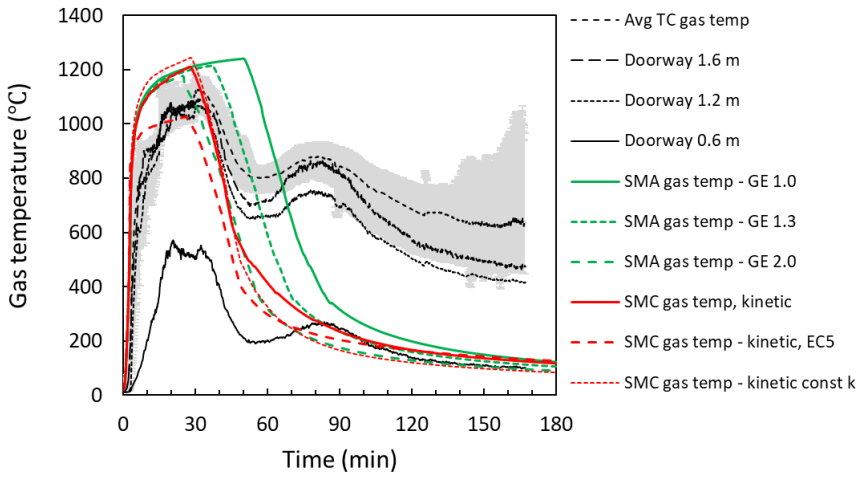

Figure 6.65: Measured and predicted enclosure gas temperatures for Config. Q using kinetic and GE (with 3 different GE factors) pyrolysis submodels.

was 1133°C at 23 min with a noticeable decline after about 30 minutes. The room temperatures slowly increased again from 60 to 90 min due to some charring behind the gypsum board protecting the CLT panels.

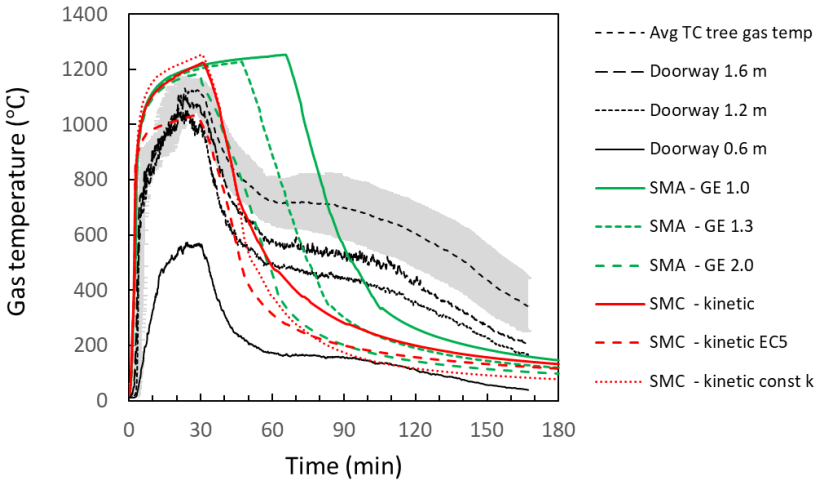

Figure 6.66: Measured and predicted enclosure gas temperatures for Config. R using kinetic and GE (with 3 different GE factors) pyrolysis submodels.

Overall the kinetic submodel with the Hankalin et al. thermal conductivity provides the best agreement with the experiment compared to either using the EC5 or constant thermal conductivity or using the alternative GE submodel.

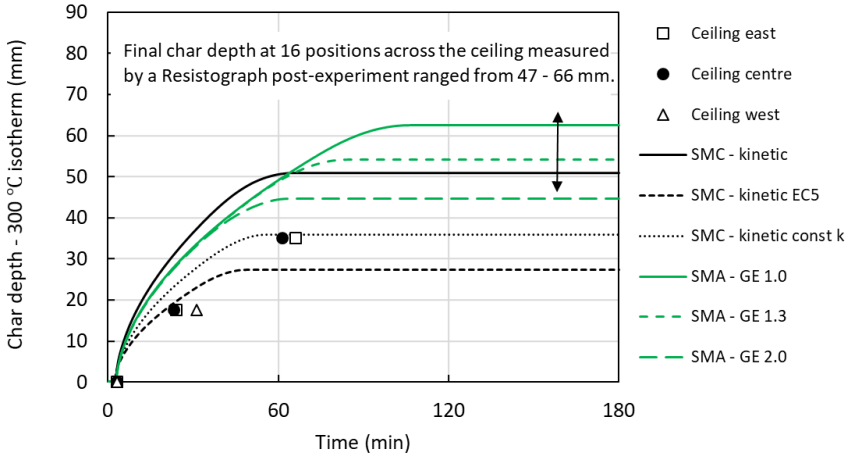

Figure 6.67: Measured versus predicted char depth in the exposed wall based on the time to reach 300°C determined from the predicted temperature/depth profile below the surface of the exposed wall for Config. R.

A resistograph was used to measure the maximum char depth after the experiment and was determined to be in the range 47-66 mm (average 54 mm – at 16 locations) in the ceiling. The predicted maximum char depth is 51 mm and within the range measured by the resistograph and greater than that derived from the embedded thermocouples as shown in Figure 6.67. Temperatures from the embedded thermocouples in the ceiling showed that the maximum temperature reached by the thermocouples located at a depth of 52.5 mm below the surface was 271°C and therefore the char line did not reach that depth at that location.

6.5.6 *Config. S - Ceiling fully exposed, walls part exposed*

This experiment was designated experiment 5 by Su et al. [171]. It had the greatest area of wood surfaces exposed to the fire compared to the previous experiments in this series with all the ceiling exposed and 35% of the wall. A view of the room showing the exposed ceiling and one of the exposed walls is shown in Figure 6.68.

The measured average gas temperature shown in Figure 6.69 was again the average of 10 thermocouple readings from two different thermocouple trees. The peak average gas temperature measured was 1158°C at 28 min with a gradual decline thereafter. The kinetic wood pyrolysis submodel and the GE submodel with GE 2 give similar times to reach the peak gas temperature with the kinetic submodel giving a temperature decay that more closely matches the experiment as shown in Figure 6.69. The GE submodel assuming a stoichiometric release (GE 1.0) of mass from the wood surfaces overestimates the

Figure 6.68: Config. S - view of exposed ceiling and wall before test. Reprinted from Su et al. [171] with permission.

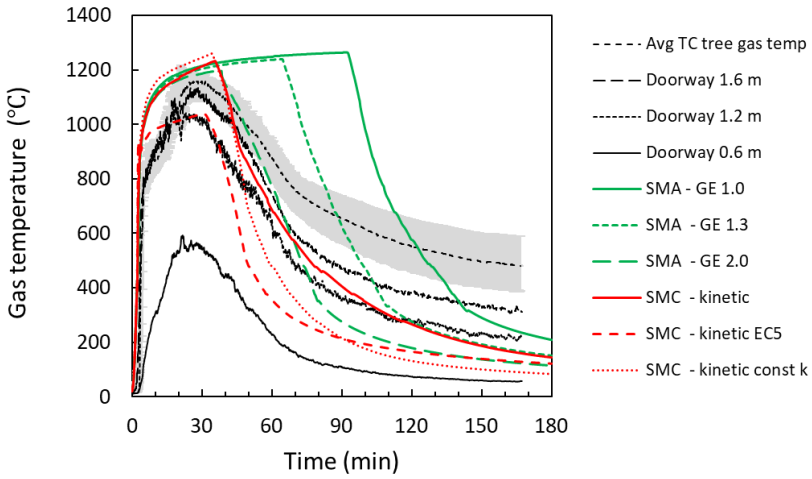

Figure 6.69: Measured and predicted enclosure gas temperatures for Config. S using kinetic and GE (with 3 different GE factors) pyrolysis submodels.

time to reach the peak gas temperature by more than a factor of two. The kinetic wood pyrolysis submodel also once again provides better

agreement with the experiment compared to using EC5 or constant thermal conductivity.

A resistograph measured char depths in the ceiling to be in the range 70-90 mm (average 78 mm – at 16 locations). In the exposed walls the char depth was 81-109 mm (average 89 mm – at 8 locations) with greater char depth measured in the lower portion of the walls compared to elsewhere. This may have been due to the positioning of the wood cribs relatively close to the wall. While the predicted char depth as seen in Figure 6.70 for the ceiling is comparable to that determined using the embedded thermocouples, depths recorded by resistograph after the experiment were much greater. Interestingly, the resistograph measured the lowest char depths (70 mm) in the centre region of the ceiling which exactly agreed with the char depth determined from the embedded thermocouples in that region. Greater char depths were recorded by the resistograph around the outer areas of the ceiling that were closer to the walls. The greater charring in these areas may have been due to the increased convective flows impinging on the ceiling from burning at the wall surface. This was not observed for Config. R which did not have any exposed wood on the walls. The maximum predicted char depth in the ceiling using the kinetic sub-model is 62 mm which under-predicts the average predicted depth from the embedded thermocouples by 11.4%.

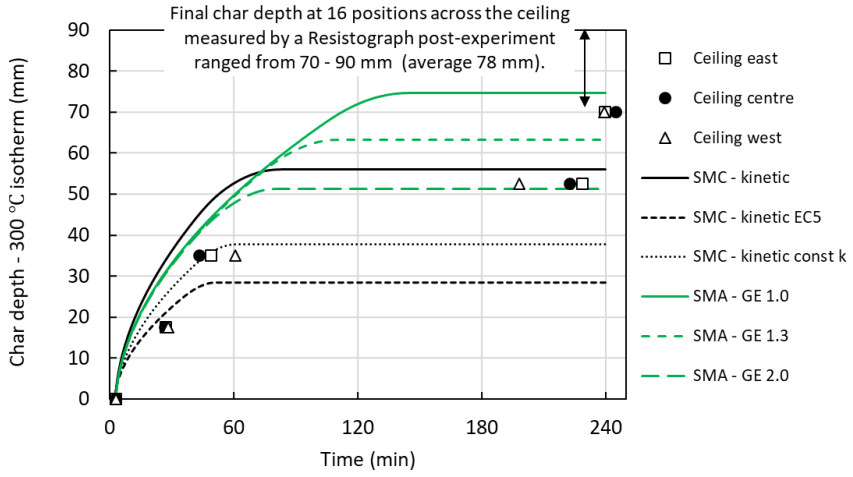

Figure 6.70: Measured versus predicted char depth in the ceiling based on the time to reach 300°C determined from the predicted temperature/depth profile below the surface of the exposed ceiling for Config. S.

6.5.7 *Discussion*

Since the CLT in this series of experiments was manufactured using a thermal resistive adhesive to bond the lamellae together it is expected

that the CLT in these cases would burn in a manner similar to solid wood. This is therefore expected to provide useful data for benchmarking the model discussed in this research without the added complexity that would be introduced with lamellae that debonded during the experiment.

Mass loss contribution from the moveable fire load (wood) during the fully developed phase is assumed to equal 1.3 × oxygen available (as for stoichiometric burning). This may not be very accurate when additional mass is also contributed by the exposed wood surfaces and in the absence of any means of accounting for other interactions between the fire and the fuel sources that could influence the mass loss rate of the moveable fire load. In Chapter 8, a fuel response effects submodel for the moveable fire load in a mass timber enclosure is discussed. This would consider the effect on the mass loss rate of the moveable fire load due to thermal feedback to the fuel surfaces and due to depletion of oxygen inside the room.

The EC5 temperature dependent thermal conductivity for wood resulted in significantly lower peak gas temperatures (in excess of 100°C lower) compared to that predicted using the properties described by Hankalin et al. [243]. As discussed previously for Config. P, while the EC5 properties may be appropriate for use with the gas time temperature curve in the standard fire resistance test, they may not be optimal when used in conjunction with enclosure fire models that solve energy conservation equations.

Representing the exposed area of the glulam beams/columns as equivalent wall area may be also inappropriate since only one dimensional heat transfer is modelled into the wall and ceiling surfaces whereas heat transfer into the beam and columns occurred on more than one side. The model is expected therefore to underestimate the contribution by the glulam elements and this is reflected in Figure 6.65 and Figure 6.66 where the divergence between the measured and predicted gas temperatures is the greatest.

The char depth predicted by the model is greater than that measured in the earlier part of each experiment. However, the difference reduced as the experiment progressed. Comparisons with char depths measured after the experiments were terminated are in most cases reasonable but not always conservative with respect to the measured char depths.

A current model limitation is that when a wall or ceiling surface is partly exposed wood and partly gypsum plasterboard, enclosure heat loss calculations assume the entire surface has the thermal properties of wood – this is expected to lead to slightly higher gas temperature than otherwise expected depending on the relative areas concerned. This is considered a conservative assumption but if necessary, the model could be refined to account for this in the future.

Overall, the kinetic pyrolysis submodel gives improved agreement compared to the GE pyrolysis submodel, with the added advantage that the user is not required to specify the global equivalence ratio in advance which governs the proportion of fuel burned inside and outside the opening. In particular, the kinetic submodel captures the shape of the decay more closely than does the GE submodel. In all five experiments, the predicted peak gas temperatures are higher and within 9% of the measured peak average value from the thermocouple tree measurements. There is however larger variation in the time at which the peak temperatures which range from -2% for experiment 3 to +49% in the case of Config. R. Closer agreement during the decay period is shown with the temperature of the gas flow leaving through the opening compared to the thermocouple tree data. There is greater disparity during the decay phase of the fire for some experiments which is partly attributed to charring and pyrolysis of wood behind failing gypsum board encapsulation which is not currently addressed in the model. Measured gas temperature data for the gas flows leaving through the opening may also be more representative of the average enclosure gases with greater mixing and therefore more consistent with the underlying basis of the two-zone enclosure fire model.

6.6 DISCUSSION

6.6.1 *SMA - global equivalence submodel*

The wood pyrolysis submodel SMA relies on a user specified GE ratio. A lower value for this ratio increases the simulated fire duration and fire severity inside the room at the expense of external flaming, whereas a higher value will increase external flaming but reduce fire duration and severity inside the room. A lower value for GE is likely to more realistic when all surfaces are protected (i.e. only the room contents burn) or where only a small proportion (e.g. 30% based on Config. E) of wall surfaces are exposed. A higher value is more representative when larger areas of exposed surfaces and/or when the ceiling is fully exposed since unreacted fuel gasified from the timber surfaces into an oxygen depleted hot gas layer will be more readily transported with the combustion products leaving through the opening.

In all cases here, where a timber ceiling was fully unprotected (i.e. Configs. B, G, H, L, R and S), assuming a GE ratio of 2.0 gives reasonable predictions for both the total HRR and the gas temperatures up until the predicted time of debonding (if any). The predictions are closer to the measured data compared with simulations using GE 1.3 or GE 1.0 with the exception of Config. L where GE 1.3 appeared to be a better fit to the measured gas temperature. As previously noted GE

2.0 is a value that is consistent with the Hakkarainen experiment [153] with unprotected glue-laminated timber on the walls and ceiling and also with the unprotected timber enclosure experiment (Config. B) by McGregor [156].

A comparison between the predicted and measured peak gas temperatures for the series of enclosure fire experiments described in Configs. A - S and using the pyrolysis submodel SMA with GE 1.3 is shown in Figure 6.71. The comparison includes an estimate of model bias and uncertainty using the procedure described by McGrattan et al. [254] and as described in Appendix C. The bias factor indicates the extent to which the model, on average, underpredicts or overpredicts the measurements. The model bias factor calculated for the simulations using SMA GE 1.3 was 1.003 indicating minimal bias.

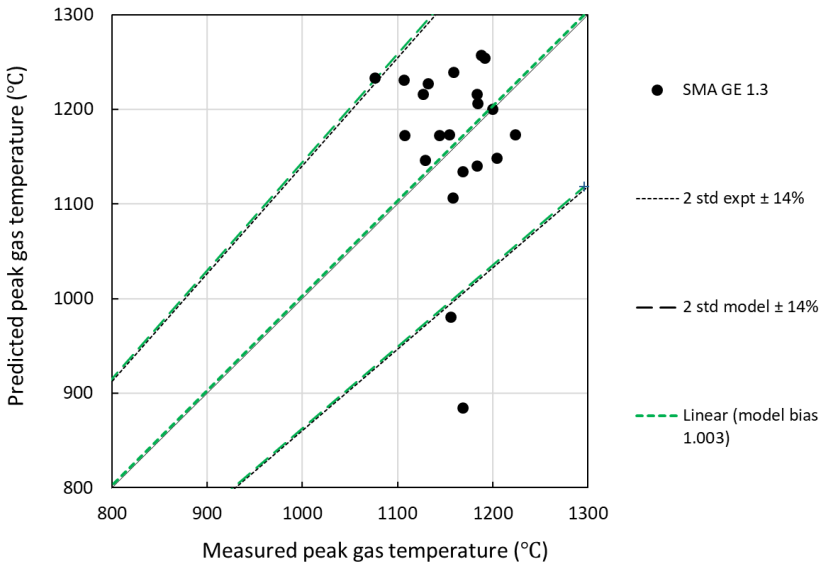

Figure 6.71: Submodel SMA GE 1.3 - Predicted versus measured peak gas temperature in rooms with and without exposed wood surfaces.

A comparison between the predicted and measured peak gas temperatures for the series of enclosure fire experiments described in Configs. A - S and using the pyrolysis submodel SMA with GE 2.0 is shown in Figure 6.72. In this case the model bias factor calculated for the simulations is 0.974. However this included the room configurations where the wood surfaces are fully protected and for which GE 2.0 would not be generally expected. The comparison between the predicted and measured peak gas temperatures for only those room configurations with at least some exposed wood surfaces is shown in Figure 6.73. In this case the model bias factor calculated for the simulations is 0.982 and in all cases the predicted peak temperatures were within experimental uncertainty. The experimental uncertainty assumed for the measurement of the peak gas temperature was a

typical value from the literature of 0.14 for the combined relative uncertainty for the measurement of a temperature rise [254, 255].

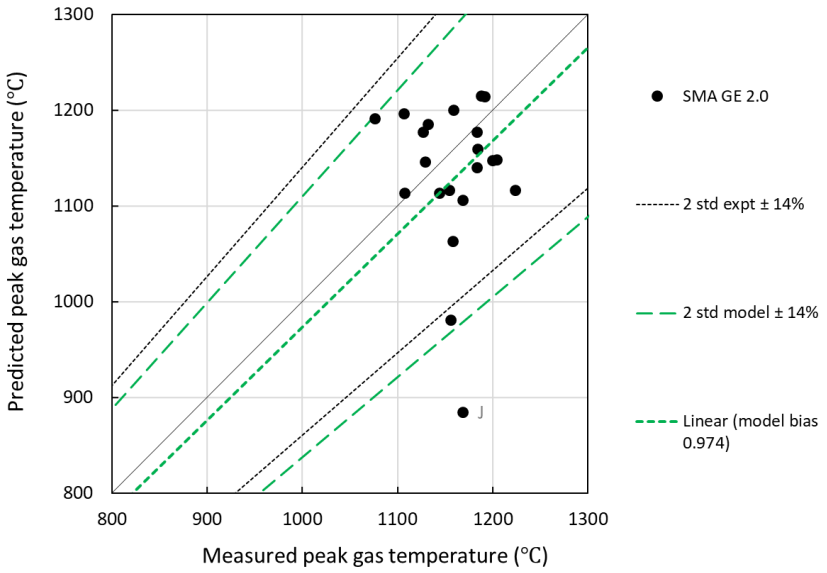

Figure 6.72: Submodel SMA GE 2.0 - Predicted versus measured peak gas temperature in rooms with and without exposed wood surfaces.

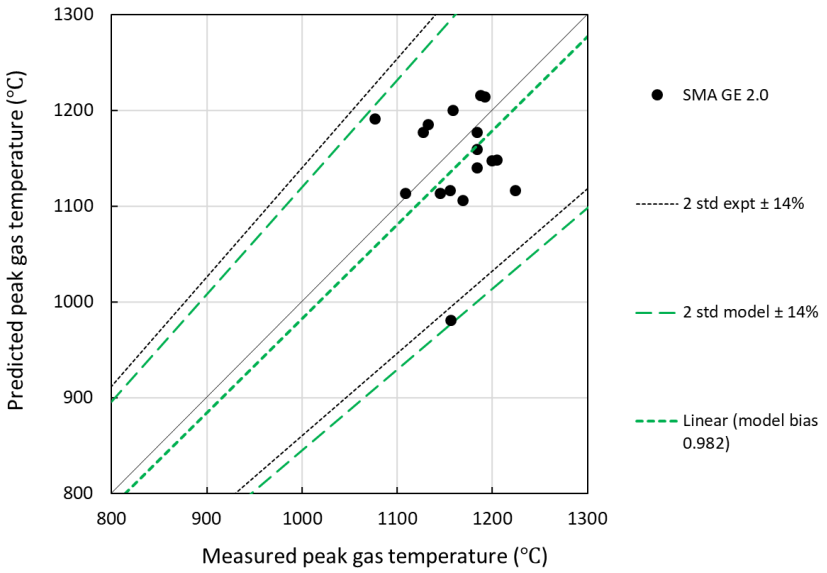

Figure 6.73: Submodel SMA GE 2.0 - Predicted versus measured peak gas temperature in only rooms with exposed wood surfaces.

Bearing in mind that wood cribs and timber linings do in practice burn quite differently, in submodel SMA where the global equivalence ratio is user-specified, the overall rate at which the fuel is made

available for burning under ventilation-control is therefore set by the user. This means a greater contribution from the surface linings will extend the duration of burning rather than the fuel gases being deposited immediately within the room only to burn in the external flame. For the case of well-ventilated enclosures where the fire may be fuel-surface controlled, the assumption that timber surfaces burn as do wood cribs could be less tenable. Furthermore, there are limited experiments that allow the current model to be validated for this scenario. This requires further research and experiments.

For design purposes, where a more conservative prediction for the gas temperatures and fire severity inside the enclosure is desired, the default GE of 1.3 would seem to be a reasonable choice when the room contents are mainly cellulosic. GE = 2.0 is reasonable where a high proportion of the timber surfaces are unprotected and particularly if the ceiling is exposed wood or where a more conservative prediction for the external flaming environment is desired. It is acknowledged that there is a high degree of uncertainty associated with these estimates and they could also be dependent on the size of the enclosure.

6.6.2 *SMC - kinetic submodel*

A comparison between the predicted and measured peak gas temperatures for the series of enclosure fire experiments for all configurations with some exposed wood surfaces and using the kinetic submodel SMC is shown in Figure 6.74. The model bias factor calculated for the simulations using the kinetic pyrolysis submodel SMC is 1.011 indicating there is a small bias toward overprediction. Assuming a combined relative uncertainty (95% confidence interval or 2 standard deviation) for the peak gas temperature measurement of 14%, all the predicted peak gas temperatures are found to be within experimental uncertainty.

With the kinetic pyrolysis submodel SMC, the initial fire growth and rate of heat release is predicted to be very steep due to the assumption that all the ceiling and all wall surfaces will contribute mass based on a single heat conduction calculation for that element i.e. the internal temperature distribution within the ceiling element is assumed to apply to the entire surface area of the ceiling and therefore the calculated generation rate of pyrolysis gases for the surface is uniform across the ceiling. This is a reasonable assumption for smaller rooms after flashover but as the area of the room increases the expectation that the burning behaviour will be uniform across the ceiling will decrease. It is also noted that in the event of there being no exposed wood surfaces, use of the SMC submodel is redundant and will provide the same result as submodel SMA.

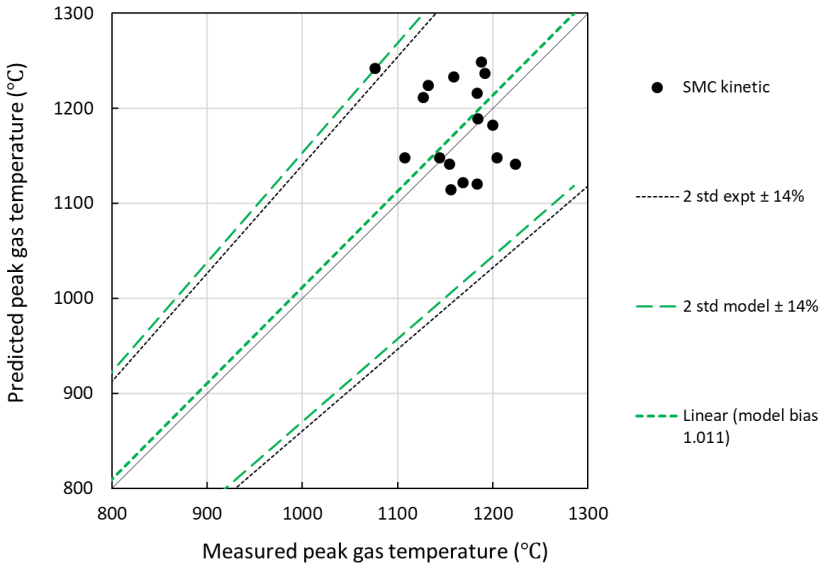

Figure 6.74: Submodel SMC - Predicted versus measured peak gas temperature in rooms with exposed wood surfaces.

6.6.3 *Debonding of timber layers*

As previously observed, use of the debonding submodel usually provided much greater predictions of char depth than was measured. This was generally true when using either 200°C or 300°C as the criterion for debonding based on temperature reached at the glueline. The idealised nature of the submodel in instantly discarding the complete facing lamella from all the walls or ceiling at the predicted debonding time is not a good representation of what is a complex and more gradual process in practice. For example Figure 6.75 shows a view of the ceiling following flaming extinction in one of the Config. G experiments where partial debonding of the facing lamella can be seen.

For engineering applications, an adhesive failure temperature of 200°C as proposed by Craft [188] is likely to be quite conservative. However, it is noted that, for the kinetic model, using a lower debonding temperature may not always be the worst case for the severity inside the enclosure, as early debonding (during the period of ventilation control) may result in more fuel mass burning outside the enclosure. A worst case approach could be when the debonding occurs later e.g. during the decay phase where a greater proportion of the fuel is able to burn inside the enclosure. This has the effect of potentially increasing the fire severity and leading to the maximum char depth.

The model could be used to assess whether debonding is expected or not depending on the design fire and the thickness of the sur-

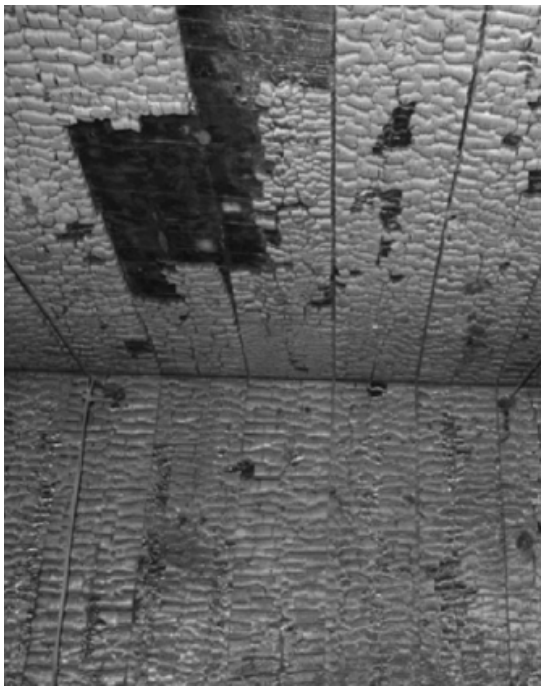

Figure 6.75: Config. G - charred timber on the ceiling and back wall after auto-extinction (note localised areas of fall-off of the first lamella on the ceiling). Reprinted from Hadden et al. [165] under a Creative Commons License.

face lamella. An appropriate thickness for the facing lamella could be specified such that the temperature at the adhesive line is kept below 200°C to avoid debonding. In the event that the adhesive is expected to reach 200°C, selecting a suitable thermal resistive adhesive to prevent debonding such that mass timber panels perform similarly to solid wood is a more reliable approach than attempting to model the debonding process, and thus reducing the uncertainty associated with the debonding phenomenon and simplifying the fire design process.

6.6.4 *Timber protection systems*

Timber encapsulation or protection systems intended to prevent timber surfaces from contributing to the fire are typically non-combustible or limited-combustible boards such as gypsum plasterboard. The degree to which protective boards help to prevent or delay pyrolysis and combustion of the underlying wood will depend on the properties, thickness and how the protective linings are fixed. They could fall off at some time during the fire or else remain in place protecting the surface beneath for the full fire duration. The latter is a more dependable means of limiting the potential contribution of timber to the fire.

While the current fire model described here cannot be used to evaluate the ability of the protection system to remain in place, it could be used to estimate the thickness of protection needed to keep the temperature of the timber beneath to below 300°C and thus avoid any burning of the protected timber. The model could also be improved by allowing two bounding surface systems (for the protected and unprotected wood surfaces) to be specified instead of one. Currently, if an estimate of char depth is needed for determining the timber contribution to the fire, timber must be the selected as the wall surface material. While the user can specify the proportion of the room with timber exposed, the heat loss calculations assume the specified material to be on all walls. Therefore, with the current model, temperatures behind an encapsulation system can only be determined for the case where exposed timber is only on the walls and the protection system is on the ceiling. The calculation may also be overly conservative for gypsum plasterboard protection unless additional allowance is made for the time taken to drive off free and bound moisture in the board.

In summary, for the current model, it is assumed that plasterboard fixed to timber surfaces for protection does not fall off, and the ability of the protection system to remain in place for the full fire duration must be separately confirmed by the model user. Including a more accurate submodel for the behaviour of gypsum board protection is expected to be a beneficial feature that could be added in the future.

6.6.5 *Autoextinction*

The predicted incident radiant heat flux to a wall for Config. E is shown in Figure 6.76. for the GE 1.3 case. The incident radiant flux drops below the Emberley et al. [167] flaming-extinction criterion of 45 kW/m^2 at 37 min and below Crielaard's [199] smouldering-extinction criterion of 5 kW/m^2 at 57 min. The latter is slightly sooner but close to the time for the char depth (as represented by the 300°C isotherm) to reach a plateau as also shown in Figure 6.76. Similarly, Figure 6.77 shows the equivalent comparison with Config. D. This supports the use of the smouldering-extinction criterion as a better choice for auto-extinction than the flaming-extinction criterion in conjunction with the present model.

It is also noted that surface erosion of the char layer where glowing combustion, char oxidation and mechanical disintegration of the char eventually erode or ablate the outer char layer [137] has not been specifically modelled here.

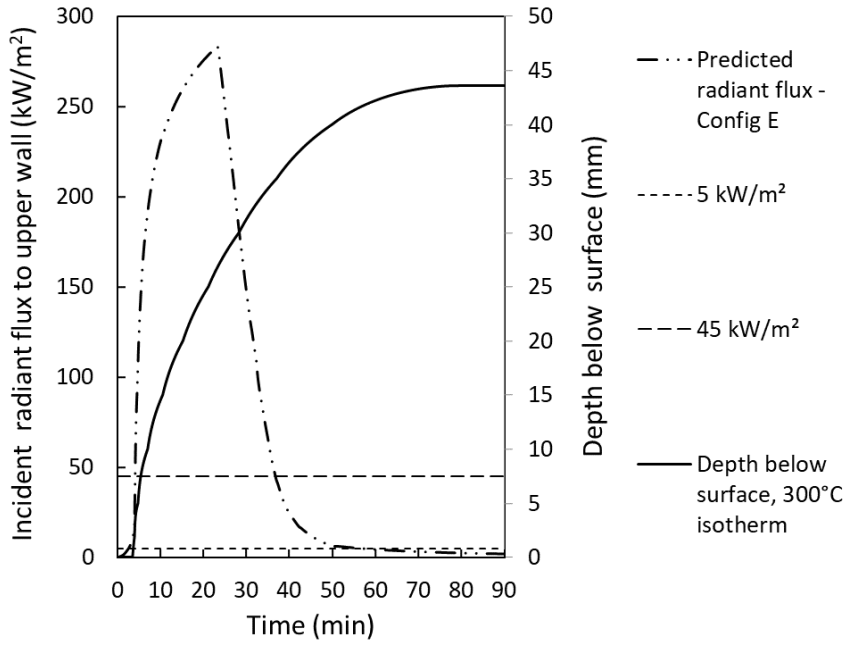

Figure 6.76: Predicted incident heat flux on wall compared with flaming and smouldering extinction criteria and char depth represented by the 300°C isotherm (for GE 1.3) for Config. E.

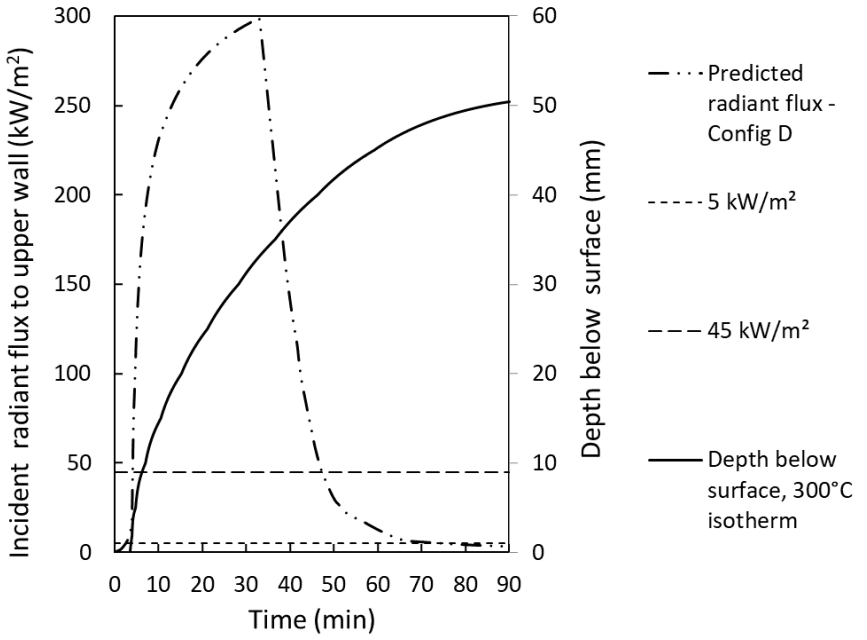

Figure 6.77: Predicted incident heat flux on wall compared with flaming and smouldering extinction criteria and char depth represented by the 300°C isotherm (for GE 1.3) for Config. D.

6.7 SUMMARY

A two-zone enclosure fire model with wood pyrolysis submodels for determining the contribution of specified areas of solid timber surfaces has been described, and a set of 19 experiments reported in the literature have been used to evaluate and benchmark the model. It has been shown that the model can be used to provide conservative predictions, as part of an engineering analysis, of the upper layer fire temperatures for enclosures with timber exposed on the walls and/or ceiling. However, there are several limitations to consider as noted below.

A debonding submodel has been presented and is likely to be conservative in estimating char depth post-debonding in its current form. However the debonding process is complex with large uncertainties such that it is not recommended that the submodel be used in a design situation, other than to determine if debonding is expected. A range of adhesive failure temperatures appear in the literature. Barlett et al. [181] report debonding temperatures as low as 90-125°C and Janssens reported 200-220°C [169]. Craft [188] suggested 200°C could be assumed and based on the submodels developed here, this is likely to be conservative. However, given the sensitivity of the debonding process to the choice of the adhesive failure temperature and possible other factors, it would be advisable to support a selected failure temperature with other supporting calibration or benchmarking studies. Preventing debonding is a preferable design strategy based on determining a suitable minimum thickness for the facing lamella or by choice of a suitable thermal-resistant adhesive.

Where timber surfaces are protected, it is assumed the protection remains in place for the full fire duration. This must be separately established and is not predicted by this model. Also, the model does not distinguish the relative position of exposed timber surfaces on the walls (e.g. adjacent walls versus opposing walls or high or low position on a given wall). It only considers the percentage of surface area of the timber exposed and able to contribute fuel to the fire. Furthermore, both the fuel provided by the contents (and from the exposed timber surfaces in the case of submodel SMA) are assumed to burn as 'equivalent wood cribs'.

The fire dynamics within a timber-lined enclosure are significantly influenced by the global equivalence ratio resulting from the specific fuel and ventilation characteristics. In the case of the GE pyrolysis submodel SMA it influences the relative proportion of heat released inside and outside the enclosure openings. This ratio can be varied by the specified user input value for the excess fuel factor. A value no greater than 1.3 is recommended in all cases where a conservative prediction for the gas temperatures and fire severity within a timber enclosure is desired. An excess fuel factor of 2.0 is recommended where

a high proportion of timber surfaces are unprotected, especially the ceiling, or where a conservative prediction for the external flaming environment is desired. The kinetic wood pyrolysis submodel SMC generally gave closer agreement with the gas temperature measured in the experiments although the rate of burning initially may be over-predicted. The kinetic submodel has the advantage of not requiring the global equivalence ratio to be a constant pre-determined value. Both submodels resulted in gas temperatures during the decay phase that were generally lower than the measured gas temperatures.

It is recommended that Eurocode 5 thermal conductivity properties not be used with the pyrolysis submodels developed in this thesis and the Hankalin et al. thermal conductivity equations be used instead as previously discussed. This is due to the coupled interaction between the surface heat conduction calculations and the energy balance calculations for the enclosure.

It was found that smouldering extinction rather than flaming extinction criterion provided extinction times closer to that corresponding to a plateau in the 300°C isotherm although it is not clear whether separate extinction criteria are required since the char depth reaches a natural plateau for a given design fire and fuel load. Other factors such as air flow velocities and oxygen concentrations during the decay phase could also influence the auto-extinction process and this is not considered in the model.

The benchmarking against the 19 experiment configurations described in this thesis gives some confidence that the model can provide conservative prediction of the fire behaviour in enclosures with varying amounts of exposed CLT surfaces provided any debonding is either avoided or accounted for. However, while there has been no systematic calibration of the model in relation to experiments used for benchmarking, recommendations regarding appropriate values for excess fuel factor (global equivalence ratio) along with debonding and auto-extinction criteria have been made considering the benchmarking results. The benchmarking also showed that predicted peak gas temperatures within the enclosures agreed with the measured peak gas temperature within the range of experimental uncertainty. However, it is recommended that further benchmarking be carried out for enclosures with a wider range of ventilation condition, geometry and fuel load. This will test the model under a wider range of conditions to further support or refine the parameters and assumptions recommended in this thesis for use in conjunction with the model.

7

FUEL RESPONSE EFFECTS IN INERT ENCLOSURES

7.1 GENERAL

The fire dynamics within a mass timber enclosure is the result of a complex coupled interaction between the fire source, the fuel response effects due to the enclosure and the burning of the enclosure wood surfaces. The simulations presented earlier in this thesis did not include any of the enclosure fuel response effects. This chapter describes the implementation of a submodel for predicting these effects on the mass loss rate and heat release rate of an item burning within a non-combustible or inert enclosure. The extension of the submodel to mass timber enclosures is then discussed in Chapter 8.

Traditional zone-type models require the user to fully define the fire in advance by specifying two of the following three parameters: mass loss rate, heat release rate and heat of combustion. These inputs are commonly based on experimental data for fuel burning in well-ventilated conditions. However, many burning objects interact with the surrounding environment. Some objects experience enhanced burning in response to radiative heating from the hot layer and heated enclosure surfaces. For example, the surface of a liquid pool fire is fully exposed to the radiative environment and may experience a large increase in the mass loss rate. This effect is smaller for wood cribs in which a large proportion of the surface area is within the crib lattice where it does not directly see the radiative environment [256]. In the case of upholstered furniture, the design and geometry of the item may be quite important for its response to the radiative environment.

In addition to the radiative effects, inside an enclosure, the availability of oxygen to the fuel may be restricted due to the size of any openings, the position of the fuel and the flow dynamics near to the openings. A descending smoke layer within the room can mix with and dilute the incoming flow of fresh air from outside the enclosure, thus reducing the oxygen concentration in the gases reaching the flame. This, in turn, can cause the flame flux, fuel mass loss rate and heat release rate to reduce or in some cases the flame to be extinguished. The radiative effects and the oxygen vitiation effects are competitive since the former acts to increase the mass loss rate while the latter acts to reduce it. For any given enclosure and fire source the combined effect could result in the total mass rate being either higher or lower than the measured loss rate for the same fire source under well-ventilated conditions.

In the rest of this Chapter, a fuel response effects submodel is described and benchmarked against a series of fourteen heptane pool fire experiments in a reduced-scale enclosure, as well as five enclosure fire experiments with single upholstered chairs in a room.

7.2 OXYGEN VITIATION

Peatross and Beyler conducted an experimental study burning diesel, wood cribs and polyurethane slabs in a full sized enclosure with both natural and forced ventilation [257]. They found that a reduced oxygen concentration at the base of the flame caused the fuel mass loss rate to be reduced and there was a linear relationship between the two variables. They developed the general linear correlation in Equation 7.1 where they normalised the mass loss rate per unit area for a given fuel by the mass loss rate per unit area under normal ambient oxygen levels of 21% by volume.

$$\frac{\dot{m}''}{\dot{m}''_{\infty}} = 0.1O_2[\%] - 1.1 \tag{7.1}$$

They included data from their pan fire experiments with forced ventilation as well as small scale data from Tewarson et al. [258] and Santo and Delichatsios [259] and plotted the data as shown in Figure 7.1 along with the proposed correlation. Peatross and Beyler came to the conclusion that -

> *"the practice of using furniture calorimeter data as input to fire models without consideration of oxygen concentrations at the flame base is questionable. In many cases, it will seriously overestimate enclosure temperatures and flashover potential"* [257].

7.3 VENT MIXING FLOW

When cool air flows into the room through a wall vent, it can entrain some of the gases from the upper layer into the lower layer. This is the driving mechanism for the reduction in oxygen in the air feeding the flame. Utiskul [225] conducted an experimental study of the near vent mixing phenomenon and developed a correlation where the incoming cold air behaves like a jet entering the vent with a characteristic velocity and diffusing downwards because of buoyancy. His correlation is given as:

$$\dot{m}_{vm} = \left\{ \begin{array}{l} 1.14\varphi\dot{m}_{o,in} \text{ for } \varphi < 1.1 \\ 1.28\dot{m}_{o,in} \text{ for } \varphi \geqslant 1.1 \\ 0 \text{ for } N < z \end{array} \right\} \tag{7.2}$$

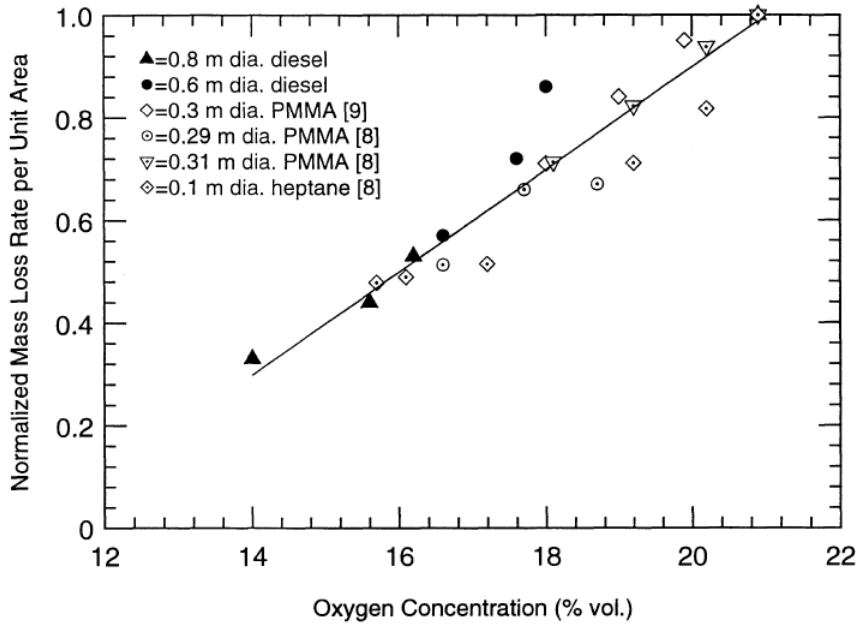

Figure 7.1: Effect of oxygen concentration on normalized mass loss rate per unit area. Reprinted from Peatross and Beyler [257] with permission from the IAFSS.

$$\varphi = \left(\frac{T_\infty}{T}\right)\left(1 + \frac{N - B}{W_o}\right)\left(\frac{N - z}{N - B}\right) \tag{7.3}$$

where $\dot{m}_{vm}$ is the mixing flow; $\dot{m}_{o,in}$ is the vent inflow; T_∞ is the gas temperature of the inflowing gases (ambient); T is the temperature of the upper layer gases; N is the neutral plane elevation; B is the sill elevation above the floor; W_o is the opening width; and z is the layer height.

Figure 7.2 shows an image from one of Utiskul's experiments illustrating the doorway mixing flow phenonema.

7.4 ENCLOSURE ENHANCEMENT EFFECT

An isolated fuel bed burning in the open will burn at a rate $\dot{m}''$ determined by the heat flux from the flame to the surface of the fuel $\dot{q}''_F$ as described by Equation 7.4 [42] where $\dot{q}''_L$ is the heat loss from the fuel surface and L_g is the heat of gasification.

$$\dot{m}'' = \frac{\dot{q}''_f - \dot{q}''_L}{L_g} \tag{7.4}$$

A number of researchers have studied the burning rate enhancement due to enclosure feedback effects. Friedman [260] burned slabs of PMMA in a reduced-scale enclosure where a hood forming the

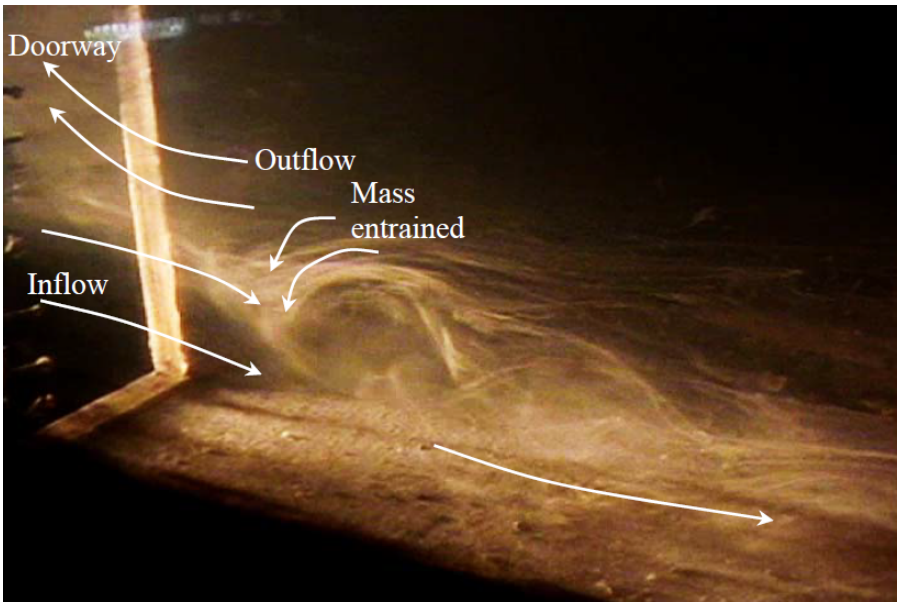

Figure 7.2: Image capturing doorway mixing phenomena. Reprinted from Utiskul [225] with permission.

ceiling and upper walls deflected the flame causing increased radiant feedback to the fuel. There was unrestricted supply of air underneath the hood on all sides. They measured maximum burning rates three times greater than in the open. The rate of burning for alcohol fires has been reported by Bullen and Thomas [261] to be up to six times higher than in the open. For methanol pool fires, Takeda and Akita [262] found the maximum burning rate was up to 7.2 times the open burning rate.

Fleischmann and Parkes [263] conducted an experimental study burning 20 cm diameter pans of heptane in a reduced-scale enclosure. They varied the width and height of the opening with opening factors in the range 0.0039 to 0.071 $m^{5/2}$ and found the mass loss rate for the highest opening factor to be almost 4 times higher than for the actual measured free burning case. This was almost 7 times higher than the value for the free-burning mass loss rate obtained using the semi-theoretical expression given later as Equation 7.15 for radiation dominated burning of 20 cm diameter heptane pool fires.

Pool fires have the fuel surface fully exposed to radiation from the flames and enclosure surfaces such that the burning enhancement effect is maximised. In the case of upholstered chair fires burning in a room of size similar to ISO 9705 then burning enhancement effect is much smaller. Babrauskas states there is approximately a 20% augmentation of the burning rate compared to the open-burn case for fires in the range 100-1000 kW [246]. He also comments on a lack of quantitative guidance for how to account for room enhancement effects for many practical cases.

7.5 RELATED MODELLING

Previous research most relevant to the present study is that by Utiskul [225]. He developed a single-zone enclosure fire model along with a fuel mass loss rate model that accounted for the thermal enhancement, oxygen-limiting feedback, fuel type and configuration. His experiments used wood cribs and heptane pool fires and were used to validate his mathematical model. He explored the range of phenomena associated with fully developed fires: extinction, oscillation, fire area shrinkage and the response of fuel to thermal and oxygen effects. Subsequently, Mizukami et al. [264] described the implementation of an enclosure burning rate algorithm into the BRI two-zone model. The BRI model modifications generally followed the Utiskul methodology [225]. They reported good agreement for small-scale enclosure data for heptane pan fires.

Wahlqvist and van Hees [265] implemented very similar equations as correlations in FDS as a simple way to compensate for the reduced radiative feedback the fuel surface receives when the oxygen concentration is lowered and the flame is cooled down, prolonged or detached from the fuel base. They made use of the oxygen volume fraction close to the flame base. They found that the model produced accurate predictions of the mass loss rate as long as the overall flow was reasonably resolved by the model.

7.6 THEORY

In this chapter, the two-zone enclosure fire model (B-RISK [114]) has been modified to include a pyrolysis submodel for predicting the fuel response effects on the mass loss rate of the fuel. Instead of providing a heat release rate for the fire source as input for the calculations, a free-burning mass loss rate is used. The model then calculates the fuel response effects depending on the enclosure geometry, thermal characteristics and ventilation and predicts mass loss rate and heat release rate for a fire in a ventilated enclosure. The two-zone model uses these calculated parameters as source terms in the mass and energy conservation calculations. The model output predicts the gas layer temperatures, smoke concentrations and other parameters required for fire safety engineering analysis.

The selected submodel for the fuel response effects follows the general approach developed by Utiskul and Quintiere [225, 264, 266–270]. The submodel accounts for the oxygen vitiation and thermal feedback effects to the fuel from the hot gases and the enclosure surfaces.

7.6.1 *Burning rate*

The burning rate $\dot{m}_b$ is defined as the rate at which the fuel is consumed by the chemical reaction within the enclosure [270] and can be expressed as:

$$\dot{m}_b = \left\{ \begin{array}{ccc} \dot{m}_f & \phi < 1 \text{ and } & T_f > 1300^o C \\ \dot{m}_o/s & \phi \geqslant 1 \text{ and } & T_f > 1300^o C \\ 0 & & T_f \leqslant 1300^o C \end{array} \right\} \tag{7.5}$$

$$\phi = \frac{\dot{m}_f}{\dot{m}_o s} \tag{7.6}$$

where $\dot{m}_f$ is the mass loss rate of the fuel; $\dot{m}_o$ is the air flow into the enclosure; s is the stoichiometric air to fuel ratio; ϕ is the global equivalence ratio; and T_f is the flame temperature. A critical flame temperature of 1300°C is assumed, below which extinction occurs and no energy is generated into the system [271]. See Equation 7.14 later.

The energy release into the enclosure is then given by:

$$\dot{Q} = \Delta H_c \dot{m}_b \tag{7.7}$$

where ΔH_c is the effective heat of combustion of the fuel.

7.6.2 *Fuel response effects*

Given that user-supplied free-burn mass loss rate data is available, Equation 7.8 gives the fuel mass loss rate [270, 272]. The first term on the right-hand side is the free-burn mass loss rate. The second term is a reduction in mass loss rate due to a vitiated oxygen environment. The third term represents enhancement of the mass loss rate (or 'thermal effect') due to re-radiation from the hot gas layers and the enclosure surfaces (i.e. walls, ceiling and floor). The first two terms combined represent the vitiated oxygen effect on the flame flux and, in this chapter, is referred to as the 'ventilation effect'.

$$\dot{m}_f = \dot{m}_{FB} - \dot{m}_{FB}\left(1 - \frac{Y_{O_{2,l}}}{Y_{O_{2,\infty}}}\right) + \frac{\dot{Q}_{ext}}{L_g} \tag{7.8}$$

where $\dot{m}_{FB}$ is the user-supplied free-burn mass loss rate; $Y_{O_{2,l}}$ is the mass fraction of oxygen in the gases feeding the flame (or in the lower layer); $Y_{O_{2,\infty}}$ is the mass fraction of oxygen under ambient free-burning conditions; $\dot{Q}_{ext}$ is the total external heating rate from the hot

gas layers and enclosure surfaces; and L_g is the heat of gasification of the fuel.

The external heating rate used in Equation 7.8 is given by:

$$\dot{Q}_{ext} = \dot{q}''_{rad,inc} \left(A_{Fp} - A_{Fp,b} \right) + A_{Fp,b} \left(1 - \epsilon_f \right) \dot{q}''_{rad,inc} \tag{7.9}$$

where $\dot{q}''_{rad,inc}$ is the incident radiation flux on the fuel surface; A_{Fp} is the surface area of the fuel exposed to the radiation; $A_{Fp,b}$ is the burning area of the fuel; and ϵ_f is the flame emissivity.

The radiation reaching the burning area on the fuel surface is attenuated by the flame based on the flame emissivity. $\dot{q}''_{rad,inc}$ is computed by the radiation submodel in B-RISK and is approximated by the incident radiation on the floor surface resulting from radiation exchange between the hot gas layers and enclosure surfaces. Figure 7.3 illustrates the flaming and non-flaming surface area of a pool fire with radiation feedback. The projected flaming fuel surface area A_{Fp} is intended to represent the area affected by (or 'seeing') the radiation. For a pool fire it is simply the area of the pool.

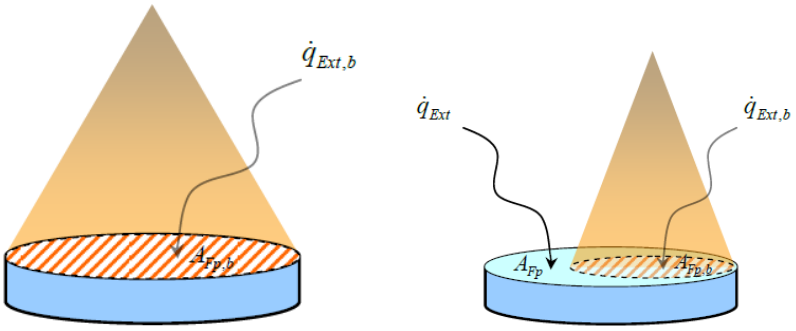

(a) (b)

Figure 7.3: External radiation feedback on flaming and non-flaming surface area for a pool fire. (a) over ventilated case (b) under ventilated case. Reprinted from Utiskul [225] with permission.

At each time step, the surface area of the fuel exposed to the radiation is calculated as:

$$A_{Fp} = \frac{\Delta H_c \dot{m}_{FB}}{\dot{q}''_c} \tag{7.10}$$

where $\dot{q}''_c$ – characteristic heat release rate per unit area for the fuel.

For a generic rectilinear object sitting on the floor and assuming that the top surface and four sides receive external radiation, a maximum value of the projected flaming fuel surface area could be given as:

$$A_{Fp} = LW + 2H(L + W) \tag{7.11}$$

where L is the object length, W is the object width and H is the object height. The lesser value of A_{Fp} calculated according to Equation 7.10 and Equation 7.11 is used in Equation 7.9.

In ventilation-limited conditions it is assumed that the burning is coupled to the rate at which air is supplied such that the flame may not cover the entire exposed surface area of the fuel. Utiskul and Quintiere [273] proposed that the flame burns only on a certain area to match the needed fuel and then moves when the local fuel is exhausted. This agreed with their own observations and those of Thomas and Bennetts [274] who observed flames burning partially over liquid fuel trays. The flame initially formed at the tray closest to the vent, and when that fuel was consumed, the flame moved towards the rear of the enclosure to the next tray.

For the underventilated condition ($\phi \geqslant 1$) where $\dot{m}_b = \dot{m}_o/s$, the flaming area $A_{Fp,b}$ is given as [264]:

$$A_{Fp,b} = \frac{\dot{m}_o/s}{\dot{m}''_{FB}\dfrac{Y_{O_{2,l}}}{Y_{O_{2,\infty}}} + (1-\epsilon_f)\dfrac{\dot{q}''_{rad,inc}}{L_g}} \tag{7.12}$$

where $\dot{m}''_{FB}$ is the free-burn mass loss rate per unit area, $\dot{m}_{FB}/A_{Fp}$, $s = \Delta H_c/\Delta H_{O2}$ and $\dot{m}_o \approx Y_{O2,l}\dot{m}_p/Y_{O2,\infty}$. The term 'fuel surface area shrinkage ratio' $(A_{Fp,b}/A_{Fp})$ is used when the calculated 'burning' surface area is less than the exposed fuel surface area. Under these conditions, Equation 7.8 is reformulated as:

$$\dot{m}_f = \dot{m}_{FB}\frac{A_{F,b}}{A_F}\frac{Y_{O_{2,l}}}{Y_{O_{2,\infty}}} + \frac{\dot{Q}_{ext}}{L_g} \tag{7.13}$$

To determine if extinction occurs, the flame temperature is calculated, and extinction is assumed to occur ($\dot{m}_b = 0$) if the calculated flame temperature is below 1300°C [271].

$$T_f = T_l + \frac{\Delta H_c - L_g + c_p\,(T_v - T_l) + \dfrac{\dot{q}_{ext,b}}{\dot{m}_f}}{c_p\,[1 + (r/Y_{O2,l})]} \tag{7.14}$$

7.7 BENCHMARKING - HEPTANE PAN EXPERIMENTS

7.7.1 *Scenario description*

The modified B-RISK model (version 2019.03) has been used to predict the mass loss rate and enclosure gas temperature for a series of 14 experiments conducted by Fleischmann and Parkes [263] burning 20 cm diameter pans of heptane in a reduced scale enclosure with a

single opening. The size of the wall opening was varied in each experiment such that the opening factor varied from 0.0039 to 0.071 $m^{5/2}$ with a total of nine different opening geometries. They measured the free-burn mass loss rate for the 20 cm diameter pan of heptane to be 0.0011 kg/s noting that it was 1.8 times greater than that calculated from Equation 7.15 a common used expression for burning organic liquids in the radiative regime.

$$\dot{m} = \dot{m}''_{\infty} \left(1 - e^{-k\beta D}\right) A \tag{7.15}$$

Babrauskas [246] gives the relevant thermophysical and empirical constants for heptane as $\dot{m}''_{\infty} = 0.101(\pm 0.009)$ $kg.m^{-2}.s^{-1}$, $k\beta = 1.1(\pm 0.3)$ m^{-1} and where D is the pool diameter in m and A is the area of the pool fire in m^2. There were 14 experiments conducted with variations in the dimensions of the wall opening. The experiments are summarised in Table 7.1 showing the vent width, height, soffit elevation and opening factor. Also shown is the measured mass loss rate and average gas temperature recorded (for the thermocouple tree nearest the opening) over the steady burning period.

Run	W (m)	H (m)	Soffit (m)	Opening factor $AH^{1/2}$ ($m^{5/2}$)	MLR (kg/s)	T_{avg} (K)
1	0.20	0.50	0.75	0.0707	0.0043	1318
2	0.13	0.50	0.75	0.0460	0.0023	1157
3	0.13	0.50	0.75	0.0460	0.0024	1234
4	0.13	0.38	0.63	0.0305	0.0021	1059
5	0.06	0.50	0.75	0.0212	0.0017	999
6	0.13	0.25	0.50	0.0163	0.0012	884
7	0.13	0.25	0.75	0.0163	0.0012	891
8	0.06	0.38	0.63	0.0141	0.0011	887
9	0.03	0.50	0.75	0.0106	0.0012	849
10	0.03	0.50	0.75	0.0106	0.0011	856
11	0.06	0.25	0.50	0.0075	0.0007	777
12	0.03	0.38	0.63	0.0070	0.0009	850
13	0.03	0.25	0.50	0.0038	*a*	
14	0.03	0.25	0.50	0.0038	*a*	

a Fire self-extinguished without reaching steady state.

Table 7.1: Experiment summary - data from Fleischmann and Parkes [263].

The apparatus used by Fleischmann and Parkes is shown in Figure 7.4 and comprised an enclosure with dimensions 1.48 m long, 0.95 m wide and 0.98 m high. The enclosure walls and ceiling was constructed with three layers of a 25 mm thick refractory fibre blanket installed over a 20 mm layer of calcium silicate board and 20 mm

layer of gypsum wallboard. The floor comprised two 20 mm layers of calcium silicate board over a 20 mm layer of gypsum wallboard [263].

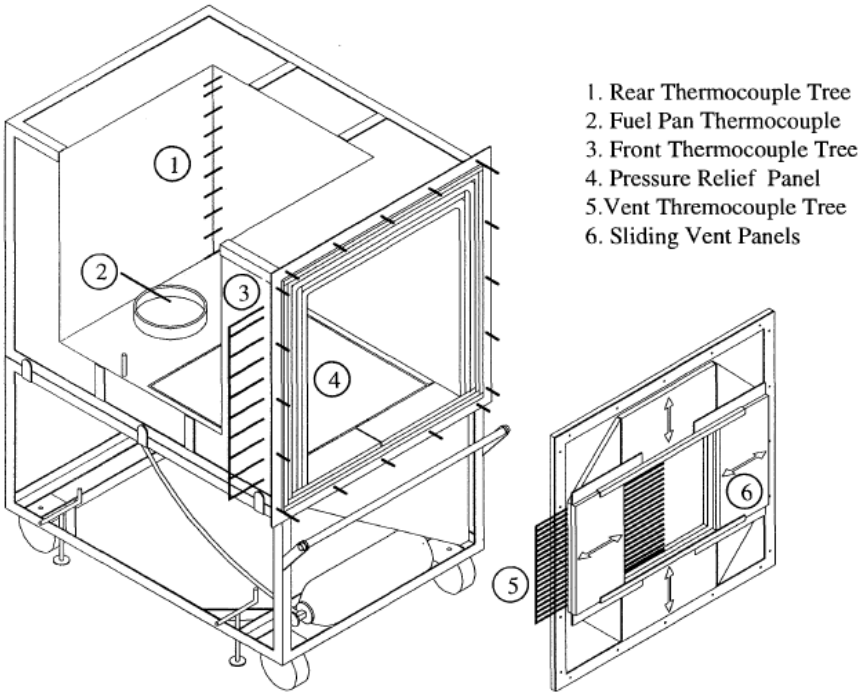

Figure 7.4: Sketch of the experimental apparatus used by Fleischmann and Parkes. Reprinted from Fleischmann and Parkes [263] with permission from the IAFSS.

7.7.2 *Model baseline parameters*

In all cases, the heptane pool was in a container 0.2 m diameter and 35 mm high (above the floor surface). The pan was placed in the rear of the enclosure with the heptane supplied from a header tank to maintain a constant fuel surface height [263]. For the simulations, fuel heat of combustion was taken as 41.2 kJ/g [229, 264], the radiant loss fraction 0.33 [229], carbon dioxide yield 2.85 g/g [229] and soot yield 0.037 g/g [229]. The effective heat of gasification for heptane burning in a 9.5 cm pan was experimentally approximated by Utiskul from experiments using a cone calorimeter as 0.87 kJ/g [225]. This value was assumed in the simulations here. Given the fuel heat of combustion, pan surface area and the free-burn mass rate are known for these pool fire experiments, a characteristic heat release rate per unit area of 1443 kW/m^2 is calculated for consistency in Equation 7.10.

The model simulations assumed the thermal properties for the enclosure selected from the B-RISK materials database as shown in Table 7.2.

Property	Refractory Fibre Blanket	calcium Silicate Board	gypsum Board
Thickness mm	75	20	20
Thermal conductivity W/m.K	0.09	0.08	0.16
Density kg/m^3	128	336	810
Heat capacity J/kg.K	1040	1090	900

Table 7.2: Thermal properties used as model input.

7.7.3 *Model predictions and discussion*

Figure 7.5 shows a scatterplot comparing the measured fuel mass loss rate over the steady burning period with the predicted mass loss rate from the model. On average the model overpredicted the mass loss rate by 15%. The expanded uncertainty in the measured mass loss rate was not reported but has been estimated as 10% for the purposes of the scatterplot. The expanded uncertainty (2 standard deviation) is estimated to be 36% for the model predictions of the mass loss rate.

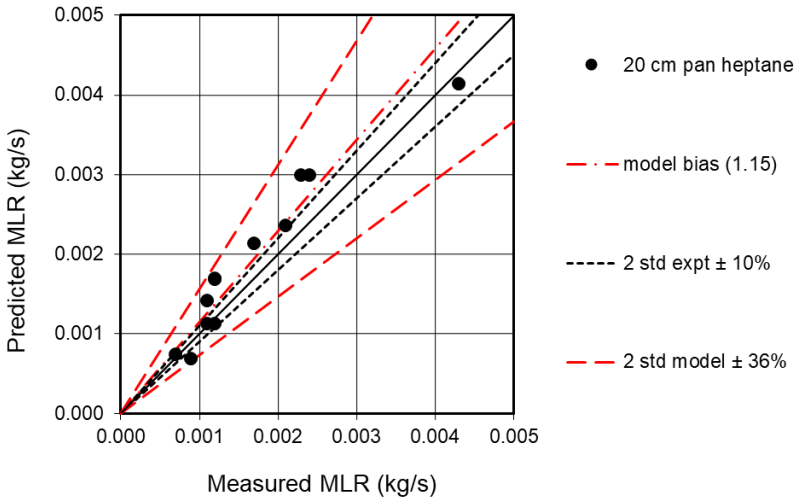

Figure 7.5: Scatterplot comparing measured and predicted mass loss rate of heptane fuel.

Figure 7.6 shows a scatterplot comparing the measured average enclosure gas temperature over the steady burning period with the predicted average enclosure gas temperature from the model. On average the model underpredicted the gas temperature by 2%. The expanded uncertainty in the measured temperatures was not reported but has been estimated from the literature as 14%. The expanded uncertainty (2 standard deviation) is estimated to also be 14% for the

model predictions of gas temperature indicating the predictions can be considered to be within experimental uncertainty.

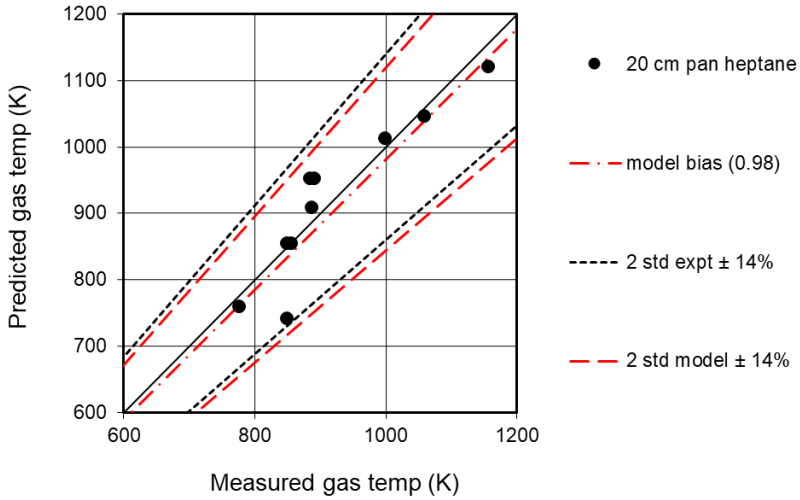

Figure 7.6: Scatterplot comparing measured and predicted enclosure gas temperature.

For runs 13 and 14, Fleischmann and Parkes observed that the fire self-extinguished before reaching a steady state regime therefore the mass loss rate and average gas temperature are not reported here. These runs are also excluded from the scatterplots shown in Figure 7.5 and Figure 7.6. For all other runs, the average values over the period 3600 - 5400 seconds were used for the predicted values. The scatterplots were generated using the methodology described by McGrattan et al. [254] (see Appendix C). The mass loss rate and gas temperature predicted by the model for runs 13 and 14 were 0.0004 kg/s and 360°C giving the lowest values of all the experiments simulated.

To demonstrate the application of the model for Run 1 which was the largest opening factor included in the Fleischmann and Parkes study, Figure 7.7 shows the contribution to the total mass loss rate due to the thermal feedback effect and due to the ventilation effect. The mass loss rate of the fuel for the free burning case in the open is also shown. The (oscillation) noise in the predicted values is a result of the predicted flame temperature switching above and below the flame extinction criterion of 1300°C.

7.8 BENCHMARKING - UPHOLSTERED CHAIR EXPERIMENTS

7.8.1 *Scenario description*

The modified B-RISK model (version 2016.031) was used to predict the mass loss and heat release rate for a series of five enclosure exper-

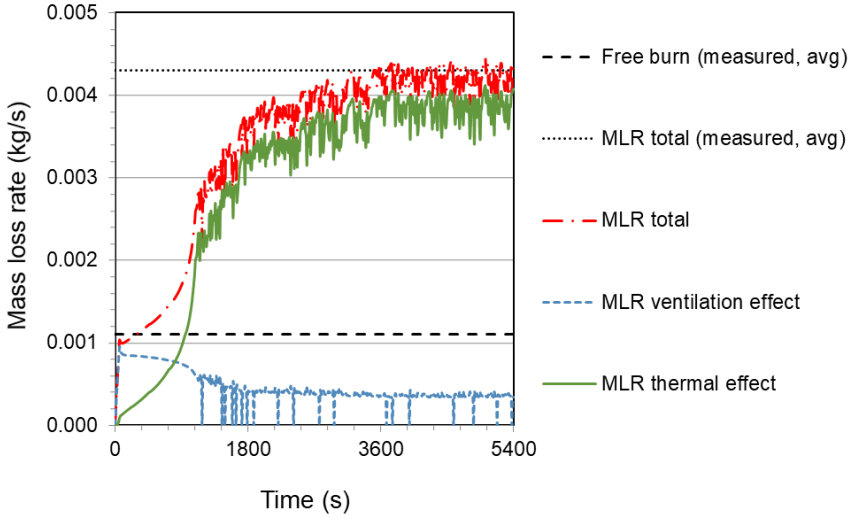

Figure 7.7: Predicted contributions to mass loss rate for Run 1 (see Table 7.1).

iments with upholstered chairs as the fuel source. These experiments were previously carried out at the University of Canterbury and reported by Girgis [275]. Only experiments where the mass loss rate of the chair was measured in both the ISO 9705 room and in the furniture calorimeter were selected as they give a meaningful comparison.

The scenario investigated involved an upholstered chair positioned in the rear corner of an ISO 9705 room [120] as illustrated in Figure 7.8. The room measured 3.6 m long, 2.4 m wide and 2.4 m high with an opening 2.0 m high and 0.8 m wide in one of the short walls. The room was lined with two layers of 12.5 mm thick paper-faced gypsum plasterboard. The ignition source was a 30 kW propane gas burner ring exposing the top surface of the chair seat. The chairs were constructed using typical upholstered furniture fabric (100% polypropylene) and polyurethane foam combinations, and the design followed that used in the CBUF study [276]. The five chair specimens reported here varied only in the foam type used.

7.8.2 *Model baseline parameters*

Free-burning mass loss rate data for each of the upholstered chairs was input to the modified B-RISK model. This free-burn data was previously obtained from the furniture calorimeter experiments conducted by Denize [277]. The mass and energy contributed by the gas burner has not been accounted for in the model predictions and was relatively small ($\approx$ 30 kW) compared to the heat output from the chairs i. e. less than 10% of the peak HRR. Details for each chair are summarised in Table 7.3.

Figure 7.8: View of an upholstered chair placed in the corner of the room with ignition gas burner in place. Reprinted from Girgis [275] with permission.

ID	Foam density kg/m^3	Foam type	Total mass loss kg	$\Delta H_{c,eff}$ kJ/g	$\dot{Q}''_{avg,300s}$ kW/m^2	$\dot{Q}''_{peak}$ kW/m^2
H	37	Superior domestic furniture (FR)	11.72	24.3	239.6	440.9
G	28	Domestic furniture seats	12.61	25.4	208.2	435.0
I	35	Superior domestic furniture, public seating	11.24	25.6	239.7	470.3
J	36	Public auditorium seating (FR)	14.42	21.1	206.9	379.8
L	36	Public auditorium and transport seating	12.53	25.0	266.8	450.4

Table 7.3: Chair details based on data from Denize [277] and Girgis [275].

The total combustible mass was estimated from the measured mass of the chair before and after the room experiment. When the model determined that all the available mass had been pyrolysed, the mass loss rate was set to zero thereafter. The effective heat of combustion for each chair was based on the cone calorimeter experiments for each

foam-fabric combination also carried out by Denize [277]. The 300-s average and peak HRRPUA based on cone calorimeter experiments for each foam-fabric combination are also shown [277]. Other model inputs included a radiant loss fraction 0.52 [229], soot yield 0.131 kg/kg [229], carbon dioxide yield 1.55 [229], stoichiometric air/fuel ratio 9.5 and latent heat of gasification 1.4 kJ/g [278]. These values were based on typical properties for flexible polyurethane foam since they were not measured by either Girgis or Denize.

The material selected for the walls, ceiling and floor was 25 mm thick 'plasterboard' from the B-RISK database with a thermal conductivity 0.16 W/(m K), density 810 kg/m^3 and specific heat 900 J/(kg K). The corner plume entrainment algorithm in B-RISK was selected to correspond with the experimental configuration with the base of the fire taken as 0.315 m above floor level.

7.8.3 *Model predictions*

Figure 7.9 shows the total mass loss rate versus time, predicted and measured in the enclosure experiments for each of the five chairs. The mass loss rate for the same chairs under free-burn conditions as measured in the furniture calorimeter and used for input to the model is also shown.

Figure 7.10 shows the heat release rate versus time predicted and measured in the enclosure experiments for each of the five chairs. The heat release rate for the same chairs under free-burn conditions as measured in the furniture calorimeter is also shown. The predicted heat release rate shown here is total theoretical HRR including the energy released both inside and outside the room. Since HRR measurements for the room experiments were from oxygen calorimetry downstream of the collection hood, it is impossible to distinguish, other than visually, between HRR inside and outside the room opening. It was therefore more appropriate in this case to compare the prediction for the total theoretical HRR with the measured data. B-RISK calculates the HRR inside the room as well as the HRR from combustion of any unburned mass transported along with the vent flow out.

Chairs 21-I-S2-1 and 21-L-S2-1 both show a sudden drop to zero in the mass loss rate (Figure 7.9(c) and (e)) and heat release rate (Figure 7.10 (c) and (e)). This occurs when the model has calculated that the total available combustible mass as shown in Table 7.3 has been consumed. A comparison between the predicted and measured peak mass loss rate of the upholstered chairs in the enclosure experiments is shown in Figure 7.11. The comparisons include an estimate of model bias and uncertainty using the procedure described by McGrattan et al [254] and as described in Appendix C. The bias factor indicates the extent to which the model, on average, underpredicts or

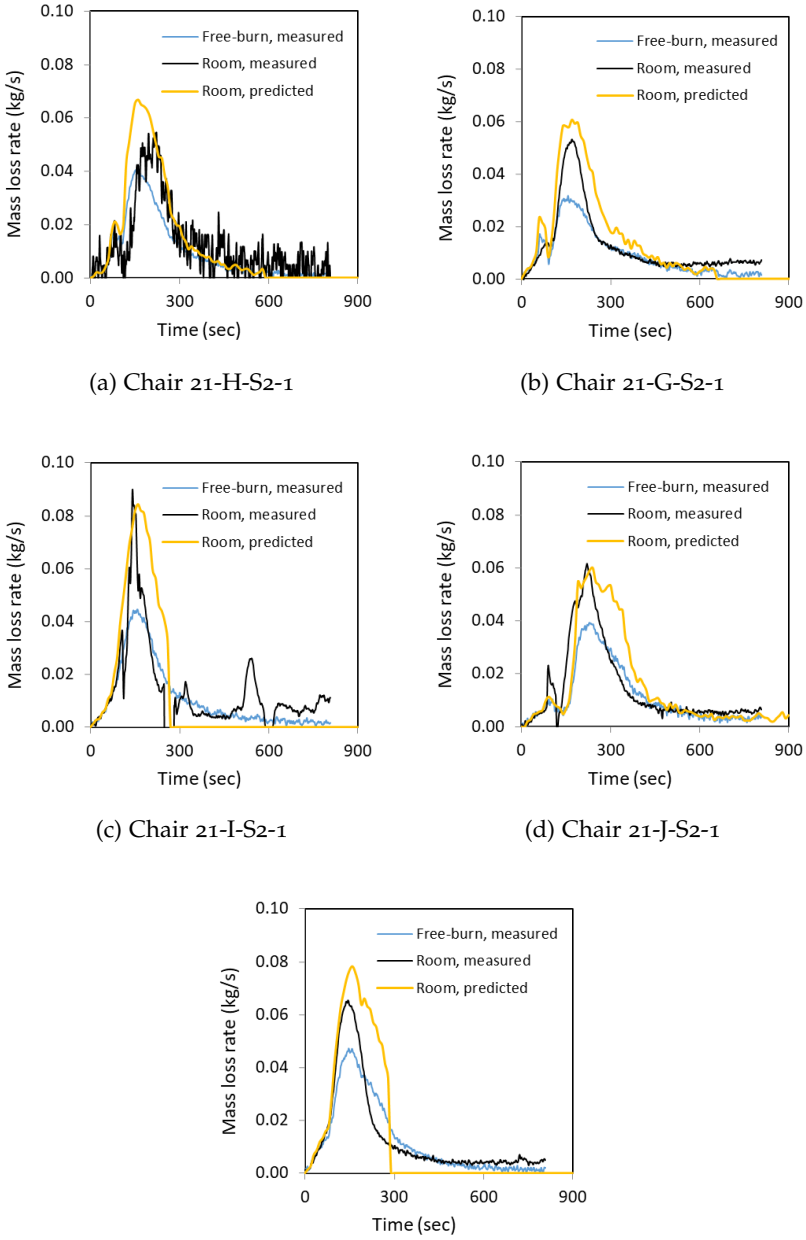

(a) Chair 21-H-S2-1

(b) Chair 21-G-S2-1

(c) Chair 21-I-S2-1

(d) Chair 21-J-S2-1

(e) Chair 21-L-S2-1

Figure 7.9: Mass loss rate versus time for furniture calorimeter and room experiments compared with model predictions.

overpredicts the measurements. The model bias factor was calculated as 1.09.

In addition, a comparison between the predicted and measured peak heat release rate of the upholstered chairs in the enclosure experiments is shown in Figure 7.12. The model bias factor for the peak heat release rate was calculated as 1.27 using the same methodology [254]. The expanded uncertainties in the mass loss rate and HRR mea-

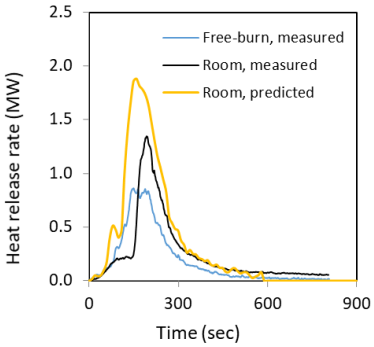

(a) Chair 21-H-S2-1

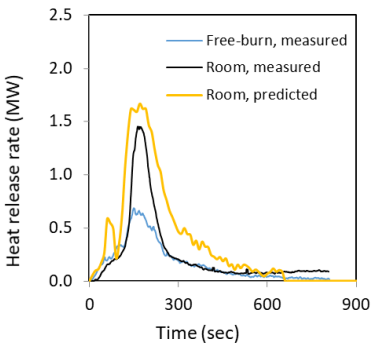

(b) Chair 21-G-S2-1

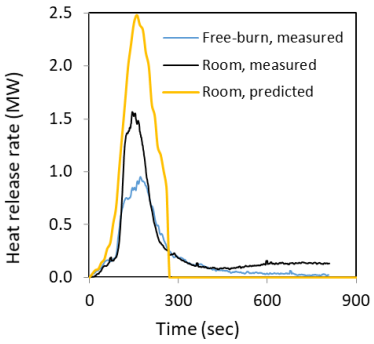

(c) Chair 21-I-S2-1

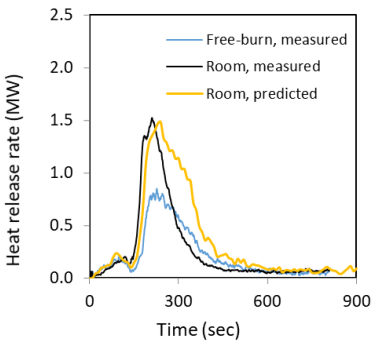

(d) Chair 21-J-S2-1

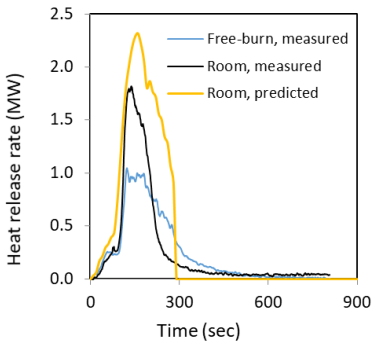

(e) Chair 21-L-S2-1

Figure 7.10: Heat release rate versus time for furniture calorimeter and room experiments compared with model predictions.

surements were not known. They have been estimated here, based on review of the literature, as ±10% and ±20% respectively at the 95% confidence interval (two standard deviation, 2 std) [279].

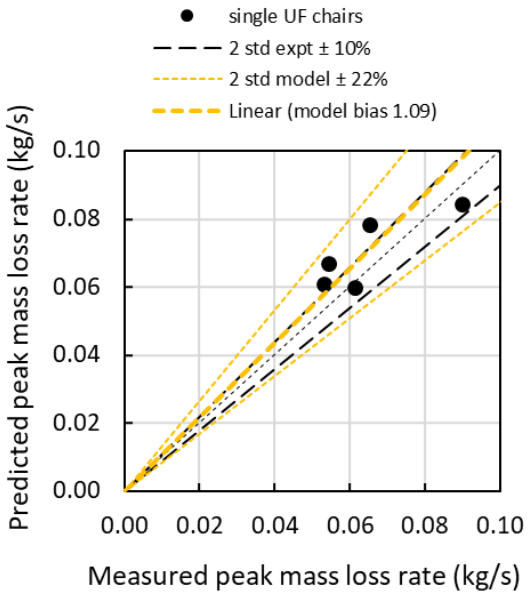

Figure 7.11: Predicted versus measured peak mass loss rate.

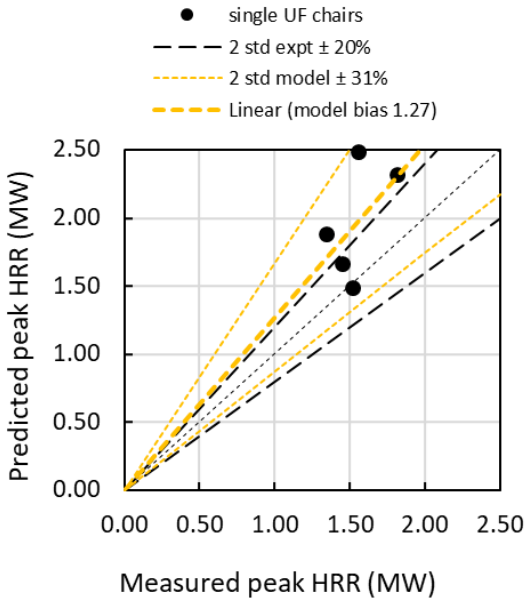

Figure 7.12: Predicted versus measured peak heat release rate.

7.8.4 *Discussion*

7.8.4.1 *General*

The heat output from the ignition burner is not included separately in the model calculations. However, the prediction does assume the

same ignition source characteristics such as position relative to the chair and heat output as used in the furniture calorimeter experiments. This is implicit in the measured free-burn mass loss rate data used as model input.

The model also assumes the same incident radiant flux on all exposed fuel surfaces at any point in time, this being equal to the flux calculated as incident on the floor surface. In practice, the incident radiant flux would vary depending on the orientation and location of the various fuel surfaces on different parts of the chair.

7.8.4.2 *Contribution to total mass loss rate*

Figure 7.13 shows the individual contributions (due to ventilation and the thermal effects) to the predicted total mass loss rate (MLR) of chair 21-G-S2-1. This is compared with the measured free-burn and the total mass loss rate versus time. Early in the fire growth period, the ventilation effect is the main contributor to the predicted total mass loss rate. During the peak burning period, the thermal effect is greater than the ventilation effect. In this example, the peak mass loss rate is approximately double that measured for the same chair in the furniture calorimeter. The plateau in the predicted ventilation effect is principally due to fuel area shrinkage during the time of ventilation control. The predicted fuel surface area shrinkage ratio $(A_{F,b}/A_F)$ to match the available air supply is shown in Figure 7.14.

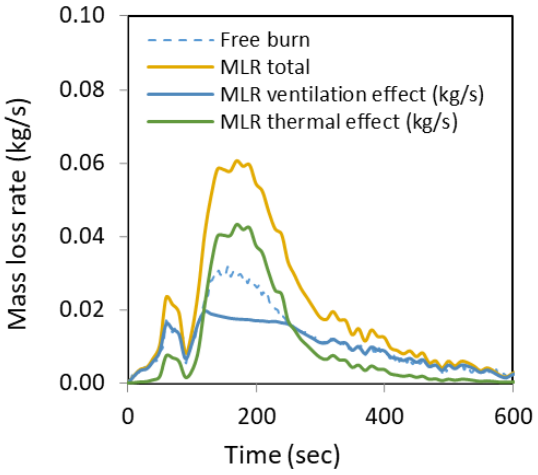

Figure 7.13: Chair 21-G-S2-1: mass loss rate model predictions.

7.8.4.3 *Sensitivity to HRRPUA input*

The model used 300-s average HRRPUA, shown in Table 7.3, obtained from cone calorimeter experiments for the same foam-fabric combination as the chair specimen in the room experiment. This was used in

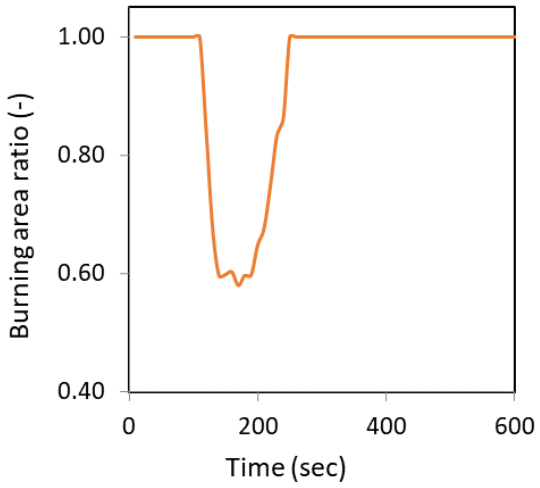

Figure 7.14: Chair 21-G-S2-1: fuel surface area shrinkage ratio.

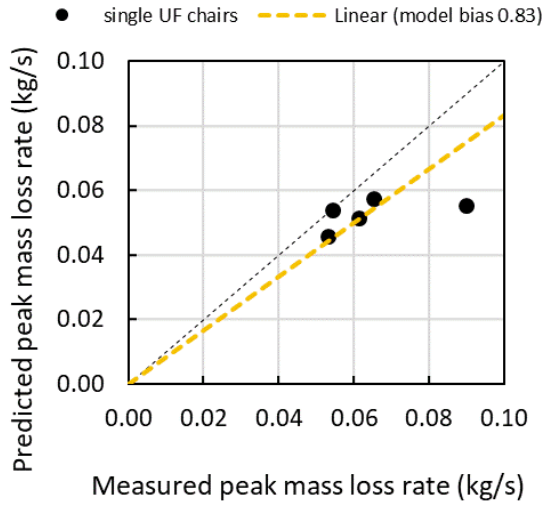

Figure 7.15: Predicted vs measured peak mass loss rate (with peak HRRPUA as input instead of 300-s average).

Equation 7.12 to determine the fuel surface area over time, which was assumed to follow the shape of the mass loss rate for the chair under free-burning conditions. The results were therefore quite sensitive to this parameter. For example, the simulations were repeated using the peak HRRPUA (also shown in Table 7.3) instead of the 300-s average from the cone calorimeter experiments. This resulted in a smaller fuel surface as well as lower mass loss rate and heat release rate predictions for the room experiment. For this case, Figure 7.15 and Figure 7.16 compare the predicted and measured peak mass loss rate and heat release rates respectively. The bias factors (see Appendix C)

were determined as 0.83 and 0.94 respectively, indicating a trend towards underpredicting the peak mass loss rate and peak heat release rate. Therefore, using the 300-s average HRRPUA is preferred over the peak HRRPUA as it provided a conservative prediction for the peak mass loss rate and peak heat release rate.

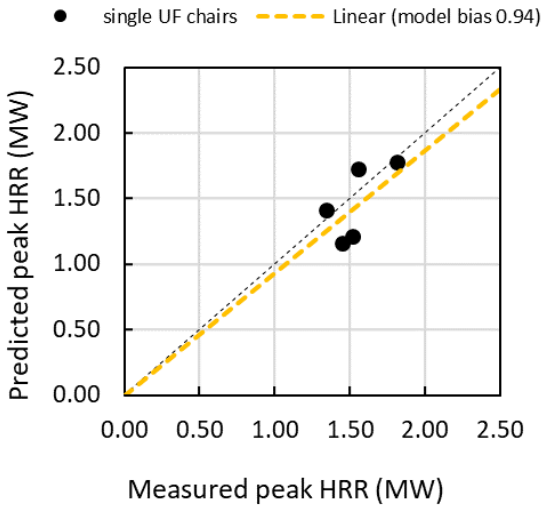

Figure 7.16: Predicted vs measured peak heat release rate (with peak HRRPUA as input instead of 300-s average).

7.8.4.4 *Sensitivity to chair position in the room*

The experiments were carried out with the chairs positioned in the rear corner of the room. B-RISK includes different plume entrainment algorithms for the centre, wall and corner location, and in this case, the algorithm for the corner location (based on Zukoski's correlation [280]) was selected. To assess the significance of this, additional simulations were carried out using a centre location and with other inputs as given in Section 7.8.2. Figure 7.17 and Figure 7.18 compare the predicted and measured peak mass loss rate and peak heat release rate respectively.

The bias factors were determined as 1.66 and 1.69 respectively (see Appendix C). The comparison of the peak values is particularly skewed by large peak values for two of the chairs (21-I-S2-1 and 21-L-S2-1). An example of this for chair 21-L-S2-1 is shown in Figure 7.19 and Figure 7.20. A higher plume entrainment rate due to a centre location increases the oxygen available for combustion in the plume and is consistent with increased mass loss and heat release rates. Therefore the use of the corner plume algorithm matching the experiment configuration was the appropriate choice.

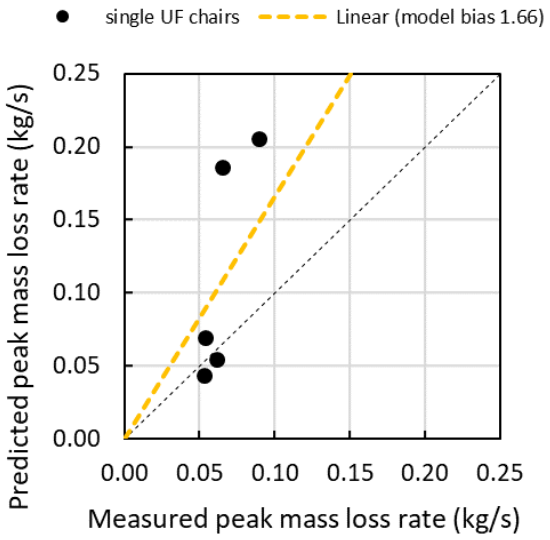

Figure 7.17: Predicted vs measured peak mass loss rate (with axisymmetric plume entrainment).

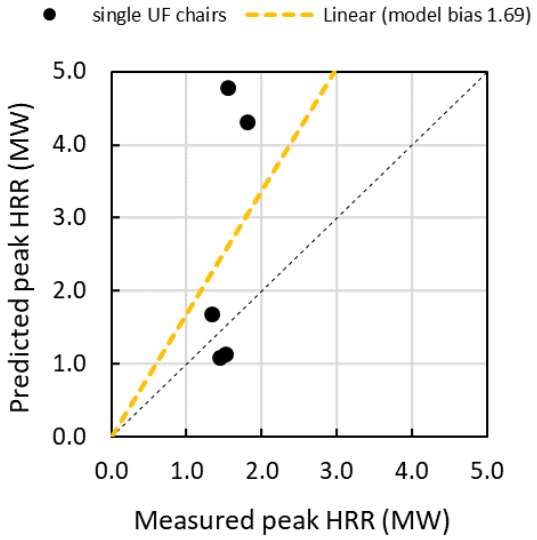

Figure 7.18: Predicted vs measured peak heat release rate (with axisymmetric plume entrainment).

7.8.4.5 *Sensitivity to heat of gasification*

Given the range for heat of gasification reported in the literature [278] for 'flexible polyurethane foam', the effect of increasing the heat of gasification from 1.4 to 2.4 kJ/g was investigated. Other inputs were as given in section 4.2 with a corner location. Figure 7.21 and Figure 7.22 compare the predicted and measured peak mass loss rate

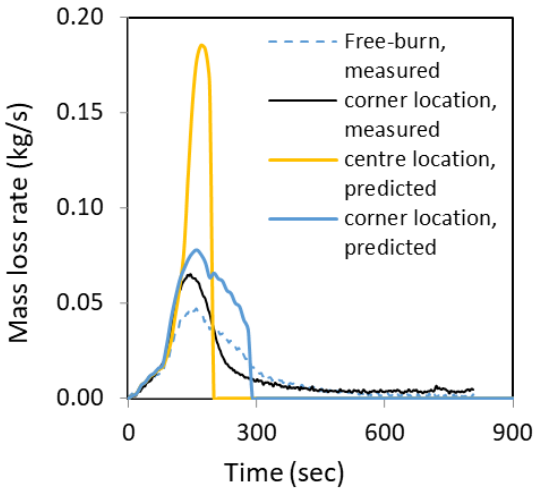

Figure 7.19: Predicted vs measured mass loss rate (21-L-S2-1 corner vs centre location).

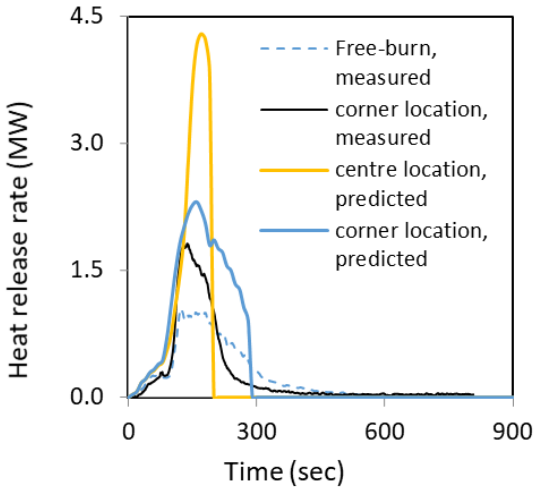

Figure 7.20: Predicted vs measured heat release rate (21-L-S2-1 corner vs centre location).

and heat release rates respectively. The bias factors were determined as 0.83 and 0.98 respectively (see Appendix C). Increasing the heat of gasification reduces the mass loss rate (as per Equation 7.8) because of the higher energy needed to gasify the fuel.

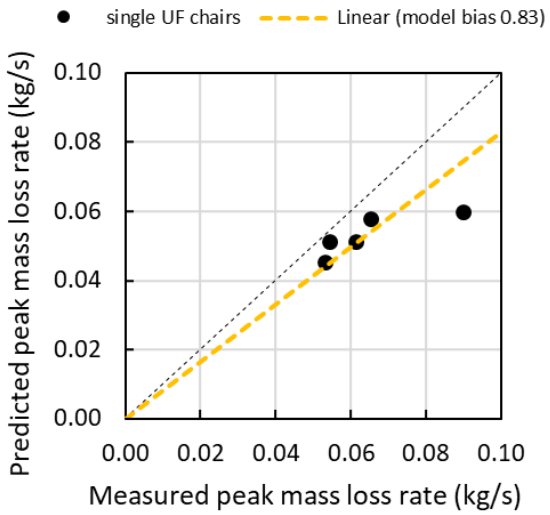

Figure 7.21: Predicted vs measured peak mass loss rate (with heat of gasification 1.4 kJ/g).

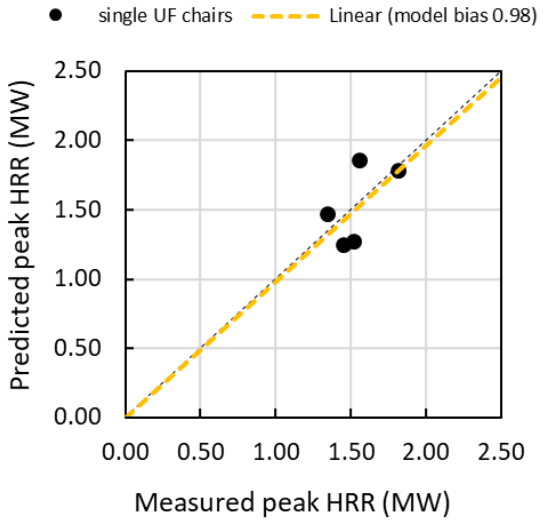

Figure 7.22: Predicted vs measured peak heat release rate (with heat of gasification 2.4 kJ/g).

7.9 SUMMARY

A predictive model for calculating the mass loss rate in an enclosure fire has been implemented within the B-RISK two-zone model. The model includes both ventilation and thermal effects on the fuel response and utilises measured free-burn data for the fire source as input. The enclosure bounding surfaces are assumed to be inert and do not contribute to the fuel load.

Free-burn mass loss rate data for upholstered furniture is readily obtained by placing the item on scales beneath a furniture calorimeter under well-ventilated ambient conditions. Correlations are available in the literature for estimating the free-burn mass loss rate for liquid pool fires and for wood cribs.

The model was used to predict the mass loss and heat release rates of 14 heptane pool fire experiments in a vented enclosure; and 5 upholstered chairs burning within a different vented enclosure. For the heptane pool fires the predicted peak mass loss rate was on average overestimated by 15% and for the upholstered chair experiments on average overestimated by 9% when the foam-fabric 300-s average HRRPUA input was used. The predicted gas temperatures for the heptane experiments were on average underpredicted by 2% but within experimental error. The predicted peak heat release rate for the upholstered chairs was on average overestimated by 27%. Therefore it is concluded that the fuel response effects submodel as implemented within B-RISK provides generally conservative prediction of the overall enclosure effects influencing the mass loss rate. This is considered relevant for engineering analysis.

However, it is noted that predictions are sensitive to the input parameters that characterise the fuel and its position in the enclosure. Further investigation and benchmarking of the submodel against other experimental datasets would be useful to confirm if the parameter selections reported here have wider applicability.

8

FUEL RESPONSE EFFECTS IN MASS TIMBER ENCLOSURES

8.1 GENERAL

This chapter describes and discusses the modified B-RISK enclosure fire model with both the fuel response effects submodel from Chapter 7 and the kinetic submodel for wood burning surfaces from Section 5.7 both active. The application of the model for predicting fire development incorporating fuel response effects and mass timber contributions is explored with reference to the experiments by Hadden et al. [165] previously presented in Section 6.3 and experiments by Su et al. [171] presented in Section 6.5. There are limited experimental data in the literature where well-characterised fuel contents have been burned both in the open (with mass loss rate measurements) and within an enclosure of exposed or partially protected mass timber construction. Therefore this feature of the model is somewhat exploratory and no strong conclusions are drawn about the overall accuracy of this part of the model.

8.2 UNIVERSITY OF EDINBURGH EXPERIMENTS

In the Hadden et al. [165] experiments there were four wood cribs as the moveable fire load as previously shown in Figure 6.24. Each crib consisted of 5 layers of 25 x 25 mm sticks, each 1 m in length with a clear spacing between sticks of 75 mm. The total mass of timber was approximately 56 kg in each experiment. Hadden et al. measured the mass loss rate of the cribs during each experiment and this is shown in Figure 8.1. Repeat experiments were conducted in the case of Config. F and Config. G.

The four wood cribs were closely spaced and here are treated as a single large crib 2 m wide $\times$ 2 long $\times$ 0.125 m high. The free burn mass loss rate of the wood cribs has been estimated from the correlations given by Babrauskas [246] and as presented in Section 5.4. The calculated free burn mass loss rate is given in Figure 8.2 however the curve was time-shifted by 4 minutes to better match the measured start of the fire growth. A 30-sec ramp up period was also added to the start. The calculated mass loss rate for the wood cribs with a peak of 0.18 kg/s is comparable to those shown in Figure 8.1 with good agreement for the peak mass loss rate. Since the fuel comprised wood cribs it is acknowledged that any burning rate thermal enhancement was not expected to be very significant (due to many surfaces in the

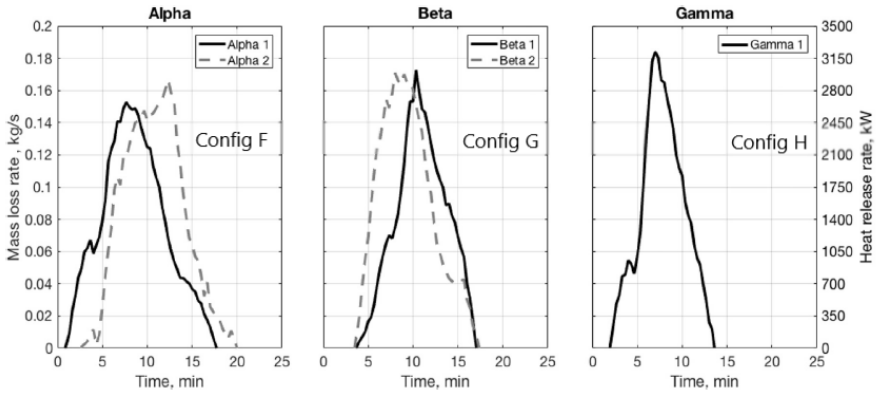

Figure 8.1: Mass loss rate of wood cribs measured during experiments by Hadden et al. Reprinted from Hadden et al. [165] under a Creative Commons License.

crib lattice being shielded from the external radiation as discussed in Section 7.1) and this is apparent by comparing Figure 8.1 and Figure 8.2. therefore, these experiments are not ideal for the evaluating this feature of the model. A more thorough evaluation in the future using a wider variety of fuel types is recommended.

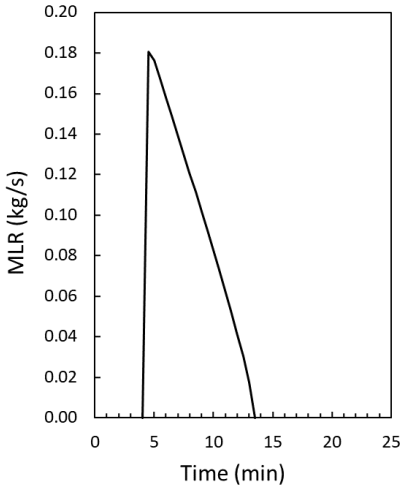

Figure 8.2: Free burn mass loss rate of wood cribs calculated from correlations in [246].

As with previous simulations an effective heat of combustion for wood of 14 MJ/kg has been assumed [146]. A carbon dioxide yield of 1.33 g/g, soot yield 0.015 g/g and a radiant loss fraction of 0.3 were also assumed [229] and a flame absorption coefficient of 0.8 m^{-1} from Lautenberger [281]. Other parameters for the enclosure dimensions, ventilation and thermal properties are as described in Chapter 6.

A characteristic HRRPUA for wood of 154 kW/m^2 for use in the fuel response effects submodel (i.e. Equation 7.10) has been used be-

ing a 300 s average from cone calorimeter experiments at an irradiance of 50 kW/m^2 as reported by Collier et al. [282]. A 300 s average value was also used for the upholstered chair fires as previously discussed in Section 7.8.4.3. However, based on the overall dimensions of these cribs, in this case Equation 7.10 is only used after the mass loss rate is below 0.055 kg/s i.e. when Equation 7.10 governs rather than Equation 7.11. This is the point at which Equation 7.10 governs rather than Equation 7.11.

The heat of gasification of wood was taken as 2.8 kJ/g [42] however it is acknowledged that a wide range of values can be found in the literature. For example, Tewarson and Pion [283] give 1.82 kJ/g while Quintiere et al. [284] quote a heat of gasification of 6.3 kJ/g for a spruce wood panel and a value of 6.2 kJ/g for an ordinary birch plywood.

The three configurations investigated by Hadden et al. [165] differed only in the proportion of timber surfaces that were unprotected or exposed within the enclosure.

8.2.1 *Config. F - 50% walls exposed*

With the free burn mass loss rate for the wood cribs from Figure 8.2 used as input to the model, the resultant mass loss rate curve including the enclosure effects on the fuel response is shown in Figure 8.3. The model prediction of the total mass loss rate shows only a small enhancement effect which is consistent with a wood crib. Since the total mass of fuel must be conserved for the moveable fire load, the mass loss rate drops to zero when the total mass loss corresponds to the initial mass of the moveable fire load.

The predicted HRR including the relative proportions burning inside and outside the enclosure is shown in Figure 8.4 along with the total measured HRR during experiments. In the experiment designated alpha-1 in Figure 8.4, plasterboard protection started to fall off from about 23 minutes. Hadden et al. reported that the load cell system indicated 26 instances of plasterboard falloff. They estimated 99 kg of plasterboard fell in total.

The HRR after the burnout of the moveable fire load is solely due to the burning exposed wood wall surfaces. Plasterboard started to fall during the alpha-1 test from 23 minutes exposing additional wood surfaces, while in alpha-2 no involvement of protected wood surfaces occurred. The predicted HRR was less than the measured HRR following the predicted burnout time of the moveable fire load. The simulation was repeated using the debonding model with a debonding criterion of 300°C and this curve is also shown in Figure 8.4. With debonding, the simulation predicted complete burn-through of the walls within 40 minutes which was not the case in the experiment. It is apparent use of the debonding submodel leads to a char rate that

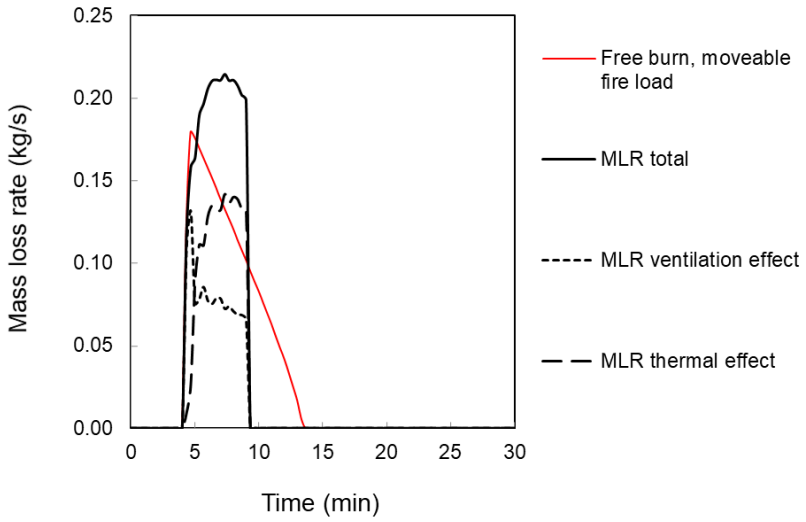

Figure 8.3: Config. F. Predicted mass loss rate (MLR) for moveable fire load based on specified free burn curve.

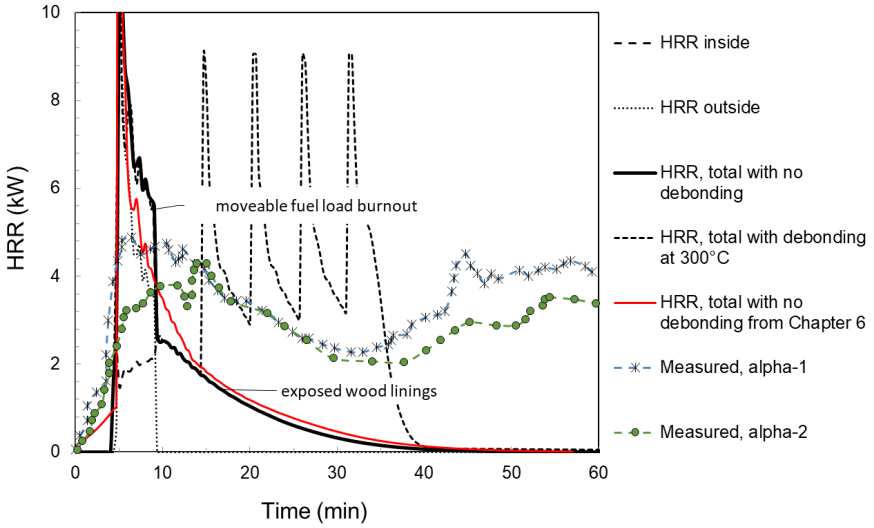

Figure 8.4: Config. F. Predicted HRR using both fuel response effects and kinetic wood pyrolysis submodels with and without debonding.

is much faster than occurred in the experiment probably due to the assumption that the entire lamella falls away instantaneously exposing the next lamella to the fire. As previously discussed in Section 5.8, debonding is a more gradual process.

8.2.2 *Config. G - 25% walls, 100% ceiling exposed*

With the free burn mass loss rate for the wood cribs from Figure 8.2 used as input to the model, the resultant mass loss rate curve for Config. G including the enclosure effects on the fuel response is shown in Figure 8.5.

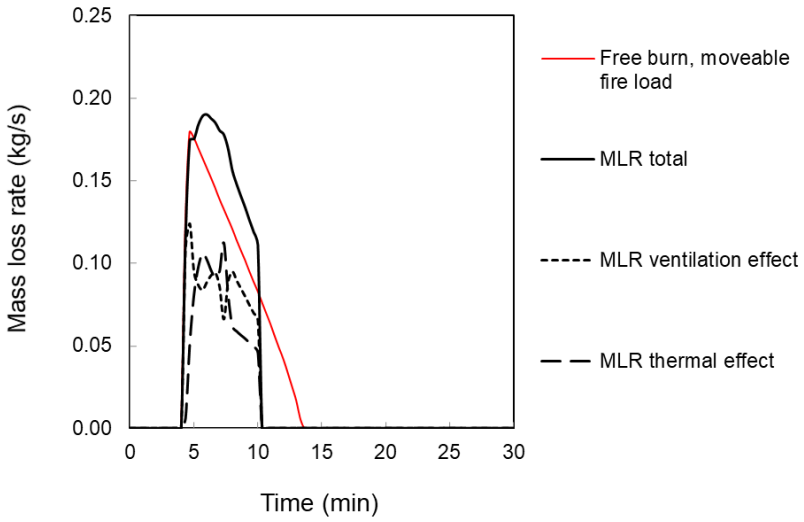

Figure 8.5: Config. G. Predicted mass loss rate (MLR) for moveable fire load based on specified free burn curve.

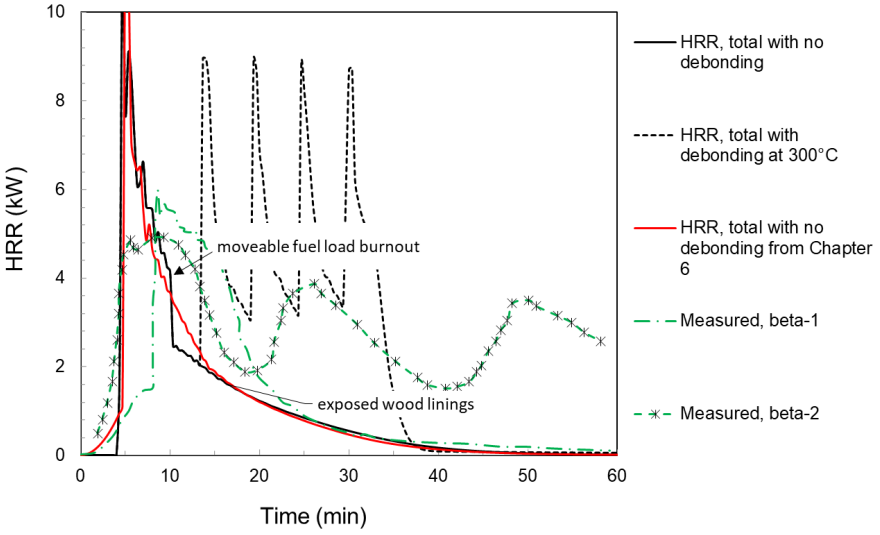

Figure 8.6: Config. G. Predicted HRR using both fuel response effects and kinetic wood pyrolysis submodels.

The predicted HRR including the proportions burning inside and outside the enclosure is shown in Figure 8.6 along with the total mea-

sured HRR during the repeated experiment designated beta-1 and beta-2. In the beta-2 experiment Hadden et al. observed there was about 8 kg of plasterboard in total that fell starting from 23 min which coincides with the regrowth as shown in Figure 8.6. There was no plasterboard fall off observed in the beta-1 experiment. At previously stated, the model does not consider the possibility of the gypsum board encapsulation falling off.

8.2.3 *Config. H - 50% walls, 100% ceiling exposed*

With the free burn mass loss rate for the wood cribs from Figure 8.2 used as input to the model, the resultant mass loss rate curve for Config. H including the enclosure effects on the fuel response is shown in Figure 8.7.

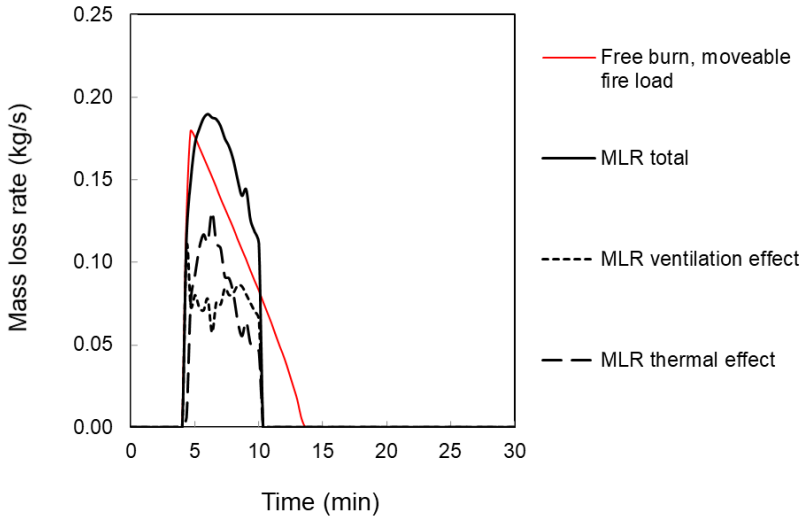

Figure 8.7: Config. H. Predicted mass loss rate (MLR) for moveable fire load based on specified free burn curve.

The predicted HRR including the proportions burning inside and outside the enclosure is shown in Figure 8.8 along with the total measured HRR during the experiment.

8.2.4 *Summary*

The results from simulations using both the fuel response effects and kinetic wood pyrolysis submodels for the Configs. F, G and H experiments show similar trends and are not greatly different from the previous results in Section 6.3 where the calculated free burn moveable fire load mass loss rate was used without enclosure effects. As previously stated this could be expected since the movable fire load was wood cribs with a large proportion of fuel surface area located

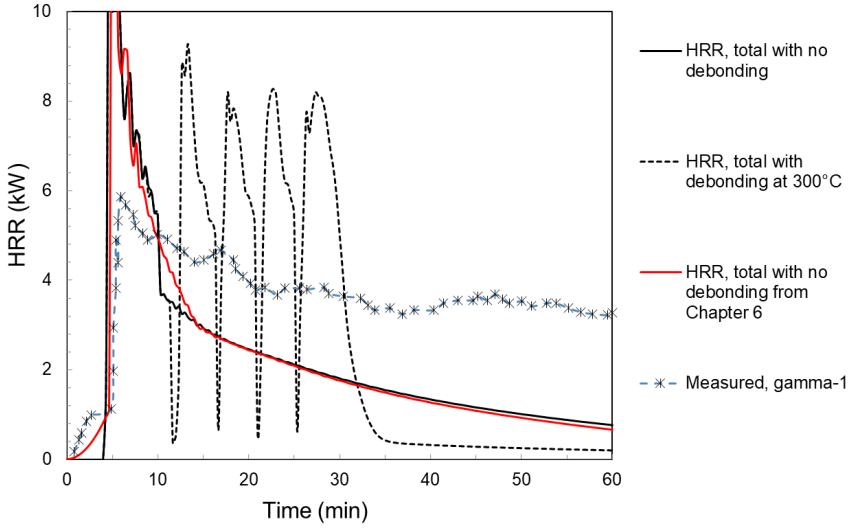

Figure 8.8: Config. H. Predicted HRR using both fuel response effects and kinetic wood pyrolysis submodels.

within the crib lattice and shielded from external radiation from the enclosure. The comparison is also made more difficult by the fall-off of charred timber lamella and failure of some of the gypsum plasterboard protection of which the latter was not modelled.

8.3 NRCC EXPERIMENTS

8.3.1 *Config. P - 33% walls, 10% ceiling exposed*

Config. P removes debonding as a variable in the simulation since the CLT was manufactured with a thermal resistive adhesive as discussed previously in Section 6.5.3. The moveable fire load was wood cribs and therefore the free burn mass loss rate could be estimated, again using the correlations in Section 5.4 from Babrauskas [246]. Three wood cribs were used weighing 120 kg each as previously described in Section 6.5 and seen in Figure 6.60. The calculated free burn mass loss rate for the wood cribs is shown in Figure 8.9 along with the mass loss rate including ventilation and thermal feedback effects during the simulation. In this case, the peak mass loss rate is predicted to be less than the peak mass loss rate under well-ventilated free burn conditions.

The measured and predicted gas temperature in the enclosure is shown in Figure 8.10 along with the previous prediction from Section 6.5.3 where the postflashover burning of the wood cribs was represented by the free burn curve. For this experiment, including the enclosure effects on the fuel has led to a significantly lower predicted peak temperature and a more extended fully developed burn-

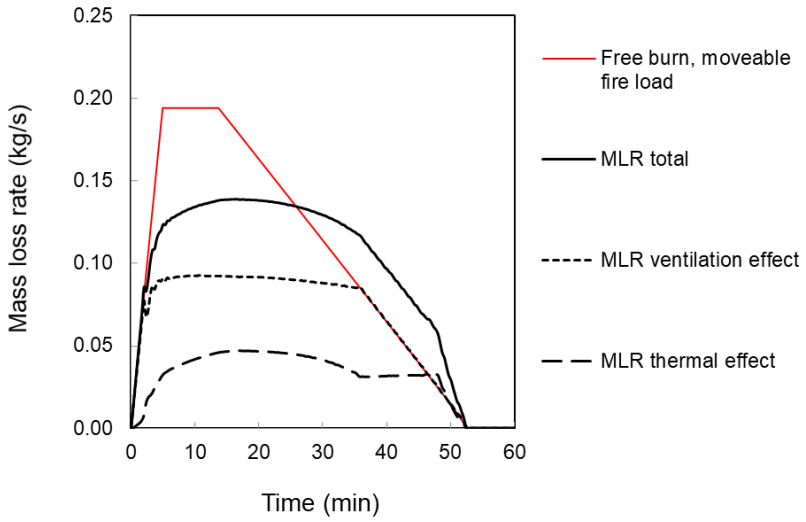

Figure 8.9: Predicted mass loss rate (MLR) for moveable fire load based on specified free burn curve for Config. P.

ing stage. This appears to follow the same trend as for the predicted mass rate with enclosure effects included as seen in Figure 8.9.

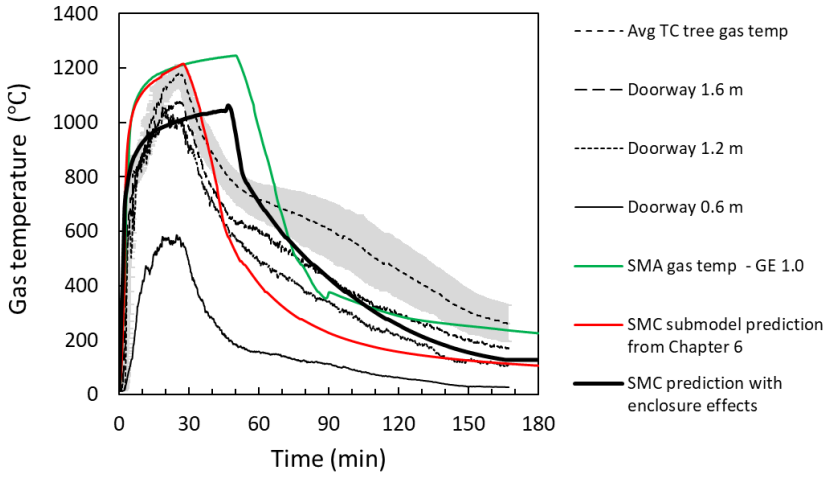

Figure 8.10: Measured and predicted enclosure gas temperatures for Config. P using kinetic pyrolysis submodel and enclosure effects.

The predicted depth of char versus time is shown in Figure 8.11 including corresponding predictions from the simulations reported in Section 6.5. The predicted char depth for the wood kinetic submodel with enclosure effects on the moveable fire load is greater than previous obtained without the enclosure effects. It was also similar to that obtained from the simpler GE pyrolysis submodel with a GE ratio of 1.0.

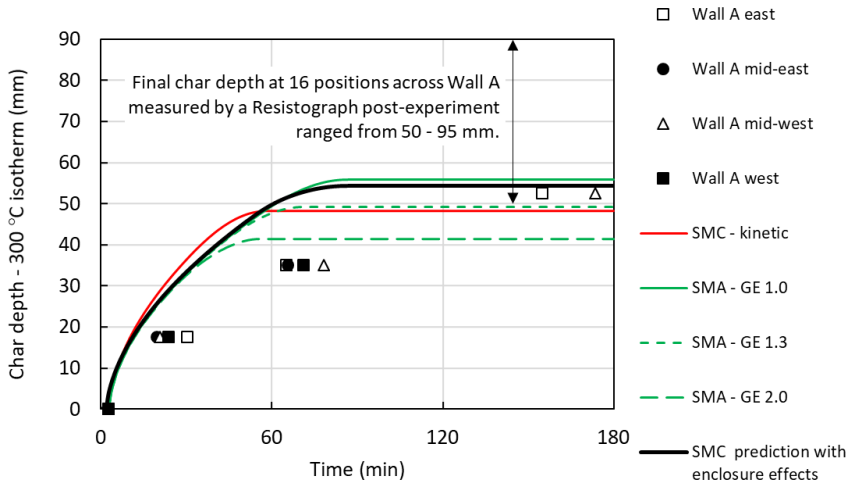

Figure 8.11: Measured versus predicted char depth in the exposed wall based on the time to reach 300°C determined from the predicted temperature - depth profile below the surface of the exposed wall for Config. P.

8.3.2 *Config. S - 35% walls, 100% ceiling exposed*

The calculated free burn mass loss rate for the wood cribs is shown in Figure 8.12 along with the mass loss rate including ventilation and thermal feedback effects during the simulation. The curve is almost identical to that from Config. P indicating that the increase in exposed surface area has little effect on the burning of the moveable fire load in this case.

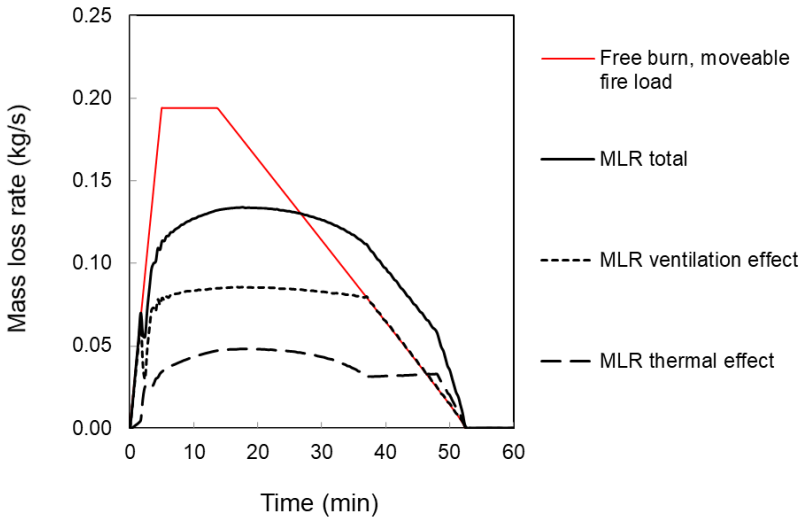

Figure 8.12: Predicted mass loss rate (MLR) for moveable fire load based on specified free burn curve for Config. S.

For Config. S, the measured and predicted gas temperature in the enclosure is shown in Figure 8.13 along with the previous prediction from Section 6.5.6 where the postflashover burning of the wood cribs was represented by the free burn curve. The additional contribution from the wood surfaces in this case leads to a much slower decay in the predicted gas temperature when compared with Config. P.

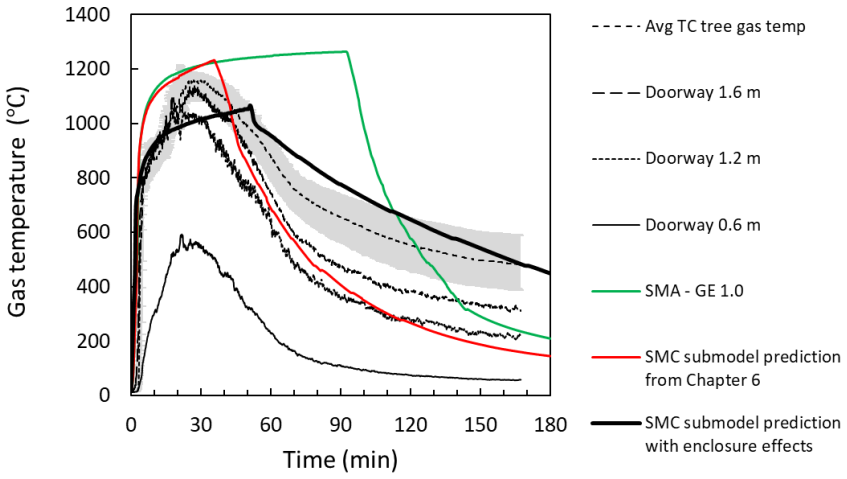

Figure 8.13: Measured and predicted enclosure gas temperatures for Config. S using kinetic pyrolysis submodel and enclosure effects.

The predicted depth of char versus time is shown in Figure 8.14 including corresponding predictions from the simulations reported in Section 6.5. The maximum predicted char depth is signficantly greater being 71 mm compared to 56 mm when the enclosure effects on the moveable fire load was ignored.

8.3.3 *Summary*

The wood cribs used in the Config. P and S experiments were predicted to have a peak mass loss rate of about 2/3 of the peak free burn mass loss rate, unlike the wood cribs used in the Config. F, G and H experiments where a small enhancement of the mass loss rate was predicted. However, since the moveable fire load was in the form of wood cribs none of the predictions indicated there would be a significant enhancement in the burning rate. The comparisons made here are illustrative to demonstrate the functionality of the fuel response effects submodel for a mass timber enclosure. A systematic study of the behaviour of the model for a wider range of fuel sources and ventilation conditions would be warranted. In any case, this feature of the model may more useful with forensic applications in mind rather than for design where exact details of the moveable fire load may not be known.

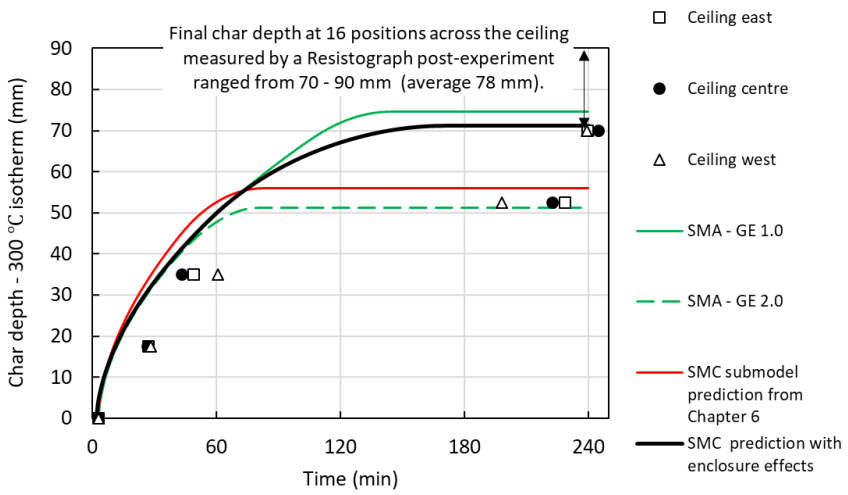

Figure 8.14: Measured versus predicted char depth in the exposed wall based on the time to reach 300°C determined from the predicted temperature/depth profile below the surface of the exposed wall for Config. S.

8.4 SENSITIVITY TO AREA OF WOOD SURFACES EXPOSED

Additional simulations were performed, again using both the kinetic wood pyrolysis and the fuel response effects submodels to illustrate the sensitivity of the overall model predictions to the area of exposed wood within the enclosure. The room dimensions, ventilation, fire load and other model inputs parameters are the same as for the NRCC experiments reported by Su et al. [171] and as previously discussed in Section 6.5 and Section 8.3. The only parameter varied here was the proportion of the walls and ceiling that were exposed wood. The simulations assume that no debonding of lamella or fall-off of any protective plasterboard in non-exposed wood areas occur.

Figure 8.15 gives the predicted enclosure gas temperature depending on the relative areas of exposed wood surface. The predicted enclosure gas temperature for the Config. P and Config. S experiments are also shown. It is clear that the area of exposed wood surfaces affects the duration of burning and time to reach the peak temperature. It also affects the rate of gas temperature decay following the burnout of the moveable fire load which is predicted to occur after about 52 minutes by reference to Figure 8.12. The more exposed wood present, the slower is the rate of temperature decay.

Figure 8.16 give the predicted char depth beneath the exposed surface of the enclosure walls depending on the relative areas of exposed wood surface. Greater areas of exposed wood results in a greater char depth being reached.

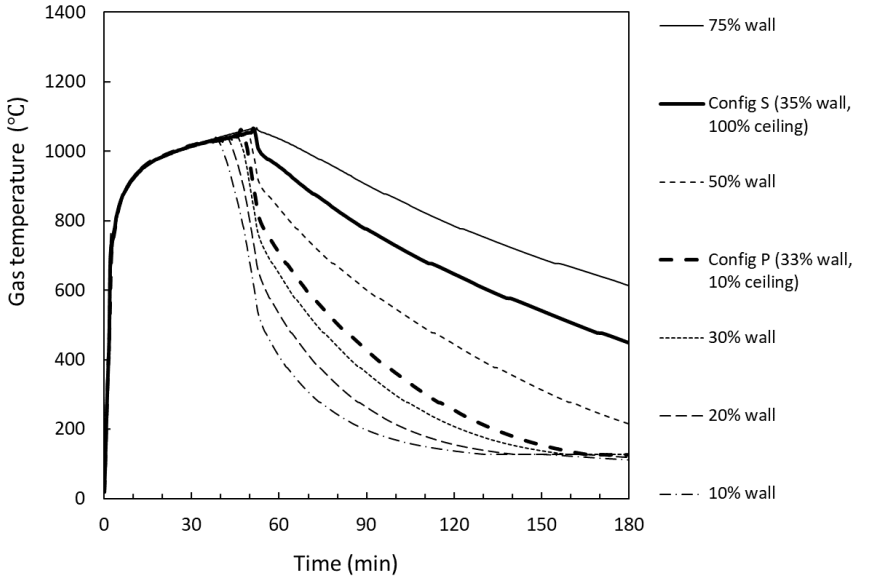

Figure 8.15: Effect of area of exposed wood on the predicted enclosure gas temperatures using kinetic pyrolysis submodel including enclosure effects on the moveable fire load.

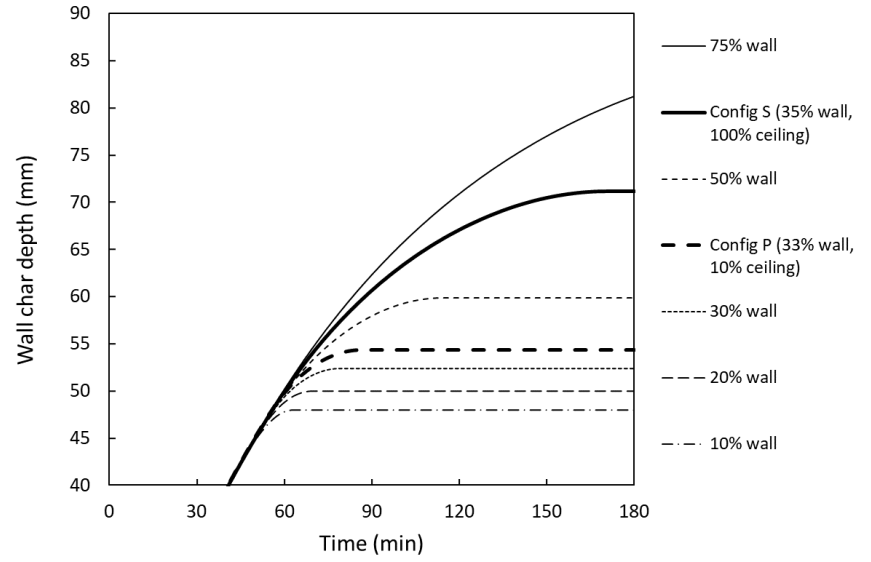

Figure 8.16: Effect of area of exposed wood on the predicted depth of char in the wall using kinetic pyrolysis submodel including enclosure effects on the moveable fire load.

9 MODEL APPLICATIONS

9.1 GENERAL

The model described in this thesis could be used to inform the structural fire engineering design of mass timber enclosures as well as noncombustible enclosures. It could also be used to help determine appropriate design FLED values to be used for mass timber enclosures instead of the values typically specified for noncombustible enclosures in a verification method such as NZBC C/VM2 [285] or when using simplified formula for determining equivalent time of fire exposure (e.g. EN 1991-1-2, Annex F [286]). These potential applications are discussed in this chapter.

9.2 STRUCTURAL FIRE ENGINEERING DESIGN

The maximum char depth calculated by the enclosure fire model with the wood pyrolysis submodels could be used directly as part of the assessment of the structural performance of solid wood walls and ceilings where the heat transfer is primarily one-dimensional. The maximum char depth determined would enable the designer to determine fire resistance based on the residual cross section area method as described in standards such as Eurocode 5 [146], NZS 3603 [145] or NZS AS 1720.1 [287]. However, char depths based on one-dimensional heat transfer may not be applicable for structural elements that are exposed to fire on more than one side such as beams and columns. In these cases, the enclosure fire model can still provide an approximate means of generating the thermal boundary conditions for use in a more detailed thermal/structural model e.g. SAFIR [218] for determining the char depth, residual cross-sections and structural response of the members. Östman et al. [24] illustrate the relevant parameters for a structural fire engineering design in Figure 9.1.

In order to allow for the fuel contribution from the beams or column, these would need to be represented as equivalent surface areas of exposed wall or ceiling as was previously done for the simulations of Config. Q (Section 6.5.4) and Config. R (Section 6.5.5).

The mass timber enclosure model calculates the thermal environment within the room in terms of the gas time-temperature and heat fluxes to the room surfaces. This allows the Adiabatic Surface Temperature (AST) over time to be calculated (also done by the model). The AST curve is used as the surface temperature boundary condition for the more detailed thermal-structural analysis, where for

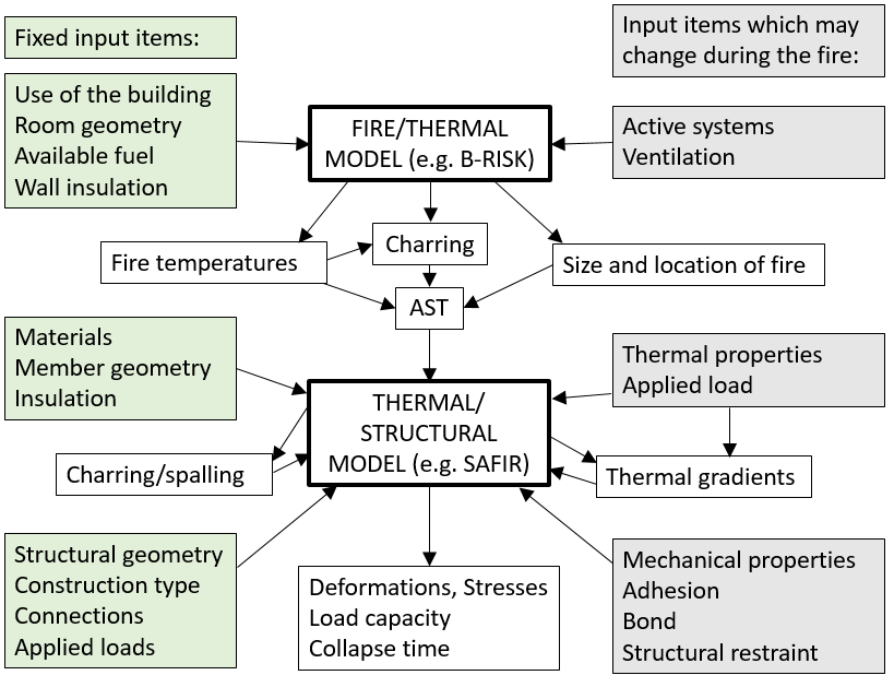

Figure 9.1: Flowchart for predicting structural fire performance. Adapted from Östman et al. [24] with permission from Elsevier.

wood components, the char depth could be recalculated (and checked against the preliminary estimate provided by the mass timber enclosure model) and the residual cross sections determined and used in the structural analysis.

9.2.1 *Theory, adiabatic surface temperature*

This description of AST follows that presented by Wickström in numerous publications in the literature [288–290], and in particular from Wickström et al. [289]. Wickström proposes that AST can be used as a means of characterising the thermal exposure to a surface as a single parameter that can easily be passed from the fire model to a thermal/structural model. The fire model is principally concerned with the gas phase and is only interested in the enclosure surfaces to the extent that they represent a source of heat loss from the enclosure and as a potential source of additional fuel. Therefore simple heat transfer submodels such as a semi-infinite solid or 1-D finite difference methods are usually incorporated within the fire model. On the other hand, a thermal/structural model is principally concerned with the detailed temperature distributions within an element exposed to the fire (in two or three dimensions) so that its structural response accounting for the elevated temperatures can be determined. The thermal/structural model is only interested in the gas phase conditions to the extent it provides the thermal boundary condition for the analysis.

The adiabatic surface temperature is used as a means of transferring the output from the fire model to the thermal/structural model.

Heat transfer to solid surfaces exposed to fire comprises convection and radiation components. The total net heat flux to a solid surface is given by:

$$\dot{q}''_{total} = \dot{q}''_{rad} + \dot{q}''_{con} \tag{9.1}$$

Ignoring any reflected radiation, the net radiant contribution is given as the difference between the absorbed radiation and the reradiated or emitted radiation from the surface.

$$\dot{q}''_{rad} = \dot{q}''_{abs} - \dot{q}''_{emi} = \alpha \dot{q}''_{inc} - \epsilon \sigma T_s^4 \tag{9.2}$$

Applying Kirchhoff's Law with $\alpha = \epsilon$ gives:

$$\dot{q}''_{rad} = \epsilon \left(\dot{q}''_{inc} - \sigma T_s^4 \right) \tag{9.3}$$

The incident radiant flux striking an enclosure surface $\dot{q}''_{inc}$ comes from several sources and is in general a complicated term involving contributions due to radiation from the fire plume (point source assumption), radiant exchange contributions from other surfaces in the enclosure (depends on view factors and absorption/transmission by the gas layers separating the surfaces) and emission from the gas layers to the surface (including emission by soot particles and absorption by CO_2 and H_2O). B-RISK uses a 4-wall radiation model assuming a rectangular shaped enclosure where the ceiling, upper wall, lower wall and floor are considered separate entities and heat transfer is calculated to each one. The incident radiant heat flux is calculated by the fire model (B-RISK) and in general terms is given by:

$$\dot{q}''_{inc} = \Sigma_i \left(\epsilon_i F_i \sigma T_i^4 \right) \tag{9.4}$$

Where the subscript i refers to the various surfaces and source terms contributing to the incident radiation striking a surface. The convective heat transfer to the surface is given by:

$$\dot{q}''_{con} = h(T_g - T_s) \tag{9.5}$$

The convective heat transfer coefficient is calculated for natural convection as a function of the Grashof and Prandtl numbers (described in the B-RISK manual) but for the mass timber enclosure fire model a constant value of 35 $Wm^{-2}K^{-1}$ is used as discussed in Appendix B. The total net heat flux to a surface is therefore given by:

$$\dot{q}''_{tot} = \epsilon \left(\dot{q}''_{inc} - \sigma T_s^4 \right) + h(T_g - T_s) \tag{9.6}$$

In the case of a perfect insulator that is exposed to the same heating conditions as the real surface, its surface temperature is designated the 'adiabatic surface temperature' or AST. In this case, by definition, the total net heat flux to the perfectly insulated surface is zero.

$$\dot{q}''_{tot} = \epsilon \left(\dot{q}''_{inc} - \sigma T_{AST}^4 \right) + h(T_g - T_{AST}) \tag{9.7}$$

Since the fire model (B-RISK) calculates $\dot{q}''_{inc}$ to the real surface with emissivity ϵ, along with the temperature of the adjacent gas layer T_g and the convective heat transfer coefficient h, Equation 9.7 can be solved for the adiabatic surface temperature T_{AST}. Incidentally, in fire resistance furnace tests and in fire enclosure experiments, the Plate Thermometer (PT) can be used to approximately measure the adiabatic surface temperature.

$$\dot{q}''_{tot} = \epsilon\sigma(T_{AST}^4 - T_s^4) + h(T_{AST} - T_s) \tag{9.8}$$

If we ignore any storage of heat by the plate thermometer, Equation 9.8 allows the net heat transfer to a surface in a fire resistance test or enclosure fire experiment to be calculated using the plate thermometer temperature (AST) and a measurement of the surface temperature of the real surface in the same test or experiment. Ignoring storage of heat by the plate thermometer is only reasonable for relatively steady heating conditions where the temperature difference between the plate and the surrounding gases are reasonably small. It cannot be ignored if the temperatures are changing rapidly. Wickström et al. [291] developed an inverse procedure for how to consider the inertia of the plate.

9.2.2 *Example application - Config Q*

This example uses the experiment described previously as Config. Q (Section 6.5.4) which was experiment 3 in the test series reported by Su et al. and which included an unprotected glulam beam and columns [171].

Figure 9.2 shows the setup for Config. Q where a beam (327 × 457 mm) was exposed to fire on three sides and the columns (457 × 457 mm) exposed on four sides. The wall and ceiling surfaces were fully protected with gypsum plasterboard. It was determined that the fire-exposed surface area of the beam and column was equivalent to 36% of the enclosure wall area (see Table 6.1), and this was how the experiment was simulated.

The measured char depth was in the range 90 mm to 160 mm for each exposed side of the glulam after four hours. The average char depth was 110 mm for each exposed beam/column side. Figure 9.3 shows the measured and predicted (using the kinetic pyrolysis model

Figure 9.2: Config. Q - Fully exposed beams and columns. Reprinted from Su et al. [171] with permission.

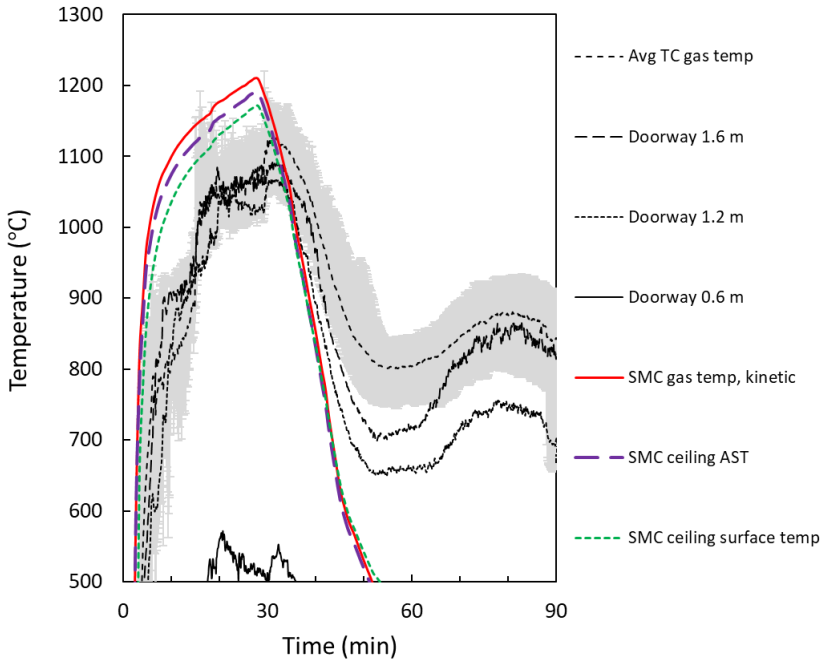

Figure 9.3: Measured and predicted enclosure gas temperatures, and predicted ceiling surface temperature and ceiling adiabatic surface temperature for Config. Q using kinetic submodel.

without enclosure effects on the moveable fire load) gas temperatures along with the calculated AST. As noted previously in Section 6.5.4 in the period from 50 min to 85 min, the room temperatures increased because the protected CLT panels started to char behind the gypsum

board protection and this was not considered by the model. The calculated AST is seen to lie between the predicted gas temperature and the surface temperature, and can be used to prescribe the temperature of the fire exposed surface (as a Dirichlet boundary condition) in a more advanced thermal and structural finite element model (e.g. SAFIR [218]). An additional check is required to ensure that the predicted char depth for a one-dimensional timber element is consistent between the fire model and the thermal/structural model.

9.2.3 *Example application - Config R*

This example uses the experiment described previously as Config. R (Section 6.5.5) which was experiment 4 in the test series reported by Su et al. [171] and which included an unprotected glulam beam and column and a fully exposed wood ceiling.

Figure 9.4 shows the setup for Config. R where a beam (327 × 457 mm) was exposed to fire on three sides and the column (457 × 457 mm) exposed on four sides. Figure 9.5 shows the position of the glulam elements in plan view. The walls were fully protected with gypsum plasterboard while the ceiling was fully exposed. The fire-exposed surface area of the beam and column was equivalent to 19% of the enclosure wall area (see Table 6.1), and again this was how the experiment was simulated. The measured char depth was in the range 60 mm to 90 mm for each exposed side of the glulam elements after four hours with an average char depth of 70 mm.

Figure 9.6 shows the measured and predicted (using the kinetic pyrolysis model without enclosure effects on the moveable fire load) gas temperatures along with the calculated AST.

9.3 EQUIVALENT TIME OF FIRE SEVERITY

Not all buildings warrant detailed structural fire engineering design or need to be designed for total burnout to prevent collapse. For many low-rise and low-risk buildings prescriptive fire resistance ratings may be specified in building code solutions to ensure fire spread is controlled for a period sufficient for occupants to escape or to limit fire spread to nearby property. Furthermore, even if a structural fire engineering analysis for load-bearing mass timber elements is undertaken for design to prevent structural collapse, there may be other construction within the same enclosure that also require fire resistance e.g. light-weight gypsum plasterboard walls, fire rated doorsets, or fire-stopping penetration systems. It is usually not practicable (and in some cases not possible) to also design these types of systems from first principles and common practice is to select systems meeting fire resistance levels specified in codes or calculated from equivalent time of severity formula.

Figure 9.4: Config. R - Fully exposed ceiling, beam and column. Reprinted from Su et al. [171] with permission.

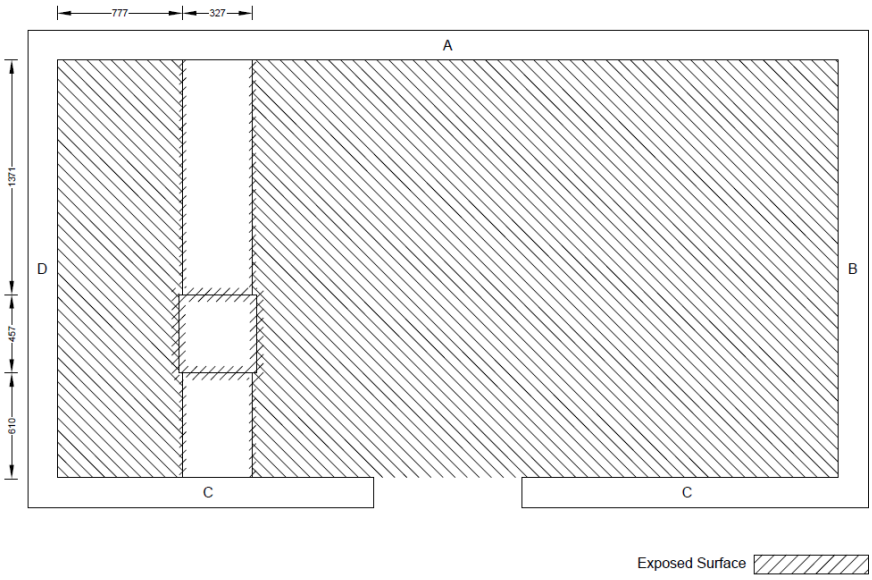

Figure 9.5: Config. R - Plan view showing position of glulam. Reprinted from Su et al. [171] with permission.

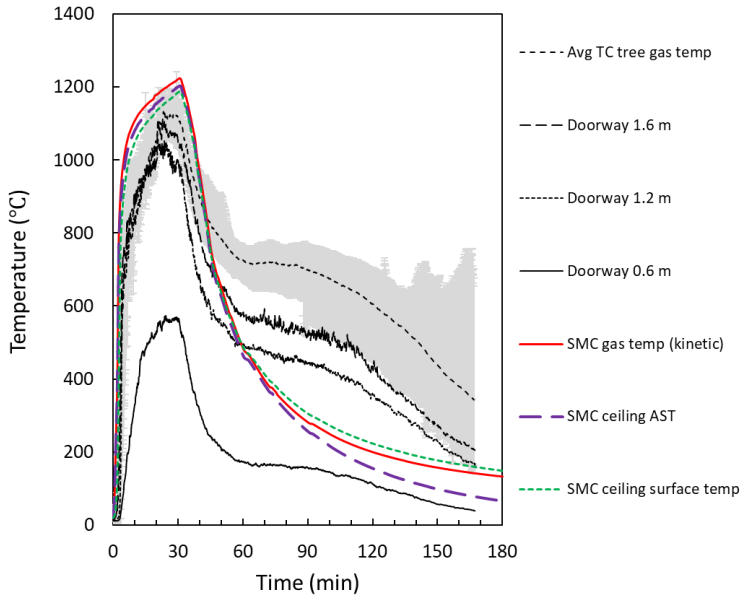

Figure 9.6: Measured and predicted enclosure gas temperatures, and predicted ceiling surface temperature and ceiling adiabatic surface temperature for Config. R using kinetic submodel.

The concept of equivalent fire severity (or the 'destructive power of a fire' as described by Harmathy [292]) is used to determine the duration of exposure in a standard fire resistance test that would produce the same destructive effect on a specified construction element as would occur when exposed to a specified real fire. This approach enables the vast amount of data collected in standard fire resistance tests over many years to still be used as part of a fire engineering analysis. It is generally not practical for construction elements to be individually tested for the large number of different time-temperature exposures possible in enclosure fires dependent on the enclosure size, ventilation thermal properties [32].

One of the first methods developed was that by Ingberg [293] who compared the area under the time-temperature curve above a certain reference temperature to that in the standard fire test. His approach did not have any real theoretical merit [294] and did not account for ventilation conditions or any variations in the thermal properties of the enclosure boundaries. Thomas [295] and Law [296] further developed the time equivalent concept using data from wood crib fires. Law went on to compare various formula spanning from Ingberg's work through to the Eurocode formula with postflashover data and did not find the correlations to be very satisfactory [297].

Harmathy [292, 298, 299] proposed the concept of the 'Normalised Heat Load (NHL)' as a method of ranking various enclosure fires on a

'potential for destruction scale'. Harmathy [300] based his proposed on an analytical solution for the maximum temperature reached at a given depth below the surface of a semi-infinite solid. His idea was applicable to reinforced or prestressed concrete elements where steel reinforcement is located at a defined depth beneath the surface and where the structural performance depended on the maximum temperature reached. Harmathy defined the normalised heat load H (with units $s^{1/2}K$) as the heat absorbed per unit area divided by the thermal inertia of the enclosure boundaries as shown in Equation 9.9 where $\dot{q}$ is an average heat flux penetrating the surface. It can be seen from this equation that NHL is proportional to a dose of absorbed energy.

$$H = \frac{1}{\sqrt{k\rho c_p}} \int_0^\tau \dot{q} dt \tag{9.9}$$

The idea of equivalent fire severity being related to an absorbed energy dose has also been proposed by others including Harada et al. [301] and Kodur et al. [294, 302]. Nyman et al. [303, 304] also proposed an energy dose method (see Section 9.6 later) but it was based on a cumulative dose of incident radiant flux.

9.4 EN 1991-1-2 ANNEX F EQUIVALENT TIME OF FIRE EXPOSURE

The simple formula given in EN 1991-1-2 Annex F to relate the equivalent time of exposure in a standard fire resistance test to a natural fire defined by the fire load, opening size and thermal properties of the enclosure was developed after extensive reviews of the previous formulations, but with more conservative estimates of the lining factor as recommended by Kirby et al. [305]. Law [297] reported that the original form of the Eurocode formula was based on correlating results from a heat balance model or computer program called MRFC developed at the University of Kassel. Kirby [305] reported the formula came from a CIB W14 report [306] which in turn was based on the DIN 18230 standard [307], thus it appears that Germany was the country of origin.

The formula for time equivalent (t_e) as it appears in C/VM2 [285] is shown in Equation 9.10 where e_f is the FLED, k_b is a conversion factor to account for thermal properties of the materials, k_m is a modification factor for the structural material and w_f is the ventilation factor.

$$t_e = e_f k_b k_m w_f \tag{9.10}$$

Purkiss and Li [308] stated that the time equivalence should only be used where structural behaviour can be characterised by a single temperature (e. g. steelwork or concrete in flexure). They also say

that time equivalence cannot be used for timber since the controlling phenomenon is char depth. Clearly the issue of time equivalence is much more complicated for a combustible material. Despite limitations and criticisms [297, 309] of the EN 1991-1-2 Annex F [286] and similar simple formulations to calculate fire severity they continue to be widely used in New Zealand [285] mainly due to their convenience and simplicity. Wade et al. [32] stated *"that time-equivalence methods seem most useful for determining the fire resistance ratings required when little is known about the specific materials and type of construction to be used, e.g. to inform prescriptive Building Code compliance documents."*

Verification method C/VM2 [285] allows fire resistance ratings to be determined by calculating the equivalent fire severity from the formula in Eurocode 1 [286] but there is no explicit guidance provided in C/VM2 as to how to address the potential for increased fire severity resulting from the presence of large areas of exposed combustibles on the walls and ceiling within an enclosure. The fire severity within an enclosure with mass timber surfaces may be similar to a non-combustible enclosure during the period of ventilation-controlled burning, however once the moveable fire load burns out, continued burning of the timber surfaces can extend the period of ventilation-controlled burning and slow the rate of temperature decay resulting in a greater fire severity.

9.5 DESIGN FIRE LOADS IN FIRE SEVERITY CALCULATIONS

NZBC C/VM2 [285] specifies the design FLED values shown in Figure 9.7 for the moveable fire load and these can be presumed to be applicable to non-combustible enclosures since there is no allowance made or required for any additional contribution from combustible construction.

Therefore, where unprotected combustible construction is exposed to the fire, the following procedure is suggested to modify the design FLED for use in fire severity calculations such as the Eurocode formula [286].

1. Use the enclosure fire model to determine the maximum char depth (d_c) in walls and ceiling in m.
2. Calculate the total mass of wood (in kg) pyrolysed from the surface area of wood exposed (A_w), the wood density (ρ_w) and the char depth.

$$m_w = d_c A_w \rho_w \tag{9.11}$$

3. Determine the total heat release (Q_{tot}) and the heat released inside the enclosure (Q_{in}) in MJ (by integrating the two respective HRR curves from the fire model).

Table 2.2 Design FLEDs for use in modelling fires in C/VM2

Design *FLED* (MJ/m²)	Activities in the space or room	Examples
400	1. Display or other large open spaces; or other spaces of low *fire hazard* where the occupants are awake but may be unfamiliar with the *building*.	1. Art galleries, auditoriums, bowling alleys, churches, clubs, community halls, court rooms, day care centres, gymnasiums, indoor swimming pools
	2. Seating areas without upholstered furniture	2. School classrooms, lecture halls, museums, eating places without cooking facilities
	3. All spaces where occupants sleep	3. *Household units*, motels, hotels, hospitals, residential care institutions
	4. Working spaces and where low *fire hazard* materials are stored	4. Wineries, meat processing plants, manufacturing plants
	5. Support activities of low *fire hazard*	5. Car parks, locker rooms, toilets and amenities, service rooms, plant rooms with plant not using flammable or *combustible* fuels
800	1. Spaces for business	1. Banks, personal or professional services, police stations (without detention), offices
	2. Seating areas with upholstered furniture, or spaces of moderate *fire hazard* where the occupants are awake but may be unfamiliar with the *building*	2. Nightclubs, restaurants and eating places, *early childhood centres*, cinemas, *theatres*, libraries
	3. Spaces for display of goods for sale (retail, non-bulk)	3. Exhibition halls, shops and other retail (non bulk)
1200	1. Spaces for working or storage with moderate *fire hazard*	1. Manufacturing and processing moderate *fire load* 2. Storage up to 3.0 m high other than *foamed plastics*
	2. Workshops and support activities of moderate *fire hazard*	3. Maintenance workshops, plant and boiler rooms other than those described elsewhere
400/tier of car storage	Spaces for multi-level car storage	Car stacking systems. The design floor area over which the design *FLED* applies is the total actual car parking area
800/m height, with a minimum of 2400	1. Spaces for working or storage with high *fire hazard*	1. Chemical manufacturing and processing, feed mills, flour mills 2. Storage over 3.0 m high of *combustible* materials, including temperature controlled storage
	2. Spaces for display and sale of goods (bulk retail)	3. Bulk retail (over 3.0 m high)

Figure 9.7: Design FLEDs used for modelling fires in C/VM2 [285]. © The Crown.

4. Determine the fraction of total energy released (λ) inside the enclosure.

$$\lambda = Q_{in}/Q_{tot} \tag{9.12}$$

5. Calculate the modified design ($FLED_c$) in MJ/m^2 of floor area, for the combustible enclosure.

$$FLED_c = FLED_{nc} + \lambda \Delta H_c m_w / A_{floor} \tag{9.13}$$

9.5.1 *Example*

This example uses the enclosure simulations presented in Section 8.4 using both the SMC kinetic wood pyrolysis and enclosure effects sub-models. The enclosure is assumed to be the same as for the NRCC

experiments reported by Su et al. [171]. The enclosure measured 4.5 m × 2.4 m × 2.7 m high with an opening 2.0 m high × 0.76 m wide. The moveable fire load (being wood cribs) was previously estimated to represent a FLED of 467 MJ/m^2 assuming an effective heat of combustion of 14 MJ/kg.

Simulations were conducted for the case of no exposed wood on the ceiling and exposed wood surfaces on the walls ranging from 0 - 50%. The predicted gas temperature curves were previously determined and shown in Figure 8.15. Following the proposed procedure the maximum char depths were determined as previously shown in Figure 8.16. The calculation results are summarised in Table 9.1.

Percentage wall exposed	0%	10%	20%	30%	50%
Area exposed (m^2)	0.00	3.73	7.45	11.18	18.63
Maximum char depth (m)	-	0.048	0.050	0.052	0.060
Mass of wood pyrolysed (kg)	0.0	92.1	191.9	301.6	574.7
Heat release fraction (-)	1.00	0.77	0.69	0.62	0.58
Movable FLED (MJ/m^2)	467	467	467	467	467
Updated FLED (MJ/m^2)	467	559	638	711	900

Table 9.1: Summary of calculation outputs to determine the FLED for the enclosure with different quantities of exposed wood on the walls.

Figure 9.8 plots the FLED against the percentage of timber wall surface exposed to the fire. The FLED for the case where all of the wall contribution burned inside the enclosure and for the case where only part of the wall contribution burned inside are both shown. The fire gas temperature curve for this example considering only the moveable fire load of 467 MJ/m^2 using the parametric equations from EN 1991-1-2 [78] were also determined. The form of the parametric equations included the suggested modifications by Reitgruber et al. [310]. A thermal inertia factor ($b = \sqrt{k\rho c}$) for insulating enclosure surfaces of 400 Jm^{-2}s$^{-1/2}$K was assumed along with a t_{lim} = 20 minutes for a medium growth rate fire. The gas temperature is shown in Figure 9.9 along with the gas temperature predicted from the fire model and the measured gas temperatures reported by Su et al. [171].

Both the fire model and the parametric equations agree reasonably well except for the latter part of the decay phase where both are seen to diverge from the measured data. Again a distinct difference is seen between the predictions with and without the enclosure effects similar to that seen earlier in Figure 8.10 for Config. P. The peak gas temperature for the parametric curve falls in between the two curves predicted using the model.

Figure 9.10 shows the predicted gas temperatures from the equations given in EN 1991-1-2 for each of FLED values corresponding to the different proportions of exposed wood wall surface.

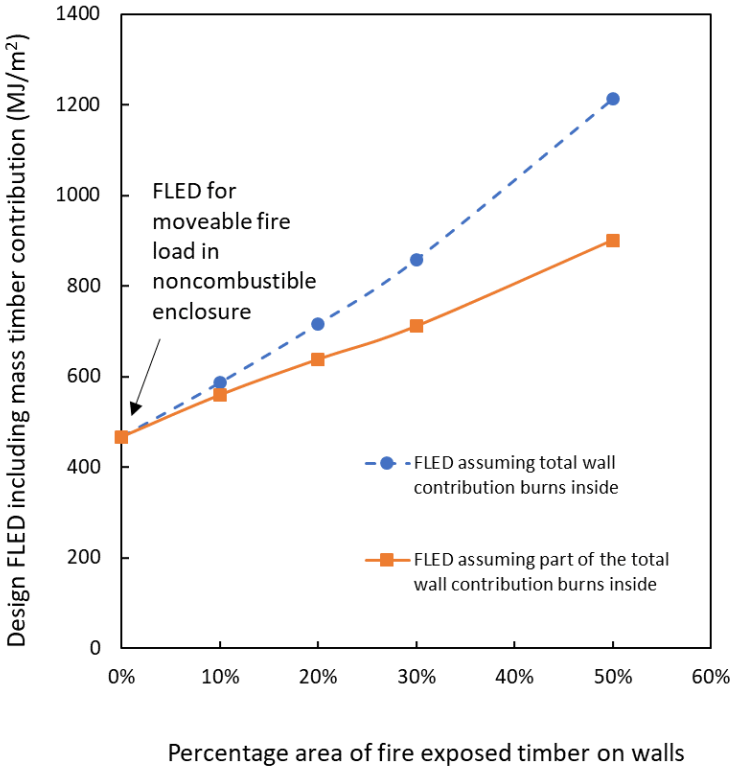

Figure 9.8: New design FLEDs versus percentage of timber wall surfaces exposed to fire (applicable to NRCC enclosure).

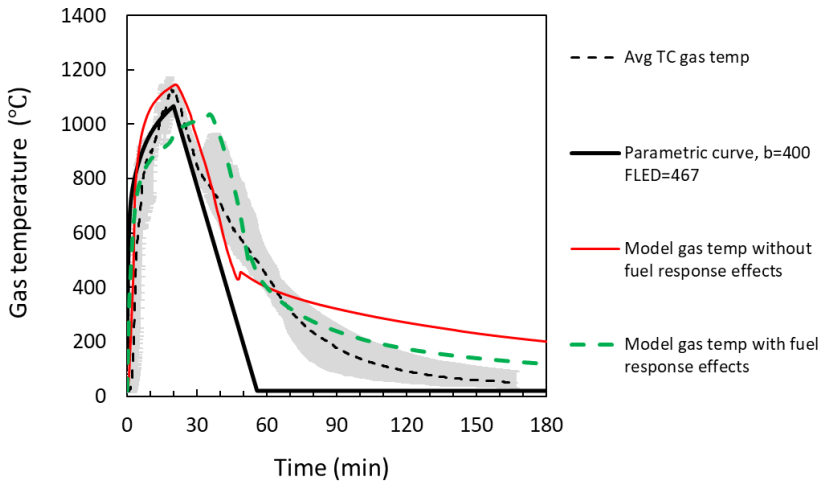

Figure 9.9: Gas temperatures for Config. O with no wood surface contribution.

Figure 9.11 compares the gas temperatures from EN 1991-1-2 using the updated FLEDs with model gas temperature predictions. The peak temperature from the parametric curve is higher but the rate of

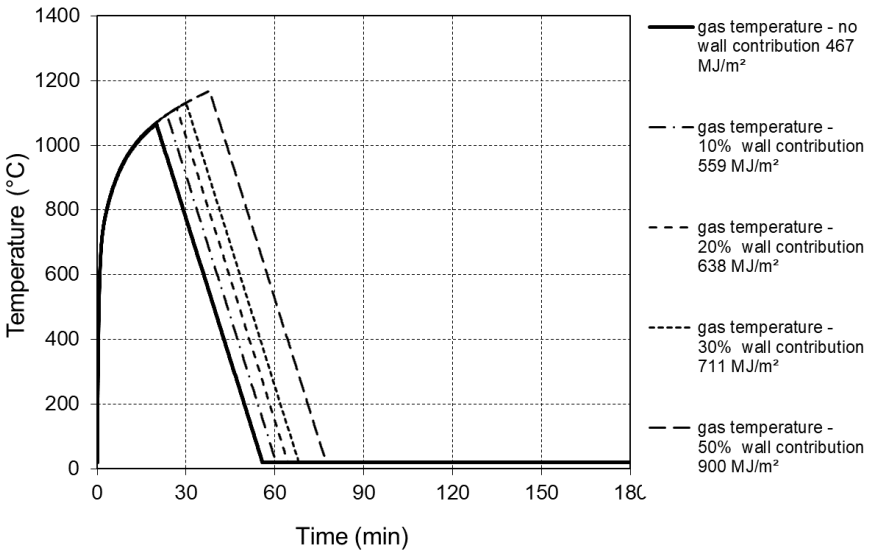

Figure 9.10: Parametric gas temperatures from EN 1991-1-2 [78] .

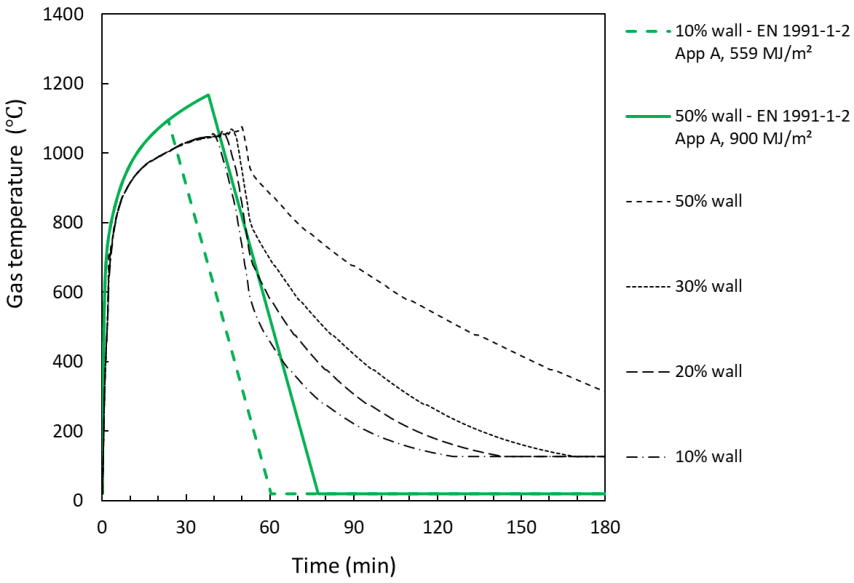

Figure 9.11: Parametric gas temperatures from EN 1991-1-2 compared with model prediction with updated FLEDs.

temperature decay is more rapid when compared to the model. However, the model shows a similar trend to EN 1991-1-2 by extending the duration of burning as the fuel load increases with a small increase in the peak gas temperature.

9.5.2 *Summary remarks*

It is not clear whether the proposed procedure for determining updated design FLED values for mass timber enclosures is conservative or non-conservative and further work is required to study this in more detail. However, since currently the verification method C/VM2 [285] is silent on how to allow for the contribution of exposed mass timber surfaces and similarly it is unaccounted for entirely in the fire resistance ratings specified in the Acceptable Solutions [311], then applying the procedure in fire safety design would be an advancement compared to designs where the wood surface contribution is entirely omitted.

9.6 CRE METHOD AND EXAMPLE

The cumulative radiant energy (CRE) method [304] involves calculating the dose (q_{inc}) of incident blackbody thermal radiation flux experienced by a construction element exposed to fire. It provides a simple means of comparing the severity of a different (non-standard) fire with a fire following a standard time-temperature curve [141]. Equation 9.14 is used for calculating the blackbody radiation dose where σ is the Stefan-Boltzmann constant, T is the gas temperature, and t is time.

$$q_{inc} = \int_0^t \sigma T^4 dt \tag{9.14}$$

When calculating the CRE dose for the standard time-temperature curve, the gas temperature relationship given in Equation 9.15 can be used.

$$T = 345 \log_{10}(8t + 1) + T_\infty \tag{9.15}$$

Nyman et al. [304] assumed that the enclosure and the furnace fire have similar heat transfer coefficients and that the ratio of the convective to total heat transfer is similar in both the enclosure and the test furnace. Their study examined the performance of light timber and light steel frame construction with gypsum plasterboard linings fixed to each side. In their enclosure experiments they found that insulation failure predictions were generally conservative, but nonconservative for the assemblies which failed structurally or on integrity (e. g. the floor/ceiling and metal stud systems). Nyman et al. concluded that the CRE method could be used for predicting insulation failure times of drywall assemblies, during the period of fire exposure where heat transfer is dominated by radiation.

The CRE method was recently evaluated by Jessop et al. [27] as a predictive tool relating the general damage experienced by the enclosure during the fire with the fire severity. This was done by comparing the CRE for two different fire severities experienced by the same enclosure using the results from a furnace experiment [40] and a natural enclosure experiment [27, 312]. They listed a series of damage markers which were used to compare the CRE dose received by the construction element at the time the event occurred in each experiment. Jessop et al. [27] concluded that CRE can be used as a general indicator to construct a timeline for the expected enclosure damage. However, they stated caution is required in extending this to other events or markers such as structural failure of the specific components without a more detailed analysis of the failure mechanisms and how they are affected by temperature and energy dose.

In the context of the present study, the fire model described in this thesis could be used to allow the calculation of the CRE and the equivalent time of exposure in a standard fire resistance test based on the predicted gas temperature history and the equivalent time of exposure in a standard fire resistance test.

Using the simulation data from the preceding example in Section 9.5.1, Figure 9.12 shows the equivalent time of exposure in a standard fire resistance test as calculated from the fire model (with kinetic and enclosure effects included); the EN 1991-1-2 Annex A parametric time-temperature equation and CRE method; and the EN 1991-1-2 Annex F equivalent time of exposure formula. All cases assume the NRCC enclosure size of 4.5 m $\times$ 2.4 m $\times$ 2.7 m high with an opening 2.0 m high $\times$ 0.76 m wide as described by Su et al. [171]. The moveable fire load (being wood cribs) was taken as 467 MJ/m^2 assuming an effective heat of combustion of 14 MJ/kg.

It can be seen in Figure 9.12 that the parametric time temperature equations [78] with the CRE method produces the lowest calculated equivalent time of exposure, probably as a result of the steeper temperature decay phase compared to the fire model gas temperature predictions. Both the calculated equivalent time of exposure from the fire model and from the EN 1991-1-2 Annex F formula give somewhat comparable results.

It is emphasised that this approach to determining the equivalent time of exposure is intended for non load-bearing elements in mass timber enclosures that require fire resistance and not for load-bearing mass timber elements where structural fire engineering procedures should be used as previously discussed in Section 9.2.

The examples presented in this chapter illustrate some possible approaches for designing mass timber buildings for fire resistance, however the examples are very limited in scope and have only been demonstrated for a single set of simulation data. Clearly there could

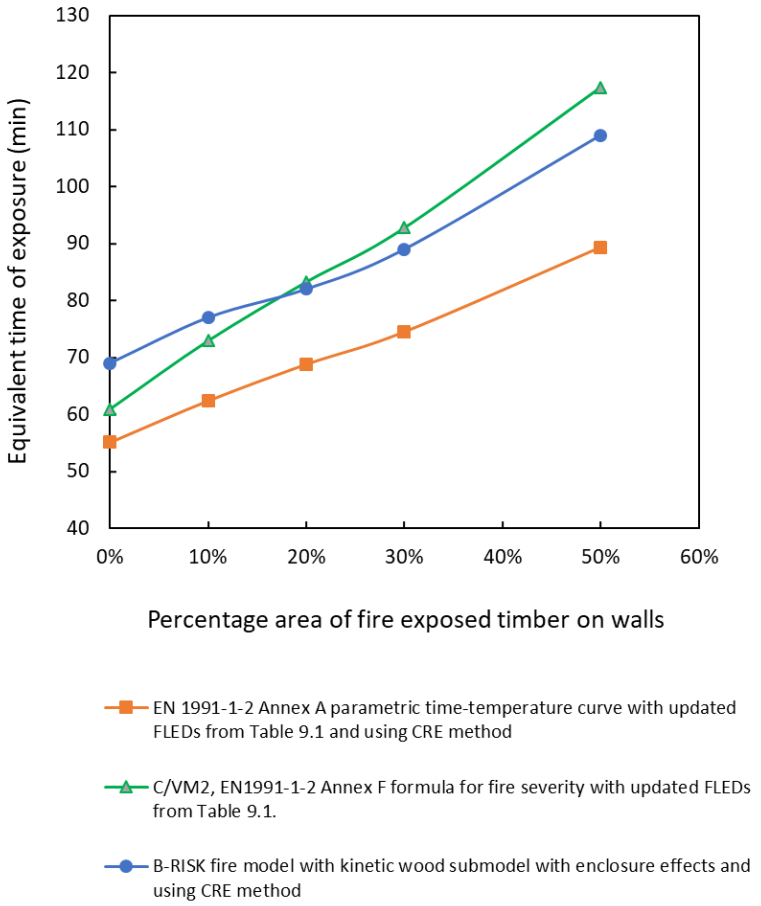

Figure 9.12: Calculated equivalent time of exposure for NRCC enclosure with movable FLED = 467 MJ/m^2 for different areas of exposed wood on the walls.

be a great deal more research done to investigate the methods further and extend the work in the future.

10 CONCLUSIONS AND RECOMMENDATIONS

10.1 CONCLUSIONS

It is concluded that where mass timber structures must be designed to 'not collapse' in fire then satisfying prescriptive time periods in standard fire resistance tests is not sufficient. The fire performance of these structures need to be specifically engineered considering the expected growth, duration and decay period of the fire. This requires a coupled interaction between the moveable fire load and the combustible enclosure surfaces to be considered. The fully developed fire model described in this thesis may be used as a basis for improving the understanding and prediction of these coupled effects. The following additional specific conclusions are made.

1. Two-zone models and postflashover fires. As demonstrated in Appendix A, a two-zone model can be used for underventilated postflashover fires since the plume flow becomes coupled to the air entering the compartment under ventilation limited conditions. While the problem can be simplified by using a one-zone model instead, it is not necessary to do so.

2. EC5 Thermal conductivity. As found in Section 6.5.3, the EN 1995-1-1 temperature dependent thermal conductivity equations for wood may not be suitable for use with enclosure fire models where energy conservation equations for the fire source are enforced. This is because a higher thermal conductivity for the solid/char at higher temperatures (i.e. nearer to the surface) as used in EC5 has the counter effect of cooling the fire gas temperature since more of the energy from the fire is conducted into the wall (and less is used to increase the fire gas temperature).

3. CLT Debonding submodel.

   It is observed that internationally there are different approaches to managing the risk of lamella debonding during a fire resulting in potential regrowth in the fire development due to adhesive failure. In Europe there seems to be greater interest in allowing for potential debonding, predicting if and when it occurs and avoiding its occurrence by ensuring that the facing lamella is sufficiently thick to prevent the adhesive reaching temperatures that would result in failure. In contrast, in North America, the emphasis is now to demand use of adhesives that have greater thermal resistance such that the element as a whole be-

haves like solid wood. The latter approach is likely to be more dependable.

While it was shown in Section 5.8 that debonding of CLT lamellae can be modelled based on the temperature reached at the adhesive line, it is a progressive process and therefore variable in nature. Early debonding may not be the worse case in terms of the fire severity. The benchmarking of the model described indicates that the proposed debonding submodel is conservative with respect to predicting the rate of charring following a debonding event which becomes more apparent as each successive lamella adhesive line reaches the specified debonding temperature. This is expected to be a result of the simplifying assumption that each lamella is completely removed from the surface at the debonding time. In reality the process of debonding is a much more progressive one occurring over a longer timeframe. It is suggested that adopting a stochastic approach to modeling debonding of lamella in engineered wood may be more appropriate.

From a design perspective, it is preferable to design to avoid the occurrence of debonding by selecting a thermal resistive adhesive in the manufacture of engineered wood products that require fire resistance. However, ensuring the facing lamella is sufficiently thick or allowing for debonding in the design process could be alternative but less dependable methods.

4. Equivalence ratio wood pyrolysis submodel SMA. The wood pyrolysis submodel described in Section 5.5 contributes mass and energy to the enclosure fire based on pyrolysis of the charred surface material as defined by the position of the 300°C isotherm. The pyrolysis gases are assumed to burn however at a rate controlled by a user-specified excess fuel factor or global equivalence ratio. This allows a more conservative approach to be used in design including assuming all the pyrolysis gases will burn inside the enclosure at a rate controlled by the available oxygen supply.

5. Kinetic wood pyrolysis submodel SMC. The alternative kinetic wood pyrolysis submodel described in Section 5.7 contributes mass and energy to the enclosure fire based on an Arrhenius equation for the temperature-dependent reaction rate that describes the thermal decomposition of the individual wood constituents lignin, cellulose and hemicellulose. Pyrolysis gases are assumed to be instantly transported to the surface with burning occurring at the time the decomposition products are released; inside the enclosure if oxygen is available or outside the enclosure openings if oxygen is not available. Benchmarking results from Chapter 6 show the kinetic wood pyrolysis sub-

model tends to be consistent with a global equivalence ratio between 1.3 and 2.0. Unlike submodel SMA, this submodel has the added advantage of providing an estimate of the proportion of heat release inside and external to the enclosure.

6. PYROLYSIS OF THE MOVEABLE FIRE LOAD. In Section 5.4, the moveable fire load is represented as wood cribs in the enclosure based on the specified fire load for the enclosure fire. The mass loss rate of the wood cribs is based on the lesser of the ventilation-controlled mass loss rate or the fuel-controlled mass loss rate using correlations for well-ventilated wood cribs from the literature. It is found that the simplified wood crib assumption provides the designer with a practical approach where the exact nature of the fire load may not be known in advance.

7. FUEL RESPONSE EFFECTS. As discussed in Chapter 7, the use of free-burning rate of heat release data as the design fire in many fire models may not be appropriate in cases where the burning may be significantly enhanced due to radiation feedback within an enclosure. This is especially true for liquid fuel fires where the fuel surface fully sees the flames and hot surfaces and where, as shown in Section 7.7, mass loss rates can be increased by a factor of 4 or more compared to burning in the open. It may be important for some upholstered furniture, but is less important for wood cribs where a significant proportion of the fuel surface area is within the crib lattice and does not directly see the flame.

   Chapter 8 demonstrated the application of the fuel response effect submodel for a mass timber enclosure however, it has not been adequately validated here due to a sparsity of experimental data. The examples presented illustrated that when the fuel response effects were included for wood crib within a mass timber enclosure, the predicted peak gas temperature was reduced but the duration of burning extended with a slower gas temperature decay compared to the kinetic submodel without fuel response effects. The predicted final char depth was also greater.

   A combined model of this type is also likely to be more useful for forensic applications rather than for fire safety design because the exact nature and arrangement of contents are usually not known at the design stage of buildings, or may regularly change over the life of the building, however it could be used where a wood crib moveable fire load is assumed.

8. APPLICATION TO STRUCTURAL FIRE ENGINEERING. Section 9.2 suggested how the fire model described in this thesis could be used to provide a boundary condition such as the adiabatic surface temperature that is useful for use in more detailed ther-

mal/structural finite element codes as may be required for evaluating structural performance of loadbearing beams and columns during and following fire exposure.

9. EQUIVALENT TIME OF FIRE EXPOSURE. The fire model described in this thesis may also be useful to determine equivalent time of fire exposure for non-structural assemblies within mass timber enclosures as discussed in Section 9.3. It is proposed that the fire load energy density contributed by mass timber elements based on the maximum char depth, and multiplied by the fraction of energy release inside the enclosure can be added to the moveable fire load and used in existing equivalent time of fire exposure formula.

10. FIRE SAFETY ENGINEERING DESIGN. The model described in this thesis may be useful as part of a performance-based design of mass timber enclosures where fire resistance is required. The zone model approach provides advantages in speed and simplicity for fire safety engineering. Given the uncertainties in basic design parameters such as ventilation and fire load, the simpler submodel SMA with a GE ratio of 1.3 may be adequate and sufficiently conservative for many cases, however the kinetic pyrolysis submodel allows the proportion of burning inside and external to the enclosure to be estimated and appears to provide a more accurate prediction. Use of the fuel response effects submodel may also provide better prediction for the rate of temperature decay.

11. THE CONVENTIONAL FIRE RESISTANCE FRAMEWORK. The applicability of the conventional fire resistance framework developed and used for decades for non-combustible construction is highly questionable when applied to combustible compartments. If mass timber structures must be designed to 'not collapse' in fire then satisfying arbitrary time periods in a standard fire resistance test is not sufficient. The fire performance of these structures needs to be specifically engineered considering the expected fire growth, burning duration and decay of the fire.

10.2 RECOMMENDED MODEL IMPROVEMENTS

The following is a list of recommended improvements to the fully developed fire model for mass timber enclosures as described in this thesis.

1. THERMAL CONDUCTIVITY OF WOOD AND CHAR.

   The thermal conductivity value given in Equation 5.22 applied to a pyrolysing wood particle at ambient temperature and was given as the average of the longitudinal and radial directions. This is inappropriate and would result in the thermal conductivity being overestimated for the typical mass timber installations. Values of thermal conductivity perpendicular to the grain or in the radial direction should be used.

   For example, TenWolde [242] gives the following equation for thermal conductivity measured across the grain for wet wood at ambient temperature. For wood with an oven dry density of 460 kg/m^3 at 10% moisture content, this equation gives a thermal conductivity of 0.127 W/mK.

$$k = 0.001\rho_{w,dry}(0.1941 + 0.4064u) + 0.01864 \tag{10.1}$$

   Janssens and Douglas [132] also provide detailed equations for the thermal conductivity of wood, char and partially charred wood at ambient and elevated temperature. In future, these should be investigated for use in the model.

2. SPECIFIC HEAT OF WOOD.

   The equations given in Section 5.3.5 do not account for the latent heat of vaporisation of the moisture in wet wood. In addition, the additional heat required, above the heat of vaporisation of free water, to evaporate water from a substance in which it has been absorbed (i.e. the heat of wetting) is also not accounted for.

   Janssens and Douglas [132] give the heat of vaporisation of water in kJ/kg of water as a function of temperature in °C as:

$$\Delta h_v = 2552 - 2.93T \tag{10.2}$$

   They also give the integral heat of wetting in kJ/kg of water as:

$$\Delta h_w = \frac{92.1}{0.07 + u} \tag{10.3}$$

   These enthalpy terms can either be accounted for directly in the heat transfer calculations or they can be included within the

temperature dependent specific heat equations over a defined temperature range (e.g. 100 - 120°C) as is done within the EC5 specific heat relationship previously shown in Figure 5.7.

Furthermore, rather than assigning each finite difference element as wood or char based on a threshold of 300°C, for the kinetic submodel after the wood starts to pyrolyse, a weighted average of the dry wood and char specific heat could be calculated for a partially charred material.

3. Temperature dependent thermal property database.

   It is recommended that in the future, model users be provided with the ability to add new materials with temperature dependent properties for thermal conductivity, specific heat and density to the B-RISK materials database. This is expected to greatly improve the accuracy of the heat conduction calculations in the post-flashover and decay phases.

   The additional option of making these properties non-reversible i.e. to hold the property value when the temperature starts to decline would also be a valuable addition to the model. While this had been done for thermal conductivity it had not been done for the specific heat of char.

4. Enclosure boundary heat loss calculations. The current model assumes that walls or ceilings that are only partially protected or exposed will have the same heat loss characteristics (as determined by the specified thermal properties) as for fully exposed wood enclosures. In future it may be desirable to modify the fire model to calculate heat losses considering the relative areas of both exposed wood and protected wood construction.

5. Account for dimensional changes in wood/char.

   The mass of wood changes as it dries and loses moisture, and as wood is converted to char. The volume also changes as the wood shrinks due to this moisture loss and charring. During fire exposure, the exposed wood surface typically recedes as the combustion progresses due to the char contraction and possible char oxidation [132].

   This contraction should ideally be accounted for in the determination of the thermal conductivity and density of the wood/char. Since the model developed in this thesis relies on finite difference calculations with a fixed grid, any char contraction effect strictly speaking should not be included in the char density and thermal conductivity values used.

   Janssens [132, 313] gives the apparent density of the wood/char (Equation 10.4) as a function of the residual mass Z at a given time, the oven-dry density of wood $\rho_{w,dry}$ and dimensional

changes due to drying and thermal expansion. f_l, f_r, f_t are the thermal expansion factors for softwoods in the longitudinal, radial and tangential directions respectively. T is the temperature and T_r is a reference temperature taken as 20°C.

$$\rho_{w,\text{corrected}} = \frac{Z}{f_l f_p^2}\rho_{w,dry} \tag{10.4}$$

$$f_l = 1 + 3.75 \times 10^{-06}(T - T_r) \tag{10.5}$$

$$f_r = 1 + \rho_{w,dry} \times 55 \times 10^{-09}(T - T_r) \tag{10.6}$$

$$f_t = 1 + \rho_{w,dry} \times 82 \times 10^{-09}(T - T_r) \tag{10.7}$$

An average expansion factor perpendicular to the grain, and also including a factor for expansion due to moisture is given in Equation 10.8 and used in Equation 10.4.

$$f_p = \sqrt{f_r f_t}\sqrt{1 + 0.00084\rho_{w,dry}u} \tag{10.8}$$

A correction to the thermal conductivity k (Equation 10.11) could be made using the average char contraction factor for the radial and tangential directions respectively from the following expressions given by Parker [314].

$$f_r = 1 - 0.64 \times (1 - (Z + u))^3 \tag{10.9}$$

$$f_t = 1 - 0.45 \times (1 - (Z + u))^{3/2} \tag{10.10}$$

$$k_{\text{corrected}} = \frac{2k}{(f_r + f_t)} \tag{10.11}$$

6. User-specified minimum oxygen concentration.

   In the model described in this thesis, a user-specified GER factor is included to allow the total mass loss rate to be increased

beyond that burned within the enclosure during ventilation controlled conditions. This in turn allows the proportion of burning inside and external to the enclosure to be adjusted. The current model assumes that the limiting oxygen concentration in the lower layer required for combustion is 10% by volume. It is recommended to make this a user-specified input to provide the user with an alternative means of controlling the combustion environment in the enclosure.

7. KINETIC PROPERTIES OF WOOD.

   It is recommended that alternative kinetic properties for the wood be investigated since there are some noted inconsistencies in the data shown in Table 5.2. In particular, the lignin fraction given is only 9% and much lower than the typically expected range of 25 to 35% [132].

   Matala et al. [315] estimated the kinetic model parameters given in Table 10.1 using thermogravimetric experiments and a genetic algorithm. The parameters were estimated by modelling thermogravimetric experiments and minimising the error between the experimental and numerical results. The sample of hemicellulose used was xylan. The residue can be assumed to be the char fraction. Janssens and Douglas [132] give the typical chemical composition of dry wood as shown in Table 10.2. Sjostrom gives the chemical composition for Spruce (Picea glauca) as 39.5% cellulose, 30.6% hemicellulose, 27.5% lignin and 2.1% extractives [316].

   Notwithstanding the above, a preliminary comparison between the predicted enclosure gas temperature and charring within the wall for Config. P showed that the impact of assuming the chemical composition for Spruce from Sjostrom [316] and using Matala's kinetic properties [315] instead of Wang's [249] was relatively minor.

COMPONENT	E_i (J/mol)	A_i (s^{-1})	n_i	RESIDUE
Hemicellulose	1.64×10^5	5.78×10^{13}	4.166	0.268
Cellulose	1.95×10^5	2.68×10^{14}	0.85	0.1
Lignin	1.38×10^5	2.18×10^{10}	7.0	0.567
Water	1.62×10^5	1.0×10^{20}	1.0	0

Table 10.1: Kinetic parameters of materials, estimated using a genetic algorithm [315].

8. DEBONDING OF WALL AND CEILING SURFACES.

   The debonding model described in Section 5.8 assumes the fall-off behaviour is uniform across the entire exposed area of tim-

Type of wood	Cellulose (%)	Hemicellulose (%)	Lignin (%)
Hardwood	40-44	23-40	18-25
Softwood	40-44	20-32	25-35

Table 10.2: Chemical composition of dry wood [132].

ber leading to much faster charring rates within the timber than seen in the experiments. This assumption is not likely to be very accurate and the current debonding submodel could be reviewed and modified to reflect the more progressive nature and time frames applicable for the debonding process. A stochastic approach might also be considered. Furthermore the continued burning of the discarded material on the floor of the enclosure is not adequately accounted for. It is recommended to develop algorithms to determine the fraction of a wall or ceiling surface that can be subject to debonding and, if debonding occurs, account for the HRR contribution of partially charred wood that falls to the floor.

9. Gypsum board fall-off.

   In the current research, any boards or lining materials used to protect the underlying timber have been assumed to remain in place and effective for the full duration of the fire. In the future, a gypsum board protection and fall-off submodel should be developed. Other materials or means of protecting the mass timber such as intumescents, or sheet linings over battens could also be investigated. Current approaches are to consider a temperature criterion on the back face of the board protection as an indicator of when the protection might fail.

10. Mixed cellulosic/polymeric fuel loads.

    It is noted that the present model, under post-flashover conditions, represents the moveable fire load as equivalent wood cribs, regardless of the actual materials and configuration of the moveable fire load within the enclosure. For some mixed cellulosic/polymeric fire loads that comprise actual furniture this may not provide a very good representation of the actual fuel surface controlled and/or porosity controlled mass loss rates. Although representing the moveable fuel load as equivalent wood cribs may be adequate for design purposes when the actual fuel composition is not well defined, an improved means of representing the burning behaviour of mixed cellulosic/polymeric fuel loads would be a useful addition to the model.

11. Progress variable for fuel response effects

When accounting for the fuel response effects on the burning behaviour of fuel packages as described in Chapter 7, the free burn mass loss rate is given as a function of time. Therefore, as the burning rate increases due to thermal feedback, the fuel is consumed more rapidly resulting in a sudden drop when the total mass has been burned. It would be more appropriate to express the free burn mass loss rate as a function of the mass loss rather than of time. For example, for an object with the free burn time-temperature mass loss rate shown in Figure 10.1, the mass loss plotted against time is shown in Figure 10.2 and the corresponding mass loss rate plotted against the mass loss is shown in Figure 10.3.

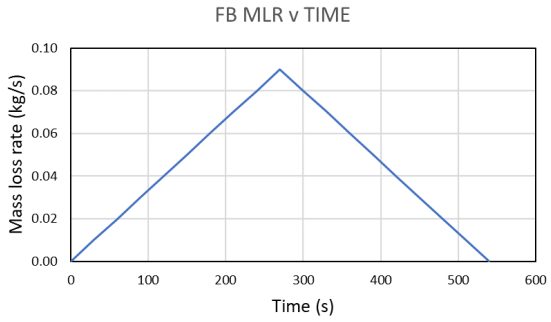

Figure 10.1: Free burn mass loss rate versus time.

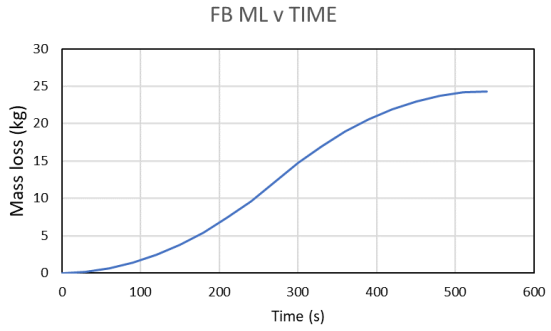

Figure 10.2: Free burn mass loss versus time.

To assess the impact of making this change, the simulation of the predicted mass loss rate for Chair 21-L-S2-1, as described in Section 7.8.3, including fuel response effects with the mass loss as the progress variable (PV) instead of time is shown in Figure 10.4. A significant improvement in the mass loss rate prediction can be seen when mass loss is used as the progress variable rather than time.

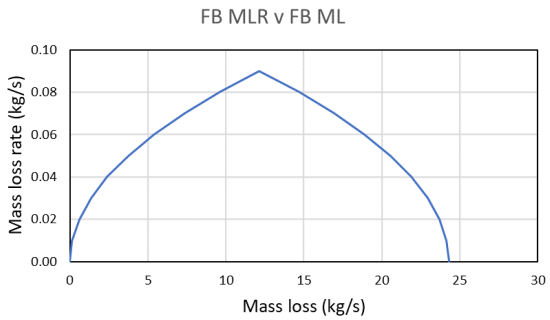

Figure 10.3: Free burn mass loss rate versus mass loss.

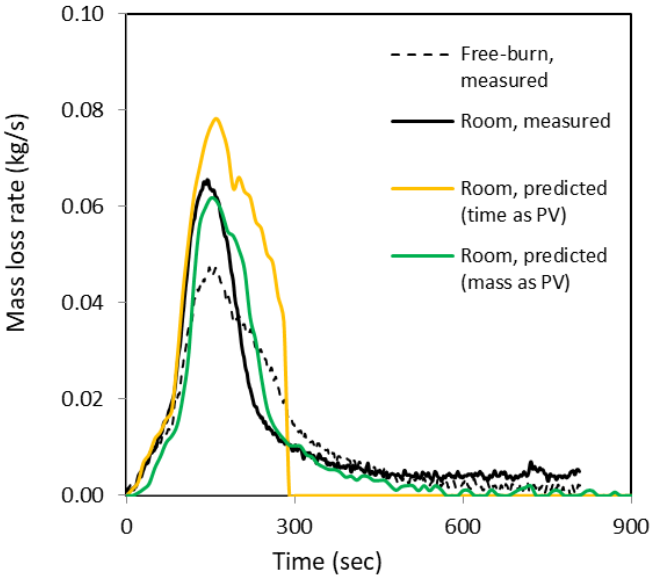

Figure 10.4: Mass loss rate versus time for Chair 21-L-S2-1 - experiment compared with model predictions.

12. INCIDENT FLUX TO THE FUEL SURFACE IN THE FUEL RESPONSE EFFECTS SUBMODEL

    In the current model, the incident flux to the fuel surface was approximated with the radiant flux incident on the floor surface. This should be updated so that the calculated radiant flux at the height of the fuel surface above the floor is used instead.

10.3 RECOMMENDATIONS FOR ADDITIONAL RESEARCH

The following is a list of recommended further research and activities relating to the content of this thesis.

1. CRACKS AND FISSURES IN WOOD CHAR. In the model developed in this research, the effect of cracking, development of surface fis-

sures and surface oxidation have not been accounted for. These phenomena may allow heat to more easily penetrate to greater depths beneath the surface accompanied by a corresponding increase in decomposition reactions. The relative importance of these phenomena should be investigated in greater detail particularly for the effect they may have on the predicted charring rates into the wood and to determine how they might be better accommodated within the model.

2. Adhesives used in New Zealand for mass timber elements. There is a need to investigate the behaviour of adhesives used in New Zealand mass timber buildings where fire performance is expected. AS/NZS 4364 does not include any content relating to the debonding characteristics of lamellae exposed to fire and the topic of fire performance requirements for adhesives should be investigated more thoroughly.

3. Char oxidation during decay phase. It would be desirable to further investigate the model capability and applicability to the decay period of the fire. It is known that oxidation of char is affected by the local oxygen concentrations. The model determines the char depth as a thermally driven process dependent on the heat transfer boundary conditions from the fire which is influenced by oxygen in the compartment. Research to determine whether the model prediction of the char depth is conservative or not in this regard would be helpful.

4. Validation and benchmarking.

   The underlying kinetic pyrolysis submodel should be more thoroughly investigated by comparison with cone calorimeter data at a fixed incident heat flux. It is also highly desirable that further benchmarking of the submodels developed in this thesis for a wider variety of enclosure sizes, fuel loads and ventilation conditions be carried out. In the case of combined fuel response effects and wood surface pyrolysis models there are very few (if any) well documented experiments available for use in a benchmarking study. Additional experiments in timber enclosures with well-characterised fuel sources are needed.

5. Char depth predictions. The ability of the model to provide conservative prediction of char depth beneath the surface of mass timber elements is critical to the reliable prediction of the structural performance in fire of these elements. This aspect of the model requires further analysis and critique. Central to this is the autoextinction behaviour during the decay phase of the fire and the influence of oxygen levels, air flows and local radiative effects. Additional, well instrumented experiments

at reduced scale where both the temperature and oxygen concentration is controlled would be very helpful for the ongoing validation of the submodels described in this thesis.

6. EQUIVALENT TIME OF EXPOSURE FOR MASS TIMBER BUILDINGS. It may be possible to develop a time-equivalence methodology, perhaps based on the ultimate char depth in real fires compared to the char depth observed in standard fire resistance tests. Further research in this area would be helpful along with further analysis and validation of the methods proposed in Chapter 9 of this thesis.

7. PREFLASHOVER VERSUS POSTFLASHOVER FIRES. The wood surface contribution during the preflashover period was not a focus of this thesis since early fire growth and flame spread does not greatly affect the fire resistance. However, a previously developed submodel for predicting fire growth and energy contribution from combustible enclosure surface linings to the enclosure fire could be integrated with the fully developed fire model described in this thesis to provide a more complete model representative of fire development from ignition to burnout.

8. REGULATORY REQUIREMENTS FOR MASS TIMBER BUILDINGS. Fire resistance requirements in the NZBC, verification method C/VM2 and acceptable solutions relating to fire severity in mass timber enclosures should be updated with provisions provided to more accurately reflect the expected fire dynamics in mass timber enclosures.

10.4 POSTSCRIPT

The kinetic wood pyrolysis submodel SMC described in Section 5.7 was subsequently amended (B-RISK version 2019.036) to evaluate the effect of making some of the changes described in Section 10.2 above. In particular:

1. The apparent density of wood/char including the char contraction correction was calculated using Equation 10.4 to Equation 10.8.

2. The thermal conductivity of wood and char were determined using the equations given by Janssens and Douglas [132] for moist wood (perpendicular to the grain) and char. A weighted average thermal conductivity based on the residual mass fractions of wood and char residue was calculated for each layer in the finite difference scheme.

3. A correction to the thermal conductivity to account for char contraction was made using Equation 10.9 to Equation 10.11.

4. The thermal conductivity and specific heat of char were treated as non-reversible with respect to temperature.

5. The latent heat of vaporisation of water and heat of wetting based on Equation 10.2 and Equation 10.3 respectively were incorporated into the specific heat term over the temperature range 100 to 120°C. It is only applied to the element during the heating phase and not during the subsequent cooling phase.

6. The kinetic properties and wood composition were changed to those given in Table 10.1.

Simulations for Config. P and Config. S were repeated and compared with the predicted and measured gas temperatures reported in Section 6.5 as shown in Figure 10.5 and Figure 10.6 respectively.

In these examples, good agreement is achieved during the heating phase along with the peak gas temperature and the time to reach the peak temperature. However the rate of temperature decay appears to be too quick. The reason for this requires further investigation but could be due to a combination of the following factors:

- Oxidation of char and/or continued burning/smouldering of the wood surfaces not accounted for during the decay phase.
- Cracking and continued degradation of the wood char during the decay phase.
- Actual temperature dependent thermal and/or kinetic properties of the wood varying from the assumed properties.
- The actual fuel surface controlled mass loss rate for the wood crib moveable fire load differing from the assumed rate due to fuel response effects, collapsing cribs or other reasons.
- Not accurately representing the conduction heat losses within the enclosure due to the thermal properties applying to the partial areas protected with gypsum plasterboard being represented by the properties of wood/char.
- Water vapour evaporating but then condensing again deeper into the enclosure surfaces.

An example of the predicted residual mass fraction for each component within the wall element located at a depth of 30 mm below the surface of the wall for Config. P is shown in Figure 10.7 with the trends shown for the decomposition of each component appearing consistent with Matala et al. [315].

Finally, if the enclosure fire model with pyrolysis sub models for mass timber is to be used to evaluate the fire severity and char depths in mass timber enclosures, then it is necessary that additional safety

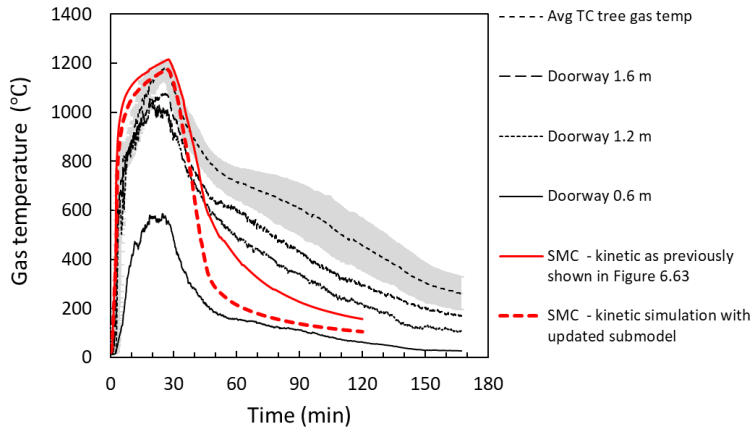

Figure 10.5: Measured and predicted enclosure gas temperatures with updated submodel SMC for Config. P.

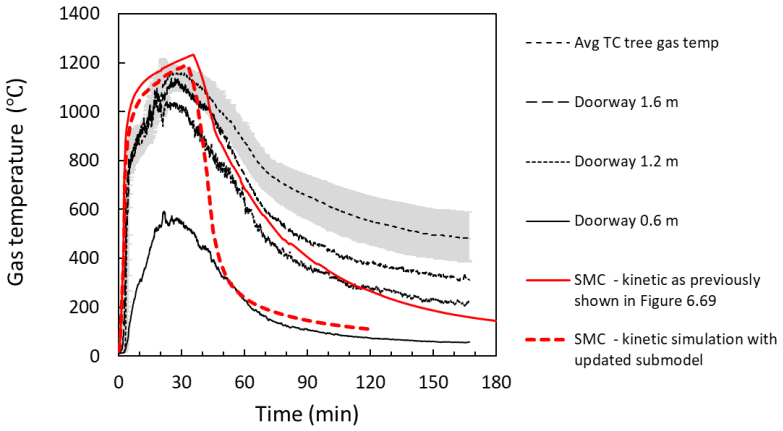

Figure 10.6: Measured and predicted enclosure gas temperatures with updated submodel SMC for Config. S.

factors for inputs and/or model calibration be undertaken. For example, Figure 10.8 shows the char depth measurements compared with predicted char depths for Config. P, where various temperatures to represent the char interface could be used to ensure a conservative char depth prediction overall. Notwithstanding this, further investigation of the decay period and the accuracy of the predicted char depths is recommended.

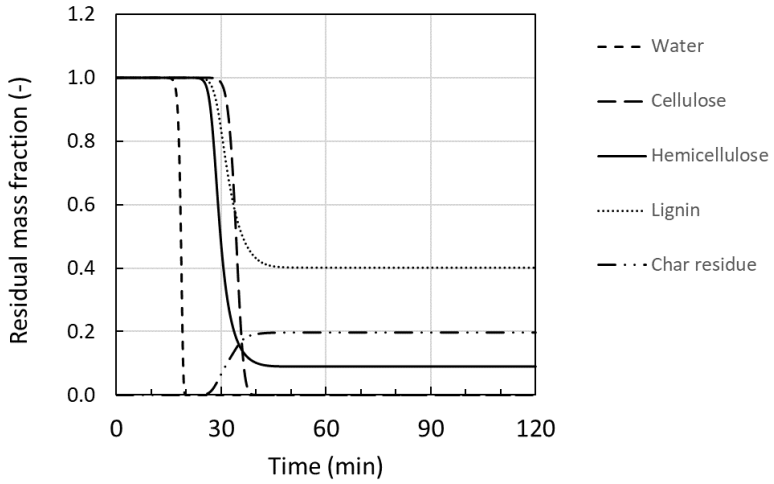

Figure 10.7: Example of the predicted residual mass fraction for each component within the wall element located at a depth of 30 mm below the surface of the wall for Config. P.

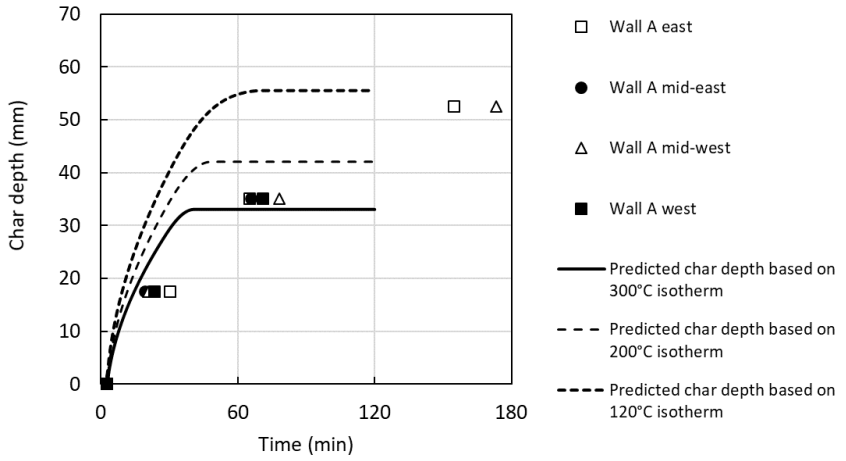

Figure 10.8: Char depth based on internal thermocouples measurement compared with predicted char depths for Config. P.

APPENDIX A

A.1 SENSITIVITY OF THE POST-FLASHOVER WOOD CRIB MODEL IN B-RISK TO THE PLUME ENTRAINMENT ALGORITHM USED

For ventilation-controlled burning, the oxygen in the plume flow is used for combustion determining the ventilation-controlled heat release rate. As for pre-flashover burning, a single axisymmetric plume is assumed. However, it doesn't seem likely that a single axisymmetric plume developed using data from small preflashover fires would be a very good assumption for a post-flashover fire. The following discussion demonstrates the significance and sensitivity of B-RISK results for ventilation-controlled burning given this assumption and shows that the the results are relatively insensitive to the exact form of the plume correlation.

The mass flow in the plume comes from both the mass inflow through the vents and from any near vent mixing flow. The near vent mixing flow deposits gases from the upper layer into the lower layer and is the sole mechanism for contamination of the lower layer gases with combustion products. The mass fraction of oxygen in the vent inflow (coming from outside) will be ambient (0.231) while the mass fraction of oxygen in the near vent mixing flow (coming from the upper layer) will be largely depleted and close to zero after flashover or during ventilation controlled burning. These two flow streams mix together in the lower layer such that the oxygen mass fraction in the mixed lower layer lies between the two source flow values. The mass flows are illustrated in Figure A.1.

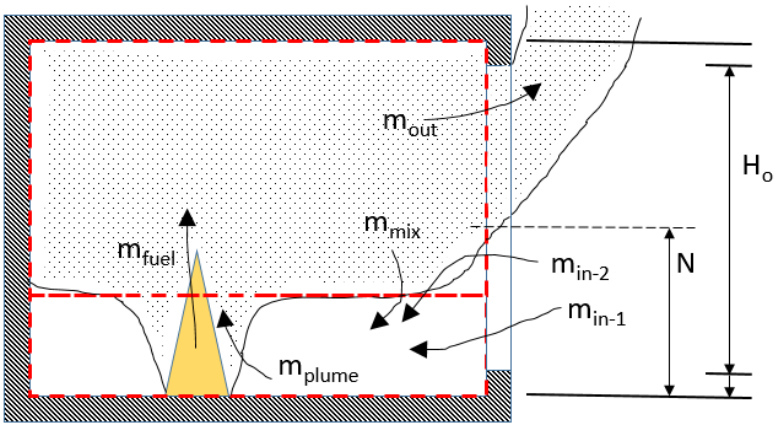

Figure A.1: Mass flows in compartment with opening with vent mixing term.

In B-RISK, after flashover and with the layer height close to the floor, the plume entrainment continues to be calculated using the McCaffrey "flaming" correlation [227] as follows, where $\dot{Q}_{max}$ is the maximum heat release rate that can be supported by the available oxygen supply:

$$\frac{\dot{m}_p}{\dot{Q}_{max}} = 0.011 \left(\frac{z}{\dot{Q}_{max}^{2/5}} \right)^{0.566} \tag{A.1}$$

The mass flow of oxygen in the plume (kg-O2/s) needed for complete combustion of the fuel is given by:

$$\dot{m}_{O_2 \text{ needed}} = \frac{\dot{Q}_f}{13100} \tag{A.2}$$

$\dot{Q}_f$ is the theoretical, free-burning heat release rate. This equation is based on the observation that approximately 13,100 kJ of energy is released for every kg of oxygen consumed during the combustion reaction [247].

The actual mass flow of oxygen in the plume (kg-O2/sec) is given by:

$$\dot{m}_{O_2 \text{ actual}} = \dot{m}_p Y_{O_{2,l}} C \tag{A.3}$$

$Y_{O_{2,l}}$ is the mass fraction of oxygen in the lower layer. C is a coefficient described by Peacock et al [115] as given by Equation A.4 representing the fraction of fuel that can be burned with the available oxygen and varies between 0 and 1 to provide a smooth cut-off of the burning over a narrow range above the oxygen limit. An oxygen limit of 10% by volume is assumed with the corresponding mass fraction given in Equation A.5.

$$C = \frac{\tanh\left(800\left(Y_{O_{2,l}} - Y_{lim}\right) - 4\right) + 1}{2} \tag{A.4}$$

$$Y_{limit} = 0.1 \frac{MW_{O_2}}{MW_{l,avg}} \tag{A.5}$$

When cool air flows into the room through a wall vent, it is assumed to entrain some of the upper layer gases from the upper layer into the lower layer. This can result in a blurring of the sharp distinction between the two stratified gas layers. The near vent mixing correlation developed by Utiskul has been applied where the incoming cold air behaves like a jet entering the vent with a characteristic velocity and diffusing downward because of buoyancy [225]. While

the cooler air descends, the surrounding hot gas is entrained with a velocity that is proportional to the incoming flow characteristic velocity. An equation for the ratio of mass entrained to the total incoming mass flow was developed by Utiskul and single-vent compartment fire experiments were conducted to establish the correlation for the mixing at the quasi-steady state. The correlation exhibited a linear relationship up to an apparent asymptote for the mixing ratio of about 1.3 and was given previously in Equation 7.2. This vent mixing mass flow, taken from the upper layer and added to the lower layer, applies both to vents to the exterior and vents to adjacent rooms.

Since the mass flow in the plume depends on the fire heat release rate, and the heat release rate depends on the oxygen available in the plume, these calculations are done iteratively at each time step until the difference between successive calculations of the oxygen constrained heat release rate is sufficiently small. Ultimately the inflow of air to the compartment determines the heat released inside the compartment rather than the total mass flow in the plume. This is demonstrated by an example.

A.2 EXAMPLE

Consider a room 8.6 m long × 5.9 m wide × 3.9 m high, with an opening 2.2 m high × 1.906 m wide. The fuel is wood cribs 285 MJ/m^2 (floor area basis). A simple estimate of the ventilation limit for this compartment using $\dot{Q}_{max} = 1500 A_o \sqrt{h_o}$ is 9329 kW.

Simulations to test the sensitivity of the compartment mass flows and heat release rate to the magnitude of the plume flow were run. The plume flow calculated using Equation A.1 for the McCaffrey flaming correlation was multiplied by factors of 0.5 and 2.0.

Figure A.2 compares the calculated plume flow using the McCaffrey correlation [227] for the flaming region (black line) with that obtained by multiplying the right hand side of Equation A.1 by a factor of 0.5 (blue) and 2.0 (red) respectively. The three cases clearly result in a different calculated total plume flow, but they are not one-half and double the original value because the plume flow and layer height are dependent on each other. If the plume flow is increased, the upper layer volume increases lowering the layer height (and reducing entrainment and plume flow). The plume flow effect on the calculated layer height is shown in Figure A.3.

In addition, if the burning is oxygen-constrained the rate of heat release is determined by the oxygen mass flow in the plume which in turn is dependent on the rate of heat release. If the plume flow increases (assuming the same mass fraction of oxygen in the plume) the rate of heat release would also increase.

Now compare the calculated heat release rate in the compartment shown in Figure A.4 for the three cases. The oxygen-constrained heat

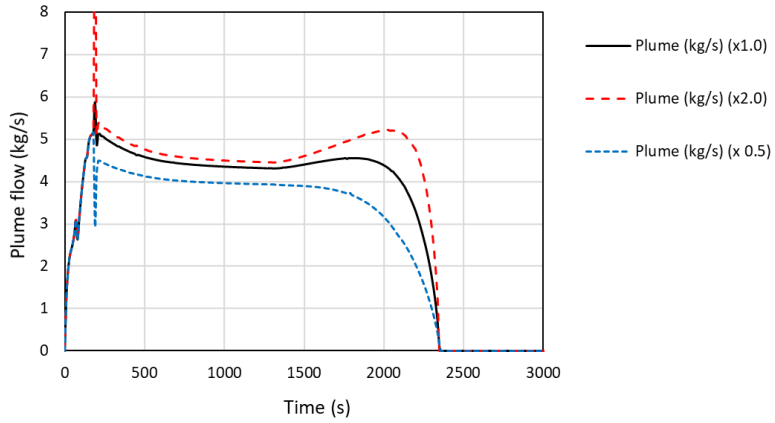

Figure A.2: Plume entrainment, flaming region.

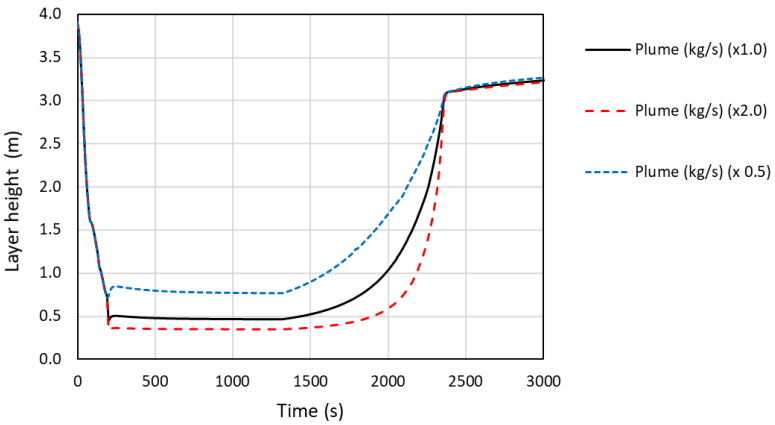

Figure A.3: Effect of plume flow on the layer height.

release rate is identical. This means that the oxygen mass flow in plume must be the same in each case even though the total plume flow is different (as per Figure A.2). This requires the oxygen mass fraction feeding the plume to be also different. For completeness, Figure A.5 shows the effect of the plume entrainment on the upper layer temperatures.

Consider a snapshot of the mass flows in the compartment at 1000 seconds for each case. In all three cases the calculated oxygen mass flow in the plume is calculated as 0.65 kg/s as shown below.

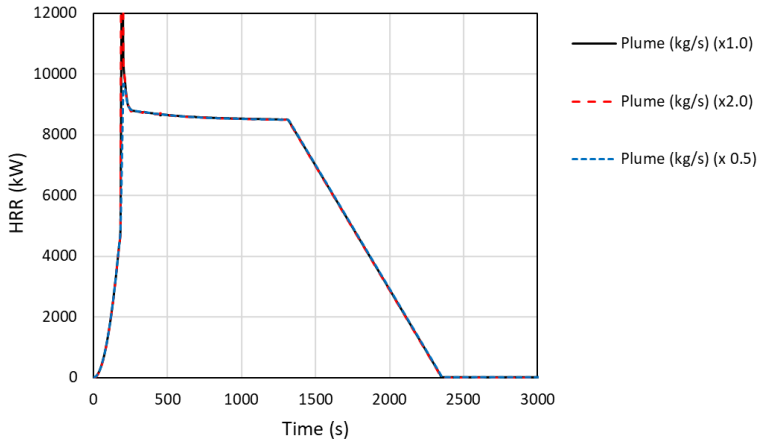

Figure A.4: Effect of plume flow on the heat release rate.

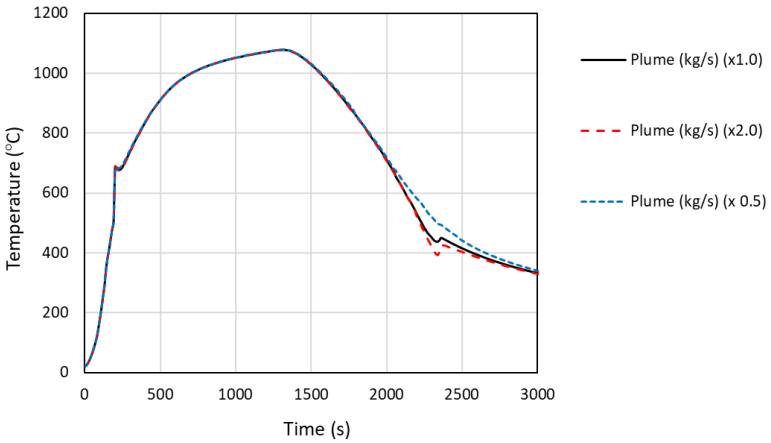

Figure A.5: Effect of plume flow on the calculated upper layer gas temperature.

At 1000 sec (using McCaffrey plume × 1.0)

Vent flow output from B-RISK is shown in Figure A.6. The corresponding flow schematic is shown in Figure A.9. The mass flow of oxygen in the plume is calculated as follows:

$$\begin{aligned} \dot{m}_{O_2} = \dot{m}_p Y_{O_{2,l}} &= \dot{m}_p V_{O_{2,l}} \frac{MW_{O_2}}{MW_{l,avg}} \\ &= \dot{m}_p V_{O_{2,l}} \frac{MW_{O_2}}{MW_{l,avg}} \\ &= 4.355 \times \frac{13.6}{100} \times \frac{32}{29.19} = 0.65 kg/s \end{aligned} \tag{A.6}$$

```
==================================
 Wall Vent Flows
==================================

Time(s)  from-room to-room  vent#  #slabs  elevation (m)     ventflow(kg/s)
0        1         2        1      1       0.900 to 3.100    1.238

1000     1         2        1      2       1.683 to 3.100    3.259
                                          0.900 to 1.683    -2.807

2000     1         2        1      3       1.773 to 3.100    3.228
                                          1.034 to 1.773    -2.449
                                          0.900 to 1.034    -0.696

3000     1         2        1      2       1.949 to 3.100    2.501
                                          0.900 to 1.949    -2.529
```

Figure A.6: B-RISK Wall vent flow output with McCaffrey plume flow × 1.0.

At 1000 sec (using McCaffrey plume × 2.0)

Vent flow output from B-RISK is shown in Figure A.7. The corresponding flow schematic is shown in Figure A.10. The mass flow of oxygen in the plume is calculated as follows:

$$\begin{aligned} \dot{m}_{O_2} = \dot{m}_p Y_{O_{2,l}} &= \dot{m}_p V_{O_{2,l}} \frac{MW_{O_2}}{MW_{l,avg}} \\ &= \dot{m}_p V_{O_{2,l}} \frac{MW_{O_2}}{MW_{l,avg}} \\ &= 4.499 \times \frac{13.2}{100} \times \frac{32}{29.205} = 0.65 \text{kg/s} \end{aligned} \tag{A.7}$$

```
==================================
 Wall Vent Flows
==================================

Time(s)  from-room to-room  vent#  #slabs  elevation (m)     ventflow(kg/s)
0        1         2        1      1       0.900 to 3.100    1.238

1000     1         2        1      2       1.683 to 3.100    3.259
                                          0.900 to 1.683    -2.806

2000     1         2        1      2       1.773 to 3.100    3.232
                                          0.900 to 1.773    -3.143

3000     1         2        1      2       1.949 to 3.100    2.487
                                          0.900 to 1.949    -2.513
```

Figure A.7: B-RISK Wall vent flow output with McCaffrey plume flow × 2.0.

At 1000 sec (using McCaffrey plume × 0.5)

Vent flow output from B-RISK is shown in Figure A.8. The corresponding flow schematic is shown in Figure A.11. The mass flow of oxygen in the plume is calculated as follows:

$$\begin{aligned} \dot{m}_{O_2} = m_p Y_{O_{2,l}} &= m_p V_{O_{2,l}} \frac{MW_{O_2}}{MW_{l,avg}} \\ &= m_p V_{O_{2,l}} \frac{MW_{O_2}}{MW_{l,avg}} \\ &= 3.961 \times \frac{14.9}{100} \times \frac{32}{29.127} = 0.65 \text{kg/s} \end{aligned} \tag{A.8}$$

```
==================================
 Wall Vent Flows
==================================

Time(s)  from-room to-room  vent#    #slabs   elevation (m)      ventflow(kg/s)
entrain (kg/s)
0        1         2        1       1        0.900 to 3.100     1.238

1000     1         2        1       2        1.683 to 3.100     3.258
                                             0.900 to 1.683     -2.807

2000     1         2        1       3        1.791 to 3.100     3.157
                                             1.689 to 1.791     -0.125
                                             0.900 to 1.689     -3.018

3000     1         2        1       2        1.947 to 3.100     2.537
                                             0.900 to 1.947     -2.567
```

Figure A.8: B-RISK Wall vent flow output with McCaffrey plume flow × 0.5.

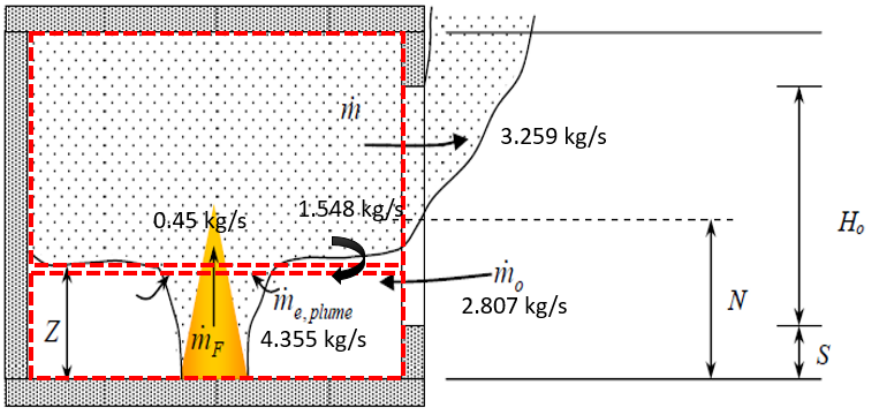

Figure A.9: Flow schematic at 1000 s with McCaffrey plume flow × 1.0.

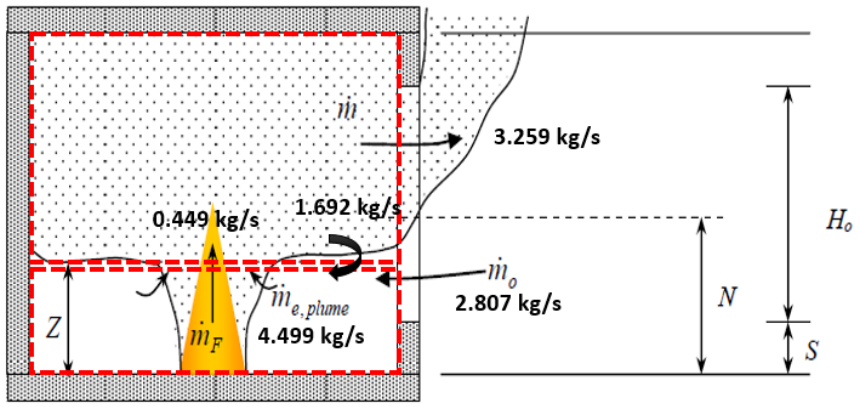

Figure A.10: Flow schematic at 1000 s with McCaffrey plume flow × 2.0.

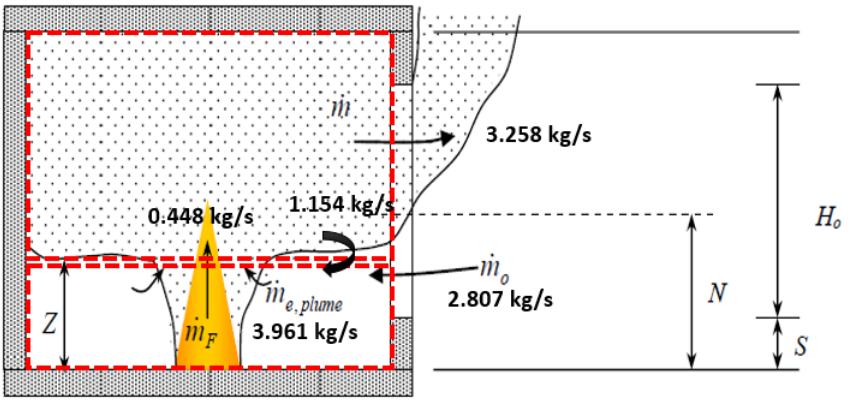

Figure A.11: Flow schematic at 1000 s with McCaffrey plume flow × 0.5.

B

APPENDIX B

B.1 CONVECTIVE HEAT TRANSFER COEFFICIENT

In B-RISK, the interior convective heat transfer coefficient used in the heat transfer calculations between the gas layers and the room surfaces is calculated following the method described by Peacock et al. [115] and as described in the B-RISK technical guide [37]. This assumes natural convective flow for the convective component of heat transfer between the gas layers and the room surfaces. However for the simulations presented in this thesis a constant convective coefficient of 35 W/m^2K has been used instead as specified in Eurocode 1 [117] for simple fire models.

The sensitivity of the calculated enclosure gas temperature to the convective coefficient is investigated for the enclosure experiment reported by Su et al. [171] and referred to as Config. P in Section 6.5.3 of this thesis. The calculated value of the convective coefficient during the Config. P experiment is shown in Figure B.1. The calculated value is much smaller than 35 W/m^2K as specified in Eurocode 1 [117].

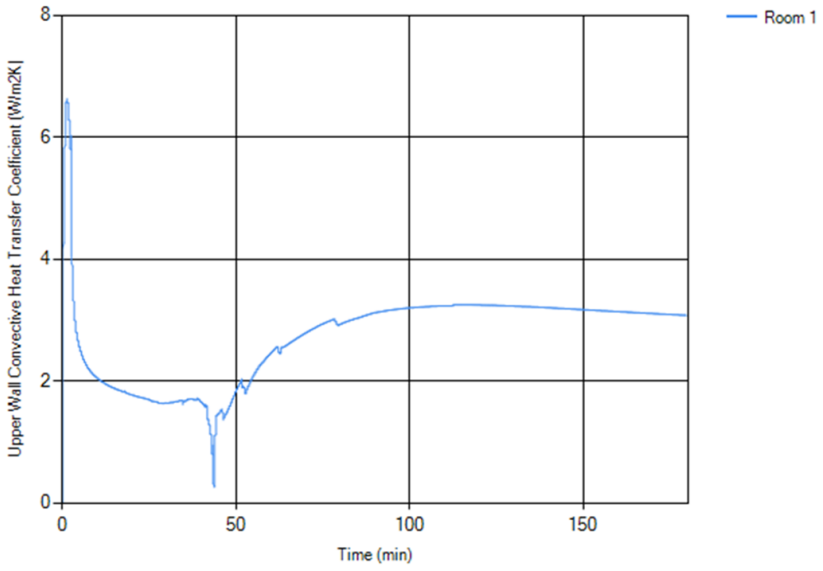

Figure B.1: Calculated convective heat transfer coefficient assuming natural convection for Config. P experiment.

Figure B.2 compares the predicted enclosure gas temperature for the case where a constant convective heat transfer coefficient of 35

W/m^2K is assumed and also for the case where the coefficient is calculated assuming natural convection. The gas temperatures are almost identical during the heating phase of the fire, and with a relatively minor difference during the decay phase where the higher value of 35 W/m^2K leads to a slightly lower gas temperature. It is concluded that assuming a constant convective heat transfer coefficient as per EN 1991-1-2 [117] or calculating the coefficient as usually done by B-RISK would both be acceptable for the types of fires and enclosures considered in this thesis.

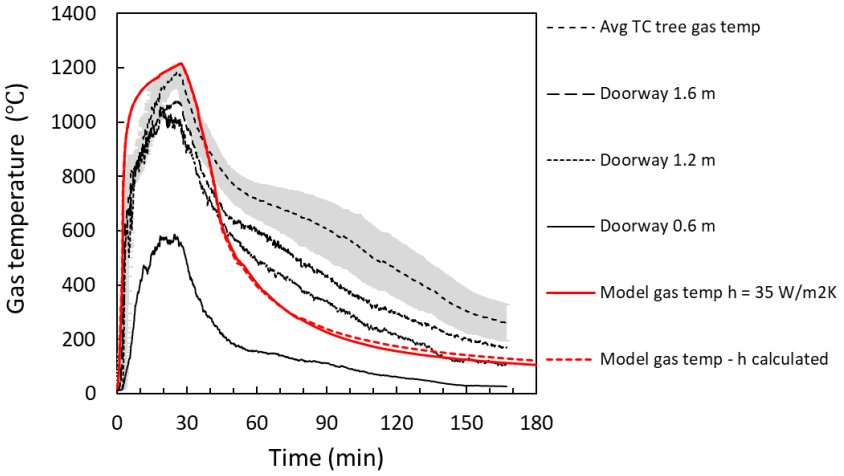

Figure B.2: Sensitivity of the enclosure gas temperatures for Config. P using kinetic pyrolysis submodel to the convective heat transfer coefficient.

While the results of this sensitivity analysis imply that the convective component of the heat flux to surfaces in a post-flashover fire is very small to negligible, that may not necessarily be the case in preflashover fires when the surface temperatures of the enclosure surfaces are still relatively cool.

APPENDIX C

C.1 ESTIMATING MODEL BIAS AND UNCERTAINTY

This procedure follows that described by McGrattan et al. [254]. If the experimental uncertainty is not reported for a specific experiment, Hill et al. [255] have estimated typical values for the combined relative uncertainty in the form of the 95th confidence interval for a range of measured quantities as shown in Table C.1.

Measured quantity	Combined relative uncertainty, $2\tilde{\sigma}_E$
Hot gas layer temperature	0.14
Hot gas layer depth	0.13
Ceiling jet temperature	0.16
Plume temperature	0.14
Gas concentrations	0.09
Smoke concentration	0.33
Pressure with ventilation	0.80
Pressure without ventilation	0.40
Heat flux	0.20
Surface temperature	0.14

Table C.1: Summary of uncertainty estimates.

The procedure aims to quantify the ability of the model to predict a given quantity using just two parameters, the 'bias' which describes the tendency to underpredict or overpredict the true value; and the 'deviation' which describes the scatter about the true value.

The relative model standard deviation is given by:

$$\tilde{\sigma}_M \approx \sqrt{\text{var}\left(\ln\left(M/E\right)\right) - \tilde{\sigma}_E^2} \tag{C.1}$$

where

$$\text{var}\left(\ln\left(M/E\right)\right) \approx \frac{1}{n-1}\sum_{i=1}^{n}\left[\ln\left(M_i/E_i\right) - \overline{\ln\left(M/E\right)}\right]^2 \tag{C.2}$$

and

$$\overline{\ln\left(M/E\right)} \approx \frac{1}{n}\sum_{i=1}^{n}\ln\left(M_i/E_i\right) \tag{C.3}$$

The bias is given by:

$$\delta \approx \exp\left(\overline{\ln(M/E)} + \frac{\tilde{\sigma}_M^2}{2} - \frac{\tilde{\sigma}_E^2}{2}\right) \tag{C.4}$$

The results of the analysis is presented in a scatterplot similar to Figure C.1. Standard deviations are reported in the form of 95% confidence intervals ($2\tilde{\sigma}$). In applying this procedure, it should be mentioned that the model uncertainty cannot sensibly be less than the experimental uncertainty.

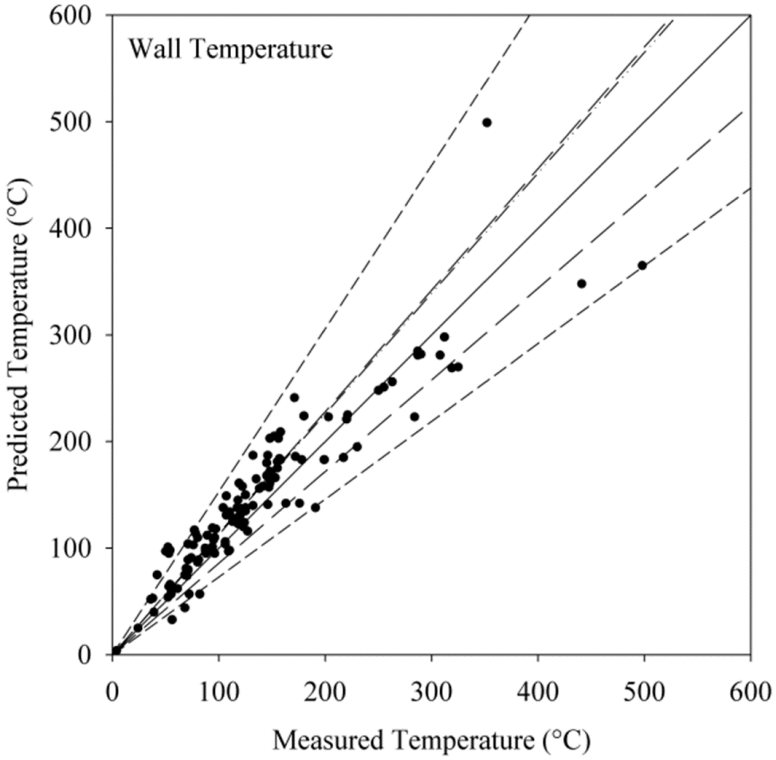

Figure C.1: Example scatterplot of measured vs predicted temperatures [254]. The off-diagonal lines indicate the $2\tilde{\sigma}$ for the experiments (long dash) and for the model (short dash). The model bias is represented as dash-dot-dot. Reprinted from [254] with permission. Copyright ©2014 International Association for Fire Safety Science.

REFERENCES

[1] P.H. Thomas. "SFPE Classic Paper Review: Fire Behavior In Rooms by Kunio Kawagoe." In: *Journal of Fire Protection Engineering* 14 2004, pp. 5–8. DOI: 10.1177/1042391504039408.

[2] D.E. Knuth. "Computer Programming as an Art." In: *Communications of the ACM* 17.12 1974, pp. 667–673. DOI: 10.1145/361604.361612.

[3] D. Barber. "Tall timber buildings – what's next in fire safety?" In: *Fire Technology* 51.6 2015, pp. 1279–1284. DOI: 10.1007/s10694-015-0497-7.

[4] D. Barber, R. Crielaard, and X. Li. "Towards fire safety design of exposed timber in tall timber buildings." In: *Proceedings of WCTE 2016 World Conference on Timber Engineering*. Vienna Austria, 2016.

[5] A.M. Harte. "Mass timber – the emergence of a modern construction material." In: *Journal of Structural Integrity and Maintenance* 2.3 July 2017, pp. 121–132. ISSN: 2470-5314. DOI: 10.1080/24705314.2017.1354156. URL: https://doi.org/10.1080/24705314.2017.1354156.

[6] D. Brandon. *Engineering methods for structural fire design of wood buildings– structural integrity during a full natural fire*. RISE Rapport 2018:44. ISBN 978-91-88695-83-3. Sweden: RISE Research Institutes of Sweden, 2018.

[7] D.C. Evison, P.D. Kremer, and J. Guiver. "Mass timber construction in Australia and New Zealand - Status, and economic and environmental influences on adoption." In: *Wood and Fiber Science* 50.(Special issue) 2018, pp. 128–138.

[8] A.H. Buchanan, A. Dunn, J. O'Neill, and D. Pau. "Fire safety of CLT buildings in New Zealand and Australia." In: *Wood and Fiber Science* 50.(Special issue) 2018, pp. 96–101.

[9] A.H. Buchanan, A. Palermo, D.M. Carradine, and S. Pampanin. "Post-tensioned timber frame buildings." In: *Structural Engineer* 69.17 2011, pp. 24–30.

[10] T. Smith, M. Fragiacomo, S. Pampanin, and A.H. Buchanan. "Construction time and cost for post tensioned timber buildings." In: *Construction Materials* 162.4 Jan. 2009, pp. 141–149. DOI: 10.1680/coma.2009.162.4.141.

[11] M. Green. *The case for tall wood buildings*. Second. Blurb, 2018. URL: https://www.trae.dk/wp-content/uploads/2012/05/tall-wood-buildings-final-report.pdf.

[12] FP Innovations and Binational Softwood and Lumber Council. *CLT Handbook US Edition*. Special Publication SP-529E. Pointe Claire, QC: FP Innovations, 2013.

[13] Arup. *Rethinking timber buildings*. Report. London, England, 2019. URL: https://www.arup.com/perspectives/publications/research/section/rethinking-timber-buildings.

[14] A.H. Buchanan and A.K. Abu. *Structural design for fire safety*. Second edition. Chichester, Sussex, United Kingdom: John Wiley & Sons, Ltd, 2017. ISBN: 978-0-470-97289-2.

[15] BBC. *Fire ravages South Korea landmark*. 2008. URL: http://news.bbc.co.uk/2/hi/asia-pacific/7238210.stm (visited on 04/19/2019).

[16] A. Groves. *Our Lady of the Angels school fire, Chicago: December 1, 1958*. 2006. URL: https://www.ideals.illinois.edu/bitstream/handle/2142/90/Our%20Lady%20of%20the%20Angels%20School%20Fire,%201958.pdf?sequence=2 (visited on 04/19/2019).

[17] D. Nam, Y. Hasemi, K. Kagiya, and T. Harada. "Role of Initial Burning Objects in the Fire Growth in a Large Enclosure-Experiments for the Investigation of a Recent Timber Gymnasium Building Fire." In: *Proceedings of the 6th Asia-Oceania Symposium of Fire Safety Science & Technology*. 2004.

[18] U. Irfan. *Why the Notre Dame fire was so destructive, according to fire experts*. News Media. Apr. 2019. URL: https://www.vox.com/2019/4/16/18312072/notre-dame-cathedral-fire (visited on 04/17/2019).

[19] A.H. Buchanan. "Fire resistance of multi-storey timber buildings." In: *Proceedings of the 10th Asia-Oceania Symposium on Fire Science and Technology*. 2015.

[20] A. Law and R.M. Hadden. "Burnout means burnout." In: *SFPE Europe Digital Magazine* Q1.5 2017. URL: https://www.sfpe.org/general/custom.asp?page=Issue5Feature1 (visited on 05/07/2019).

[21] Department of Building and Housing (DBH). *Schedule 1 of the Building Regulations 1992. New Zealand Building Code Clauses C1–C6 Protection from Fire.* Apr. 2012.

[22] S. Deeny, R. Hadden, B. Lane, and A. Lawrence. "Fire safety design in modern timber buildings." In: *The Structural Engineer* 96.1 Jan. 2018, pp. 48–53. URL: https://www.istructe.org/journal/volumes/volume-96-(2018)/issue-1/fire-safety-design-in-modern-timber-buildings.

[23] R. Gerard, D. Barber, and A. Wolski. *Fire Safety Challenges of Tall Wood Buildings*. Final Report. Quincy, MA: The Fire Protection Research Foundation, 2013.

[24] B. Östman, D. Brandon, and H. Frantzich. "Fire safety engineering in timber buildings." In: *Fire Safety Journal* 91 2017, pp. 11–20. ISSN: 0379-7112. DOI: 10.1016/j.firesaf.2017.05.002. URL: http://www.sciencedirect.com/science/article/pii/S0379711217302977.

[25] C.A. Wade, G.B. Baker, K. Frank, A.P. Robbins, R. Harrison, M.J. Spearpoint, and C.M. Fleischmann. *B-RISK user guide and technical manual*. Study Report 282. Porirua, New Zealand: BRANZ Ltd, 2013. URL: http://www.b-risk.com.

[26] C.A. Wade, D. Hopkin, J. Su, M.J. Spearpoint, and C.M. Fleischmann. "Enclosure fire model for mass timber construction - benchmarking with a kinetic pyrolysis submodel." In: *Interflam 2019: 15th International Conference on Fire Science and Engineering*. Royal Holloway College, Nr Windsor, UK: InterScience Communications Limited, 2019.

[27] D. Jessop, A.K. Abu, C.A. Wade, M.J. Spearpoint, J.T Gerlich, and A.H. Buchanan. "Performance of a light timber-framed compartment in natural fire subjected to lateral load." In: *Fire and Materials* 43.2 2019, pp. 175–188. DOI: 10.1002/fam.2684.

[28] C.A. Wade, M.J. Spearpoint, C.M. Fleischmann, G.B. Baker, and A.K. Abu. "Predicting the fire dynamics of exposed timber surfaces in compartments using a two-zone model." In: *Fire Technology* 54.4 2018, pp. 893–920. ISSN: 0015-2684. DOI: 10.1007/s10694-018-0714-2.

[29] C. A. Wade, M.J. Spearpoint, and C.M. Fleischmann. "Engineering Methods for Evaluating the Contribution of Exposed Timber to Post-Flashover Enclosure Fires." In: *SFPE Europe Magazine* 11 2018. URL: https://www.sfpe.org/page/Issue11Feature2?&_zs=hc01d1&_zl=sx9e5.

[30] C.A. Wade, C.M. Fleischmann, M.J. Spearpoint, and A.K. Abu. "Prediction model for compartment effects on burning upholstered furniture." In: *Proceedings of Fire Safety 2017 International Conference on Research and Advanced Technology in Fire Safety*. Ed. by D. Alvear. Santander, Spain: Editorial de la Universidad de Cantabria, 2017, pp. 315–330.

[31] C.A. Wade, C.M. Fleischmann, M.J. Spearpoint, and A.K. Abu. "Revisiting normalised heat load and its application in a compartment fire model." In: *Proceedings Fire and Materials 2015*. San Francisco, USA: InterScience Communications Limited, 2015.

[32] C.A. Wade, J.T. Gerlich, and A.K. Abu. *The Relationship between Fire Severity and Time-Equivalence*. BRANZ Study Report 314. Porirua, New Zealand, 2014.

[33] C.A. Wade. "Fire hazard assesssment of wall and ceiling fire spread in rooms." In: *Flammability testing of materials used in construction, transport and mining*. Ed. by V. Apte. 2nd Edition. (Chapter under revision). Cambridge, England: Woodhead Publishing Limited, 2019.

[34] C.A. Wade. "Fire ratings in industrial buildings." In: *BUILD* 171.April/May 2019, pp. 53–54. URL: http://www.buildmagazine.org.nz/articles/show/fire-resistance-in-industrial-buildings.

[35] C. A. Wade and K. Frank. "Evaluating fire resistance requirements in New Zealand industrial and storage buildings." In: *SFPE Europe Magazine* 2019. Submitted March 2019. URL: https://www.sfpe.org/page/Issue11Feature2?&_zs=hco1d1&_zl=sx9e5.

[36] G.B. Baker, C.A. Wade, and K. Frank. "Reaction-to-Fire Behaviour of Partial Quantities of Timber Surface Linings in Compartments." In: *Research and Advanced Technology in Fire Safety*. Ed. by D. Alvear. Santander, Spain: Editorial de la Universidad de Cantabria, 2017, pp. 331–346.

[37] C.A. Wade, G.B. Baker, K. Frank, R Harrison, and M.J. Spearpoint. *B-RISK 2016 User guide and technical manual*. Study Report SR364. Porirua, New Zealand: BRANZ, 2016.

[38] H. Peel, C.A. Wade, M.J. Spearpoint, and C.M. Fleischmann. "Experiments to develop a performance based assessment method for rooms partially lined with timber." In: *Proceedings of the 11th Conference on Performance-Based Codes and Fire Safety Design Methods*. Warsaw, Poland, 2016.

[39] H. Peel, C.A. Wade, and M.J. Spearpoint. "Comparison of partially lined timber room experiments with the modified B-RISK flame spread capability." In: *Proceedings of 14th International Conference on Fire Science and Engineering (INTERFLAM)*. University of London, UK, 2016.

[40] D. Jessop, A.K. Abu, C.A. Wade, M.J. Spearpoint, J.T Gerlich, and A.H. Buchanan. "Full-scale fire test of a laterally loaded light timber-framed compartment." In: *Proceedings of the 9th International Conference on Structures in Fire*. Princeton, USA, 2016.

[41] J.G. Quintiere and C.A. Wade. "Chapter 29 Compartment Fire Modeling." In: *SFPE Handbook of Fire Protection Engineering*. 5th Edition. New York, NY: Springer, 2015, pp. 981–995. ISBN: 978-1-4939-2564-3. URL: https://doi.org/10.1007/978-1-4939-2565-0_29.

[42] D. Drysdale. *An Introduction to Fire Dynamics*. 2nd ed. Chichester, Sussex, United Kingdom: John Wiley & Sons Ltd, 1998. ISBN: 978-047197291.

[43] J. Stern-Gottfried and G. Rein. "Travelling fires for structural design–Part I: Literature review." In: *Fire Safety Journal* 54 2012, pp. 74–85. DOI: 10.1016/j.firesaf.2012.06.003.

[44] J. Stern-Gottfried and G. Rein. "Travelling fires for structural design-Part II: Design methodology." In: *Fire Safety Journal* 54 2012, pp. 96–112. DOI: 10.1016/j.firesaf.2012.06.011.

[45] W.D. Walton and P.H. Thomas. "Chapter 30 Estimating temperatures in compartment fires." In: *SFPE Handbook of Fire Protection Engineering*. 5th Edition. Gaithersburg MD: Society of Fire Protection Engineers, 2016. URL: https://doi.org/10.1007/978-1-4939-2565-0_30.

[46] P.H. Thomas. "Testing products and materials for their contribution to flashover in rooms." In: *Fire and Materials* 5.3 1981, pp. 103–111. ISSN: 1099-1018. DOI: 10.1002/fam.810050305.

[47] K. Kawagoe. *Fire behaviour in rooms*. Report 27. Tokyo: Building Research Institute, 1958.

[48] T.Z. Harmathy. "A New Look at Compartment Fires, Part II." In: *Fire Technology* 8 1972, pp. 326–351. DOI: 10.1007/BF02590537.

[49] T.Z. Harmathy. "Mechanism of burning of fully-developed compartment fires." In: *Combustion and Flame* 31.1 1978, pp. 265–273. DOI: 10.1016/0010-2180(78)90139-6.

[50] T.Z. Harmathy. "Experimental Study on the Effect of Ventilation on the Burning of Piles of Solid Fuels." In: *Combustion and Flame* 31 1978, pp. 259–264. DOI: 10.1016/0010-2180(78)90138-4.

[51] H.W. Emmons. "The Needed Fire Science." In: *Proceedings of the First International Fire Safety Symposium*. University of California, Berkeley, 1986. DOI: 10.3801/IAFSS.FSS.1-33.

[52] J.G. Quintiere. "A Perspective on Compartment Fire Growth." In: *Combustion Science and Technology* 39.1-6 Aug. 1984, pp. 11–54. ISSN: 0010-2202. DOI: 10.1080/00102208408923782.

[53] J.G. Quintiere. "Fundamentals of Enclosure Fire Zone Models." In: *Journal of Fire Protection Engineering* 1.3 1989, pp. 99–119. DOI: 10.1177/104239158900100302.

[54] M.L. Janssens. "Heat Release in Fires." In: *Heat Release in Fires*. Ed. by V. Babrauskas and S.J. Grayson. Essex, England: Elsevier Applied Science, 1992. ISBN: 978-0-419-16100-4.

[55] N.D. Fowkes. "A Mechanistic Model of the 1973 and 1974 Bedroom Test Fires." In: *A Study of Room Fire Development: The Second Full-Scale Bedroom Fire Test of the Home Fire Project*. FMRC Technical Report No. 21011.4. FMRC, 1975, pp. 8–50.

[56] H.E. Mitler. *The Physical Basis for the Harvard Computer Fire Code*. Home Fire Project Technical Report 34. Cambridge, MA: Harvard University, 1978.

[57] H.E. Mitler and H. Emmons. *Documentation for CFC, the Fifth Harvard Computer Fire Code*. NBSGCR 81-344. National Bureau of Standards, U.S. Department of Commerce, 1981.

[58] T. Tanaka. *A Mathematical Model of a Compartment Fire*. BRI Research Paper 70. Tokyo, Japan: Building Research Institute, 1977.

[59] H.E. Mitler. "The Harvard Fire Model." In: *Fire Safety Journal* 9.1 1985, pp. 7–16. DOI: 10.1016/0379-7112(85)90026-8.

[60] H.E. Mitler and J.A. Rockett. *User's Guide to FIRST, A Comprehensive Single-Room Fire Model*. NBSIR 87-3595. National Bureau of Standards, U.S. Department of Commerce, 1987.

[61] L.Y. Cooper. *Estimating Safe Available Egress Time from Fires*. NBSIR 80-2172. National Bureau of Standards, U.S. Department of Commerce, 1980.

[62] H.E. Nelson. *FPETOOL - Fire Protection Tools for Hazard Estimation*. NISTIR 4380. National Institute of Standards and Technology, 1990.

[63] R. Portier, P.A. Reneke, W.W. Jones, and R.D. Peacock. *A User's Guide for CFAST Version 1.6*. Report NISTIR 4985. Gaithersburg, MD: National Institute of Standards and Technology, Dec. 1992.

[64] D. Satterfield and J.R. Barnett. *User's Guide for WPI/Fire Version 2 - Compartment Fire Model*. Report. Worcester, MA: Worcester Polytechnic Institute, 1990.

[65] E. Haynes. "Development of WPI/Fire 3.0 - A Multiroom Model." PhD thesis. Worcester, MA: Worcester Polytechnic Institute, Dec. 1994.

[66] G.P. Forney, L.Y. Cooper, and W.F. Moss. *The Consolidated Compartment Fire Model (CCFM) Computer Code Application CCFM.VENTS - Part IV: User Reference Guide*. NISTIR 4345. National Institute of Standards and Technology, 1990.

[67] C.A. Wade. "A Room Fire Model Incorporating Fire Growth on Combustible Lining Materials." Master of Science Thesis. Worcester, MA: Worcester Polytechnic Institute, Apr. 1996.

[68] C.A. Wade. *BRANZFIRE Technical Reference Guide*. BRANZ Study Report 92. Porirua, New Zealand: BRANZ, 2000.

[69] W.D. Davis. *Zone Fire Model Jet: A Model for the Prediction of Detector Activation and Gas Temperature in the Presence of a Smoke Layer*. NISTIR 6324. National Institute of Standards and Technology, May 1999.

[70] B. Gautier, O. Pages, and E. Thibert. "MAGIC: Global Modelling of Fire Into Compartments." In: *Proceedings of the 8th Interflam Conference*. Edinburgh, Scotland, 1999.

[71] T. Tanaka and S. Yamada. "BRI2002 : Two layer zone smoke transport model." In: *Fire Science & Technology* 23.1 2004, pp. 1–131. DOI: 10.3210/fst.23.IV.

[72] R.D. Peacock, G.P. Forney, and P.A. Reneke. *CFAST – Consolidated Fire And Smoke Transport (Version 7) Volume 3: Verification and Validation Guide*. NIST Technical Note 1889v3. Gaithersburg, MD: National Institute of Standards and Technology, 2017. URL: http://dx.doi.org/10.6028/NIST.TN.1889v3.

[73] R.D. Peacock. *CFAST – Consolidated Fire and Smoke Transport (Version 7) Volume 4: Configuration Management*. NIST Technical Note 1889v4. Gaithersburg, MD: National Institute of Standards and Technology, 2017. URL: http://dx.doi.org/10.6028/NIST.TN.1889v4.

[74] R.D. Peacock, K. McGrattan, G.P. Forney, and P.A. Reneke. *CFAST – Consolidated Fire And Smoke Transport (Version 7) Volume 1: Technical Reference Guide*. NIST Technical Note 1889v1. Gaithersburg, MD: National Institute of Standards and Technology, 2017. URL: http://dx.doi.org/10.6028/NIST.TN.1889v1.

[75] Electric Power Research Institute (EPRI), Palo Alto, CA, and U.S. Nuclear, Regulatory Commission, Office of Nuclear Regulatory Research (RES), and Electric Power Research Institute (EPRI), Palo Alto, CA. *EPRI/NRC-RES Fire PRA Methodology for Nuclear Power Facilities: Volume 1: Summary and Overview*. Tech. rep. EPRI - 1011989 and NUREG/CR-6850. Rockville, MD, 2005.

[76] S.E. Magnusson and S. Thelandersson. *Temperature-time curves for the complete process of fire development – a theoretical study of wood fuels in enclosed spaces*. Acta Polytechnica Scandinavica, Civil Engineering and Building Construction Series 65. Stockholm: The Royal Swedish Academy of Engineering Sciences, 1970.

[77] U. Wickström. "Application of the Standard Fire Curve for Expressing Natural Fires for Design." In: ASTM STP 882. Philadelphia: American Society for Testing and Materials, 1985.

[78] CEN. *EN 1991 Actions on structures – Part 1-2: General actions – Actions on structures exposed to fire, Annex A*. European Standard. Brussels: European Committee for Standardization, 2002.

[79] V. Babrauskas. *COMPF – A Program for Calculating Post-Flashover Fire Temperatures*. Report UCB FRG 75-2. Berkeley, CA: Fire Research Group, University of California, 1975.

[80] V. Babrauskas and R.B. Williamson. "Post-flashover Compartment Fires: Basis of a Theoretical Model." In: *Fire and Materials* 2.2 1978, pp. 39–53. DOI: 10.1002/fam.810020202.

[81] V. Babrauskas and R.B. Williamson. "Post-flashover Compartment Fires: Application of a theoretical model." In: *Fire and Materials* 3.1 1979, pp. 1–7. DOI: 10.1007/BF02380810.

[82] V. Babrauskas. *COMPF2 – A Program for Calculating Post- Flashover Fire Temperatures*. Technical Note 991. Gaithersburg, MD: National Bureau of Standards, 1979.

[83] J.M. Franssen. *The Design Fire Tool OZone V2.0 - Theoretical Description and Validation on Experimental Fire Tests*. Report. Belgium: Civil and Structural Engineering Department, University of Liege, 2000.

[84] J.F. Cadorin, D. Pintea, and J.M. Franssen. *The Design Fire Tool OZone V2.0 - Theoretical Description and Validation On Experimental Fire Tests*. Internal Report. Belgium: University of Leige, June 2001.

[85] J.F. Cadorin, D. Pintea, J-C Dotreppe, and J.M. Franssen. "A tool to design steel elements submitted to compartment fires - OZone V2. Part 2: Methodology and application." In: *Fire Safety Journal* 38.5 2003, pp. 429–451. DOI: 10.1016/S0379-7112(03)00015-8.

[86] K. McGrattan and S. Miles. "Chapter 32 Modeling Fires Using Computational Fluid Dynamics (CFD)." In: *SFPE Handbook of Fire Protection Engineering*. Ed. by M.J. Hurley. 5th Edition. New York, NY: Springer, 2016. ISBN: 978-1-4939-2565-0. URL: https://doi.org/10.1007/978-1-4939-2565-0.

[87] V. Novozhilov. "Computational fluid dynamics modeling of compartment fires." In: *Progress in Energy and Combustion Science* 27.6 Jan. 2001, pp. 611–666. ISSN: 0360-1285. DOI: 10.1016/S0360-1285(01)00005-3.

[88] S.M. Olenick and D.J. Carpenter. "An updated international survey of computer models for fire and smoke." In: *Journal of Fire Protection Engineering* 13.2 2003, pp. 87–110. DOI: 10.1177/1042391032033367.

[89] K. McGrattan, S. Hostikka, R. McDermott, J. Floyd, C. Weinschenk, and K. Overholt. *Fire Dynamics Simulator User's Guide*. NIST Special Publication 1019 Sixth Edition. FDS Version 6.3.2. Gaithersburg, MD: National Institute of Standards and Technology, 2015. URL: http://dx.doi.org/10.6028/NIST.SP.1019.

[90] J. Ewer, E.R. Galea, M.K. Patel, S. Taylor, B. Knight, and M. Pedritis. "Smartfire: an intelligent CFD based fire model." In: *Journal of Fire Protection Engineering* 10.1 1999, pp. 13–27. DOI: 10.1177/104239159901000102.

[91] FM Global. *FireFOAM*. 2017. URL: https://github.com/fireFoam-dev/fireFoam-dev.

[92] T.T. Lie. "Characteristic temperature curves for various fire severities." In: *Fire Technology* 10.4 Nov. 1974, pp. 315–326. ISSN: 1572-8099. DOI: 10.1007/BF02589990.

[93] K. Kawagoe and T. Sekine. *Estimation of fire temperature-time curve in rooms*. BRI Occasional Report 11. Tokyo, Japan: Building Research Institute, 1963.

[94] K. Kawagoe. *Estimation of fire temperature-time curve in rooms*. Research Paper 29. Tokyo, Japan: Building Research Institute, 1967.

[95] Z. Ma and P. Mäkeläinen. "Parametric temperature–time curves of medium compartment fires for structural design." In: *Fire Safety Journal* 34.4 2000, pp. 361–375. DOI: dx.doi.org/10.1016/S0379-7112(00)00008-4.

[96] C.R. Barnett. "BFD curve: a new empirical model for fire compartment temperatures." In: *Fire Safety Journal* 37.5 2002, pp. 437–463. DOI: 10.1016/S0379-7112(02)00006-1.

[97] C.R. Barnett. "Replacing international temperature–time curves with BFD curve." In: *Fire Safety Journal* 42.4 2007, pp. 321–327. DOI: 10.1016/j.firesaf.2006.11.001.

[98] N.D. Pope and C.G. Bailey. "Quantitative comparison of FDS and parametric fire curves with post-flashover compartment fire test data." In: *Fire Safety Journal* 41.2 Mar. 2006, pp. 99–110. ISSN: 0379-7112. DOI: 10.1016/j.firesaf.2005.11.002.

[99] A. Jowsey, S. Welch, and J.L. Torero. "Chapter 4 Heat and mass transfer effects to be considered when modelling the effect of fire on structures." In: *Transport Phenomena in Fires*. Ed. by B Sundén and M Faghri. Great Britain: WIT Press, 2008. ISBN: 978-1-84564-160-3.

[100] J.L. Torero, A.H. Majdalani, C Abecassis-Empis, and A Cowlard. "Revisiting the Compartment Fire." In: *Fire Safety Science - Proceedings of the Eleventh International Symposium*. Christchurch, New Zealand, 2014.

[101] D. Barber, L. Sieverts, R. Dixon, and J. Alston. "A methodology for quantifying fire resistance of exposed structural mass timber elements." In: *Proceedings of the 10th International Conference on Structures in Fire*. Belfast, UK, 2018, pp. 217–224.

[102] K.A Notarianni. "The Role of Uncertainty in Improving Fire Protection Regulation." PhD Thesis. Pittsburgh, PA, US: Carnegie Mellon University, 2000.

[103] T. Elicson, J. Bouchard, H. Lucek, and B. Harwood. "Calculation of fire severity factors and fire nonsuppression probabilities for a DOE facility fire PRA." In: Wilmington, NC.: American Nuclear Society, 2011.

[104] G.B. Baker, M.J. Spearpoint, C.M. Fleischmann, and C.A. Wade. "Development of a design fire generator for a risk-informed fire safety engineering tool." In: *Proceedings 9th International Conference on Performance-Based Codes and Fire Safety Design Methods*. Hong Kong, 2011.

[105] G.B. Baker, C.A. Wade, M.J. Spearpoint, and C.M. Fleischmann. "Developing Probabilistic Design Fires for Performance based Fire Safety Engineering." In: *Procedia Engineering* 62 (9th Asia-Oceania Symposium on Fire Science and Technology) Jan. 2013, pp. 639–647. ISSN: 1877-7058. DOI: 10.1016/j.proeng.2013.08.109. URL: http://www.sciencedirect.com/science/article/pii/S1877705813012915.

[106] G.B. Baker. "Quantification of the Variability in Heat Release Rate Curves Used to Model Fires in Residential-Scale Occupancies." PhD Thesis. Christchurch, New Zealand: University of Canterbury, Department of Civil and Natural Resources Engineering, 2016.

[107] R. Harrison, C.A. Wade, and M. Spearpoint. "Predicting Spill Plumes with the Fire Risk Zone Model B-RISK." In: *Fire Technology* 50 2014, pp. 205–231. DOI: 10.1007/s10694-013-0364-3.

[108] G.B. Baker, M.J. Spearpoint, C.M. Fleischmann, and C.A. Wade. "Selecting an Ignition Criterion Methodology for use in a Radiative Fire Spread Submodel." In: *Fire and Materials* 35.6 2011, pp. 367–381. DOI: 10.1002/fam.1059.

[109] G.B. Baker, M.J. Spearpoint, C.M. Fleischmann, and C.A. Wade. "Experimental Validation for an Item-to-Item Fire Spread Model." In: *Proceedings of the 12th Fire and Materials International Conference*. San Francisco, USA, 2011.

[110] G.B. Baker, P.C.R. Collier, C.A. Wade, M.J. Spearpoint, C.M. Fleischmann, K. Frank, and S. Sazegara. "A comparison of a priori modelling predictions with experimental results to validate a design fire generator submodel." In: *Proceedings of the 13th Fire and Materials Conference*. San Francisco, USA, 2013.

[111] K. Frank, M.J. Spearpoint, C.M. Fleischmann, and C.A. Wade. "Modelling the activation of multiple sprinklers with a risk-informed design tool." In: *Proceedings of the 9th International Conference on Performance-Based Codes and Fire Safety Design Methods*. Hong Kong: SFPE, 2012.

[112] C. Hopkin and M.J. Spearpoint. "Evaluation of sprinkler actuation times in FDS and B-RISK." In: *International Fire Professional* 28 May 2019, pp. 22–27. URL: www.ife.org.uk.

[113] C.A. Wade, D. LeBlanc, J. A. Ierardi, and J. R. Barnett. "A Room-Corner Fire Growth & Zone Model for Lining Materials." In: Gaithersburg, MD, 1997.

[114] C.A. Wade. *B-RISK 2013 Software Benchmarking Examples*. Study Report SR292. Porirua: BRANZ, 2013.

[115] R.D. Peacock, G.P. Forney, P.A. Reneke, R. Portier, and W.W. Jones. *CFAST, the Consolidated Model of Fire and Smoke Transport*. NIST Technical Note 1299. National Institute of Standards and Technology, Feb. 1993.

[116] G.P. Forney. "Computing radiative heat transfer occurring in a zone model." In: *Fire Science & Technology* 14.1/2 1994, pp. 31–47.

[117] CEN. *EN 1991 Actions on structures – Part 1-2: General actions – Actions on structures exposed to fire*. European Standard. Brussels: European Committee for Standardization, 2002.

[118] D.C. Jr Eagle. *BNALib A Basic Numerical Analysis Library for Personal Computers*. Report. 1997.

[119] C.A. Wade. "Fire hazard assesssment of wall and ceiling fire spread in rooms." In: *Flammability testing of materials used in construction, transport and mining*. Ed. by V. Apte. 1st Edition. Cambridge, England: Woodhead Publishing Limited, 2006, pp. 123–148. ISBN: 978-1-85573-935-2.

[120] ISO. *ISO 9705 Fire tests – full-scale room tests for surface products*. International Standard. Geneva, Switzerland: International Organization for Standardization, 1993.

[121] J.G. Quintiere. "A Simulation Model for Fire Growth on Materials Subject to a Room-Corner Test." In: *Fire Safety Journal* 20.4 1993, pp. 313–339. DOI: 10.1016/0379-7112(93)90053-S.

[122] ISO. *ISO 5660-1 Reaction-to-fire tests – Heat release, smoke production and mass loss rate – Part 1: Heat release rate (cone calorimeter method) and smoke production rate (dynamic measurement)*. International Standard. Geneva, Switzerland: International Organization for Standardization, 2015.

[123] American Society for Testing Materials. *ASTM E 1321-18 Standard Test Method for Determining Material Ignition and Flame Spread Properties*. Philadelphia, 2018.

[124] H. Peel. "Fire Development in Rooms Partially Lined with Timber." Master of Eng. Thesis. Christchurch, New Zealand: University of Canterbury, Department of Civil and Natural Resources Engineering, 2016.

[125] M. Gong. "Lumber-Based Mass Timber Products in Construction." In: *Timber Buildings and Constructions*. IntechOpen, Apr. 2019. DOI: 10.5772/intechopen.85808.

[126] J. Schmid, M. Klippel, A. Just, A. Frangi, and M. Tiso. "Simulation of the Fire Resistance of Cross-laminated Timber (CLT)." In: *Fire Technology* May 2018. ISSN: 1572-8099. DOI: 10.1007/s10694-018-0728-9.

[127] Think Wood. *Nail-Laminated Timber (NLT)*. 2019. URL: https://www.thinkwood.com/products-and-systems/nail-laminated-timber (visited on 03/12/2019).

[128] Think Wood. *Dowel-Laminated Timber (DLT)*. 2019. URL: https://www.thinkwood.com/products-and-systems/dowel-laminated-timber-dlt (visited on 03/12/2019).

[129] Structurecraft. *DowelLam™ – DLT*. URL: https://structurecraft.com/materials/mass-timber/dlt-dowel-laminated-timber#photos (visited on 03/16/2019).

[130] M. Abu Ghalia and Y. Dahman. "Synthesis and utilization of natural fiber-reinforced poly (lactic acid) bionanocomposites." In: *Lignocellulosic Fibre and Biomass-Based Composite Materials: Processing, Properties and Applications*. Woodhead Publishing, Dec. 2017, pp. 313–345. ISBN: 978-0-08-100959-8. URL: DOI:10.1016/B978-0-08-100959-8.00015-9.

[131] P.E.A. Debiagi, C. Pecchi, G. Gentile, A. Frassoldati, A. Cuoci, T. Faravelli, and E. Ranzi. "Extractives Extend the Applicability of Multistep Kinetic Scheme of Biomass Pyrolysis." In: *Energy & Fuels* 29.10 Oct. 2015, pp. 6544–6555. ISSN: 0887-0624. DOI: 10.1021/acs.energyfuels.5b01753.

[132] M.L. Janssens and B. Douglas. "Wood and wood products." In: *Handbook of building materials for fire protection*. Ed. by C.A. Harper. McGraw-Hill, 2004. ISBN: 978-0-07-138891-7.

[133] F.L. Browne. *Theories of the combustion of wood and its control. A survey of the literature.* Report 2136. Madison, Wisconsin: Forest Products Laboratory, US Department of Agriculture, 1958.

[134] V. Babrauskas. *Ignition handbook*. Fire Science Publishers, 2003. ISBN: 0-9728111-3-3.

[135] A. Bartlett, R. Hadden, and L. Bisby. "A Review of Factors Affecting the Burning Behaviour of Wood for Application to Tall Timber Construction." In: *Fire Technology* Nov. 2018. DOI: 10.1007/s10694-018-0787-y.

[136] C. Di Blasi. "Modeling and simulation of combustion processes of charring and non-charring solid fuels." In: *Progress in Energy and Combustion Science* 19.1 Jan. 1993, pp. 71–104. ISSN: 0360-1285. DOI: 10.1016/0360-1285(93)90022-7.

[137] R. White. "Analytical methods for determining fire resistance of timber members." In: *SFPE Handbook of Fire Protection Engineering*. Ed. by M.J. Hurley. 5th Edition. New York, NY, USA: Springer, 2016. ISBN: 978-1-4939-2565-0. URL: https://doi.org/10.1007/978-1-4939-2565-0_55.

[138] M.L. Janssens. "Modeling of the thermal degradation of structural wood members exposed to fire." In: *Proceedings of the 2nd International Conference on Structures in Fire*. Christchurch, New Zealand, 2002.

[139] K.W. Ragland, D.J. Aerts, and A.J. Baker. "Properties of wood for combustion analysis." In: *Bioresource Technology* 37.2 Jan. 1991, pp. 161–168. ISSN: 0960-8524. DOI: 10.1016/0960-8524(91)90205-X.

[140] J. König. "Effective thermal actions and thermal properties of timber members in natural fires." In: *Fire and Materials* 30.1 Jan. 2006, pp. 51–63. ISSN: 0308-0501. DOI: 10.1002/fam.898.

[141] Standards Australia. *AS 1530 Part 4 Fire-resistance Tests of Elements of Building Construction*. Standard. Sydney, Australia, 2005.

[142] ISO. *ISO 834-1: Fire-resistance tests – Elements of building construction, Part 1: General Requirements*. Standard. Geneva, Switzerland: International Organization for Standardization, 1999.

[143] V. Babrauskas. "Charring rate of wood as a tool for fire investigations." In: *Fire Safety Journal* 40.6 Sept. 2005, pp. 528–554. ISSN: 0379-7112. DOI: 10.1016/j.firesaf.2005.05.006.

[144] P.C.R. Collier. *Charring Rates of Timber*. Study Report 42. Porirua, New Zealand: BRANZ, 1992.

[145] Standards New Zealand. *NZS 3603 Timber Structures Standard (Amendment 4)*. Standard. Wellington, New Zealand, 1993.

[146] CEN. *EN 1995 Eurocode 5 Design of timber structures Part 1-1: General - Common rules and rules for buildings*. European Standard. Brussels: European Committee for Standardization, 2004.

[147] F. Richter, P. Kotsovinos, and G. Rein. "The role of chemistry and physics in the charring of timber in realistic fires." In: *SFPE FPE Extra Issue* 28 Apr. 2018. URL: https://sfpe.site-ym.com/default.asp?page=FPEExtraIssue28&_zs=HCo1d1&_zl=rMOm4.

[148] B. Fredlund. "Modelling of heat and mass transfer in wood structures during fire." In: *Fire Safety Journal* 20.1 Jan. 1993, pp. 39–69. ISSN: 0379-7112. DOI: 10.1016/0379-7112(93)90011-E.

[149] ASTM. *ASTM E 119 - oo Standard Test Methods for Fire Tests of Buildings Construction and Materials*. 2000.

[150] C. Lautenberger. "A Generalized Pyrolysis Model for Combustible Solids." PhD Thesis. University of California, Berkeley, 2007.

[151] J. Torero. "Chapter 21 Flaming Ignition of Solid Fuels." In: *SFPE Handbook of Fire Protection Engineering*. 5th. Gaithersburg MD: Society of Fire Protection Engineers, 2016.

[152] D. Brandon and B. Östman. *Fire safety challenges of tall wood buildings – Phase 2: Task 1 – Literature review*. Report FRPF-2016-22. Quincy, MA: Fire Protection Research Foundation, 2016.

[153] T. Hakkarainen. "Post-flashover fires in light and heavy timber construction compartments." In: *Journal of Fire Sciences* 20.2 2002, pp. 133–175. DOI: 10.1177/0734904102020002074.

[154] A. Frangi and M. Fontana. "Fire performance of timber structures under natural fire conditions." In: *Fire Safety Science – Proceedings of the Eighth International Symposium*. Beijing, China, 2005, pp. 279–290. DOI: 10.3801/IAFSS.FSS.8-279.

[155] A. Frangi, G. Bochicchio, A. Ceccotti, and M.P. Lauriola. "Natural Full-Scale Fire Test on a 3 storey XLam Timber Building." In: *Proceeding of the 10th World Conference on Timber Engineering (WCTE 2008)*. Vol. 1. Miyazaki, Japan: Curran Associates, Inc, 2008, pp. 528–535. ISBN: 978-1-61567-088-8.

[156] C.J. McGregor. "Contribution of cross laminated timber panels to room fires." Master of Applied Science Thesis. Ottawa, Canada: Carleton University, 2013.

[157] A.R. Medina Hevia. "Fire resistance of partially protected cross-laminated timber rooms." Master of Engineering Thesis. Ottawa, Canada: Carleton University, 2014.

[158] X. Li, X. Zhang, G. Hadjisophocleous, and C. McGregor. "Experimental study of combustible and non-combustible construction in a natural fire." In: *Fire Technology* 51 2015, pp. 1447–1474. DOI: 10.1007/s10694-014-0407-4.

[159] X. Li, C. McGregor, A.R. Medina, X. Sun, D. Barber, and G. Hadjisophocleous. "Real-scale fire tests on timber constructions." In: *Proceedings of WCTE 2016 World Conference on Timber Engineering*. Vienna, Austria: Vienna University of Technology, 2016. ISBN: 978-3-903024-35-9.

[160] J. Su and G.D. Lougheed. *Fire safety summary: Fire research conducted for the project on midrise wood construction (Report to research consortium for wood and wood-hybrid mid-rise buildings)*. Client Report A1-004377.1. Ottawa, Canada: National Research Council of Canada, 2014.

[161] B.C. Taber, G. D. Lougheed, J. Su, and N. Benichou. *Solutions for mid-rise wood construction: apartment fire test with encapsulated cross laminated timber construction (Test APT-CLT) (Report to research consortium for wood and wood-hybrid mid-rise buildings)*. Client Report A1-100035-01.10. Ottawa, Canada: National Research Council of Canada, 2014.

[162] K. Hox and G.B. Baker. "Full-scale fire test of CLT structure used for student housing." In: *Proceedings of the 14th International Conference on Fire Science and Engineering*. Royal Holloway College, Nr Windsor, UK: InterScience Communications Limited, 2016.

[163] K. Hox. *Branntest av massivtre*. Norwegian. SPFR Report 15101. Norway: SP Fire Research AS, 2015.

[164] M.L. Janssens. *Full-scale tests in a furnished living room to evaluate the fire performance of protected cross-laminated and nail laminated timber construction*. Report SwRI Project No. 01.21428.01.001. San Antonio, Texas: Southwest Research Institute, Sept. 2015.

[165] R.M. Hadden, A.I. Bartlett, J.P. Hidalgo, S. Santamaria, F. Wiesner, L.A. Bisby, S. Deeny, and B. Lane. "Effects of exposed cross laminated timber on compartment fire dynamics." In: *Fire Safety Journal* 91 2017, pp. 480–489. ISSN: 0379-7112. DOI: 10.1016/j.firesaf.2017.03.074.

[166] E.G. Butcher, G.K. Bedford, and P.J. Fardell. "Further experiments on temperatures reached by steel in building fires." In: *Joint Fire Research Organisation Symposium*. United Kingdom: HMSO, 1967.

[167] R. Emberley et al. "Description of small and large-scale cross laminated timber fire tests." In: *Fire Safety Journal* 91 2017, pp. 327–335. ISSN: 0379-7112. DOI: 10.1016/j.firesaf.2017.03.024. URL: http://www.sciencedirect.com/science/article/pii/S0379711217300954.

[168] J. Su, P. Lafrance, M. Hoehler, and M. Bundy. *Fire safety challenges of tall wood buildings – Phase 2: Task 2 & 3 – Cross Laminated Timber Compartment Fire Tests*. Report FPRF-2018-01. Quincy, MA: Fire Protection Research Foundation, 2018.

[169] M.L. Janssens. *Development of a fire performance assessment methodology for qualifying cross-laminated timber adhesives*. Client Report SwRI Project No 01.23086.01.001a. San Antonio, Texas: Southwest Research Institute, 2017.

[170] APA - The Engineered Wood Association. *ANSI/APA PRG 320-2018 Standard for performance-rated cross-laminated timber*. American National Standard. Tacoma, WA: APA - The Engineered Wood Association, 2018.

[171] J. Su. "Fire safety of CLT building in Canada." In: *Wood and fiber science* 50 (Special issue) 2018, pp. 102–109.

[172] S. Zelinka, L. Hasburgh, K. Bourne, D. Tucholski, and J. Ouellette. *Compartment fire testing of a two-story cross laminated timber (CLT) building*. General Technical Report FPL-GTR-247. Madison, Wisconsin: U.S. Department of Agriculture, Forest Service, Forest Products Laboratory, 2018.

[173] L. Hasburgh, S. Zelinka, K. Bourne, D. Tucholski, and J. Ouellette. "Full-scale fire tests of a two-story cross-laminated structure." In: *Proceedings of WCTE 2018 World Conference on Timber Engineering*. Seoul, Republic of Korea, 2018.

[174] A.L. Bartlett, R.M. Hadden, L.A. Bisby, and A. Law. "Analysis of cross-laminated timber charring rates upon exposure to non-standard heating conditions." In: *Proceedings Fire and Materials 2015*. San Francisco, USA: InterScience Communications Limited, 2015.

[175] A. Bartlett, K. Gajewski, S. Lineham, R. Hadden, L. Bisby, and N. Butterworth. "Overcoming the Fire Barrier to Tall Timber Construction." In: *Proceedings of the Infrastructure and Environment Scotland 3rd Postgraduate Conference*. Heriot-Watt University, Edinburgh, Scotland, 2015.

[176] M. Aguanno. "Fire resistance tests on cross-laminated timber floor panels: an experimental and numerical analysis." Master of Applied Science Thesis. Ottawa, Canada: Carleton University, 2013.

[177] A. Frangi, M. Fontana, E. Hugi, and R. Jübstl. "Experimental analysis of cross-laminated timber panels in fire." In: *Fire Safety Journal* 44.8 2009, pp. 1078–1087. ISSN: 0379-7112. DOI: 10.1016/j.firesaf.2009.07.007.

[178] M. Klippel, C. Leyder, A. Frangi, and M. Fontana. "Fire tests on loaded cross-laminated timber wall and floor elements," in: *Proceedings of the Eleventh International Fire Safety Symposium*. Christchurch, New Zealand: International Association for Fire Safety Science, 2014, pp. 626–639. DOI: 10.3801/IAFSS.FSS.11-626.

[179] M. Klippel, J. Schmid, and A. Frangi. "Fire Design of CLT – comparison of design concepts." In: *Proceedings of the Joint Conference of COST Actions FP1402 & FP1404 KTH Building Materials, 10.3.2016*. Stockholm, Sweden: KTH Royal Institute of Technology, Division of Building Materials, 2016, pp. 101–122.

[180] R. Emberley, A. Inghelbrecht, N. Doyle, and J.L. Torero. "Components and Consequences of Cross-Laminated Timber Delamination," in: *Proceedings of the 10th Asia-Oceania Symposium on Fire Science and Technology.* Tsukuba, Japan, 2015.

[181] A.I. Bartlett, K. Gajewski, R.M. Hadden, N. Butterworth, and L. Bisby. "Fire-Induced Delamination of Cross-Laminated Timber." In: *Proceedings of the 1st European Workshop Fire Safety of Green Buildings*. 2015.

[182] M. Hoehler, J. Su, P. Lafrance, M. Bundy, A. Kimball, D. Brandon, and B. Östman. "Fire safety challenges of tall wood buildings: Large-scale cross laminated timber compartment fire tests." In: *Proceedings of the 10th International Conference on Structures in Fire*. Belfast, UK, 2018.

[183] M. Klippel. "Fire safety of bonded structural timber elements." PhD Thesis. Zurich, Switzerland: Aachen University, 2014.

[184] C. Lehringer and J. Gabriel. "Review of Recent Research Activities on One-Component PUR-Adhesives for Engineered Wood Products." In: *Materials and Joints in Timber Structures*. Ed. by S Aicher, H.W. Reinhardt, and H. Garrecht. Vol. 9. RILEM Bookseries. Springer, Dordrecht, 2014.

[185] S. Clauß, M. Joscak, and P. Niemz. "Thermal stability of glued wood joints measured by shear tests." In: *European Journal of Wood and Wood Products* 69.1 Feb. 2011, pp. 101–111. ISSN: 1436-736X. DOI: 10.1007/s00107-010-0411-4.

[186] S. Clauß, J. Gabriel, A. Karbach, M. Matner, and P. Niemz. "Influence of the adhesive formulation on the mechanical properties and bonding performance of polyurethane prepolymers." In: *Holzforschung* 65 2011, pp. 835–844. DOI: 10.1515/HF.2011.095.

[187] A. Frangi, M. Fontana, M. Knobloch, and G. Bochicchio. "Fire behaviour of cross-laminated solid timber panels." In: *Fire Safety Science – Proceedings of the Ninth International Symposium*. 2008, pp. 1279–1290. DOI: 10.3801/IAFSS.FSS.9-1279.

[188] S. Craft. *Development of small-scale evaluation methods for wood adhesives at elevated temperature*. Report. Ottawa, Canada: FP Innovations - Forintek Division, 2008.

[189] S. Craft, R. Desjardins, and L. Richardson. "Development of Small-scale Evaluation Methods for Wood Adhesives at Elevated Temperatures." In: *Proceedings of WCTE 2008 World Conference on Timber Engineering*. Miyazaki, Japan, 2008. ISBN: 978-1-61567-088-8.

[190] European Committee for Standardization (CEN). *EN 301 Adhesives, phenolic and aminoplastic, for load-bearing timber structures. Classification and performance requirements*. Tech. rep. Brussels, 2017.

[191] Glue Laminated Timber Association. *Principal choices - adhesives*. URL: http://www.glulam.co.uk/principalChoices_adhesives.htm (visited on 03/17/2019).

[192] CEN. *EN 15425 Adhesives. One component polyurethane (PUR) for load-bearing timber structures. Classification and performance requirements*. European Standard. Brussels: European Committee for Standardization (CEN), 2017.

[193] European Committee for Standardization (CEN). *EN 15416 Adhesives for load bearing timber structures other than phenolic and aminoplastic.* European Standard. Brussels: European Committee for Standardization (CEN), 2017.

[194] S. Pei, D. Rammer, M. Popovski, T. Williamson, P. Line, and J.W. van de Lindt. "An Overview of CLT Research and Implementation in North America." In: *Proceedings of WCTE 2016 World Conference on Timber Engineering*. Vienna, Austria, 2016.

[195] D. Brandon and C. Dagenais. *Fire safety challenges of tall wood buildings – Phase 2: Task 5 - Experimental study of delamination of cross laminated timber (CLT) in fire*. Report FRPF-2018-05. Quincy, MA: Fire Protection Research Foundation, 2018.

[196] S. Earnshaw, M. Nowicki, and C. Campbell. "Adhesives for load-bearing timber structures - classification and performance." In: *New Zealand Timber Design Journal* 17.3 2009, pp. 12–17.

[197] Standards Australia. *AS/NZS 4364:2010 Timber-bond performance of structural adhesives*. Standard AS/NZS 4364. 2010.

[198] R. Emberley, A. Inghelbrecht, Z. Yu, and J.L. Torero. "Self-extinction of timber." In: *Proceedings of the Combustion Institute* 36.2 Jan. 2017, pp. 3055–3062. ISSN: 1540-7489. DOI: 10.1016/j.proci.2016.07.077. URL: http://www.sciencedirect.com/science/article/pii/S1540748916303352.

[199] R. Crielaard. "Self-extinguishment of cross-laminated timber." Master of Science in Civil Engineering. Netherlands: Delft University of Technology, 2015.

[200] R. Crielaard, J-W. van de Kuilen, K. Terwel, G. Ravenshorst, and P. Steenbakkers. "Self-extinguishment of cross-laminated timber." In: *Fire Safety Journal* Feb. 2019. ISSN: 0379-7112. DOI: 10.1016/j.firesaf.2019.01.008. URL: http://www.sciencedirect.com/science/article/pii/S0379711219300189.

[201] Alastair L Bartlett, Rory M. Hadden, Luke A. Bisby, and Barbara Lane. "Auto-extinction of engineered timber: the application of firepoint theory." In: Royal Holloway College, Nr Windsor, UK, 2016.

[202] R. Emberley, T. Do, J. Yim, and J.L. Torero. "Critical heat flux and mass loss rate for extinction of flaming combustion of timber." In: *Fire Safety Science: Proceedings of the 12th International Symposium* 91 July 2017, pp. 252–258. ISSN: 0379-7112. DOI: 10.1016/j.firesaf.2017.03.008. URL: http://www.sciencedirect.com/science/article/pii/S037971121730187X.

[203] C. Bateman, A.I. Bartlett, L. Rutkauskas, and Rory M. Hadden. "Effects of Fuel Load and Exposed CLT Surface Configuration in Reduced- Scale Compartments." In: *Proceedings of WCTE 2018 World Conference on Timber Engineering*. Seoul, Republic of Korea, 2018.

[204] S. Craft, R. Desjardins, and J.R. Mehaffey. "Investigation of the behaviour of CLT panels exposed to fire." In: *Proceedings of the 12th International Fire and Materials Conference*. San Francisco, USA: InterScience Communications Limited, 2011.

[205] J. Schmid, A. Santomaso, D. Brandon, U. Wickström, and A. Frangi. "Timber under real fire conditions – the influence of oxygen content and gas velocity on the charring behavior." In: *Journal of Structural Fire Engineering* Sept. 2017. ISSN: 2040-2317. DOI: 10.1108/JSFE-01-2017-0013.

[206] F.X. Jervis. "Application of fire calorimetry to understand factors affecting flammability of cellulosic material: Pine needles, tree leaves and chipboard." PhD Thesis. The University of Edinburgh, 2012.

[207] D. Brandon, J. Schmid, J. Su, M. Hoehler, B. Östman, and A. Kimball. "Experimental fire simulator for post-flashover compartment fires." In: *Proceedings of the 10th International Conference on Structures in Fire*. Belfast, UK, 2018.

[208] P.C.R. Collier. *Post-earthquake performance of passive fire protection systems*. BRANZ Study Report 304. Porirua, New Zealand: BRANZ, 2013.

[209] C. Maluk, L. Bisby, M. Krajcovic, and J.L. Torero. "A Heat-Transfer Rate Inducing System (H-TRIS) Test Method." In: *Fire Safety Journal* June 2016. ISSN: 0379-7112. DOI: 10.1016/j.firesaf.2016.05.001. URL: http://www.sciencedirect.com/science/article/pii/S0379711216300650.

[210] T. Moser and M. Spearpoint. "Delay of onset of charring to CLT using different encapsulation board materials." In: *SESOC Journal* 29.1 Jan. 2016, pp. 104–111.

[211] D. Brandon. *Fire safety challenges of tall wood buildings – Phase 2: Task 4 Engineering methods*. Report FRPF-2018-04. Quincy, MA: Fire Protection Research Foundation, 2018.

[212] A. Just. "Structural fire design of timber frame assemblies Insulated by glass wool and covered by gypsum plasterboards." PhD Thesis. Estonia: Tallinn University of Technology, 2010.

[213] G.V. Hadjisophocleous and Z. Fu. "Development and Case Study of a Risk Assessment Model CUrisk for Building Fires." In: *Fire Safety Science - Proceedings of the Eighth International Symposium*. 2005. DOI: 10.10.3801/IAFSS.FSS.8-8773801/IAFSS.FSS.8-877.

[214] X. Zhang, X. Li, and G. Hadjisophocleous. "A design fire model for the full process of fire." In: *Proceedings of the International Fire Safety Symposium 2015*. Coimbra, Portugal, 2015, pp. 381–390.

[215] M. Salminen and J. Hietaniemi. "Performance-based fire design of a 14-storey residential mass timber building." In: *Applications of Fire Engineering: Proceedings of the International Conference of Applications of Structural Fire Engineering (ASFE 2017)*. Manchester, UK: CRC Press, 2018. ISBN: 978-1-138-09291-4.

[216] D. Brandon. *Practical method to determine the contribution of structural timber to the rate of heat release and fire temperature of post-flashover compartment fires*. Report 2016:68. Borås, Sweden: SP Technical Research Institute of Sweden, 2016.

[217] J. Schmid, D. Brandon, A. Santomaso, U. Wickström, and A. Frangi. "Timber under Real Fire Conditions – the Influence of Oxygen Content and Gas Velocity on the Charring Behavior." In: *Proceedings of the 9th International Conference on Structures in Fire*. Princeton University, USA: DesTech Publications Inc, 2016.

[218] J-M. Franssen. "SAFIR: A thermal/structural program for modeling structures under fire." In: *Engineering Journal* 42 Sept. 2005, pp. 143–150.

[219] J. König and L. Walleij. *Timber frame assemblies exposed to standard and parametric fires Part 2: A design model for standard fire exposure*. Report 0001001. Stockholm, Sweden: Trätek - Swedish Institute of Wood Technology Research, 2000.

[220] D.J. Hopkin, S. Anastasov, and D. Brandon. "Reviewing the veracity of a zone-model-based-approach for the assessment of enclosures formed of exposed CLT." In: *Applications of Fire Engineering: Proceedings of the International Conference of Applications of Structural Fire Engineering (ASFE 2017)*. Ed. by M. Gillie and Y. Wang. First edition. Manchester, UK, 2017. ISBN: 978-1-138-09291-4.

[221] X. Wang, C.M. Fleischmann, M.J. Spearpoint, and X. Huang. "The application of different component schemes to predict wood pyrolysis and fire behaviour." In: *Proceedings of IFireSS – International Fire Safety Symposium*. Coimbra, Portugal, 2015.

[222] R.D. Peacock, W.W. Jones, P.A. Reneke, and G.P. Forney. *CFAST – Consolidated Model of Fire Growth and Smoke Transport (Version 6) User's Guide*. NIST Special Publication 1019 Sixth Edition 1041. Washington, DC: National Institute of Standards and Technology, 2005.

[223] L.Y. Cooper and G.P. Forney. *The Consolidated Compartment Fire Model (CCFM) Computer Code Application CCFM.VENTS – Part III: Catalog of Algorithms and Subroutines*. NISTIR 4344. Gaithersburg, MD: National Institute of Standards and Technology, 1990.

[224] L.Y. Cooper and G.P. Forney. *The Consolidated Compartment Fire Model (CCFM) Computer Code Application CCFM.VENTS – Part I: Physical Basis*. NISTIR 4342. Gaithersburg, MD: National Institute of Standards and Technology, 1990.

[225] Y. Utiskul. "Theoretical and experimental study on fully developed compartment fires." NIST GCR 07-907. PhD. College Park, MD: University of Maryland, 2007.

[226] ISO. *ISO 16734 Fire safety engineering – Requirements governing algebraic equations – Fire plumes*. International Standard. Geneva, Switzerland: International Organization for Standardization, 2006.

[227] B.J. McCaffrey. "Momentum implications for buoyant diffusion flames." In: *Combustion and Flame* 52 1983, pp. 149–167. DOI: 10.1016/0010-2180(83)90129-3.

[228] G.P. Forney. *Computing radiative heat transfer occurring in a zone fire model*. NISTIR 4709. Gaithersburg, MD: National Institute of Standards and Technology, 1991.

[229] "Appendix 3: Fuel properties and combustion data. Table A39." In: *SFPE Handbook of Fire Protection Engineering*. Ed. by M.J. Hurley. Fifth edition. DOI 10.1007/978-1-4939-2565-0_36. New York, NY: Springer, 2016, p. 3468. ISBN: 978-1-4939-2564-3.

[230] A. Tewarson, F.H. Jiang, and T. Morikawa. "Ventilation Controlled Combustion of Polymers." In: *Combustion and Flame* 95.1-2 1993, pp. 151–169. DOI: 10.1016/0010-2180(93)90058-B.

[231] F.P. Incropera and D.P. DeWitt. *Fundamentals of heat and mass transfer*. NJ, USA: John Wiley and Sons, 1990. ISBN: 978-0-471-30460-9.

[232] H.C. Tran and R.H. White. "Burning rate of solid wood measured in a heat release rate calorimeter." In: *Fire and Materials* 16.4 Oct. 1992, pp. 197–206. ISSN: 1099-1018. DOI: 10.1002/fam.810160406. URL: http://dx.doi.org/10.1002/fam.810160406.

[233] H.C. Tran. "Experimental data on wood materials." In: *Heat Release in Fires*. Ed. by V. Babrauskas and S.J. Grayson. Essex, England: Elsevier Applied Science, 1992, pp. 357–372. ISBN: 978-0-419-16100-4.

[234] M. Janssens. "Rate of heat release of wood products." In: *Fire Safety Journal* 17.3 Jan. 1991, pp. 217–238. ISSN: 0379-7112. DOI: 10.1016/0379-7112(91)90003-H. URL: http://www.sciencedirect.com/science/article/pii/037971129190003H.

[235] M.J. Spearpoint and J.G. Quintiere. "Predicting the burning of wood using an integral model." In: *Combustion and Flame* 123.3 Nov. 2000, pp. 308–325. ISSN: 0010-2180. DOI: 10.1016/S0010-2180(00)00162-0. URL: http://www.sciencedirect.com/science/article/pii/S0010218000001620.

[236] M.J. Spearpoint. *Predicting the ignition and burning rate of wood in the cone calorimeter using an integral model*. NIST GCR 99-775. (Master of Science in Fire Protection Engineering Thesis, University of Maryland). Gaithersburg, MD: National Institute of Standards and Technology, 1999.

[237] Forest Products Laboratory. *Wood Handbook - Wood as an Engineering Material*. General Technical Report FPL-GTR-190. Madison, Wisconsin: Department of Agriculture, Forest Service, Forest Products Laboratory, 2010, 508p.

[238] Nordic Wood Structures. *Technical Data - Nordic X-Lam*. 2013. URL: http://nordic.ca/data/files/datasheet/file/T-S22_eTechnicalData.pdf (visited on 07/04/2017).

[239] Y. Shi, L. Chrusciel, and A. Zoulalian. "Production of charcoal from different wood species." In: *Récents Progrès en Génie des Procédés*. Vol. 96. Paris, France, 2007. ISBN: 2-910239-70-5. URL: https://hal.archives-ouvertes.fr/hal-00265340.

[240] F. Beall. "Properties of Wood during Carbonization under Fire Conditions." In: *Wood Technology: Chemical Aspects (Symposium Series 43)*. Ed. by Irving S. Goldstein. Vol. 43. 1977. ISBN: 978-0-8412-0373-0. DOI: 10.1021/bk-1977-0043.

[241] X. Wang, C.M. Fleischmann, and M.J. Spearpoint. "Parameterising study of tunnel experiment materials for application to the Fire Dynamics Simulator pyrolysis model." In: *Journal of Fire Sciences* 2016, pp. 1–25. DOI: 10.1177/0734904116667738.

[242] A. TenWolde, J.D. McNatt, and L. Krahn. *Thermal Properties of Wood Panel Products Buildings*. Report DOE / USDA-21697/ 1. Madison, Wisconsin: USDA, Forest Products Laboratory, 1988.

[243] V. Hankalin, T. Ahonen, and R. Raiko. "On Thermal Properties of a Pyrolysing Wood Particle." In: *Proceedings of Finnish-Swedish Flame Days 2009*. Tampere University of Technology: IFRF National Committees of Finland and Sweden, 2009.

[244] D. Hopkin. "The Fire Performance of Engineered Timber Products and Systems." PhD Thesis. Loughborough University, Sept. 2011.

[245] D. Hopkin, J. El-Rimawi, V. Silberschmidt, and T. Lennon. "An effective thermal property framework for softwood in parametric design fires: Comparison of the Eurocode 5 parametric charring approach and advanced calculation models." In:

Construction & Building Materials 25.5 2011, pp. 2584–2595. DOI: 10.1016/j.conbuildmat.2010.12.002.

[246] V. Babrauskas. "Heat release rates." In: *SFPE Handbook of Fire Protection Engineering*. Ed. by M.J. Hurley. 5th Edition. New York, NY: Springer, 2016. ISBN: 978-1-4939-2565-0. URL: https://doi.org/10.1007/978-1-4939-2565-0_26.

[247] C. Huggett. "Estimation of rate of heat release by means of oxygen consumption measurements." In: *Fire and Materials* 4 1980, pp. 61–65. DOI: 10.1002/fam.810040202.

[248] W.M. Pitts. *The Global Equivalence Ratio Concept and the Prediction of Carbon Monoxide Formation in Enclosure Fires*. NIST Monograph 179. National Institute of Standards and Technology, June 1994.

[249] X. Wang, C.M. Fleischmann, M.J. Spearpoint, and K. Li. "A simple hand calculation method to estimate the pyrolysis kinetics of plastic and wood materials." In: *Fire Science and Technology 2015*. Ed. by K. Harada, K. Matsuyama, K. Himoto, Y. Nakamura, and K. Wakatsuki. Springer, Singapore, 2017. ISBN: 978-981-10-0376-9.

[250] K. McGrattan, S. Hostikka, R. McDermott, J. Floyd, and M. Vanella. *Fire Dynamics Simulator User's Guide*. NIST Special Publication 1019 Sixth Edition Revision: FDS6.7.1. Gaithersburg, MD: National Institute of Standards and Technology, Feb. 2019. URL: dx.doi.org/10.6028/NIST.SP.1019.

[251] Transmetra. *Table of emissivity of various surfaces for infrared thermometry*. http://www.transmetra.ch. 1999. URL: http://www.transmetra.ch (visited on 07/25/2017).

[252] U.S. Nuclear Regulatory Commission. *Verification and Validation of Selected Fire Models for Nuclear Power Plant Applications: Volume 2 Experimental Uncertainty*. Report NUREG-1824. Washington, DC: United States Nuclear Regulatory Commission, 2007.

[253] APA - The Engineered Wood Association. *ANSI/APA PRG 320-2012 Standard for performance-rated cross-laminated timber*. American National Standard. Tacoma, WA: APA - The Engineered Wood Association, 2012.

[254] K. McGrattan, R.D. Peacock, and K. Overholt. "Fire model validation – eight lessons learned." In: *Fire Safety Science – Proceedings of the Eleventh International Symposium*. Christchurch, New Zealand: International Association for Fire Safety Science, 2014.

[255] K. Hill, J. Dreisbach, F. Joglar, B. Najafi, K. McGrattan, R.D. Peacock, and A. Hamins. *Verification and Validation of Selected Fire Models for Nuclear Power Plant Applications*. Report NUREG 1824. Washington, DC: United States Nuclear Regulatory Commission, 2007.

[256] J.G. Quintiere. "Fire behavior in building compartments." In: *Proceedings of the Combustion Institute* 29.1 2002, pp. 181–193. DOI: 10.1016/S1540-7489(02)80027-X.

[257] M.J. Peatross and C.L. Beyler. "Ventilation Effects on Compartment Fire Characterization." In: *Proceedings of the Fifth International Symposium Fire Safety Science*. Vol. 5. Melbourne, Australia: IAFSS, 1997, pp. 403–414.

[258] A. Tewarson, J.L. Lee, and R.F. Pion. "The Influence of Oxygen Concentration on Fuel Parameters for Fire Modeling." In: *Symposium (International) on Combustion* 18.1 1981. DOI: 10.1016/S0082-0784(81)80061-6.

[259] G. Santo and M.A. Delichatsios. *Effects of Vitiated Air on Radiation and Completeness of Combustion in Propane Pool Fires*. Report FMRC J.I. oFoN4.BU. Norwood, Massachusetts: Factory Mutual Research, 1982.

[260] R. Friedman. "Behavior of Fires in Compartments." In: *International Symposium on Fire Safety of Combustible Materials*. Edinburgh, Scotland: University of Edinburgh, Centre for Industrial Consultancy and Liaison, 1975, pp. 100–113. ISBN: 0-903042-03-7.

[261] M.L. Bullen and P.H. Thomas. "Compartment fires with non-cellulosic fuels." In: *Seventeenth Symposium (International) on Combustion* 17.1 Jan. 1979, pp. 1139–1148. ISSN: 0082-0784. DOI: 10.1016/S0082-0784(79)80108-3.

[262] H. Takeda and K. Akita. "Critical phenomenon in compartment fires with liquid fuels." In: *Eighteenth Symposium (International) on Combustion* 18.1 Jan. 1981, pp. 519–527. ISSN: 0082-0784. DOI: 10.1016/S0082-0784(81)80057-4.

[263] C.M. Fleischmann and A.R. Parkes. "Effects of ventilation on the compartment enhanced mass loss rate." In: *Fire Safety Science - Proceedings of the Fifth International Symposium*. Melbourne, Australia: International Association for Fire Safety Science, 1997, pp. 415–426. DOI: 10.3801/IAFSS.FSS.5-415.

[264] T. Mizukami, Y. Utiskul, and J.G. Quintiere. "A compartment burning rate algorithm for a zone model." In: *Fire Safety Journal* 79 2015, pp. 57–68. DOI: 10.1016/j.firesaf.2015.11.005.

[265] J. Wahlqvist and P. van Hees. "Implementation and validation of an environmental feedback pool fire model based on oxygen depletion and radiative feedback in FDS." In: *Fire Safety Journal* 85 2016, pp. 35–49. DOI: 10.1016/j.firesaf.2016.08.003.

[266] Y. Utiskul, J.G. Quintiere, A.S. Rangwala, B.A. Ringwelski, K. Wakatsuki, and T. Naruse. "Compartment fire phenomena under limited ventilation." In: *Fire Safety Journal* 40.4 2005, pp. 367–390. DOI: 10.1016/j.firesaf.2005.02.002.

[267] T. Mizukami, Y. Utiskul, and J.G. Quintiere. "Application of zone models for under-ventilated compartment fires." In: *ASME 2006 International Mechanical Engineering Congress and Exposition Heat Transfer, Volume 2*. Chicago, Illinois, USA: ASME, 2006, pp. 69–77. DOI: 10.1115/IMECE2006-15135.

[268] Y. Utiskul and J.G. Quintiere. "Theoretical And experimental study on fully-developed compartment fires." In: *Proceedings of the 7th Asia-Oceania Symposium on Fire Science & Technology*. 2007.

[269] T. Mizukami, Y. Utiskul, T. Naruse, and J.G. Quintiere. "A compartment burning rate model for various scales." In: *Fire Safety Science – Proceedings of the Ninth International Symposium*. University of Karlsruhe, Germany, 2008, pp. 839–848. DOI: 10.3801/IAFSS.FSS.9-839.

[270] Y. Utiskul and J.G. Quintiere. "An application of mass loss rate model with fuel response effects in fully-developed compartment fires." In: *Fire Safety Science - Proceedings of the Ninth International Symposium*. 2008, pp. 827–838. DOI: 10.3801/IAFSS.FSS.9-827.

[271] J.G. Quintiere and A.S. Rangwala. "A theory for flame extinction based on flame temperature." In: *Fire and Materials* 28 2004, pp. 387–402. DOI: 10.1002/fam.835.

[272] J.G. Quintiere and B. McCaffrey. *The burning of wood and plastic cribs in an enclosure: volume 1*. NBSIR 80-2054. Gaithersburg, MD: National Bureau of Standards, 1980.

[273] Y. Utiskul and J.G. Quintiere. "Oscillation and fire area shrinkage phenomena of wood crib and heptane pool in ventilation-controlled compartment fires." In: *International Interflam Conference, 11th Proceedings*. Vol. 1. London, England, 2007, pp. 465–476.

[274] I.R. Thomas and I.B. Bennetts. "Fires in enclosures with single ventilation openings – comparison of long and wide enclosures." In: *Fire Safety Science – Proceedings of the Sixth International Symposium*. Poitiers, France: International Association for Fire Safety Science, 1999.

[275] N. Girgis. "Full-scale Compartment Experiments on Upholstered Furniture." Master of Engineering Thesis. Christchurch, New Zealand: University of Canterbury, Department of Civil Engineering, 2000.

[276] B. Sundström, ed. *Fire safety of upholstered furniture — the final report on the CBUF research programme*. London, England: InterScience Communications Limited, 1996.

[277] H. Denize. "The Combustion Behaviour of Upholstered Furniture Materials in New Zealand." Master of Engineering Thesis. Christchurch, New Zealand: University of Canterbury, Department of Civil Engineering, 2000.

[278] M.M. Khan, A. Tewarson, and M. Chaos. "Chapter 36 Combustion characteristics of materials and generation of fire products." In: *SFPE Handbook of Fire Protection Engineering*. 5th Edition. Vol. 1. DOI 10.1007/978-1-4939-2565-0_36. Gaithersburg MD: Society of Fire Protection Engineers, 2016, pp. 1162–1232. ISBN: 978-1-4939-2564-3.

[279] A. Lock, G.H. Ko, M. Bundy, E. Johnsson, and A. Hamins. "Measurements in standard room scale fires." In: *Fire Safety Science – Proceedings of the Ninth International Symposium*. Karlsruhe, Germany: International Association for Fire Safety Science, 2008, pp. 873–882.

[280] B. Karlsson and J.G. Quintiere. *Enclosure Fire Dynamics*. Boca Raton, Florida: CRC Press, 2000.

[281] C. Lautenberger. "Chapter 4 Radiation heat transfer." In: *SFPE Handbook of Fire Protection Engineering*. Ed. by M.J. Hurley. 5th Edition. New York, NY: Springer, 2016, pp. 102–137. ISBN: 978-1-4939-2565-0. URL: https://doi.org/10.1007/978-1-4939-2565-0_4.

[282] P.C.R. Collier, P.N. Whiting, and C.A. Wade. *Fire Properties of Wall and Ceiling Linings: Investigation of Fire Test Methods for Use in NZBC Compliance Documents*. Study Report SR160. Porirua, New Zealand: BRANZ, 2006.

[283] A. Tewarson and R.F Pion. "Flammability of Plastics - I. Burning Intensity." In: *Combustion & Flame* 26 1976, pp. 85 –103. DOI: 10.1016/0010-2180(76)90059-6.

[284] J.G. Quintiere, G. Haynes, and B.T. Rhodes. "Applications of a Model to Predict Flame Spread Over Interior Finish Materials in a Compartment." In: *Journal of Fire Protection Engineering* 7.1 1995, pp. 1–13. DOI: 10.1177/104239159500700101.

[285] MBIE. *C/VM2 Verification Method: Framework for Fire Safety Design for New Zealand Building Code Clauses C1-C6 Protection from Fire*. Compliance Document. Amendment 5. Effective 24 Nov 2017. Wellington, New Zealand: The Ministry of Business, Innovation and Employment, 2017.

[286] CEN. *EN 1991 Actions on structures – Part 1-2: General actions – Actions on structures exposed to fire, Annex F*. European Standard. Brussels: European Committee for Standardization, 2002.

[287] Standards New Zealand. *AS/NZS 1720.4 Timber structures - Fire resistance of timber elements*. Standard. Wellington, New Zealand, 2018.

[288] U. Wickström, A.P. Robbins, and G.B. Baker. "The Use of Adiabatic Surface Temperature to Design Structures For Fire Exposure." In: *Journal of Structural Fire Engineering* 2.1 2011, pp. 21–28. DOI: 10.1260/2040-2317.2.1.21.

[289] U. Wickström, D. Duthinh, and K. McGrattan. "Adiabatic surface temperature for calculating heat transfer to fire exposed structures." In: *Proceedings of the 11th International Conference on Fire Science & Engineering (INTERFLAM)*. Royal Holloway College, Nr Windsor, UK: InterScience Communications Limited, 2007.

[290] U. Wickström. "Adiabatic Surface Temperature and the Plate Thermometer for Calculating Heat Transfer and Controlling Fire Resistance Furnaces." In: *Fire Safety Science – Proceedings of the Nineth International Symposium*. Karlsruhe, Germany, 2008, pp. 1227–1238. DOI: 10.3801/IAFSS.FSS.9-1227.

[291] U. Wickström, R. Jansson, and H. Tuovinen. *Validation fire tests on using the adiabatic surface temperature for predicting heat transfer*. Tech. rep. SP Report 2009:19. Borås: SP Technical Research Institute of Sweden, 2009.

[292] T.Z. Harmathy. "On the Equivalent Fire Exposure." In: *Fire and Materials* 11.2 1987, pp. 95–104. DOI: 10.1002/fam.810110206.

[293] S.H. Ingberg. "Tests of the Severity of Building Fires." In: *National Fire Protection Quarterly* 22.1 1928, pp. 43–61.

[294] V.K.R. Kodur, P. Pakala, and M.B. Dwaikat. "Energy based time equivalent approach for evaluating fire resistance of reinforced concrete beams." In: *Fire Safety Journal* 45.4 2010, pp. 211–220. DOI: 10.1016/j.firesaf.2010.03.002.

[295] P.H. Thomas. *The fire resistance required to survive a burnout*. Fire Research Note 901. Borehamwood: Fire Research Station, 1970.

[296] M. Law. *A Relationship between Fire Grading and Building Design and Contents*. Fire Research Note 877. Fire Research Station, 1971.

[297] M. Law. "A Review of Formulae for T-Equivalent." In: *Fire Safety Science – Proceedings of the Fifth International Symposium*. 1997, pp. 985–996. DOI: 10.3801/IAFSS.FSS.5-985.

[298] T.Z. Harmathy and J.R. Mehaffey. "Normalized Heat Load: A Key Parameter in Fire Safety Design." In: *Fire and Materials* 6.1 1982, pp. 27–31. DOI: 10.1002/fam.810060108.

[299] T.Z. Harmathy and J.R. Mehaffey. *Design of Buildings for Prescribed Levels of Structural Fire Safety*. Special Technical Testing Publication ASTM STP 882. American Society for Testing and Materials, 1985, pp. 160–175.

[300] T.Z. Harmathy. "The possibility of characterizing the severity of fires by a single parameter." In: *Fire and Materials* 4.2 1980, pp. 71–76. DOI: 10.1002/fam.810040204.

[301] K. Harada, R. Kogure, K. Matsuyama, and T. Wakamatsu. "Equivalent Fire Duration Based On Time-Heat Flux Area." In: *Proceedings of the 4th Asia-Oceania Symposium on Fire Science & Technology*. 2000.

[302] V.K.R. Kodur and P. Pakala. "Energy Based Time Equivalent Approach for Evaluating Fire Resistance under Design Fire Exposures." In: *Proceedings of the 2010 Structures Congress*. 2010. DOI: 10.1061/41130(369)117.

[303] J.F. Nyman. "Equivalent Fire Resistance Ratings of Construction Elements Exposed to Realistic Fires." Master of Engineering. Christchurch, New Zealand: University of Canterbury, Department of Civil Engineering, 2002. URL: http://www.civil.canterbury.ac.nz/fire/pdfreports/JNyman02.pdf.

[304] J.F. Nyman, H.J.T. Gerlich, C. A. Wade, and A.H. Buchanan. "Predicting Fire Resistance Performance of Drywall Construction Exposed to Parametric Design Fires – A Review." In: *Journal of Fire Protection Engineering* 18 2008, pp. 117–139. DOI: 10.1177/1042391507080811.

[305] B.R. Kirby, D.E. Wainman, L.N. Tomlinson, T.R. Kay, and B.N. Peacock. "Natural Fires in Large Scale Compartments." In: *International Journal on Engineering Performance-Based Fire Codes*, 1.2 1999, pp. 43–58.

[306] P.H. Thomas. "Design guide: Structure fire safety CIB W14 Workshop report." In: *Fire Safety Journal* 10.2 Mar. 1986, pp. 77–137. ISSN: 0379-7112. DOI: 10.1016/0379-7112(86)90041-X. URL: http://www.sciencedirect.com/science/article/pii/037971128690041X.

[307] Deutsches Institut Fur Normung E.V. *DIN 18230 Part 1 Structural fire protection in industrial buildings*. German National Standard. 1982.

[308] J. A. Purkiss and L-Y. Li. *Fire Safety Engineering: Design of Structures*. 3rd Edition. Boca Raton, Florida: CRC Press, 2014. ISBN: 798-1-4665-8547-8.

[309] G.C. Thomas, A.H. Buchanan, and C.M. Fleischmann. "Structural Fire Design: The Role of Time Equivalence." In: *Fire Safety Science - Proceedings of the fifth International Symposium*. Melbourne, Australia, 1997, pp. 607–618. DOI: 10.3801/IAFSS.FSS.5-607.

[310] S. Reitgruber, C. Pérez-Jiménez, C. Di Blasi, and J-M. Franssen. *Some Comments on the Parametric Fire Model of Eurocode 1*. 2006. URL: https://orbi.uliege.be/bitstream/2268/70848/1/2006%20Some%20comments%20on%20the%20parametric%20fire%20model%20of%20Eurocode%201.pdf.

[311] MBIE. *C/AS1 to C/AS7 Acceptable Solutions for New Zealand Building Code Clauses C1-C6 Protection from Fire (including Amendment 3)*. Compliance Document. Wellington, New Zealand: The Ministry of Business Innovation and Employment, 2014.

[312] D. Jessop. "Fire performance of a laterally loaded light timber-framed compartment." Master of Eng. Thesis. Christchurch, New Zealand: University of Canterbury, Department of Civil Engineering, 2016.

[313] M.L. Janssens. "Thermo-physical properties for wood pyrolysis models." In: *Proceedings of the Pacific Timber Engineering Conference*. Gold Coast, Australia, 1994, pp. 607–618.

[314] W.J. Parker. "Prediction of the Heat Release Rate of Douglas Fir." In: *Fire Safety Science - Proceedings of the Second International Symposium*. Hemisphere Publishing Corporation, 1989.

[315] A. Matala, S. Hostikka, and J. Mangs. "Estimation of pyrolysis model parameters for solid materials using thermogravimetric data." In: *Fire Safety Science - Proceedings of the 9th International Symposium*. Karlsruhe, Germany: International Association for Fire Safety Science, 2008, pp. 1213–1224. DOI: 10.3801/IAFSS.FSS.9-1213.

[316] E. Sjostrom. *Wood chemistry fundamentals and applications*. 2nd edition. San Diego: Academic Press, 1993.